

THÈSE

Pour obtenir le grade de

DOCTEUR DE L'UNIVERSITÉ DE GRENOBLE

Spécialité : **Physique pour les Sciences du Vivant**

Arrêté ministériel : 7 août 2006

Présentée par

Laurent NAULT

Thèse dirigée par **Franz BRUCKERT** et **Yves BRECHET**
codirigée par **Marianne WEIDENHAUPT**

préparée au sein du **Laboratoire des Matériaux et du Génie
Physique (LMGP)**

dans l'**École Doctorale de Physique**

Mécanismes moléculaires de l'agrégation de l'insuline induite par la surface des matériaux.

Thèse soutenue publiquement le **24 octobre 2012**,
devant le jury composé de :

Mme. Séverine SIGRIST

Directeur de Recherche au Centre Européen d'Étude du Diabète, Rapporteur

Mr. Hilal LASHUEL

Professeur associé à l'École Polytechnique de Lausanne, Rapporteur

Mr. Vincent FORGE

Directeur de Recherche à l'iRTSV, Président

Mr. Arnaud PONCHE

Directeur de Recherche à l'Institut de Science des Matériaux, Membre

Mr. Arnaud BAHUON

Ingénieur Pharmacotechnie à Novo Nordisk, Membre

Mr. Franz BRUCKERT

Professeur à Grenoble INP, Directeur de thèse

Mr. Yves BRÉCHET

Professeur à Grenoble INP, Directeur de thèse



Acknowledgements

Je tiens à remercier grandement mon directeur de thèse, Dr Franz Bruckert, pour m'avoir permis de travailler sur ce sujet passionnant qu'est l'agrégation des protéines. Sa supervision et ses conseils ont permis le succès de cette thèse. Je remercie également le Dr Marianne Weidenhaupt pour son aide, ses idées et conseils qui m'ont été précieux tout au long de ma thèse et de la rédaction de ce manuscrit et des articles scientifiques qui lui sont associés. Enfin, dernier cité mais pas des moindres, un grand merci à mon co-directeur de thèse Dr Yves Bréchet, avec qui les discussions sont toujours à la fois fructueuses, passionnantes et distrayantes. Merci également pour avoir réussi à corriger si rapidement mon manuscrit, qui traite pourtant d'un domaine qui ne lui est pas totalement familier. Lucky Yves, l'homme qui corrige plus vite que son ombre.

Enfin, je me dois de dire un grand merci également à la caféine, composant absolument nécessaire au fonctionnement cérébral de mes 2 directeurs de thèse. Merci donc aux marchands Vénitiens d'avoir importé ce breuvage en Europe !

J'aimerais également remercier les membres de mon jury, Dr Séverine Sigrist, Dr Hilal Lashuel, Dr Vincent Forge, Dr Arnaud Ponche et Dr Arnaud Bahuon pour s'être ainsi intéressé à mes travaux et m'avoir donné de précieux conseils pour améliorer ce manuscrit.

Je tiens à remercier aussi les agences qui ont financé ce projet, le CNRS, l'ANR et la Région Rhône-Alpes. Merci aussi à l'École Doctorale de Physique et en particulier à sa secrétaire, Mme Ferrari, pour son aide sur les questions administratives.

Merci également au LMGP de m'avoir accueilli et d'avoir mis à ma disposition tout ce dont j'ai eu besoin durant ma thèse. Merci en particulier au Dr Catherine Picart pour nous avoir la première fait remarquer l'article d'Ivanova *et al.*, qui a été très utile dans mes travaux, comme peuvent en témoigner ses très nombreuses citations dans ce manuscrit.

Merci aux autres membres permanents du groupe IMBM, le Dr Didier Delabouglisse et le Dr Valérie Stambouli-Sene pour leurs conseils sur l'utilisation de leurs équipements et leurs réactifs dont j'ai eu besoin durant cette étude. Merci à Isabelle Paintrand et Laetitia Rapenne pour m'avoir permis d'observer mes agrégats en TEM.

Un immense merci à tous les autres membres du groupe IMBM et du LMGP en général : Mouna Messaoud, Laure Fourel, Claire Holtzinger, Marius Socol, Rached Salhi, Germain Rey, Nicolas Karst, Philipp Achatz, Mael Guennou, Nicolas Chaban, Sebastien Forissier, Claire Nicolas, Raphael Guillot, Fabien Dalonneau, Flora Da-Silva Gilde, Ophelia Manitis, Pratamesh Kharkar, Lalit Pandey, Varvara Gribova, Hoang Phuong Uyen Nguyen, Louis Fratedal, Pauline Serre, Claire Monge, Jorge Almodovar, Gael Giusti, Etienne Puyoo, Sophie Guillemain, Ionela Iliescu, Valentin Gate et tous les autres, restés plus ou moins longtemps au LMGP mais tous très agréables. Merci également à Arnaud Robin pour avoir trouvé le temps de trouver un bureau pour tous les stagiaires avec qui j'ai eu le plaisir de travailler, en particulier Jain, Gagan, Stacey et Mike.

Thomas Ballet mérite ma reconnaissance éternelle à la fois pour l'énorme travail qu'il a fourni durant ses années de thèse au LMGP et à BD et qui ont servi de base à mes travaux, mais également pour sa bonne humeur, son efficacité et ses nombreuses compétences. Travailler avec toi fut un véritable plaisir. Merci en particulier d'avoir mis au point les protocoles d'agrégation en plaque 96 puits et m'avoir ainsi évité de travailler en tube borosilicate + billes. Toi seul sais à quel point je peux t'en être reconnaissant !

Je veux également remercier mes parents, mes frères chéris et toute ma famille pour leur soutien et sans qui ce manuscrit n'aurait jamais pu exister. J'adresse une pensée particulière à mes grands-parents qui auraient été très heureux et fiers de me voir finir cette thèse.

Un grand merci également à ma Mélie qui a supporté mes soirées à rallonge au labo et mes week-ends rédaction. Tu mériterais un prix Nobel de la paix pour ta patience ! Merci également à toute ta famille pour leur accueil et pour la recette de la brioche à la saucisse !

Enfin, je remercie tous mes amis non-Grenoblois. Manu, Jojo, Mandine et Elie (vivent les mariés !), Isa, Pipette, Steph, Yann-pas-colloc, Bubulle, Fillote, Tom, Sylvie, Alexia, Dany, Grand-chef, Vince et Perrine (vivent les mariés bis repetita), Bounette et les tous les autres que j'ai eu le plaisir de rencontrer et fréquenter à Lyon. Merci aussi à Yann B pour tout ce que tu n'a pas fait pour moi, merci de t'être abstenu ! Et un merci tout particulier à ma Juju pour être celle que tu es. Mais j'avais également des amis avant de vous rencontrer (étonnant non ?). Je salue donc tous mes amis Nantais, qu'ils datent du collège comme Pierre, du lycée comme Sylvain, ou de la prépa comme Tanguy, Choupinet, Economimi, Mouet, Elo, et tous les autres. Sans oublier tous les anciens du Loquidy, d'Aulon ou du club théâtre de Lyon. Le moins que l'on puisse dire c'est que vous m'avez marqué, voire changé (en mieux ?), et que le monde est meilleur avec vous !

Pour finir, je remercie le nutella et le chocolat en général d'exister. Je remercie aussi Grenoble d'être une ville où il fait si chaud l'été que l'on est heureux d'aller rédiger au labo puisqu'il est climatisé, ça aide beaucoup. Merci également à mon rat Choucroute d'avoir accepté de ne grignoter significativement les corrections de ce manuscrit qu'après que j'ai eu le temps d'en corriger la version électronique. Enfin, merci à la Science d'avoir daigné me laissé un peu de vie sociale durant ces années.

Abstract

Material surface-induced protein aggregation is important for the stability of therapeutic proteins. Using human insulin, we first study its amyloid aggregation on neutral hydrophobic or hydrophilic surfaces and show that nucleation takes place on the hydrophobic surfaces at both pH 2.5 and 7.3. We show that the activation energy for nucleation is lower on hydrophobic surfaces than in solution. We observed that agitating the solution has several antagonistic effects. In particular, the hydrodynamic shear stress detaches surface-borne fibrils. Using Surface Plasmon Resonance imaging, infrared spectroscopy and fluorescence microscopy we then define the sequence of molecular events that happen at the interface between hydrophobic materials and fluid phase. Insulin first adsorbs rapidly on the surface and then continues to accumulate, in parallel with an α -to β -structural transition leading to amyloid fibril formation. Hereafter, we study the mechanism of action of a small peptide known to accelerate insulin aggregation (LVEALYL). This peptide stably adsorbs in β -conformation on the surface and helps accumulating insulin on the surface. Moreover, it appears that its sequence is not essential for its effectiveness, since several peptides, having a β -sheet structure on the surface, induce insulin aggregation. The presence of prolines abolishes its pro-aggregative activity. These results shed light on the molecular details of insulin self-association. The hydrophobic nature of material surfaces facilitates the unfolding of adsorbed insulin, resulting in the exposure of the LVEALYL peptide segment. This peptide promotes the propagation of conformational changes among incoming proteins. Counteracting this propagation could help stabilizing protein solutions.

Résumé

L'agrégation protéique induite par la surface des matériaux est un phénomène important dans la stabilité des protéines thérapeutiques. En utilisant l'insuline humaine, nous avons étudié les phénomènes d'agrégation en présence de surfaces neutres hydrophobes ou hydrophiles et avons montré que la nucléation a lieu sur les surfaces hydrophobes que l'on soit à pH 2.5 ou 7.3. Nous avons montré que l'énergie d'activation de la nucléation est abaissée sur surface hydrophobe. De plus, il apparaît que l'agitation de la solution a des effets antagonistes. En particulier, les forces hydrodynamiques de cisaillement détachent de la surface les fibres. Par Résonance Plasmonique de Surface, spectroscopie infrarouge et microscopie à fluorescence, nous avons pu définir les étapes moléculaires ayant lieu à l'interface matériaux hydrophobe/solution. L'insuline s'adsorbe tout d'abord rapidement sur la surface, puis s'accumule lentement parallèlement à une transition de la structure α initiale vers une structure β , aboutissant à la formation de fibres amyloïdes. Par la suite, nous avons étudié le mécanisme d'action d'un peptide connu pour accélérer l'agrégation de l'insuline (LVEALYL). Ce peptide s'adsorbe de façon stable sur la surface hydrophobe en structure β et facilite l'accumulation d'insuline. De plus, il apparaît que la séquence du peptide n'est pas essentielle à son action car différents peptides adoptant une structure β sur la surface sont également capables d'induire l'agrégation de l'insuline. La présence de prolines abolit cette action. Ces résultats apportent d'importantes informations sur les mécanismes moléculaires d'auto-association de l'insuline. L'hydrophobicité du matériau facilite le dépliement de l'insuline adsorbée, aboutissant à l'exposition du segment LVEALYL. Cette séquence facilite la propagation du changement de conformation vers les molécules nouvellement adsorbées. Agir contre ce phénomène pourrait permettre de stabiliser les solutions protéiques.

Table of Contents

Table of Contents.....	1
Chapter 1: Introduction.....	6
1.1. Protein conformation and aggregation	7
1.1.1. Generality on protein structure and protein solutions	7
1.1.2. Importance of protein stability in medical application.....	8
1.1.3. Protein aggregation thermodynamics and kinetics.....	8
1.1.4. Physico-chemical parameters affecting protein aggregation kinetics	10
1.2. Insulin as a model of protein aggregation	11
1.2.1. Diabetes	12
1.2.2. Insulin therapy.....	12
1.2.3. Insulin administration modes	14
1.2.4. Insulin composition and conformation.....	15
1.2.5. Physiological formation of insulin complexes	17
1.2.6. Aggregation of insulin solutions	17
1.3. Minimum peptide sequence responsible for protein aggregation	20
1.3.1. Background knowledge.....	20
1.3.2 Case of insulin: minimum peptide responsible for insulin aggregation.....	21
1.4. Influence of material surfaces in insulin aggregation	25
1.4.1. Previous studies.....	25
1.4.2. Mechanisms of insulin aggregation on hydrophobic surfaces	28
1.5. Other cases of surface-induced protein aggregation	30

1.6. Additives used to inhibit or accelerate protein aggregation.....	30
1.7. PhD project and experimental strategy	33
1.8. Thesis overview.....	35
Chapter 2: Material and methods.	38
2.1. Chemicals and products	39
2.2. Methodologies	41
2.2.1. Protein Aggregation Assays: Physical Set-Up	41
2.3. Material Surface Preparation.....	42
2.3.1. Silanization of glass slides and silicon ATR-FTIR prisms	42
2.3.2. Surface treatment of SPRi prisms	43
2.3.2.1. PEG side	44
2.3.2.2. C ₁₆ side	44
2.3.3. Water Contact Angle Analysis.....	44
2.4. Biochemical methods	45
2.4.1. Protein Desorption from material surfaces.....	45
2.4.2. Determination of protein concentration	45
2.4.2.1. Absorbance at 280nm.....	45
2.4.2.2. Bicinchoninic Acid Protein Assay (BCA) and QuantiPro™ BCA Assay (QPBCA)	46
2.5. Biophysical methods	48
2.5.1. SPRi experiments	48
2.5.2. FTIR experiments.....	49
2.5.3. Microscopy experiments	49
2.6. Insulin aggregation kinetics	49

Chapter 3: Insulin adsorbed on hydrophobic surfaces stimulates the formation and release of insulin amyloid fibers. 52

3.1. Aim of the study 53

3.2. Effect of temperature on insulin aggregation: activation energy of insulin aggregation 54

3.3. Effect of pH on insulin aggregation 56

3.4. Importance of agitation in insulin aggregation 57

3.5. Submitted Manuscript 60

Chapter 4: Human insulin adsorption kinetics, conformational changes and amyloid aggregate formation on hydrophobic surfaces..... 80

4.1. Aim of the study 81

4.2. Insulin adsorption kinetic and conformational changes..... 82

4.3. Submitted Manuscript 89

Chapter 5: Kinetic modification of surface-induced insulin aggregation by short peptide sequences. 100

5.1. Aim of the study 101

5.2. Surface-dependant effect of LVEALYL peptide on insulin aggregation 101

5.3. Minimum structure of an amyloidogenic peptide consists of alternating hydrophilic and hydrophobic amino-acids..... 102

5.4. Model of action of amyloidogenic peptides on surface-induced insulin aggregation 107

5.5. Submitted Manuscript 110

Chapter 6: Discussion and conclusion..... 126

6.1. Thesis summary..... 127

6.2. Surface-induced aggregation mechanism	128
6.3. Thesis discussion.....	132
6.4. Future directions.....	133
7. References	138
8. Appendix: Ballet <i>et al.</i> (2012)	148

Chapter 1: Introduction

1.1. Protein conformations and aggregation

1.1.1. Generality on protein structure and protein solutions

Proteins are heteropolymers of amino-acids connected by amide bounds. Their characteristic size varies from a few nanometers to a few micrometers. 20 different amino-acids are present in proteins, each one having different physico-chemical properties. The amino-acid sequence, also called primary structure, is defined by the DNA sequence of the gene coding for that protein. Since amino-acid side chains have different size, are polar or apolar, charged or neutral, the interactions of the amino-acid polypeptide chain(s) with their environment ¹ (solvent, salts, surfaces, other proteins and small molecules) defines protein 3D structure. Three structural levels are commonly described. Secondary structures are stabilized by interactions between main chain atoms (C=O and N-H) and consist of α -helices, parallel and anti-parallel β -sheets, extended helices, β -hairpins and disordered segments. Tertiary structures also involve the interactions between amino-acid side chains that results in domain formation. The formation and assembly of protein domains, called folding, is supervised *in vivo* by other proteins called chaperones. About 1000 different protein domains are known, with different biological functions. When correctly folded, proteins are in their biologically active conformation, also called native conformation, and can act in cell processes *in vivo*, depending on their biological function (enzymes, cell signaling components, cytoskeleton, transcription factors...). Nowadays, artificial proteins, called recombinant proteins, are also engineered, produced and purified to be used as therapeutical drugs.

Protein solutions consist of colloidal suspensions stabilized by the electrostatic repulsive forces between the proteins. Proteins often present several energetically favorable 3 dimensional structures or conformations, depending on the environmental conditions. Consequently, changes in pH, ionic strength or temperature, or protein/protein or protein/surfaces interactions can lead to the destabilization of native protein metastable structures ² and to the formation of other protein structures ³. It must be noticed that the order of magnitude of folding energy in a protein is 10 kcal per mole of amino-acid, while the order of magnitude of conformational transition activation energy is ~ 100 times less, from 10 to 20 kcal per mole of protein. Consequently, conformational changes induce only small variations in protein energy. Nevertheless, it may reduce the protein biological activity. Charged and neutral groups positions at the surface of the protein may also be

modified, which can reduce the repulsive forces between the proteins, leading to flocculation. Many different flocculation processes have been observed, with formation of large protein aggregates that precipitate. Depending on the self-assembly process, proteins can form low structured amorphous aggregates, or highly ordered structures such as fibrils or crystals ⁴.

1.1.2. Importance of proteins stability in medical applications

In pharmaceutical industry, the use of proteins as drugs has been widely extended since the US Food and Drug Administration (FDA) approval in 1982 of the first therapeutic recombinant insulin. This was made possible by the very high purity (> 99.9 %) obtained with the purification techniques ⁵. The protein produced can be either identical to their natural counterpart, or modified to enhance their activity or stability, and several protein domains can be fused together to obtain more complex functions in a recombinant protein. Currently, many proteins are already used to treat a large number of diseases, from cancers to diabetes or growth hormone deficiency, and many other proteins are still currently in preclinical or clinical development. Consequently, protein stability becomes a very important issue, in addition to its observed biological effect; a protein which cannot be stabilized correctly over a period of 18 to 24 months, will not be authorized for medical use ^{6,7}.

Two major sources of protein instability and flocculation are: (i) chemical degradation like asparagines oxidation and glutamine deamidation ⁸, and (ii) unfolding leading to protein self-association. These processes can lead to the irreversible formation of non functional high molecular weight species of self-assembled proteins. Proteins with very different amino-acid sequences can form protein aggregates stabilized by similar structures, suggesting that a generic mechanism is governing the process ⁹⁻¹¹. Proteins can aggregate in ordered or disordered high molecular mass structures but little is known about the conditions that favor formation of aggregates at a given order level compare to another order level. Nevertheless, aggregates are often rich in β -sheet structures and protein fibril is a typical protein aggregate ^{12,13}.

1.1.3. Protein aggregation thermodynamics and kinetics

Assuming that no chemical degradation occurs, the conformational stability of a protein in solution can be defined as the free energy change at a given temperature, pressure and buffer composition, for the equilibrium between the native protein state (N) and the denaturated or

unfolded protein state (U), with the possible existence of intermediate conformed proteins states (I). The $U \leftrightarrow I \leftrightarrow N$ reactions, involving the structuration/destructuration of the protein by intra-protein interactions are called folding/unfolding reactions ¹⁴⁻¹⁶. Protein interactions involve specific electrostatic interactions, H-bonding and van-der-Vaals forces or originate from the hydrophobic effect. Moreover, N, U or I proteins states can be involved in protein/protein interactions. The same kind of interactions can lead to the formation of aggregates (A) of self-associated proteins. Consequently, the formation of proteins in an aggregated state is considered as a process that competes with the natural folding reaction ¹⁷. These aggregates can even precipitate when their size became large enough for gravity force to compensate Brownian motion. These aggregates can be low-order and form amorphous structures or can be highly structured and form fibrils or crystals ⁴, depending on the aggregation pathway in action. Kinetically speaking, protein aggregations generally proceeds in 3 steps (see Figure 1.1): (i) a slow nucleation phase (lag phase), where sites of nucleation slowly form, (ii) the growth phase where aggregates rapidly form and (iii) a steady state when aggregated proteins and monomers are at equilibrium ^{18,19}.

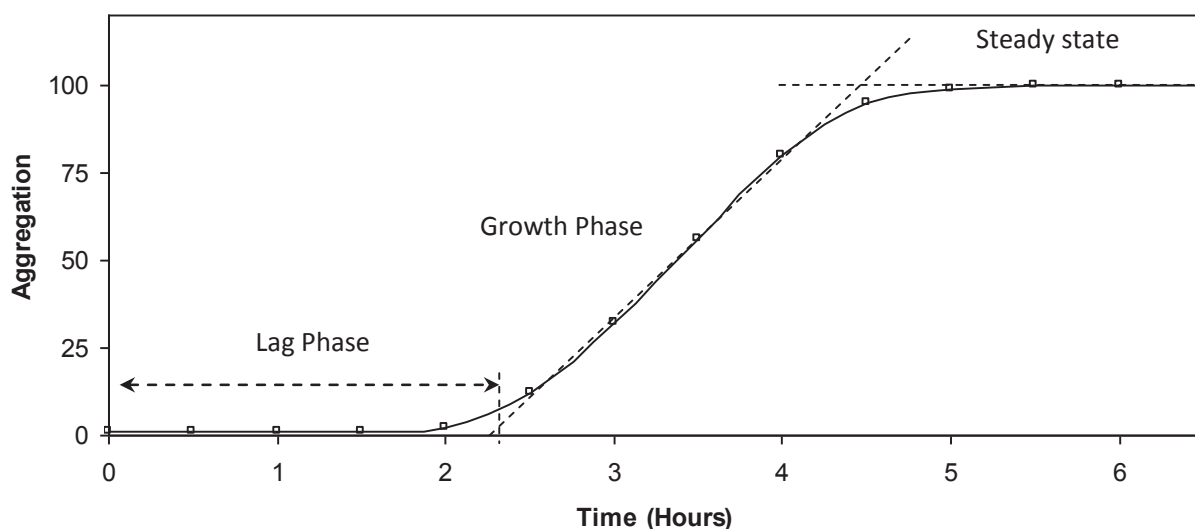


Figure 1.1: Typical kinetics of insulin aggregation: Lag phase, growth phase and plateau (steady state).

It is often observed that protein aggregates are stabilized by intermolecular hydrophobic interactions. In the native conformation of soluble proteins, hydrophobic side chains are buried

inside the proteins. It is known that individual proteins can undergo conformational rearrangement, also called unfolding, leading to non-favorable hydrophobic domains exposure to solvent. Aggregation therefore implies collective unfolded proteins interactions and stabilizations mostly through exposed hydrophobic domains interactions.

Even before the completion of their synthesis, proteins start to fold. As unfolded proteins expose their hydrophobic segments to solvent, these segments rapidly minimize the free energy by changing their conformation and removing hydrophobic parts from water contact. Consequently, the first folding event is the burying of hydrophobic lateral chains. This partially folded state is called the “molten globule”, which is characterized by a backbone resembling the completely folded protein, but lacking the extensive specific side-chain packing interactions of the native structure. This state corresponds to higher energy level than the native state but lower energy than the completely unfolded state. Since the protein structure is flexible and continuously fluctuating around an average conformation, soluble protein can spontaneously expose hydrophobic segment to solvent²⁰. This is revealed by the binding of the hydrophobic fluorophore ANS, which is increased dramatically near the unfolding temperature. If the protein is near a hydrophobic surface, this segment can minimize its free energy by making a contact with this dehydrated surface. This protein adsorption on hydrophobic surfaces thus possibly leads to partial unfolding and exposition of hydrophobic segments. In addition, adsorption increases the protein local concentration. The exposed hydrophobic protein domains can then interact together, forming initial protein aggregates.

1.1.4. Physico-chemical parameters affecting protein aggregation kinetics

In different studies, protein aggregation can be accelerated or slowed down by different physico-chemical factors. The most important are ionic strength, temperature and pH variations, that can induce changes in protein stability²¹.

When the temperature is raised, non covalent bounds in the proteins, particularly hydrogen bounds, are weakened. This affects the interactions that are necessary for the stabilization of tertiary structure and proteins become more flexible. As heating continues, hydrogen bounds will begin to break, leading to partial loss of secondary structure of the protein and the possible exposure of hydrophobic residues. Consequently, thermally induced protein

unfolding often leads to fast aggregation due to intermolecular interactions of proteins hydrophobic residues. Since the native soluble protein conformation corresponds to a local energy minimum and the aggregate form to a more stable conformation, the protein aggregation process is spontaneous and is governed by the activation energy, in respect to Arrhenius law. A temperature increase thus leads to accelerated aggregation. It follows that temperature is the most commonly used parameter to control protein aggregation. The temperature effect on protein conformation and stability can be determined using microcalorimetry.

A second common parameter that affects protein aggregation is the pH. Many amino acids charges are determined by the solution pH. Consequently, pH determines the charge distribution in the protein, which affects intramolecular interactions and its structural stability. For instance, in areas of large charge density of the same sign, electrostatic repulsion can lead to partial unfolding. Therefore, if the protein structure depends on electrostatic charges interactions, an inappropriate pH can destabilize protein structure. The solution pH also determines the net global charge of the protein, which highly influences protein/protein electrostatic repulsion and so the intermolecular interactions. Identical charges repel each other in solution, but if pH is not far from the isoelectric pH (pI), proteins will have a zero global charge, which facilitates protein association, hence aggregation.

In addition to the pH effects, ionic strength also affects protein stability because, at low concentration counterions screen out charges on proteins, and disturb the water hydrogen bonds network at high concentration. That changes the energy associated with hydrophobic interactions and the hydrogen bonds. The effect of ionic strength on protein aggregation is highly protein dependent. Finally, it is often observed that strongly bound ions, especially divalent ones, and protein cofactors are required for protein stability and function.

1.2. Insulin as a model of protein aggregation

Insulin is one of the two main hormones involved in glucose metabolism regulation in mammals in general, and humans in particular. Consequently, insulin is of great importance for diabetes treatment, and insulin stability and aggregation are essential for safe diabetes therapy. In non-diabetic people, its concentration in blood oscillates between 60 and 800 pM²². Insulin is synthesized and secreted in blood by the β cells of the islets of Langerhans in the pancreas. It is

released in the blood when glucose concentration in the bloodstream increases above a threshold (~ 4 to 6 mM). Due to the therapeutic importance of this protein, to the fact that insulin regulative function is known since 1922 ²³, to the relative cheapness of highly pure insulin and to the fact that it can fibrillate rapidly *in vitro*, a large number of studies has been performed on insulin. A lot is thus known about its composition, conformation and self-association behavior in solution.

1.2.1. Diabetes

Diabetes designates a number of very different diseases characterized by excessive urination and thirst as a common symptom. Among them, the most common are diabetes mellitus (particularly type 1 and type 2), characterized by high blood sugar concentration, that affect almost 350 million people worldwide ²⁴.

Type 1 diabetes mellitus, also called insulin-dependent diabetes, represent almost 10% of total number of diabetes mellitus cases. This disease is due to the auto-immune destruction of pancreatic insulin-producing β -cells. As insulin is essential to the cell ability to absorb glucose, reduced insulin production results in glucose accumulation in the blood, which is then flushed out into the urine. This disease is mostly treated by insulin replacement therapy, which requires frequent blood glucose concentration monitoring and subcutaneous insulin injections. Left untreated, the lack of glycemic control may lead to diabetic coma which is fatal in absence of medical assistance.

Type 2 diabetes mellitus represent almost 90% of diabetes mellitus cases. It is caused by cell resistance to insulin, and also results in decreased cellular glucose absorption. Medication can act (i) on the amount of secreted insulin by the pancreas, (ii) on cells sensitivity to insulin and/or (iii) on the gastrointestinal rate of glucose absorption. Quite often, insulin injections can be added to the treatment.

1.2.2. Insulin Therapy

In order to treat type 1 diabetes mellitus patients, a lot of research has been done to improve insulin therapy and acceptability. First, research focused on increasing insulin purity to decrease allergic reactions and to decrease the potency variations between the batches. The purity increased thanks to the discovery of insulin crystallization in 1926 ²⁵ and the effect of zinc in

insulin crystallization in 1934²⁶. Finally, 99% purity was reached by the mid-1970 thanks to HPLC methods.

First insulin was extracted from bovine or pigs insulin. Due to the similarity between human insulin and bovine or pig insulin (respectively 3 and 1 amino acid difference), bovine and pig insulins are functional in humans. Nevertheless, their use increases the risk of immune reaction. In 1982, the first synthetic human insulin, Humulin, was commercialized, increasing the patient tolerance to the treatment.

Another problem of insulin subcutaneous injections is the time of action of the injection. Insulin tends to complex with other insulin molecules and zinc to form hexamers. In hexameric form, insulin does not interact with its receptor. Consequently, the effects of insulin injections are delayed, as active insulin concentration in plasma is maximum 3 hours after the injection, and decreased to zero 6 to 10 hours after the injection. The delay before the maximum effect of insulin can give rise to inappropriate patient responses, for instance after a meal. Furthermore, the lack of long-term effect forced patients to have multiple injections per day. To control the insulin time of action, researches were undertaken to obtain insulin preparations with various pharmacokinetic properties.

One of the most important ideas was to play on insulin solubility in order to control insulin monomer release in blood. For instance, the addition of protamine decreases insulin solubility at neutral pH. As a result, insulin precipitate at the site of injection and is then slowly released in the blood. Similarly, the addition of zinc produces long-term acting insulin solutions. This reduces the number of injections per day.

With the development of biological engineering, it became possible to produce insulin analogues. Non hexameric insulin were then produced and commercialized, that act faster than unmodified insulin. These new solutions reduces the patients constrains in meal planning. Nowadays, new insulin analogues are used, to obtain fast (Novorapid insulin for instance) or long-acting (Lantus insulin for instance) effects.

1.2.3. Insulin administration modes

After the discovery of insulin and of its importance in type 1 diabetes mellitus treatments in 1921-1922 by Banting, Best, MacLeod and Collip, it was very rapidly established that subcutaneous and intravenous injections were the only efficient administration mode. Over the years, researches have been done to develop administration modes that should be painless and easier to handle, but with few success. For instance, an inhalable powdered form of insulin was developed and commercialized in 2006 (Exubera insulin) but production has been stopped due to poor success of the product among patients and physicians.

Artificial delivery systems were developed in the late 1970's and the early 1980's. Insulin automatic pumps allow continuous therapy with automatic adjustment of the insulin infusion to control glucose blood concentration. This system reduces the number of painful injections and was less time-consuming. They could be a perfect solution to type 1 diabetes mellitus. Nevertheless, the development of such systems appeared to be extremely difficult due to insulin aggregation in delivery systems. Studies reported that insulin precipitation appeared due to the continuous agitation of the protein²⁷ at a temperature comprised between 25°C (external pump) and 37°C (internal systems). This leads to the obstruction of the delivery system and necessitated frequent replacements of the catheters²⁸. Moreover, it was observed that the materials used in the pump were of high importance. Insulin solution presented faster aggregation on silicone rubber and hydrophobic materials than on hydrophilic materials^{29,30}.

In pharmaceutical insulin solutions, some additives are used that affect insulin aggregation behavior. Sugar/polyols are often used to reduce protein-solvent interactions, which reduces the possible conformational variations of the proteins. Moreover, by decreasing the protein solvent access and ionic strength increase, some amino-acids like arginine, histidine or lysine have aggregation inhibition activity. Surfactant, like Polysorbate 20 and 80 (Tween 20 and Tween 80) are also often used to stabilize protein solutions in general and insulin solutions in particular. Their effect on protein stability is due to their weak binding to hydrophobic areas on surfaces and proteins. Consequently, on the one hand, protein-surfactant and surface-surfactant complexes becomes more hydrophilic, which facilitates the protein solubility and on the other hand, the presence of the surfactant on proteins and surfaces induces steric effects that makes more difficult for proteins to interact together or with the surfaces. In pharmaceutical solutions,

the surfactant concentration is usually fixed just above the Critical Micelle Concentration (CMC) to obtain a monolayer of oriented surfactant molecules self-assemble at the interface.

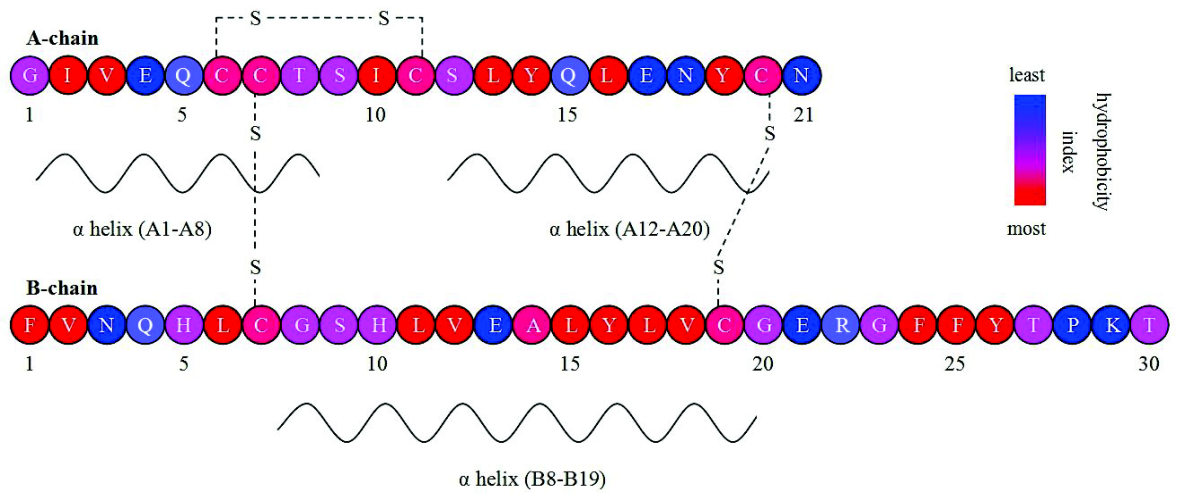
1.2.4. Insulin composition and conformation

Insulin amino-acid sequence has been determined in 1955 by Frederick Sanger³¹. Insulin is a small globular protein of 51 amino-acids. It is composed of two chains, A and B chains, of 21 and 30 amino-acids respectively (see Figure 1.2). Those chains are linked covalently by two disulfide bridges, between residues A7 and B7, and between residues A20 and B19. The A chain also contains an internal disulfide bridge between residues A6 and A11.

X-ray analysis of insulin crystals reveals that A chain is structured in two α -helices (A1-A8 and A12-A20) with a non structured region between those two helices. The B chain presents an α -helix structure in the center of the chain (residues B8-B19). The B chain is mostly unstructured outside of this α -helix center region.

Hydrophobic interactions between hydrophobic amino-acids of the two chains (A2, A3, A13, A16, B11, B12, B15, B18 and B24) form the hydrophobic core of insulin molecule³², which is of great importance for its stability. The stability is reinforced by those disulfide bridges on the polypeptide chains organization, as shown by the strong pro-aggregative effect of the disulfide-reducing agent β -mercaptoethanol and dithiothreitol³³ (Ballet private communication).

A.



B.

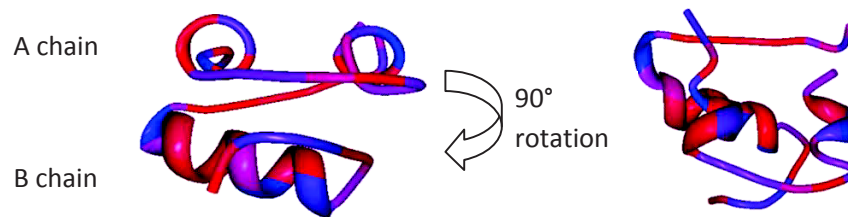


Figure 1.2: A. Structure of human insulin. Each letter code for one amino-acid, see appendix, and are colored according to the side chain hydrophobicity (blue: least hydrophobic, red: most hydrophobic). **B.** 3-Dimensional structure of insulin monomer. Each amino-acids are colored according to the side chain hydrophobicity (blue: least hydrophobic, red: most hydrophobic).

1.2.5. Physiological formation of insulin complexes

In vivo, insulin binds to its receptor in monomeric form, but in the blood insulin can associate into dimers when the insulin concentration is higher than 0.08 μM . Moreover, in presence of Zn^{2+} , dimers can associate and form hexamers stabilized by two zinc ions, provided that the insulin concentration is sufficient (insulin concentration $> 2.5 \mu\text{M}$). It can be noticed that hexamer is the storage form of insulin *in vivo* in pancreatic β cells. In the blood, insulin is only monomeric, because of its low concentration (concentration $< 0.1 \text{ nM}$) but in pancreas β cells³⁴ and in therapeutic insulin preparations, insulin is mainly in hexameric form (insulin concentration $> 200 \mu\text{M}$).

Equilibrium constants of monomer-dimer-hexamer insulin formation have been determined by equilibrium ultracentrifugation in the 1970's on bovine^{35,36} and porcine³⁷ insulins and for human insulin, at pH 7, 25°C. For human insulin, $K_{\text{dimer}} \sim 14 \cdot 10^{-4} \text{ M}^{-1}$, $K_{\text{hexamer}} \sim 3 \cdot 10^{-8} \text{ M}^{-2}$ for zinc-free insulin and $K_{\text{hexamer}} \sim 15 \cdot 10^{-10} \text{ M}^{-2}$ for insulin with zinc³⁸. These values show that an increase in insulin concentration or in Zn^{2+} concentration shifts the equilibrium to higher amounts of hexamer.

It must be noticed that in the experiments exposed in this thesis, insulin concentration is fixed at 86 μM . Using the above equilibrium constants, one can calculate that more than 85 % of insulin is in hexameric form, 10 % is in dimeric form and only 5 % is in monomeric form.

1.2.6. Aggregation of insulin solutions

As the clinical applications of insulin in diabetes therapy rapidly expanded in the late 1970's and the early 1980's, it became rapidly prominent that insulin aggregates rapidly *in vitro* in artificial delivery systems, particularly in the presence of hydrophobic surfaces^{29,30,39} and under agitation^{27,40}. Insulin precipitation leads to the obstruction of delivery systems²⁸, which slowed the development of artificial devices to deliver insulin to patients. Moreover, some insulin treated patients developed injection amyloidosis, characterized by the presence of high molecular mass insulin fibrils at the site of frequent injections⁴¹⁻⁴³.

One of the most important types of protein aggregate organizations is amyloid fiber. They are observed as insoluble fibrous protein aggregates and are characterized by extended cross- β -

sheet structure, orientated perpendicular to fibril main axis. These β -sheets are stabilized through hydrogen bonding between the protein backbone and by hydrophobic interactions between hydrophobic amino-acids.

Both *in vitro* and *in vivo*, formed aggregates are fibrils which present all of the characteristics of amyloid fibrils⁴⁴ (Figure 1.3):

- binding of the Congo red dye with “apple-green” birefringence.
- binding of the thioflavin T (ThT) fluorophore with red-shift of the excitation and emission wavelengths
- an elongated, unbranched fibrillar morphology
- a nucleation step preceding fast aggregation
- a characteristic cross- β X-ray diffraction pattern⁴⁵ (see Figure 1.4.A) revealing a repeated core structure consisting of predominantly β -sheets, orientated perpendicular to the fibril main axis^{46,47}.

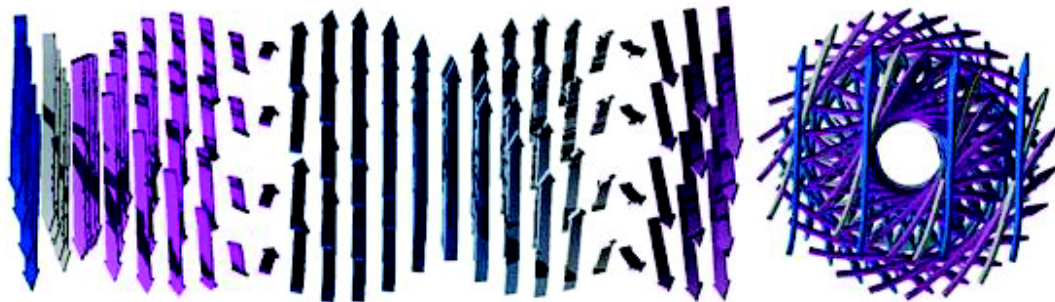


Figure 1.3: 3-Dimensions structure of A β peptide amyloid fibril

(Figure modified from Blake et al.¹⁰⁸)

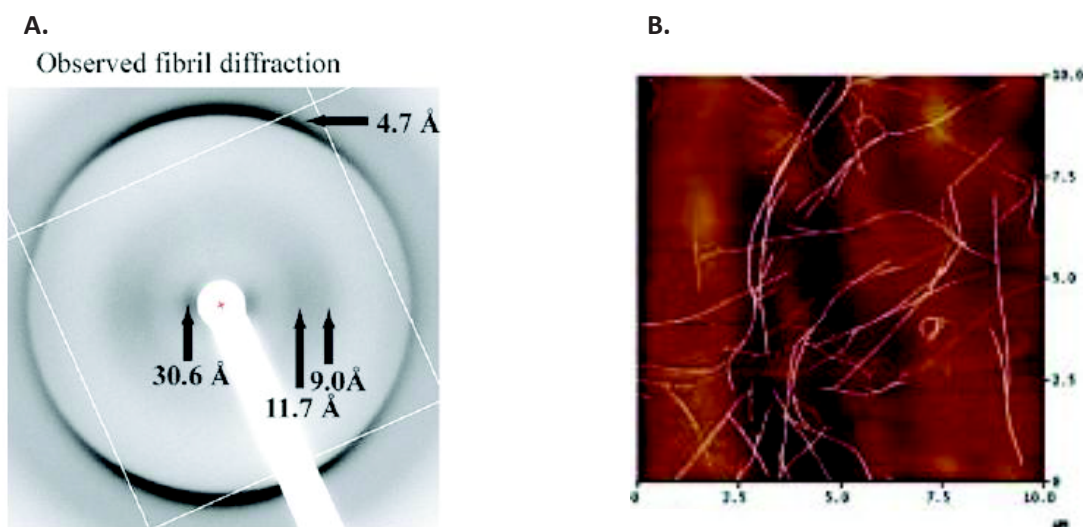


Figure 1.4: **A.** X-ray diffraction of insulin amyloid fibrils (Obtained from Ivanova *et al.*⁴⁸) **B.** Insulin fibrils observed in AFM (Obtained from Jansen *et al.*⁴⁹)

The insulin β -sheet structure is stabilized by hydrogen bonding between the proteins backbones and by hydrophobic interactions between hydrophobic amino-acids Ile^{A2}, Val^{A3}, Leu^{B11} and Leu^{B15}⁵⁰. In electron microscopy (Figure 1.4.B), these fibrils are seen as long unidirectional fibers whose diameter ranged from 3 to 15 nm and whose length ranges from hundred nanometers to several micrometers⁵¹. Consequently, understanding the molecular mechanism of insulin instability and fibrillation has been a widely studied issue in order to develop safer insulin solutions and delivery devices.

By studying the mechanism of insulin inactivation and precipitation at pH 2, 100°C, it was realized that insulin fiber formation precedes its precipitation⁵¹⁻⁵⁶. Furthermore, these fibrils are formed in three steps: (i) formation of nuclei, which are active centers of fibril formation, where protein association is faster than protein dissociation; (ii) growth of fibrils on these nucleation centers; and (iii) formation of large fibrils aggregates that precipitates. Consequently, the nuclei formation appears to be the first phenomena of insulin aggregation. The study of this process shows that the nucleus formation requires simultaneous interaction of 3 to 4 insulin molecules⁵⁶, which suggests that the nucleation core is formed from insulin monomers.

Since the late 1920's and the availability of high purity insulin solutions, it has been observed that insulin is irreversibly inactivated and precipitates in acid conditions^{57,58}, with a reaction rate that progressively increases as the pH decreases below 3. Moreover, the inactivation rate of insulin in acid conditions appears to be proportional to insulin concentration and to obey

the Arrhenius law for temperatures above 50°C⁵⁸. This shows that activation energy is the most important parameter on insulin aggregation, at least for tested pH (2 < pH < 4). It was found later that, if aggregation nucleus formation requires temperature above normal, insulin fibril growth at pH 2 is also possible at ambient and even low temperatures⁵⁶. Moreover, the aggregation of insulin in neutral therapeutic solutions used in clinical applications showed that low pH and high temperatures were not prerequisites for insulin aggregation, indicating the formation of insulin fibrils did not require complete unfolding of insulin molecules.

1.3. Minimum peptide sequence responsible for protein aggregation

1.3.1. Background knowledge

To understand the structural mechanisms of protein aggregation, and in order to develop strategies to inhibit that phenomenon, different studies have been done to discover the minimum peptide sequence explaining the full-length protein aggregation. The researched peptides were proposed (i) to be able to aggregate by themselves; (ii) the corresponding sequence in full length protein should be structurally involved in stability of the final aggregate and (iii) in solution, the peptide should interact with the full length protein, which may change the protein aggregation kinetic. As a result, some peptide sequences, derived from protein sequence and able to act on the full-length protein aggregation were discovered in different proteins known to be prone to aggregation. It is observed that those peptides are mostly hydrophobic, that they have tendencies to adopt mostly β -strand structures and to form by themselves large oligomers organized in fibrils, even for peptides as short as 3 or 4 amino-acids⁵⁹⁻⁶³. For instance, an 8 amino-acids prion peptide segment (residues 113–120: AGAAAAGA), a 6 amino-acids modified peptide from A β peptide (residues 16–20: KLVFF) and an IAPP peptide 5 amino-acids segment (residues 22–27: NFGAIL) can delay fibril formation of their respective full-length protein⁶⁴⁻⁶⁷. Moreover, β -synuclein, the non-amyloidogenic homolog of α -synuclein can inhibit the α -synuclein aggregation⁶⁸. A derived approach has been successfully studied on A β peptide with the use of small hybrid peptides, consisting in of a recognition domain (here the residues 15 to 25 of A β peptide) designed to bind a specific protein and a disrupting domain, here a polylysine that would alter the protein aggregation^{69,70}. Nevertheless, all those anti-aggregative activities are observed only at high relative concentration, since effective protective compound concentration ranged from equimolar concentrations to 10 times the protein concentration. On the contrary, some

peptides derived from protein sequences have been discovered that induces accelerated the full-length protein aggregation kinetic at low relative concentrations compare to the protein concentration ^{48,71,72}. Those peptides which enhance protein aggregation can be called pro-aggregative peptides or amyloidogenic peptides. Their aggregative effects on proteins are observed for relative concentrations of 1 pro-aggregative peptide for 10 to 100 proteins.

An interesting fact is that many proteins or peptides presents both an enhancement and inhibition activity on proteins aggregation kinetics, depending on their relative concentrations. For instance, α 1-antichymotrypsin has been observed to both accelerate (for α 1-antichymotrysin / A β peptide molar ratios lower than 1 to 100) and inhibit β -amyloid (A β) fibrillation (for molar ratios raised to 1 to 10) ^{73,74}. Apolipoprotein E (ApoE) is another example of protein presenting both A β peptide aggregation enhancement and inhibition activity, depending on the relative concentration of the two proteins ^{73,75,76}. In contrast with α 1-antichymotrypsin, the apo E4 dual effect on A β fibrillation is reversed: Apo E4 inhibits fibrillation when incubated at concentrations lower than those that accelerate fibril formation.

These stoichiometric effects are important information in understanding molecular mechanisms of aggregation and the molecular effects of compounds affecting the aggregation kinetic. Indeed, according to the nucleation theory, a compound that acts at a higher concentration than the protein concentration is a compound that is changing monomer/monomer interactions or monomer/aggregation nuclei interactions. At the opposite, a compound that has effects at lower concentrations than protein concentration must act on the aggregation nuclei formation.

1.3.2 Case of insulin: minimum peptide responsible for insulin aggregation

In the case of insulin, kinetic x-ray solution scattering and cryo-electron microscopy images show that before fibrillation, the α -helical structures of insulin molecules undergo conformational transition into a flat β -sheet rich state ^{77,78}. The first atomic-level view of the interactions between insulin segments which may be part of fibrillar spine came from single crystal structures of the fibril forming peptide segments LYQLEN (residues A13 to A18) and VEALYL (residues B12 to B17) ⁷⁹. Moreover, different studies have proposed the B chain, or at least a segment of it, to be of very high importance in insulin fibril structure stabilization. The

LVEALYLV segment (residues B11 to B18) is able to recognize and bind insulin⁸⁰. Moreover, the addition of hexameric arginine tail on that peptide induces a reduction of insulin aggregation rate at equimolar amounts of peptide and insulin. Consequently, this sequence was especially proposed to be a main contributor to the spine formation of insulin fibrils⁸⁰ (see Figure 1.5).



Figure 1.5: Human insulin amino-acid sequence. A chain in red, B chain in blue, disulfide bridges in yellow. Segments SLYQLENY and LVEALYL emphasized in dark red and dark blue respectively.

(Figure from Ivanova *et al.*⁴⁸)

Ivanova *et al.*⁴⁸ shown that the LVEALYL peptide and the SLYQLENY peptide (residues B11 to B17, and A12 to A19 respectively, see Figure 1.5) were able to aggregates in amyloid fibrils by themselves (Figure 1.6). Moreover, it appears that the LVEALYL peptide was able at sub-stoichiometric amounts (1 peptide for 10 to 40 insulin molecules) to highly reduce the insulin aggregation lag-time (from 10 hours to 1 hour) and to increase the aggregation growth phase at pH 2.5 (Figure 1.7). According to the nucleation theory, these effects at low peptide/protein stoichiometry show that this LVEALYL peptide must accelerate the aggregation nuclei formation. Consequently, that LVEALYL peptide was proposed to be the central structure of the insulin fibrils, stabilizing the fibril by hydrophobic lateral chain interaction which leads to the formation of dehydrated, highly complementary interface of the type termed “steric zipper” (see Figure 1.8)⁷⁹. This model suggests that fibril is stabilized in the long axis by H-bonding between parallel^{81,82} or antiparallel β -sheets^{79,83,84} main chains. Moreover, due to the B chain β -sheet organization and to the disulfide bridges binding the A and B chains of insulin, the A chain also has to be organized in β -sheet in the fibrils. Molecular dynamics calculations suggest that the A chain segment SLYQLENY (residues A12 to A19) is in a β -sheet structure in a peripheral position in the fibril⁴⁸.

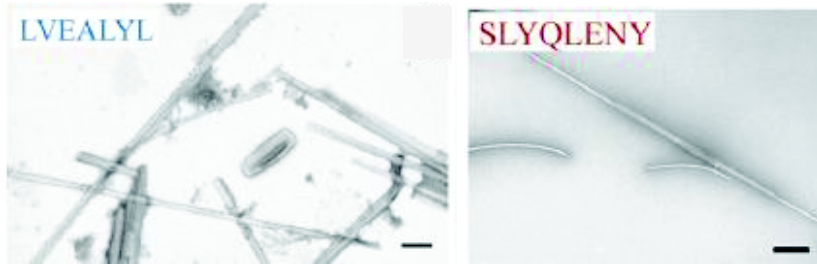


Figure 1.6: Electron microscopy images showing that LVEALYL and SLYQLENY peptides aggregate by themselves in fibril structures. Scale bars: 400nm.

(Figure from Ivanova et al. ⁴⁸)

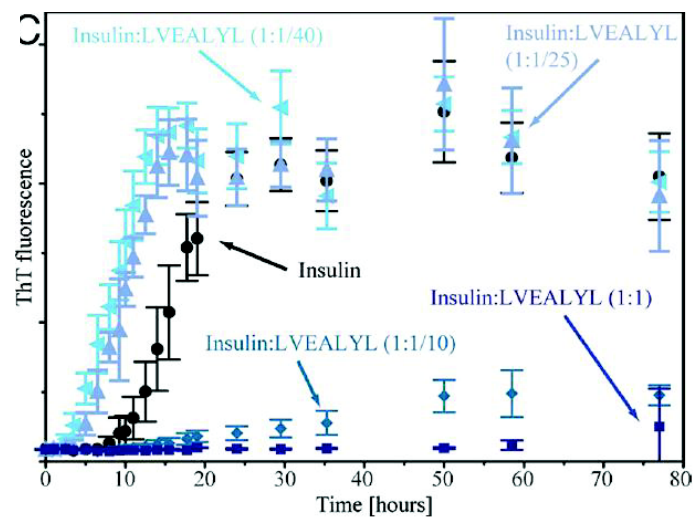


Figure 1.7: Fibrillation assay showing that B-chain LVEALYL accelerates insulin fibril formation when added to the reaction mixture at low concentrations, but inhibits insulin fibril formation at higher concentrations.

(Figure from Ivanova et al. ⁴⁸)

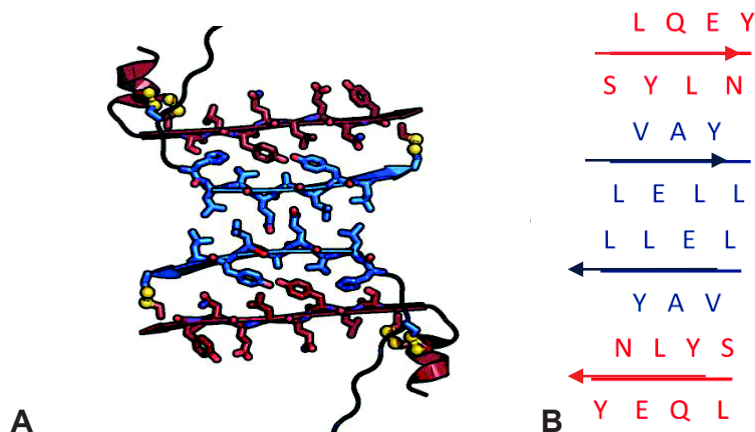


Figure 1.8: **A.** View down fibril axis showing one layer of interdigitated pair of insulin molecules, which interlock tightly to form the dry steric zipper interface. **B.** Scheme of amino-acid position in the dry steric zipper.

(Figure from Ivanova *et al.* ⁴⁸)

In the model, fibril formation involves by insulin monomer partial denaturation, leads to energetically unfavorable exposure of the VEALYL segment to solvent. This model is supported by the fact that insulin at equimolar concentration with the RRRRRRLVEALYLV peptide, containing residues B11-B17 of the B chain and a long arginine end which is known to disturb aggregation through reduction of protein/solvent interactions, can increase by a factor of 2 the insulin fibrillation lag time at pH 2 without shaking ⁸⁰. Moreover, in 2009, Ivanova *et al.* ⁴⁸ shows that the 7 amino-acids peptide sequence LVEALYL, similar to the insulin sequence in chain B (LVEALYL, residues B11–B17), was able at sub-stoichiometric concentrations to decrease the nucleation step of human insulin at pH 2.5. At the contrary, the peptide SLYQLENY derived from the insulin segment in A chain (residues A12 to A19) had no effect on insulin aggregation kinetic, showing that this segment should be peripheral in the spine of insulin fibril structure.

One problem with these reports is that experiments on pro or anti-aggregative peptides have often been performed without any considerations of the container surface chemistry and hydrophobicity, and the type of containers used in the aggregation experiments is information that is often not even present in the experimental procedures. Nevertheless, most of the experiments are done in plastic (hydrophobic) containers (plastic 96 well plates, or eppendorfs usually). But, as this LVEALYL peptide is mostly hydrophobic, it is probably able to interact strongly with hydrophobic surfaces. Since it is known that surface hydrophobicity has important

effect on insulin nucleation rate^{40,85}, the effect of that peptide on insulin aggregation kinetic has to be studied in respect to the presence or not of hydrophobic surface. Conversely, realizing that specific peptides are involved in insulin aggregation on material surfaces allow to study the molecular mechanism of insulin aggregation by mutating this peptide. This will be an element of the strategy explained in part 1.7.

1.4. Influence of material surfaces in insulin aggregation

1.4.1. Previous studies

At neutral pH, insulin aggregation is greatly enhanced by agitation and presence of hydrophobic surfaces, including air/water surfaces^{29,86,87}. Using an experimental system made of glass container filled with insulin solution and agitated at selected speed and temperature, in presence of air/water interface or various material beads, Sluzky *et al.*^{40,85} reproduced the conditions present in many drug delivery systems (temperature, mechanical stresses, presence of liquid/solid interface and air/liquid interface) (see Figure 1.9). Systematic studies were performed in 1991 and 1992 on insulin aggregation kinetic of the effects of insulin concentration, agitation rates, air/water interface, hydrophobicity of the container surface and surface area.

Those studies at neutral pH showed that insulin stability is increased at high concentration in the presence of air-water interface (see Figure 1.10.A) and Teflon-water interface (see Figure 1.10.B). Since high concentrations favor hexamer formation, it was concluded that insulin hexamers have fewer propensities to participate to aggregates formation, and that insulin monomers instead take part to aggregate formation. It must be noted that insulin aggregation kinetics at pH 7 also exhibit the 3 characteristic phases (see Figure 1.10): (i) a long lag-phase where insulin concentration is not significantly modified and where no fibrils can be detected in solution. (ii) a fast aggregation phase, where soluble insulin concentration decreases rapidly and where fibrils concentration in solution increases and (iii) a plateau phase where the amounts of aggregates and monomers reached steady state.

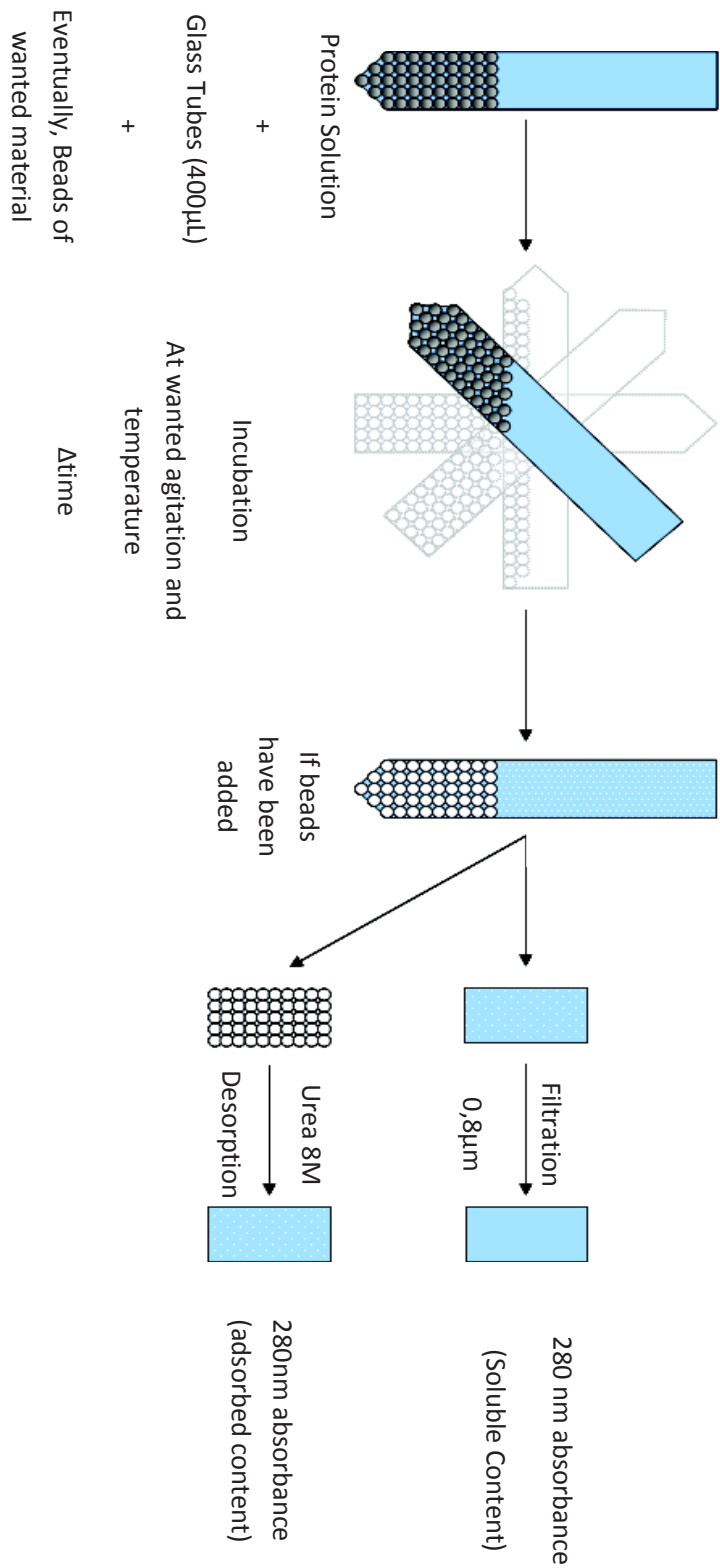


Figure 1.9: Experimental system used by Sluzky et al. for studying insulin aggregation at neutral pH.

Image from Ballet PhD Thesis

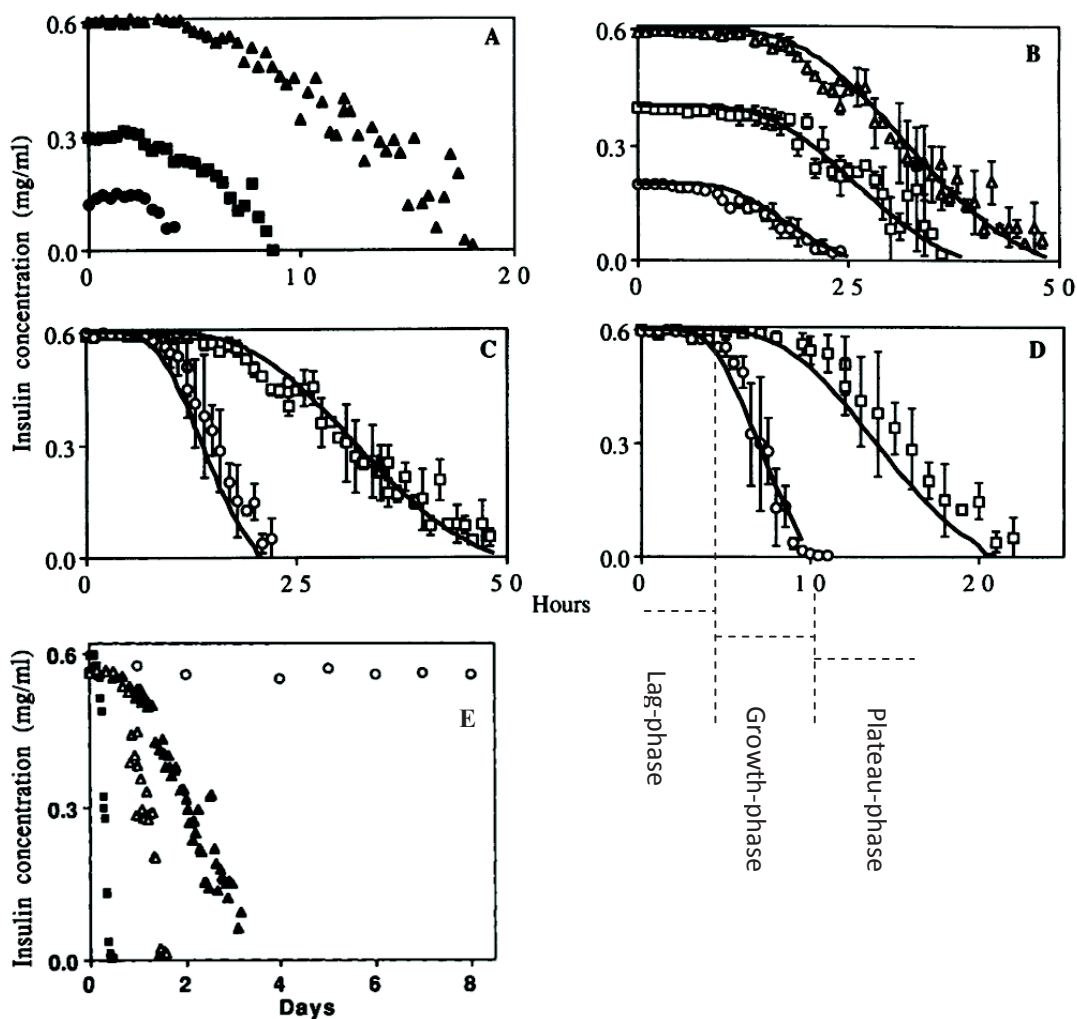


Figure 1.10: Concentration profiles of insulin aggregation upon shaking at 37°C.

(A) Effect of concentration at the air-water interface: Samples agitated at 250rpm at initial insulin concentrations of 0.6 (▲), 0.3 (■), and 0.1 (●) mg/mL. (B) Effect of concentration at the teflon-water interface: Samples with 5 teflon spheres agitated at 80rpm at initial insulin concentrations of 0.6 (Δ), 0.4 (□), and 0.2 (○) mg/mL. (C) Effect of hydrophobic surface area: Samples with 5 (□) and 10 (○) teflon spheres agitated at 80rpm. (D) Effect of agitation rates: Samples agitated at 80 (□) and 160rpm (○) at initial insulin concentration of 0.6mg/mL. (E) Effect of surface hydrophobicity on agitation-induced insulin fibrillation: Samples at initial concentration of 0.6mg/mL agitated at 160rpm in the presence of teflon (■), polypropylene (▲), siliconized glass (Δ), and unmodified glass spheres (○).

(Figure modified from Sluzky et al. ^{40,85})

Moreover, when the hydrophobic surface area (see Figure 1.10.C) or the agitation rate are increased (see Figure 1.10.D), insulin aggregates with both a shorter lag time and a higher fibril growth rate. It was also noticed that increasing the hydrophobicity of the material increased the aggregation rate of insulin (Figure 1.10.E).

More recently, Ballet *et al.*⁸⁸ developed a new setup, that allows multiple conditions to be tested in parallel using 96 microwells plates: replicates and different insulin solution conditions can be tested in the same time and different plate coating are commercialize and their effect on insulin aggregation kinetics can be tested easily. Particularly, hydrophilic PEG coated plates, proposed to be protein non-binding, were used as negative control in surface induced insulin aggregation. Ballet shows that an insulin pre-incubated hydrophobic surface was able to further shorten the nuclei formation time of fresh insulin solution. At the contrary, an insulin solution which has been pre-incubated on a hydrophobic surface was not able to aggregate faster than a fresh insulin solution when put in contact with a new hydrophobic surface. This showed that the nuclei are formed on the hydrophobic surface and remained strongly adsorbed on the surface. Moreover, it was shown that fibril growth was a mechanism which needed an interaction with the hydrophobic surface, as no fibril growth has been observed in solution.

1.4.2. Mechanisms of insulin aggregation on hydrophobic surfaces

Based on these observations, a model describing the mechanism of insulin aggregation at neutral pH in aqueous solutions in contact with hydrophobic surfaces was proposed⁸⁸, see Figure 1.11. In this model, insulin monomers, dimers and hexamers would reversibly adsorb on the material surface, exposing hydrophobic amino-acid side-chains. A new energetically favorable conformation would appear for insulin monomers, which involved a deformation of the protein to expose its hydrophobic core to the hydrophobic surface, detected by DnaK chaperone recognition of adsorbed insulin. Then, different partially unfolded proteins expose their hydrophobic core would interact together on the hydrophobic surface and form aggregation intermediates that eventually growth. After reaching a certain size, those intermediates would have sufficient surface area to become stable, leading to the construction of a nucleus of aggregation, and can start reacting with native molecules. As a result, a surface pre-incubated long enough with insulin solution is able to act as seed for a fresh insulin solution, reducing the nucleation time of that insulin aggregation kinetic. As the insulin hydrophobic core would be also involved in

protein/protein contact within dimers and hexamers, the hydrophobic core is more stabilized in the insulin complexes. So, the hydrophobic core interaction with the hydrophobic surface is less energetically favorable for insulin complexes than for monomeric insulin, which explains why dimers and hexamers are more stable than monomers and have fewer propensities to participate into the aggregation process ⁸⁹. Other studies proposed the effect of low pH on insulin aggregation kinetic mainly results from the influence of pH on dimer and hexamer stability of insulin, because in acidic conditions, dimers and hexamers are unstable ⁹⁰.

After the nucleus formation on the surface, insulin monomers would interact with this nucleus and grow into fibril. Then, when the fibril reaches a certain size, mechanical stress could break the fibril, which is released in solution, and the nucleus is able to form a new insulin fibril.

In this model, the increased stability of higher concentrated insulin solution is due to the occupation of the hydrophobic surface by dimers and hexamers, which reduced the surface available for the steps of nucleus formation: monomer adsorption, unfolding and interaction with other unfolded monomers. This model would also explain the insulin aggregation kinetic. The slow formation of stable nuclei on the surface would explain the lag-phase observed in insulin aggregation experiments. The fast insulin depletion following the end of the lag-phase would be explained by the involvement of native insulin molecules into the fibril growth on the surface.

Nevertheless, unanswered questions remained. Amino-acids involved in insulin nucleation and fibril formation are still unknown. Moreover, the insulin conformational change kinetic on the surface is yet not understood. These questions will be the aim of this thesis.

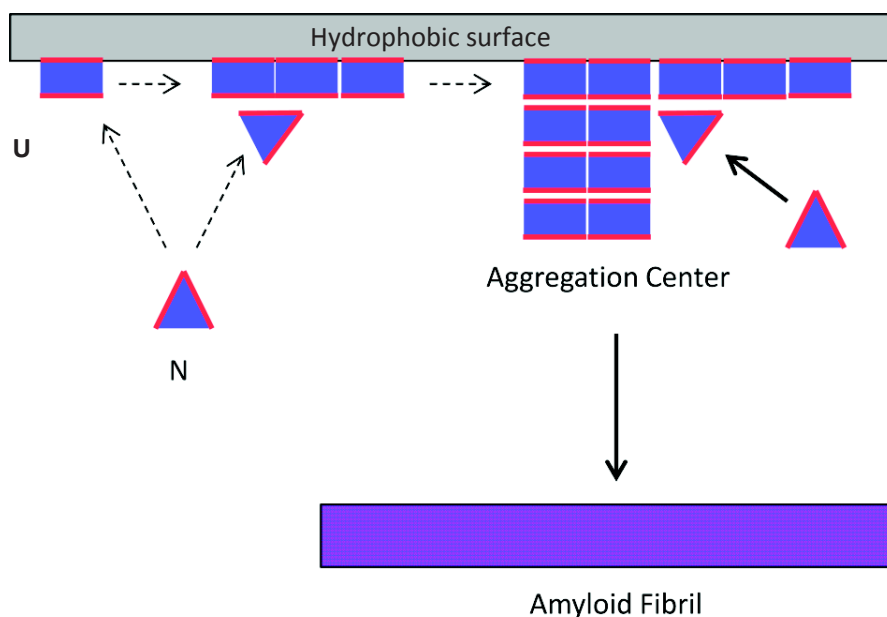


Figure 1.11: Insulin surface-induced aggregation model as proposed in Ballet *et al.* N: Native insulin, U: Unfolded insulin.

1.5. Other cases of surface-induced protein aggregation

It must be noted that this surface dependant mechanism, characterized by nuclei formation on the surfaces are observed for other proteins than insulin. For instance, IgG antibodies have been shown to aggregate at the hydrophobic air/water interface ⁹¹ and β amyloid peptide is known to present a surface induced aggregation behavior ⁹². Moreover, Ballet shows that calcitonin also aggregates in presence of hydrophobic surface. Similarly to what is observed for insulin, preincubated surfaces can act as seeds for fresh calcitonin solution. Furthermore, DnaK chaperone is able to bind adsorbed calcitonin, whereas it does not bind to soluble calcitonin, which proves that adsorbed calcitonin presents structural changes upon hydrophobic surface adsorption. Consequently, it appears that insulin material dependant aggregation studies can be generalized to other proteins of therapeutic interest.

1.6. Additives used to inhibit or accelerate protein aggregation

Additives, like arginine ⁸⁰ and small molecules found *in vivo* in organisms in stress conditions (high or low temperature, presence of free radical compounds that oxidize proteins and can leads to denaturation and aggregation) like ectoine, citrulline, betaine and trehalose (see

Table 1.1) can inhibit proteins aggregation⁹³ by interacting with and stabilizing hydrophilic groups on protein by solvent hydration (also see page 14). Other compounds such as lecithins, 2-hydroxypropyl- β -cyclodextrins, and polymeric surfactants reduce protein aggregation by binding either to hydrophobic interfaces or to hydrophobic protein domains^{43,86,94,95}. These aggregation inhibitors are fairly nonspecific and are generally effective only at relatively high molar concentrations above the targeted unstable proteins. For example, 300 mM betaine suppressed aggregation of 0.17 mM insulin, a ~1700-fold molar excess⁹³. On the contrary, some compounds can enhance protein aggregation. For instance, it is known that aluminium (AlCl_3), copper and cyclodextrins are able to induce faster A β peptide aggregation^{96,97}. But, in the same way than the previously exposed aggregation inhibitors, these aggregation enhancers are effective only at a high molar excess (~400-fold molar excess).

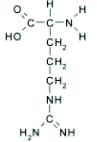
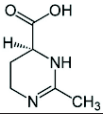
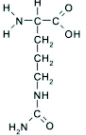
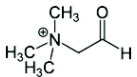
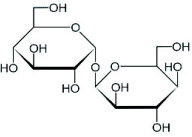
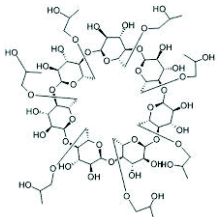
molecule	chemical structure	concentration	effect	reference
arginine		100mM	75 h protection of 0.52mM insulin solution	Gibson <i>et al.</i> (2006)
ectoin		300mM	suppress 0.17mM insulin aggregation	Arora <i>et al.</i> (2004)
citrulline		300mM	suppress 0.17mM insulin aggregation	Arora <i>et al.</i> (2004)
betaine		300mM	suppress 0.17mM insulin aggregation	Arora <i>et al.</i> (2004)
trehalose		300mM	suppress 0.17mM insulin aggregation	Arora <i>et al.</i> (2004)
2-hydroxypropyl- β -cyclodextrin		5.2mM	suppress 0.17mM insulin solution aggregation	Brewster <i>et al.</i> (1991)

Table 1.1: Chemical structures and effects of compounds known to inhibit protein aggregation, and particularly insulin aggregation.

In vivo, some proteins also exist that prevent protein aggregation. Heat shock proteins (hsp), also called chaperones are able to inhibit proteins aggregation and some can disaggregate precipitated proteins^{98,99}. For instance, in *E. coli* ~250 proteins are disaggregated by the combination of chaperones DnaK, DnaJ and ClpB¹⁰⁰. Moreover, *in vitro*, DnaK chaperone and α -crystallin can prevent insulin aggregation^{88,101,102}. These chaperones are able to recognize exposed hydrophobic segments of proteins. *In vivo*, chaperones assist the folding of nascent polypeptide chains, the refolding of denatured proteins and prevent aggregation of unfolded proteins that expose hydrophobic parts. They were identified as “heat-shock” proteins because their expression increases after a brief cell exposure to heat that induces formation of large

number of protein aggregates^{103,104}. Nevertheless, chaperone proteins cannot be used easily in therapeutic protein stabilization, because their injection to patients induces immune response.

1.7. PhD project experimental and strategy

This literature review shows that surfaces, agitation, temperature and aggregation-enhancer peptides all have a profound influence on protein aggregation. A better understanding of the interactions between these parameters on insulin aggregation could allow the development of more efficient insulin solutions and automatic delivery systems which may improve diabetes mellitus therapies. Nevertheless, agitation, temperature and aggregation enhancer peptides have never been studied with respect to the container surface physico-chemical properties, particularly its hydrophobicity, albeit the presence of hydrophobic surfaces have been shown to be of high importance on insulin aggregation kinetic. Moreover, it has been proved that aggregation nuclei formed on the hydrophobic surface but, due to the small amounts of protein involved in this process, few data are available to understand the molecular mechanism of protein adsorption and nuclei formation on the surfaces.

Nevertheless, different questions have yet to be answered. (i) The number of insulin molecules that are necessary to form a stable aggregation nucleus is not known. Moreover, the number of nuclei on the surface and their distribution has to be studied. (ii) Furthermore, even if final insulin fibril structure has been resolved, aggregation insulin nucleus structure and on the surface is not known. (iii) It has been observed that insulin aggregation at pH 2 respect Arrhenius law. It can be supposed that it is the case at neutral pH, so it should be possible to calculate activation energy of the different phases of insulin aggregation. (iv) Moreover, the binding energy of insulin monomer/insulin aggregation nucleus interaction should be measured to describe the fibril growth from the nucleus. (v) Finally, the orientation of the nuclei and of the fibril growth on the surface will be studied.

In order to solve these questions, different experimental strategies have been used in this thesis. (i) The aggregation nuclei distribution on the surface can be studied both by Atomic Force Microscopy (AFM) and by direct measurements of adsorbed mass on insulin incubated surface by Bicinchoninic Acid Assay (BCA) experiments. Combining these two techniques, it is possible to obtain the average mass of one aggregation nucleus, and so the number of insulin monomers involved in the nucleus. (ii) Nucleus structure on the surface can be analyzed by Fourier

Transformed Infrared Spectroscopy in Attenuated Total Reflection mode (ATR-FTIR), which gives information on the secondary structures of the proteins at the proximity of the studied surface. Moreover, Thioflavin T fluorescence can be used to detect the formation of extended intermolecular β -sheets. (iii) Studying insulin aggregation kinetics at different temperatures for constant insulin concentrations may determine if insulin aggregation at neutral pH respects Arrhenius equation, which should make possible to calculate activation energy for the nucleation and the fibril growth, depending on the surface chemistry. (iv) Surface Plasmon Resonance imaging (SPRi) will be used to analyze insulin adsorption and desorption kinetics for different surface chemistry. This should give information on insulin/surface and insulin monomer/insulin aggregation nucleus interaction energy. (v) The use of LVEALYL peptide and of mutants of that peptide will be able to understand the nucleus and fibril orientation on the surface.

Previous studies on insulin aggregation on hydrophobic surfaces have been done at scales that makes difficult to detect events on the surface. For instance, in Sluzky studies, 2 mL of solution was in contact with 5 cm² of surface. In Ballet experiments, 200 μ L of solution was in contact with 1.5 cm² of surface. In these conditions, in solution analysis the events that happen on the surface gives too small signals compared to overall solution signals to be easily detectable. Consequently, to obtain information on molecular events that happen on the surface, different surface analysis techniques were used. These techniques (ATR-FTIR, SPRi, fluorescence microscopy) allow surface analysis thanks to a limited penetration sensibility (see Figure 1.13). As a result, in these techniques, adsorbed proteins are easily detectable, with only small signals due to protein in solution.

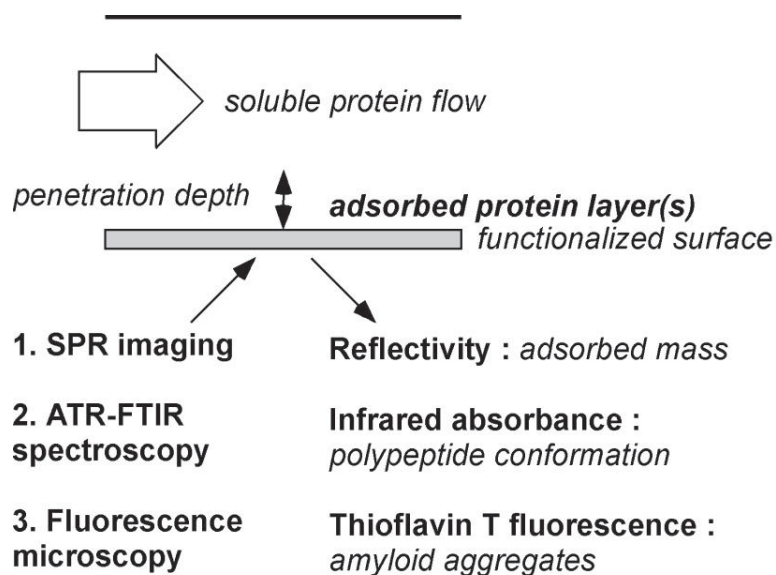


Figure 1.13: Scheme of the experimental procedures of SPRi, ATR-FTIR and fluorescence microscopy as used in this thesis.

1.8. Thesis overview

This thesis is organized around 3 main articles, to which I made essential or substantial contributions. In the first chapter (Ballet *et al.* 2012¹⁰⁵) of the results section, insulin aggregation was monitored using the ThT fluorescence. I analyzed the effect of temperature, agitation and pH variations on insulin aggregation kinetic in hydrophobic and hydrophilic 96 micro-wells plates. Particularly, I studied the effects of those parameters on the two phases of insulin aggregation: the lag-phase or nucleation phase, and the aggregates growth-phase. Our results show that the insulin aggregation nucleus formation requires lower activation energy in the presence of hydrophobic surfaces than in the presence of hydrophilic ones. But the further growth of the aggregates appears to be independent of the underlying materials. The studies as a function of temperature show that 2 mechanisms of insulin aggregation coexist: homogeneous aggregation in the bulk solution and heterogeneous aggregation on hydrophobic surfaces. This quantitative analysis allows delineating the respective part of each mechanism as a function of temperature.

In the second chapter of the results section (Nault *et al.* 2012 a ¹⁰⁶), SPRi, ATR-FTIR and microscopy fluorescence were combined to analyze the insulin aggregation mechanism on the material surface and in real time. In SPRi, it was observed that insulin adsorbs on the hydrophobic surface. Interestingly, it appears that a fraction of this adsorbed insulin population binds very strongly on the surface, as it is not easily washed. Moreover, this pool of strongly adsorbed insulin increases when insulin stays in contact for longer times, and become more and more strongly adsorbed. In infrared spectroscopy (FTIR and ATR-FTIR), it was observed that insulin structure is considerably modified by the adsorption on the surface, exhibiting a new conformation, different from soluble insulin and from aggregated insulin. This conformation is enriched in β -sheet structure. This is confirmed by fluorescence microscopy results, which shows an increase in ThT fluorescence on the hydrophobic surface, revealing the formation of extended β -sheets in adsorbed insulin structures. I will therefore distinguish several steps in the formation of amyloid fibers on the surface.

Finally, in the third and last part of the results section (Nault *et al.* 2012 b ¹⁰⁷), the effect of peptides acting as insulin nucleation-enhancers was studied. It appears that these peptides act only when adsorbed on the hydrophobic surface, independently to the pH, where they formed β -sheets. Moreover, using mutated peptides, I observed that peptides accelerate insulin nucleation more efficiently when they are more likely to form β -strand structures when adsorbed on hydrophobic surfaces.

These results are discussed thoroughly in the last chapter of this thesis. I present a model describing our mechanistic understanding of peptide-nucleation enhancement on hydrophobic surfaces during insulin aggregation.

Chapter 2: Materials and methods

2.1. Chemicals and Products

Filters

Millex-GV Durapore PVDF 0.22 μ m (33mm) were purchased from Millipore.

Microplates

Greiner Bio One flat bottom clear polystyrene 96-well microplates, Nunc Nunclon™ Δ Surface 96-well black microplates, and Corning flat bottom polystyrene “non-binding surface” 96-well black with clear bottom microplates were purchased from Sigma-Aldrich or Dutscher.

Proteins

Recombinant human insulin (HI), expressed in yeast (Ref I2643), albumin from bovine serum Cohn Fraction V (BSA) (Ref A7906) were purchased from Sigma Aldrich.

Protein Assays/Dyes/Reagents

Bicinchoninic acid kit (Ref BCA1), QuantiPro™ BCA assay kit (Ref QPBCA), thioflavin-T (Ref T3516) and hexadecanethiol (Ref 674516) were purchased from Sigma-Aldrich. PEG-thiol (polyethylene glycol thiol, 8 monomer units, MW=569.8 g.mol⁻¹) was purchased from Iris Biotech GmbH.

Insulin solution aggregation preparation

The buffer used in the experiments is TBS (25mM TRIS-HCl, pH 7.3, 125mM NaCl, 2mM MgCl₂) were freshly prepared and sterilized by filtration through 0.22 μ m Millipore Stericup filter units. Human insulin (HI) (recombinant, expressed in yeast - Purity \geq 98%) was purchased from Sigma-Aldrich (I2643) and used without further purification. The zinc content was \leq 1% (w/w), corresponding to approximately 5.5 Zn²⁺ per insulin hexamer. As Zn²⁺ influences the equilibrium of insulin hexamer formation, we tested the effect of Zn²⁺ addition (up to 10 μ M) on HI aggregation: HI aggregation kinetics was not modified. All solutions of HI were prepared at a concentration of 0.5 mg.mL⁻¹ (86 μ M) by adding human insulin to TBS. The resulting cloudy mixture was dissolved by lowering the pH to about 3.0 to 3.5 using HCl 1M (100 μ L for 20 mL of HI solution). The pH was then adjusted with 1M NaOH (volume added \sim 90 μ L for 20 mL of HI solution) to pH 7.3 \pm 0.1.

For experiments performed in acidic conditions, HI solutions were also prepared at pH 2.5 in 50 mM Glycine buffer without further pH re-adjustments. The HI concentration was determined by UV absorbance at 280 nm using an extinction coefficient of $5.53 \text{ mM}^{-1}\text{cm}^{-1}$ and molecular weight of $5807.57\text{g}\cdot\text{mol}^{-1}$. Exact concentrations were obtained by dilution with buffer prior to the final filtration through sterile $0.22\mu\text{m}$ Millex GV low-protein binding filters, to obtain a maximum seed-free condition at the onset of kinetics. The insulin concentration was checked after filtration, confirming that no material was lost during filtering.

Peptide solution preparation

peptide	solubilisation concentration	dissolved in
LVEALYL	4.3mM	20mM NaOH (pH=12.3)
LVDALYL		
LVTALYL		
LPEALYL		
LVEPLYL		
SLYQLENY		
LVEALWL	860 μM	10mM NaOH (pH=12)
LVAELYL		
LVEVLYL	2.15mM	
LVEVLFL		
SVSASYS		
LYQLENY	860 μM	
LYQLEAY		
LVPTPYL	4.3mM	20mM HCl (pH=1.7)
FSFSFSF		
LVOALYL	4.3mM	H ₂ O
LVKALYL		
LVPTLYL		
SVSPSYS		
LVTPLYL		
LSPSPSL		
LYALANY		
LSSALSL		

Table 2.1: Solubilisation conditions of peptides used in this thesis. Basic conditions are used to obtain charged glutamate (E), aspartate (D) and terminal carboxyl residues on peptides, which help solubilisation. Acid conditions are used to obtain peptides with charged terminal amine residues and Lysine (K) or Ornithine (O) residues, which help solubilisation. All peptides were purchased from Genecust, with >99% purity.

Fluorescence microscopy filters

The light filters system used in fluorescence microscopy was purchased from Olympus (U-MCFPHQ).

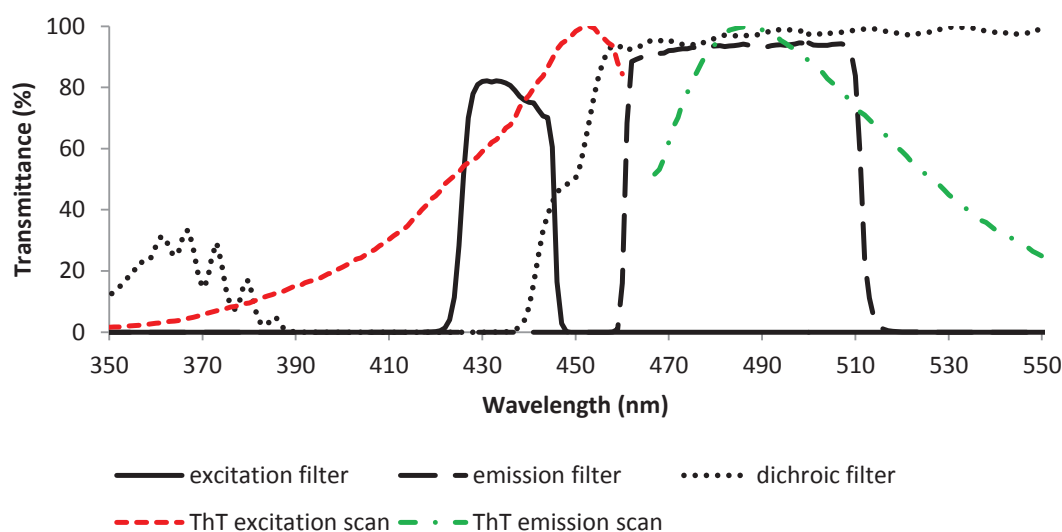


Figure 2.1: Fluorescence filters used in fluorescence microscopy experiments and Thioflavin T excitation and emission spectra.

2.2. Methodologies

2.2.1. Protein Aggregation Assays: experimental Set-Up

To study the effects of agitation, temperature or material surfaces on insulin aggregation kinetics, it is necessary to have an experimental setup allowing a fast and easy monitoring of insulin aggregation in replicates. Consequently, 96 micro-wells plates have been used, as they offer easy handling and allow good statistics. Moreover, different surface treatments are commercially available. Particularly, untreated polystyrene plates, which are hydrophobic, and PEG-coated plates, which are non-charged highly hydrophilic plates, have been used. Insulin aggregation, which is characterized by the formation of large intermolecular β -sheets, was

monitored by the binding of thioflavin T (ThT). ThT binding to β -sheets results in a characteristic fluorescence signal (excitation wavelength = 450 nm, emission wavelength = 482 nm). Furthermore, 96 micro-wells plates can be agitated and can be incubated at a chosen temperature easily.

Protein aggregation assay used plastic 96 multi-well plates as a material surface to which protein solutions were exposed. Plain polystyrene [Greiner Bio One (clear) or Nunc Nunclon (black), contact angle = $85^\circ (\pm 5)$] or (PEO)-like treated [“Non-Binding” Corning (black with clear bottom), contact angle = $5^\circ (\pm 5)$] surfaces were chosen as a model of hydrophobic or hydrophilic surfaces, respectively. Protein binds to untreated polystyrene through hydrogen bonding and hydrophobic interactions. The non-ionic hydrophilic layer on the well surface of (PEO)-treated microplates strongly reduces hydrophobic and ionic interactions with proteins.

Protein aggregation was monitored by ThT (20 μ M) fluorescence and/or turbidity measurements. A minimum of 8 replicates, corresponding to 8 wells, were measured for each sample to explore the well-to-well variation. The plates were filled with 200-250 μ L protein (86 μ M) solution and covered by plastic sheets to prevent evaporation, incubated at 37°C and shaken at 1200 rpm (Heidolph Titramax vibrating platform microplate shaker) with a small vibration orbit of 1.5 mm. No cross-contamination between wells was measured. The plates were removed at indicated times from the incubator and turbidity measurements ($\lambda=600$ nm) or free and bound ThT fluorescence were performed on a Tecan Infinite M1000 multimode microplate reader (TECAN USA, Boston, MA).

Adsorption of insulin on the plate could also be quantified by QuantiPro™ BCA after 2 washes of the plate with 200 μ L of buffer and desorption with 100 μ L of 5% SDS as described in the glass bead assay (see 3.1).

2.3. Material Surface Preparation

2.3.1. Silanization of glass slides and silicon ATR-FTIR prisms:

Glass slides used in fluorescence microscopy were treated with Dimethyldichlorosilane (DDS, see Table 2.2). Slides were cleaned by rinsing with 0.1% SDS, acetone, ethanol and then

H₂O. Glass surface was then hydroxylated in oxygen plasma, 12W, 4 minutes. Glass slides were then siliconized by an immersion of 2 hours in DDS 5% diluted in toluene with smooth agitation. Then, glass slides are washed with toluene, ethanol and water and cured at 100°C for 1 hour.

ATR-FTIR silicon prism was treated using the same protocol, replacing the DDS by phenyldimethylmethoxysilane (PDMMS). While cleaning and handling the silicon prism, some solutions should be avoided, particularly acid solutions, because they destroy the covalent linkage.

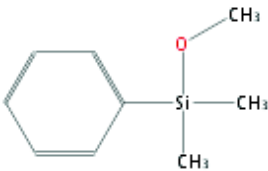
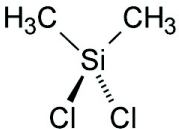
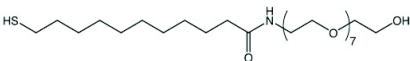
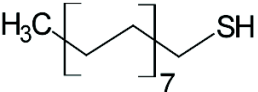
surface treated	silane used	chemical structure	forbidden solutions
ATR-FTIR	Phenyl Dimethyl Methoxysilane (PDMMS)		Acid conditions
Microscopy glass slides	Dimethyl Dichlorosilane (DDS)		
PEG side of SPR prism	Thiol Polyethylenglycol		NaBH ₄
C ₁₆ side of SPR prism	Hexadecanethiol		NaBH ₄

Table 2.2: Chemical structures of the compounds used for surface treatments in this thesis.

2.3.2. Surface treatment of SPRi prisms treatments

Clean prisms with 0.1% SDS, acetone, ethanol then H₂O. If not enough for successfully clean the prism, liquid soap can be **gently** applied on the surface with fingers, handling **gloves**. Do not try to clean gold surface with anything solid. Dry and clean prisms in oxygen plasma, 12W for 4 minutes.

2.3.2.1. PEG side

In a closed chamber containing water, put a clean glass slide on half of the prism gold surface. Prevent it to move adding some liquid mass at its surface. Add $\sim 2\mu\text{L}$ of PEG-SH solution ($1\text{ mg}\cdot\text{mL}^{-1}$) under the glass slide. Let the thiol react for ~ 2 hours. Then remove the glass slide, clean the prism with water and dry it. The C_{16} side can then be functionalized.

2.3.2.2. C_{16} side

In a closed chamber containing toluene, add approximately $400\mu\text{L}$ of C_{16} diluted at $1\text{ mg}\cdot\text{mL}^{-1}$ in toluene on top of the prism. Let it react for 2 hours. Clean the prism with toluene, ethanol and water. Store at 4°C .

2.3.3. Water Contact Angle Analysis

In order to confirm the efficiency of the material surface treatments, we measured water contact angles by the sessile drop method, using a contact angle goniometer. In this method, an optical system captures the profile of a pure liquid deposited on a solid substrate. The contact angle is defined as the angle made by the intersection of the liquid-solid interface and the liquid-air interface. It can be alternately described as the angle between the solid sample's surface and the tangent of the droplet's ovate shape at the edge of the droplet. A high contact angle indicates a low solid surface energy or chemical affinity between H_2O and the mature surface (see Figure 2.1). This is also referred to as a low degree of wetting (hydrophobic). A low contact angle indicates a high solid surface energy or chemical affinity, and a high degree of wetting (hydrophilic).

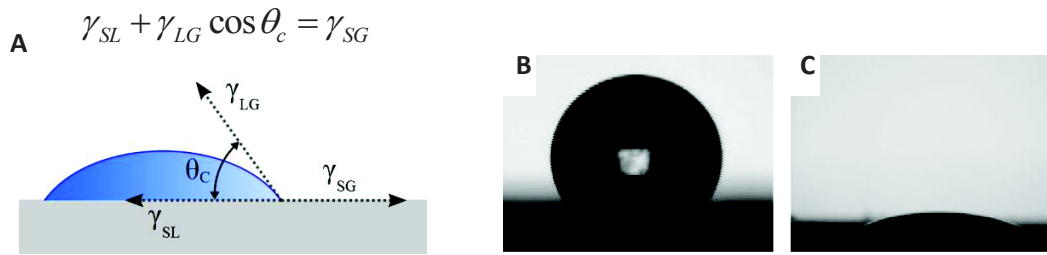


Figure 2.1: **A.** Sessile drop measuring method and Young equation with the solid-gas, the solid-liquid and the liquid-gas interfacial energies denoted as γ_{SG} , γ_{SL} , γ_{LG} , respectively, and the contact angle θ_c . (figure adapted from the Wikimedia Foundation, Inc.). **B.** Water contact angle on gold surface treated with C₁₆. **C.** Water contact angle on gold surface treated with PEG.

The water contact angle was measured with a drop shape analysis system DSA100 (Krüss) and was $38^\circ \pm 3^\circ$ and $100^\circ \pm 2.5^\circ$ for the hydrophilic (PEG) and hydrophobic (C₁₆) prisms sides, respectively. For DDS treated glass surface, contact angle was $102.1 \pm 1.3^\circ$. ATR-FTIR treated with PDMMS, contact angle was $103.1 \pm 3.7^\circ$.

2.4. Biochemical methods

2.4.1. Protein Desorption from material surfaces

Sodium dodecyl sulfate (SDS) is an anionic surfactant commonly used for protein desorption. The molecule (see Figure 2.2) has a tail of 12 carbon atoms, attached to a sulfate group, giving the molecule the amphiphilic properties required of a detergent. In most cases, SDS-mediated protein removal is assumed to proceed mainly by a displacement mechanism, i.e., by SDS adsorption to the surface. The critical micelle concentration (CMC) of SDS in phosphate buffer (pH 7.0) at 25°C is 0.0038 M (0.10% (w/w)). We used 5% (w/w) SDS (0.173M), which is thus well above its CMC, at 37°C for 30 minutes.

2.4.2. Determination of protein concentration

2.4.2.1. Absorbance at 280nm

The simplest and most direct method to measure pure protein concentration in solution is its 280nm absorbance. Indeed, no additional reagents or incubations are required, and no protein standard needs to be prepared, provided that the protein sequence is known, since the ϵ_{280} can be calculated. Amino acids containing aromatic side chains (i.e., tryptophan, tyrosine, and to a lesser

extent cysteine and phenylalanine) exhibit strong UV-light absorption. Consequently, proteins and peptides absorb UV-light in proportion to their aromatic amino acid content and total concentration.

The Beer-Lambert law states that the absorbance is directly proportional to the path length of the sample (ℓ) and its concentration (c):

$$OD_{280} = \epsilon_{280} \times \ell \times c, \text{ thus: } c = \frac{OD_{280}}{\epsilon \times \ell}$$

OD_{280} : Absorbance at 280nm

ϵ_{280} : Molar Extinction Coefficient ($M^{-1} \cdot cm^{-1}$)

The molar extinction coefficient is constant for a particular protein, and is wavelength-dependent. For most proteins, UV-light absorption allows detection of concentrations higher than $50 \mu g \cdot mL^{-1}$ of protein only. Consequently, we used absorbance at 280nm only for quantitation of working solutions while we used colorimetric and/or fluorescent protein assay methods such as BCA or QuantiPro BCA for accurate measurements of protein concentrations during aggregation assays. OD_{280} measurements were performed on a Tecan Infinite M1000 multimode microplate reader (TECAN USA, Boston, MA).

2.4.2.2. Bicinchoninic Acid Protein Assay (BCA) and QuantiPro™ BCA

Assay

The principle of the BCA assay combines the protein-induced biuret reaction with the highly sensitive and selective colorimetric detection of the resulting cuprous cation Cu^{1+} , by bicinchoninic acid (BCA). Thus, two steps are involved (see Figure). First is the biuret reaction, whose faint blue color results from the reduction of the cupric ion Cu^{2+} to the cuprous ion Cu^{1+} . Second is the chelation of two molecules of BCA with one cuprous ion, resulting in an intense purple color. The BCA/copper complex is water-soluble and exhibits a strong absorbance at 562 nm, increasing linearly with the protein concentration.

It has been shown that cysteine/cystine, tryptophan, tyrosine, and the peptide bond are able to reduce Cu^{2+} to Cu^{1+} . Thus, the amount of reduction is a sum of contributions. However,

studies performed with di- and tripeptides indicate that the peptide produces more color than the sum of each amino acid alone. Therefore, the peptide backbone (and thus the total amount of protein) is the major contributor to the reduction of copper in the biuret reaction and color development in the BCA assay. Slight protein-to-protein variation in the BCA protein assay results from differences among proteins in composition with respect to these three amino acids. The binding of BCA to cuprous ion effectively removes the weakly chelated peptides of the biuret reaction. Those peptide groups are then free to bind another molecule of cupric ion. Therefore, if bicinchoninic acid and copper are present in large excess (as they always are in BCA protein assay reagents), the protein assay does not reach an end-point. In addition, the rate of BCA color formation is dependent on the incubation time and the temperature. Consequently, the key to obtaining accurate results with the BCA assay method is to assay standards and unknown samples simultaneously so that they both receive identical incubation time and temperature.

A.

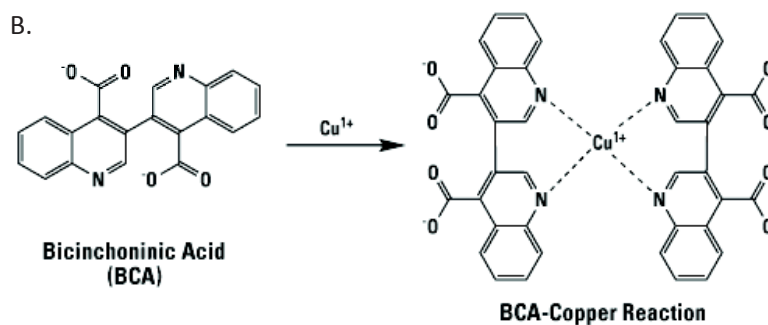
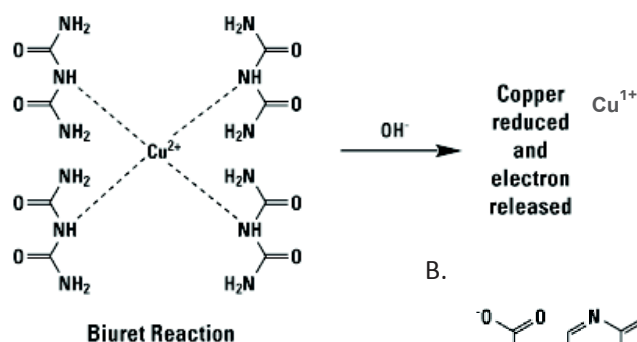


Figure 2.2: The principle of the bicinchoninic acid (BCA). (A) Biuret reaction. (B) Chelation of two molecules of BCA with one cuprous ion.

*(Figure adapted from Thermo Scientific. Pierce Protein Research Products. Chemistry of Protein Assays
www.piercenet.com. 2010)*

One particular benefit is that, unlike other protein assays (e.g., Bradford and Lowry assays), the BCA Protein Assay is compatible with samples that contain up to 5 % surfactants which allowed us to quantify protein adsorption using a solution 5 % (w/v) SDS solution. In addition, the BCA Assay responds more uniformly to different proteins than the Bradford method and has a linear concentration range between 50 and 1000 $\mu\text{g.mL}^{-1}$ of protein. The BCA assay was performed as per manufacturer's instructions (Sigma BCA1 Technical Bulletin).

The QuantiPro™ BCA Assay Kit is based on the same principles as the BCA Kit, except that the QuantiPro™ BCA Kit gives a linear response from 0.5 to 50 $\mu\text{g.mL}^{-1}$ of protein. Since the QuantiPro™ BCA assay can detect low concentrations of protein in small volumes of solution, it is especially adapted to the quantification of protein adsorption. The QuantiPro BCA assay was performed as per manufacturer's instructions (Sigma QPBCA Technical Bulletin). At the end of the color development of BCA or QPBCA assays, the absorbance at 562nm was read on a Tecan Infinite M1000 multimode microplate reader (TECAN USA, Boston, MA).

2.5. Biophysical methods

2.5.1. SPRi experiments:

Surface Plasmon Resonance imaging (SPRi) was used to monitor the mass adsorption on analyzed surfaces. SPRi is a useful real-time tool sensitive to local changes in refractive index on the first 100 nanometers of a metal surface, usually a gold layer. At a certain angle, called critical angle of resonance, a metal layer does not reflect light as the electric and magnetic fields of the light are in resonance with an electron wave forming in the metal layer. This critical angle of resonance is decreased when the refractive index on the first nanometers of the surface is increased. As an accumulation of proteins on the surface will locally increase the refractive index, the reflectivity of the gold layer will be increased. This reflectivity change of the gold layer is monitored in real-time, revealing material adsorption as small as tens of picograms per millimeter square on the gold surface. Here, a protocol was developed to obtain a gold layer treated with PEG-thiol, a hydrophilic compound, and alkyl (C16)-thiol, a hydrophobic compound. So, SPRi recording could be simultaneously obtained on both hydrophilic and hydrophobic surfaces.

Starting SPRi experiments, some 2% SDS or 1mM HCl injections must be done until signal stabilization. Regeneration can be done using 2% SDS, 5% SDS or 1mM HCl.

2.5.2. FTIR experiments

Protein structures are possibly modified during aggregation and, in proteins, atoms covalent bounds vibrations are affected by the protein structure. Vibrations changes can thus be detected through infrared spectroscopy. Consequently, Fourier Transformed Infra-Red spectroscopy (FTIR) was used to study the structures of insulin in soluble or aggregated states. Insulin structures during insulin interaction and accumulation on hydrophobic surfaces were obtained using a silicon prism in Total Attenuated Reflectance FTIR (ATR-FTIR). The prism was treated with phenyldimethylmethoxysilane (PDMMS), to obtain a hydrophobic surface in contact with the studied solutions.

2.5.3. Microscopy experiments

A flow chamber was built on a DDS-coated glass coverslip using a Glycotech flow chamber (channel width = 2.5 mm, channel thickness = 0.127 mm). A $20 \mu\text{L}\cdot\text{min}^{-1}$ flow rate was applied by a syringe pump. When indicated, thioflavin T was added to buffer and protein solutions at a $20\mu\text{M}$ final concentration. The surface fluorescence was observed by a 63x objective (N.A. = 1.4) on an IX-71 Olympus microscope fitted with a DAPI fluorescence cube ($\lambda_{\text{ex}} = 435 \pm 10 \text{ nm}$, $\lambda_{\text{em}} = 485 \pm 25 \text{ nm}$) and connected to an Olympus DP30BW camera. The image of the field stop was used to ensure proper focusing on the glass surface. Fluorescence images of the surface were recorded at the indicated times. To avoid photobleaching, each image was recorded at a different position, using a motorized stage. Using the ImageProPlus software, the average fluorescence intensity was calculated on the image of the field stop and the value of the dark background was subtracted.

2.6. Insulin aggregation kinetics

At regular time intervals, insulin ThT fluorescence was measured. ThT fluorescence values were then plotted against time (see Figure). Growth rate value was then measured as the slope of the linear ThT fluorescence increase of the growth phase. Lag time was further defined

as the intersection of the growth phase linear prolongation and the ThT fluorescence level at time 0 (see Figure 2.3).

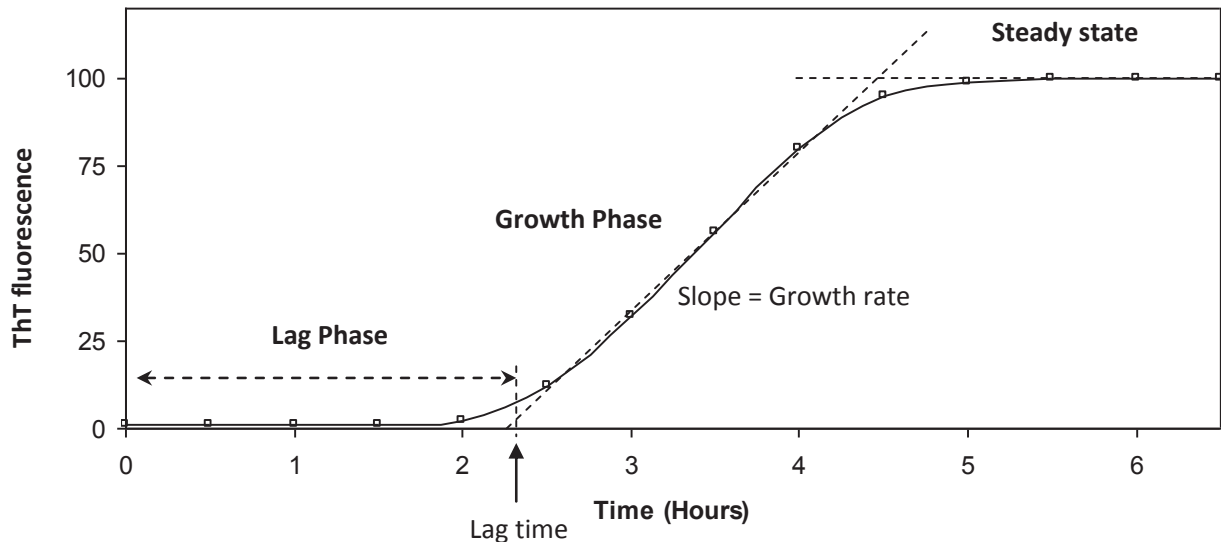


Figure 2.3: Typical kinetics of insulin aggregation: Lag phase, growth phase and plateau (steady state).

**Chapter 3: Insulin adsorbed on
hydrophobic surfaces stimulates the
formation and release of insulin
amyloid fibers**

3.1. Aim of the study

In literature, it can be seen that 2 major ways exist studying insulin aggregation. One involved insulin aggregation at pH 2 and high temperature, usually 60 °C^{48,49,54,93}. In these conditions, insulin aggregates in few minutes, but because of Arrhenius law, aggregation time highly depends on the temperature. However, in these conditions (low pH, high temperature) insulin aggregation appears to be surface independent. Since, these conditions are far from the conservation conditions of therapeutic insulin solutions, the second one consists in studying insulin aggregation at neutral pH and physiological temperature (37 °C), under agitation^{40,85,88,89}. These studies demonstrated that insulin aggregation is enhanced by surfaces, particularly hydrophobic surfaces. Consequently, insulin aggregation appears to be able to take place in solution, or on surfaces. In both cases, the final insulin state is identical, characterized by large (up to 1µm) amyloid fibers in solution. Moreover, insulin aggregation kinetic appears to be similar, with a nucleation phase preceding a growth phase. Thus, the 2 insulin aggregation mechanisms (in solution or on surfaces) are involved in kinetic competition, and systematic studies of insulin aggregation in function of temperature and surfaces was not available to determine the relative importance in given conditions of these competing mechanism. Nevertheless, it must be noted that amyloid fibrils are not the only possible insulin aggregate state. For instance, I proved in my studies that, at pH near insulin isoelectric point (4.5), insulin spontaneously form amorphous aggregates in few seconds, which are negative to ThT staining and can be disassembled by changing the pH away from the pI (see Fig. 7 of the article).

In order to study the competition between the 2 insulin amyloid aggregation mechanisms, the first part of my thesis was to study the effect of temperature and agitation on human insulin aggregation kinetics in homogeneous phase (insulin aggregation in solution) and heterogeneous phase (insulin aggregation induced by surfaces) at different temperature, pH and agitation rates. This was possible thanks to the use of microwells plates. Indeed, commercial microplates can be found that are hydrophobic or highly hydrophilic with protein very low binding properties, through a PEG-coating of the wells. In hydrophobic plastic plates, insulin can aggregate in heterogeneous phase, whereas in the hydrophilic PEG-coated plates, insulin only aggregates in homogeneous phase. This work is directly related to previous work by Sluzky and Ballet on insulin aggregation on hydrophobic surfaces exposed in Sluzky *et al.*^{40,85} and Ballet *et al.*⁸⁸. In Ballet study, human insulin was demonstrated to adsorb on hydrophobic surfaces and different

chaperones were able to recognize that adsorbed insulin. It was concluded that adsorbed insulin should be partially unfolded, exposing hydrophobic segments that can be recognized by the chaperones. That insulin partial unfolding on hydrophobic surfaces is consistent with surface-induced insulin aggregation model proposed by Sluzky *et al.*^{40,85} In that model, it is proposed that hydrophobic surfaces induce a faster aggregation of insulin monomers through (i) partial denaturation of the protein on the surface, (ii) desorption of the unfolded insulin monomer, and (iii) nucleus formation and fibril growth in the solution. Nevertheless, in Ballet's study⁸⁸, unfolded insulin remained adsorbed on the surface strongly enough to be detectable by BCA and chaperone binding after buffer washes. This shows that partially unfolded insulin monomers accumulate on the surface. Moreover, hydrophobic surface incubated with insulin solution appears to be able to seed insulin aggregation of a new solution. At the contrary, insulin solution incubated with hydrophobic surface shows similar aggregation kinetic if transferred on a fresh hydrophobic surface. These results prove that insulin unfolded monomers associate on the hydrophobic surface instead of in solution. Consequently, insulin fibrils nuclei formation and at least a part of fibril growth happen on the surface itself. In this second article, this hypothesis is formally proved, through insulin aggregation kinetics monitoring in respect of the surface chemistry. My contribution to this work has been to analyze and explain the observed influence of agitation, pH and temperature.

3.2. Effect of temperature on insulin aggregation: activation energy of insulin aggregation

In order to get a quantitative estimation of the energy change involved in the nucleus formation and the fibril growth mechanism, insulin aggregation experiments has been done at different temperature. Indeed, these two processes require the conformational change of insulin monomers, as shown by InfraRed spectroscopic signature of the soluble and aggregated insulin states. Arrhenius law relates the molar reaction rate (k) to the molar activation energy (E_a) by the relationship: $k = k_0 \cdot \exp(-E_a/RT)$, where k_0 is a constant. E_a is the energy of the transition state with respect to the initial state energy. The Arrhenius equation gives a linear relation between the logarithmic nucleation rate and the inverse of temperature ($1/T$). The nucleus formation is characterized by the nucleation rate ($= 1 / \text{lag time}$ assuming that the lag time is the characteristic nucleation time). Similarly, the growth rate is characterized by the slope of the aggregation phase divided by the plateau value (see Figure 1.1). As a result, two activation energies will be

obtained, one for the nucleation and one for fibril growth and release. Here, the activation energy is the slope of the linear relation obtained. It must be noticed that the Arrhenius law is acceptable only for activation energies that are not changing with the temperature, which implies small temperature amplitudes. This is consistent with the temperature range (from 12 to 60°C) studied here.

Consequently, I calculated the lag-time and the growth rate variations (see Fig. 2.3 in previous chapter) with the temperature, in the presence of hydrophilic and hydrophobic surfaces. In the presence of hydrophobic surface, the nucleation activation energy is decreased compared to the presence of hydrophilic surface. Moreover, on hydrophobic surface, the nucleation activation energy is smaller than the activation energy for fibril growth. These data shows that hydrophobic surfaces act as a catalyst for nucleus formation. But no significant difference has been found between the activation energy of fibril growth on hydrophobic and hydrophilic surface. So, fibril growth rate seems to be a surface independent mechanism, and insulin aggregation is controlled by the nucleation rate.

This nucleation controlled aggregation kinetic implies that according to Arrhenius equation, the activation energies can be used to evaluate the kinetic constants of the two mechanisms and their evolution with temperature. Comparing these two constants relative at a given temperature allows evaluating the part of insulin aggregation that happens in homogeneous or heterogeneous phases (See Figure 3.1).

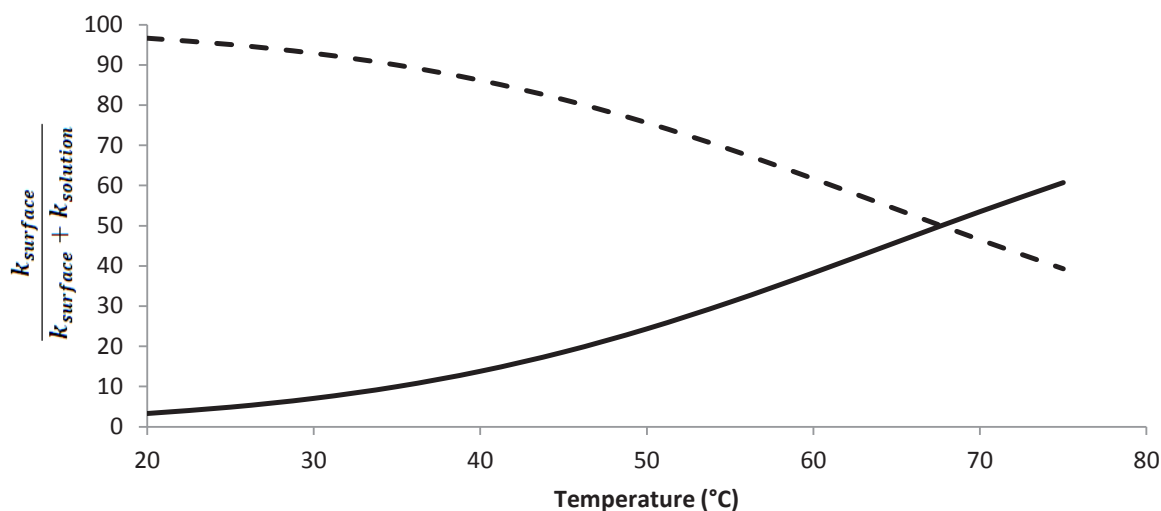


Figure 3.1: Relative contribution of heterogeneous (dotted line) and homogeneous (full line) nucleation mechanisms in human insulin nucleation for an insulin solution (86 μM , pH 7.3) incubated in a hydrophobic polystyrene microwell plate. Calculated by the comparison of heterogeneous phase nucleation constant (k_{surface}) and homogeneous phase nucleation constant (k_{solution}).

This figure shows that, when temperature raises, the quantity of unfolded protein increases and therefore the driving force for precipitate increases favorable to homogeneous aggregation. According to our results, at 37°C, 90% of the nucleation is done on the surface. At this temperature, insulin aggregation is governed by heterogeneous phase, which explains that no aggregation is observed at this temperature for 24 hours of insulin incubation on hydrophilic surfaces. At 50°C, 25 % of the aggregation is governed by homogeneous phase, and aggregation of insulin solution starts to be detectable for 24 hours of insulin incubation on hydrophilic surfaces. At 67°C, aggregation is equally governed by homogeneous and heterogeneous phases.

3.3. Effect of pH on insulin aggregation

The pH effect on insulin aggregation was also studied. Infrared Spectroscopy shows that insulin aggregates structures at pH 2 and pH 7 shows high β -sheet content compared to soluble insulin. It shows that insulin aggregates at these two pHs are amyloid fibrils, which is also confirmed by ThT fluorescence. Indeed, insulin aggregates formed at pH 2 or pH 7 seems to be similar, but with higher β -sheet amounts in pH 2 insulin aggregates (see Fig. 4F in following article). Nevertheless, at pH 2 soluble insulin conformation is similar to soluble insulin at pH 7. Moreover, at room temperature, insulin stability in hydrophilic plates at pH 2 and pH 7 are comparable. Consequently, acidic pH does not induce fast insulin amyloid fibers formation. We

also noticed that for temperatures higher than 46 °C insulin aggregation in homogeneous phase is favored at both pHs 2 and 7. Moreover, for both pHs, the presence of hydrophobic surfaces catalyze insulin aggregation. Consequently, our results show that insulin aggregation mechanisms are similar at pH 2 and pH 7. In both cases, material surface and temperature induces insulin aggregation, leading to formation of insulin amyloid fibrils on the surfaces (for temperature < 44°C) or in solution (temperature > 48°C).

I further observed that at a pH close to pI (pH = 4.5), an insulin aggregation appears in few seconds. Nevertheless, these aggregates show almost no ThT fluorescence, and FTIR confirms the absence of any structural modifications. The aggregate formation is due to the disappearance of protein/protein electrostatic repulsion at the isoelectric pH.

3.4. Multiples roles of agitation during insulin aggregation

As explained in the article, at neutral pH and 37°C nuclei formation and fibril growth take place on the hydrophobic surface and not in solution. Nevertheless, it has been reported in the literature ⁴⁰ that agitation of the insulin solution is a key determinant of aggregation, as an unstinted insulin solution contained in a hydrophobic container is stable for months (BD private communication). It is easily understandable that increases the rate of insulin molecules collisions, so that the aggregates can be formed more rapidly. This explains why insulin aggregation is highly reduced in the absence of shaking, since in this case only diffusion allows soluble insulin to encounter the surface or the growing fibrils. The initial adsorption of insulin with the surface leads to a local insulin concentration decrease at the vicinity of the surface. Nevertheless, as soon as enough agitation is provided for the solution to be maintained homogeneous, the effect of agitation on insulin aggregation kinetic should be highly reduced and hardly detectable. But this is not what is observed. My contribution has been to explain that high agitation effect on insulin aggregation kinetic.

I first varied the agitation rate of the samples and measured the obtained variations in the lag-time observed before the apparition of detectable fibrils in solution. Then, I measured the variations obtained on the rate of aggregate formation in solution after the nucleation. Aggregation formation was monitored using Thioflavin T (ThT) fluorescence and/or optical density measurements. Under a certain agitation (600 rpm), no insulin aggregation was

measurable. This was due to the absence of efficient solution mixing at that rotation speed in our experimental setup. For agitation speed between 600 rpm and 900rpm, the lag time decreased, as the solution mixing becomes more efficient and insulin fibrils formation becomes detectable after a few hours. This is consistent with diffusion being the limiting parameter, explaining why agitation accelerates the insulin aggregation. Surprisingly, the lag-time increased again with the rotation speed for agitation speeds higher to 900 rpm. These observations show that once the solution mixing has become efficient, the agitation is also an inhibiting factor of aggregation nucleus formation on the surfaces. To explain that phenomena, it must be noticed that increasing the mixing of the solution does not only increases the homogeneity of the solution but it also increases the mechanical shear stress at the surface, where the aggregates form. In the article, Thomas Ballet shows in Figure 2.B that the nuclei structures on the surface are fragile structures that can be removed by several buffer washes. We proposed that the increase of agitation induces an increase of the wall shear stress that breaks the forming nuclei on the surface. It is confirmed by the lag time linear increase with the calculated hydrodynamic wall shear stress.

After the lag phase, the aggregates become detectable in solution, and aggregate concentration increased linearly with time (growth phase). This linear increase allows calculating the fibril formation rate in the solution, also called fibril growth rate. As observed in literature, increasing the agitation rate induces a high increase of the fibril growth rate. As less than 900 rpm mixing is inefficient to produce aggregation nuclei on the surface, we first obtained nuclei at 1200 rpm, then studied fibril growth rate by reducing the agitation speed to the wanted value. I observed that the fibril growth rate increases linearly with the calculated average hydrodynamic wall shear stress ($k(\omega) = A \cdot \omega^{3/2}$). As Thomas Ballet shows that the fibril growth only happen on the surfaces, we proposed that the fibril accumulation in the solution is a shear stress-dependant mechanism: aggregates nuclei are formed and fibrils growth on the surface, but as soon as a fibril becomes long enough, shear stress breaks its attach to the surface. That liberates space on the surface which is further used as a new fibril growth site.

Consequently, agitation has three important and antagonist effects on surface dependant aggregation: (i) it homogenizes the solution, facilitating the molecular collisions; (ii) it detaches the fibrils from the surface, inducing the apparition of fibril accumulation in the solution and allowing the formation of new fibrils on the liberated free surface. But (iii) it breaks the

nucleation centers on the surface, increasing the stability of the solution. The two first parameters increase the aggregation rate, the last one decreases the aggregation rate.

This indicates that the fibrils growth from the nuclei on the surface and are then released in solution when they become large enough to be sensitive to the wall shear stress. Consequently, our data show that nucleus formation and fibril growth both takes place on the surface.

INSULIN ADSORBED ON HYDROPHOBIC SURFACES STIMULATES THE FORMATION AND RELEASE OF INSULIN AMYLOID FIBERS

Thomas Ballet^{1,2}, Laurent Nault¹, Lalit Pandey¹, Franz Bruckert¹, Christophe Bureau², Laurence Boulangé^{2,3}, Paolo Mangiagalli², Marianne Weidenhaupt¹.

From the ¹ Laboratoire des Matériaux et du Génie Physique, Grenoble Institute of Technology, 3 parvis Louis Néel, 38016 Grenoble Cedex 1, France. ² Becton-Dickinson Pharmaceutical Systems, 11, Rue Aristide Bergès, 38801 Le Pont de Claix, France. ³ Current address : EIFFAGE Travaux Publics, Centre d'Etudes et de Recherches, 8 rue du Dauphiné, 69960 Corbas, France

Running head: DnaK prevents insulin amyloid fiber formation on materials

Address correspondance to: Marianne Weidenhaupt ¹Laboratoire des Matériaux et du Génie Physique, Grenoble Institute of Technology, 3 parvis Louis Néel, 38016 Grenoble Cedex 1. France ; tel : 0033 4 56 52 93 66 ; fax : 0033 4 56 52 93 01 ; Email : marianne.weidenhaupt@grenoble-inp.fr

We investigated the impact of surface hydrophobicity on the adsorption and aggregation of human insulin. Our study shows that, under specific formulation conditions, hydrophobic surfaces can induce strong insulin adsorption, a conformational change leading to thioflavin T-positive staining and the release of amyloid-like aggregates from the surface. In contrast, insulin adsorbs very weakly and does not aggregate on plain glass or PEG-coated hydrophilic surfaces. The kinetics of insulin aggregation progresses in two phases. First, a lag-phase during which pre-fibrillar aggregates form on the material surface. These material-borne intermediates act as seeds and are essential for the subsequent formation of amyloid fibers. Second, a growth phase, during which amyloid fibers are progressively released in the bulk solution. We show that the initiation of HI amyloid aggregate formation requires lower activation energy in the presence of hydrophobic surfaces than in the presence of hydrophilic ones, but that the ongoing growth of the aggregates is material-independent. These results show that HI is able to form prefibrillar aggregates on hydrophobic surfaces, which act as seed for the growth of large micron-sized amyloid fibers. Material surfaces can therefore assist protein unfolding leading to aggregate formation.

INTRODUCTION

Protein adsorption on material surfaces is a widespread phenomenon with multiple and sometimes unwanted consequences in biology, pharmacy and medicine. The extracellular matrix, a well-defined protein network that conveys mechanical support as well as growth and differentiation signals to eukaryotic cells, naturally mediates their adherence to materials. In biotechnology, recombinant protein stability can be affected by the nature of the container used to store it ^{1, 2}. In medicine, implantable materials often trigger an inflammatory response driven by the adsorption and reaction of the complement with their surface ³. Blood-contacting materials provide another example where the binding and activation of specific proteins may trigger blood clotting ⁴.

The mechanisms that drive protein adsorption on materials are governed by a complex combination of physico-chemical characteristics of the protein and the material, as well as the solution environment. The size, charge, hydrophobicity and conformational stability are specific to each protein and influence its propensity to adsorb and stay bound to a given material. In an aqueous environment enhanced protein adsorption and conformational change are mostly observed on hydrophobic surfaces because of the entropy increase resulting from both the dehydration of a hydrophobic protein domain and the release of water from a hydrophobic surface upon binding. On the material site, not only its hydrophobicity and charge but also its topography influences the interaction with a given protein. Temperature and agitation are important parameters governing the collision rate between the protein molecules in solution and with the material. Moreover thermal and mechanical energy also affect protein tertiary structure. With increasing temperature long-range interactions are weakened and the overall protein structure becomes

more flexible and therefore more likely to adsorb on a material surface. Finally the pH of the solution determines the type and distribution of surface charges and therefore affects protein conformation and protein-material interaction via electrostatic forces.

Protein adsorption can be measured either biochemically after desorption or in situ by sensitive biophysical methods like IR spectroscopy or fluorescence using conformation-sensitive dyes. These techniques are sensitive to both the amount of protein and to their folding state while AFM allows to image the protein layers adsorbed on a material.

We chose human insulin (HI) as a model because its aggregation has been studied in different physico-chemical conditions⁵⁻⁷. It has been known for a long time that HI forms inactive aggregates at elevated temperature and acidic pH and since the discovery of amyloid fibers in the 1960s, it is known that these HI aggregates exhibit the properties of amyloid fibers. More recently, studies by Brange et al⁷ have shown that HI forms fibrils within 2 hours at acidic pH and 55°C whereas fibrillation only starts after 2 days at acidic pH and 37°C. Besides acidic pH and elevated temperature, insulin aggregation has also been studied under agitation in the presence of hydrophobic materials. Sluzky and coworkers⁶ have shown that insulin undoubtedly changes its conformation upon binding to hydrophobic surfaces at pH 7 and 37°C. From a concentration-dependence study, they deduced that the HI monomer was the molecular species leading to aggregation. They hypothesized that HI changes its conformation upon binding to hydrophobic surfaces and that the released, unfolded HI monomer forms aggregates in solution⁶. In this article, we show that HI aggregation in fact proceeds exclusively on the material surface, once the latter is covered with adsorbed HI. This holds true at acidic and neutral pH and is dependent on agitation and the presence of a hydrophobic material surface. The properties of the material surface therefore act as a catalyst that triggers a propagative conformational change in the protein.

EXPERIMENTAL PROCEDURES

If not otherwise stated, all chemicals were purchased from Sigma-Aldrich. Experiments were conducted in PBS (10mM phosphate, pH 7.4, 154mM NaCl) or TBS (25mM TRIS-HCl, pH 7.4, 125mM NaCl). HI (recombinant, expressed in yeast) solutions were prepared at 0.5 mg/mL (86 μ M), a concentration suitable for protein quantification. Moreover previous work by Sluzky *et al.*⁵ showed that HI, at this concentration, readily adsorbs and aggregates upon contact with hydrophobic surfaces. All solutions were filtered (0.22 μ m) before use.

Glass bead surface treatments—Acid-washed borosilicate glass beads (diameter 1mm) were siliconized by immersing in SurfaSil[®] (Pierce) 10% (w/w) in acetone and stabilized by curing at 100°C for 1h. The water contact angle was measured (DSA100 Krüss) and was <15° and 93.5° (\pm 3.5°) for plain and SurfaSil[®]-treated surfaces, respectively.

Insulin aggregation assays—HI aggregation assays were conducted on two types of model surfaces, glass beads or plastic 96-well microplates. All reactions were performed with 3 (glass beads) or 8 (microplate) replicates.

Glass Bead Assay—A 6 x 29 mm borosilicate glass tube was filled with 200mg of unmodified or siliconized glass beads (6 cm² area) and 325 μ L HI in PBS, sealed with Parafilm, and incubated at 37°C with agitation (PTR-60 Grant 60 rpm end-on-end rotation). At each time point, the solution was separated from beads. Part of the solution was filtered to remove aggregated HI (100 nm cut-off). The beads were washed 3 times with 500 μ L PBS. The adsorbed HI fraction was desorbed with 100 μ L of 5% SDS for 1h agitation at 37°C. Negligible protein material remained on the bead surface thereafter. The total amount of HI in solution (non-filtered), of soluble HI and of HI adsorbed to the beads was determined using the Bicinchoninic Acid Assay⁸⁻¹¹. In addition, non-filtered solutions were used for turbidity (λ =600nm) or Thioflavin T (ThT, 20 or 50 μ M) fluorescence measurements. Free and bound forms of ThT were

measured at $\lambda_{\text{ex}}=342\text{nm}$, $\lambda_{\text{em}}=430\text{nm}$ and $\lambda_{\text{ex}}=450\text{nm}$, $\lambda_{\text{em}}=482\text{nm}$, respectively¹², with a 5 nm excitation and emission slit (Tecan Infinite M1000). For seeding experiments, an HI aggregation assay was performed for the indicated time. At the end of the pre-incubation, beads and the solution were separated. The “pre-incubated” beads were washed and incubated with a fresh HI solution. The “pre-incubated” solution was directly incubated with fresh plain borosilicate beads. Seeding with aggregates was performed by adding “pre-formed” aggregates (10% (w/w)) from a overnight incubated solution to a fresh HI solution and plain beads. The results are the average and standard deviation of 3 samples. They are representative of several independent experiments. Lines are hand-drawn and provided as a guide for the eye.

96-well microplate assay—Polystyrene (Greiner Bio-One, contact angle = $85^\circ \pm 4.7$), or PEO-coated, (Corning, contact angle = $3.5^\circ \pm 5.8$) microplates were used. In fluorescence assays, black polystyrene microplates were used (Nunc Nunclon[®] Δ Surface). The plates were covered by plastic sheets, incubated at 37°C and shaken at 1200 rpm (Heidolph Titramax, 1.5 mm vibration orbit). This setup allows to obtain similar aggregation kinetics when compared to the bead assay. Indeed the hydrophobic surface area of an individual well is smaller than that of the beads (2 cm^2 and 6 cm^2 , respectively). This decrease is compensated for by agitation at 1200 rpm so as to favour protein-material contact. At the indicated times, turbidity or free and bound ThT fluorescence were measured. Quantification of soluble HI was conducted after filtration using Millipore $0.22\mu\text{m}$ MultiScreen[™]. Adsorption of HI on the plate was quantified by BCA assay after 2 washes and desorption with 5% SDS. ThT staining of the adsorbed proteins was done after 2 washes. Seeding experiments were performed as previously described with glass beads. The results are the average and standard deviation of 8 samples. They are representative of several independent experiments. Lines are hand-drawn and provided as a guide for the eye.

Kinetic analysis—The aggregation kinetics proceeded in three phases: a lag phase, where the signal was not statistically different from the baseline (mean \pm standard deviation), a linear growth phase and a plateau phase. Experimentally, the lag time was defined by the intercept between the linear growth phase and the baseline. The lag-time is variable between 2 and 4 hours according to the experimental set-up. The nucleation rate (h^{-1}) is defined as the inverse of the lag time. The slope of the aggregate growth was defined as the slope of the linear phase and the plateau as the maximum value attained. Growth slopes were normalized to the maximum value to the signal to define the growth rate (h^{-1}). These parameters were calculated on individual kinetics corresponding to different samples, and the given statistics represent the average and the standard deviation for each parameter.

In order to determine activation energies, HI solutions were incubated in hydrophobic multi-well plates at different temperatures, with agitation (1200 rpm). HI aggregation was monitored by ThT fluorescence or turbidity. The nucleation and aggregation growth rate were determined as explained above and fitted to the following equation $k(T) = k_0 \exp(-E_a/RT)$ to calculate activation energies.

Dynamic Light Scattering (DLS) / Micro-Flow Imaging (MFI[™])—In order to estimate the size of the aggregates formed during the experiment, insulin aggregation was monitored by Dynamic Light Scattering (DLS : Wyatt Dynapro Plate Reader Plus) and Micro-Flow Imaging (MFI[™] : DPA4200 Series A, Brightwell Technologies). These experiments were conducted in the microplate assay format. At each time point, solutions were removed from the incubation and assayed for particles size and quantity using those two instruments. DLS analysis of filtrated samples (100 nm cut-off) showed that in the 1-100 nm range, a single 2.7 nm peak was present, corresponding HI monomers, dimers and hexamers, but no aggregates of sizes up to 100 nm were present during the whole aggregation process (data not shown). Using MFI[™], increasing amounts of particles were observed during the growth phase (2-3 μm average size).

Insulin aggregation at different pH—Aggregation and seeding experiments performed in acidic conditions (50 mM Glycine-HCl, pH 2) were conducted in microplates. Aggregation was monitored by turbidity or

fluorescence. Seeds were obtained either using a 0.5mg/mL HI solution in TRIS-HCl, pH 1.6, 125 mM NaCl, incubated at 60°C without agitation or using a 0.5mg/mL HI solution in TBS, incubated in contact with hydrophobic surfaces. Both types of seeds were added at a 5% (w/w) ratio to a fresh 0.5 mg/mL HI solution (TRIS-HCl, pH 1.6, 125 mM NaCl), in a new microplate and incubated at 60°C without agitation. Aggregation kinetics studied at different pH were performed in various buffer solutions, at a constant 100 mM ionic strength.

FTIR experiments— The FTIR instrument used is a Bruker Vertex 70 and the software is OPUS. The liquid cell was a CaF₂ cell from Perkin Elmer Instruments. HI solutions were prepared in D₂O (from Sigma-Aldrich) at 86μM in PBS (0.01 M phosphate buffer, 0.0027 M KCl and 0.137 M NaCl). The pD was adjusted to 6.89, 2.09 or 5 using a pH-meter, which corresponds to pH 7.3, 2.5 or 5.41 respectively, in H₂O. Aggregated HI solutions were prepared in 96 well plates as described above. Using the OPUS software, compensation was applied to filter H₂O and CO₂ contributions to the spectra. Smoothing was done using the Savitzky-Golay equation. Baselines were flattened using a linear correction. Spectral decomposition of the amide I band (1600-1700 cm⁻¹) was done using the second derivative of the spectra to find peak positions. Then, using the Levenberg-Marquardt algorithm, 2 to 3 peaks were fitted to the experimental data (residual relative error less than 0.8%).

RESULTS

Insulin aggregates in the presence of insulin adsorbed on hydrophobic surfaces

Identical HI solutions were incubated in hydrophilic borosilicate glass tubes containing small glass beads (6 cm² surface area), that were either plain and hydrophilic or modified by SurfaSil[®], which renders them hydrophobic. After different times at 37°C under agitation, the amount of HI adsorbed on the bead surface and the amounts of HI present in the fluid phase in soluble or aggregated form were quantitatively analyzed as explained in Materials and Methods (Fig 1A). In the presence of hydrophobic beads, the amount of soluble HI in the fluid phase remained constant for about 2 hrs (lag phase) after which it started to decrease sharply (growth phase) until only trace amounts of soluble HI were left (plateau phase). The amount of aggregated HI in the fluid phase increased symmetrically, starting at about 2 hrs and reaching a maximum after 4 hrs. In contrast, in the presence of hydrophilic beads, HI did not aggregate even after several days. Concerning HI adsorption on hydrophobic glass beads (Fig.1A), we observed a slow but significant increase of adsorbed HI during the lag phase. After 3.5 hrs, a maximum amount of about 40 μg of HI was adsorbed, followed by a decrease of adsorbed HI to about 20 μg during the plateau phase. In contrast, the amount of adsorbed protein on hydrophilic glass beads remained at the detection limit (less than 1μg) during all the incubation.

Seeding experiments were performed to study whether aggregation took place in the bulk solution or at the material surface. A HI solution was pre-incubated at 37°C and pH 7.4 for 2 hrs in the presence of hydrophobic beads then the fluid phase was separated from the beads, which were washed three times with buffer to remove the interstitial liquid. When this pre-incubated HI solution was put in contact with fresh borosilicate beads (Fig 1B), no aggregation was observed, showing that the fluid phase carried no 'aggregation center'. In contrast, pre-incubated beads induced the aggregation of a fresh HI solution after a reduced 1-hr lag phase. Large amounts of HI adsorbed rapidly (up to 60 μg) when the pre-incubated beads were put in the fresh HI solution, then it decreased to about 20 μg (Fig 1B). After a longer pre-incubation time (12 hrs), HI aggregation started immediately on hydrophobic surfaces (data not shown). HI aggregation therefore takes place on hydrophobic surfaces, where HI is already adsorbed. To confirm this point, 5 % (w/w) of insulin aggregates recovered from a fully aggregated solution were added to a fresh HI solution and incubated at 37°C in the presence of hydrophilic beads under agitation. No aggregation occurred under these conditions, showing that HI aggregation takes place on hydrophobic surfaces, and not in solution, at pH7 and 37°C.

In order to increase the statistics of the data and to screen more rapidly different experimental conditions, a 96-well plate assay was developed for HI aggregation assays. The amount of soluble, aggregated and adsorbed HI was quantified in eight microwells in parallel. HI aggregation could also be monitored by turbidity changes^{13, 14} or using thioflavin T (ThT), a dye specific for the formation of extensive intermolecular β -sheets¹⁵. The protein concentration and the temperature were identical to the bead assay, but the agitation conditions were quite different, in order to obtain comparable aggregation kinetics. The effect of agitation will be studied below. As for the glass bead assay, HI typically started to aggregate after 2h and was fully aggregated after 8 hrs in hydrophobic microplates, whereas it was stable for days in hydrophilic microplates (Fig. 2A). The kinetics of HI adsorption onto hydrophobic plastic microwell plates were also quantitatively very similar to those obtained on hydrophobic borosilicate beads. No protein adsorption could be detected on hydrophilic multiwell plates. Seeding experiments also confirmed the results obtained with glass beads. A hydrophobic surface pre-incubated with HI triggered aggregation of a fresh HI solution more rapidly than a hydrophobic surface, which had never been exposed to HI. Increasing the pre-incubation period resulted in a parallel decrease of the aggregation lag time (Fig 2B). Interestingly, when the pre-incubated hydrophobic surface was washed, the lag time was less decreased, showing that the washing partially removed 'aggregation centers' from the plastic surface.

Dynamic Light Scattering (DLS) and Micro-Flow Imaging (MFITM) experiments were conducted to estimate the size of the aggregates formed along the aggregation process and present in the fluid phase (Fig. 3). DLS analysis of the filtrated solution (100 nm cut-off) showed that, during both the lag and growth phase, a single peak was present, at about 2.7 nm (30-35 kDa), corresponding to the expected signature of a mixture of HI monomers, dimers and hexamers (Fig. 3A). Interestingly, during the growth phase, DLS analysis revealed the very same single peak, which demonstrated that no aggregate of intermediate size comprised between 2.7 and 100 nm was present in solution during the whole aggregation process. DLS analysis of non-filtrated samples was impracticable after the lag time, showing the presence of aggregates larger than 100 nm in the fluid phase. Using MFITM, no particle could be detected during the lag phase, but increasing amounts of particles comprised between 1 and 10 μm (2-3 μm on average) were observed during the growth phase, that closely paralleled the amount of aggregated HI (Fig. 3C). The size distribution of these particles slightly increased during the aggregation process (Fig. 3B). At the onset of aggregation ($t = 135$ min), more than 50% of the particles had a size comprised between 1 and 1.25 μm , and almost no particle was larger than 2.5 μm . At $t = 180$ min, 45% of the particles had that size, while the remaining 55% had a size comprised between 1.25 and 2.5 μm . At later times ($t = 225$ or 255 min), 70% of the particles had a size lower than 3 μm , and the remaining ones had a size comprised between 3 and 10 μm . Altogether, these results show that HI aggregates contained in the fluid phase range between 0.1 and 10 μm .

FTIR spectra were recorded of the initial HI solutions and of HI aggregates in the supernatant at the end of the aggregation process at pH2 and pH7 (Fig. 4A-D). The spectra obtained from soluble HI at pH2 and 7 are very similar, with a dominant α -helical component (1650-1656 cm^{-1}) (80 % of the total absorbance) and minor β -sheet (1626-1636 cm^{-1}) and β -sheet/ β -turn (1672-1677 cm^{-1}) contributions. When aggregated in the presence of hydrophobic surfaces, HI contains less α -helical structure and this is especially prominent at pH2. Indeed, the α -helical component contributes 10% to the overall absorbance in aggregated HI at pH2 whereas at pH7 it contributes about 50%. On the other hand, the β -sheet contribution becomes dominant in aggregated HI, indicating that α -helical structures of soluble HI are converted into extensive β -sheet structures after aggregation (compare Fig.4 A and C, B and D). This α -helical to β -sheet conversion has also been observed by Bouchard and colleagues when heating bovine insulin to 70°C at pH 2.3¹⁶. These data support the idea that hydrophobic surfaces trigger an α -helix to β -sheet transition in HI upon adsorption and this holds true at neutral and acidic pH.

AFM observations of the surface of washed and dried hydrophobic beads after incubation with HI for different times revealed that the surface roughness of the material dramatically increased during the incubation, up to 100 nm (Fig. 5). The presence of many 20 nm large filamentous structures with a dendritic morphology was noticeable, especially at the end of the lag time (1.5 hrs). During the

aggregation phase, aggregates had a more spherical morphology. At the end of the aggregation process, the surface still contained large aggregates (about 50 nm diameter), separated by large flat surfaces, that could correspond to precursors of HI aggregates remaining on the surface. These structures were absent on the surface of hydrophilic beads incubated with HI solutions (data not shown). Hydrophobic surfaces are therefore covered with prefibrillar protein aggregates, which are later released in solution.

Altogether, these AFM observations, the decreased lag time exhibited by HI-covered hydrophobic beads, the decrease in the amount of adsorbed insulin observed after the growth phase and the fact that only aggregates larger than 100 nm are present in the fluid phase suggest that the aggregates form on the surface up to a quasi-micron size, and are later released in the fluid phase. Since, at the end of the aggregation kinetics, no more soluble insulin is present in the fluid phase, new aggregates cannot form on the surface, whereas the shear stress induced by shaking can possibly detach already formed micron-sized aggregates. To confirm this sequence of events, we studied the effect of agitation speed on aggregation kinetics. Below 600 rpm, no aggregation occurred because the fluid phase is not mixed and accompanies the movement of the well as a solid (grey zones in Fig. 6). This was supported by the following experiment. A water layer was carefully deposited on top of a slightly denser sucrose solution containing bromophenol blue. After 10 min rotation at different speeds below 600 rpm, no mixing was observed whereas the solution became homogenous above 600 rpm. Interestingly, once aggregation had started, the agitation speed could be reduced down to 100 rpm (Fig. 6 A). It is likely that the surface roughness due to HI massive adsorption on the plastic surface (Fig. 1, 2 and 5) help mixing the solution. It should be noted that in the absence of agitation, HI solutions remain stable for months, even in the presence of hydrophobic surfaces. Diffusion of HI molecules alone is therefore too slow to allow efficient building up of HI aggregates at the material surfaces. Mass transfer to surfaces is determined by the dimensionless Damköhler number $Da = k_{on}C_{s0}h/D$, where k_{on} is the association rate constant ($\text{mole}^{-1}.\text{m}^3.\text{s}^{-1}$), C_{s0} the surface density of binding sites ($\text{mole}.\text{m}^{-2}$), h the microwell size (m) and D the HI diffusion constant ($\text{m}^2.\text{s}^{-1}$)¹⁷. This number represents the ratio of the reaction rate with the surface ($k_{on}C_{s0}h$) to the inverse of the characteristic diffusion time to the surface (D/h^2). Assuming $k_{on} = 10^9 \text{ M}^{-1}.\text{s}^{-1}$ and C_{s0} corresponding to 1 HI molecule per 4 nm^2 results in $Da = 10^{15}$ proving that HI transport to the surface is strongly diffusion-limited. Mixing therefore ensures a constant HI concentration near the material surface, which is favourable for HI aggregation. Between 600 and 700 rpm, the insulin aggregation lag time decreased sharply, indicating that the nucleation layer is efficiently formed beyond 700 rpm. Above 900 rpm, the lag time increased again in parallel to the hydrodynamical shear stress, possibly because 'aggregation centers' detach from the well surface (Fig. 6A).

To study aggregation growth rate at a low rotation speed, hydrophobic microwell plates were filled with HI and agitated at 1200 rpm during the lag time until the aggregation just started, then they were further agitated at different rotation speed, and the aggregation kinetics was recorded using ThT to stain amyloid aggregates in the fluid phase (Fig. 6B open squares). At rotation speeds higher than 600 rpm, the HI solution was continuously agitated at the indicated speed (Fig. 6B, filled squares). There is a continuous increase of the growth rate with the rotation speed, in proportion to the average hydrodynamic shear stress experienced at the well-fluid interface, which shows that agitation induces the release of aggregates in solution (solid line, Fig. 6B).

Agitation has therefore three effects : (i) it allows mixing, preventing the formation of a diffusion layer, (ii) it detaches large aggregates from the surface and (iii) it slows down aggregation because it detaches seeds from the material surface. It is also possible, although we have not yet evidence for it, that shear stress at the interface helps protein conformational change.

Effect of pH, temperature and material surfaces on insulin aggregation

It is well known that HI solutions spontaneously form amyloid fibers at pH 2 and 60°C, without agitation^{7, 18, 19}. Under these conditions, HI aggregation also proceeds after a 2-hr lag phase, which can be reduced by seeding with 5% aggregates²⁰. The aggregates formed under these conditions bear some similarity with those obtained at pH 7.4 and 37°C with agitation: both indeed contain extensive intermolecular β -sheets revealed by IR spectroscopy and ThT fluorescence. The ThT fluorescence intensity per μg of aggregates is the same, whatever the pH during aggregation. Furthermore, the aggregates formed at pH 7.4 and 37°C with agitation in the presence of hydrophobic surfaces are able to seed the formation of HI fibers at pH 2 and 60°C without agitation (Table 1). The morphology of the aggregates is nevertheless different since the aggregates observed on hydrophobic surfaces (Fig. 5) are much smaller than the long fibers observed at low pH²¹.

The absence of agitation required for HI aggregation at pH2 and 60°C could be indicative that in these conditions, the nature of material surfaces played no role. We therefore investigated HI aggregation at different pH and temperature in hydrophobic and hydrophilic multi-well plates using ThT fluorescence.

First we studied the effects of surfaces and temperature on HI aggregation at pH 2 and 7. At 37°C, HI aggregation at pH 2 was strictly dependant on the presence of hydrophobic surfaces, as it is at pH 7 (Fig. 7A). At pH 7, when the temperature was raised, the HI aggregation rate increased on both hydrophobic and hydrophilic surfaces (Fig. 7B). The activation energy for the nucleation rate was three times higher in the presence of hydrophilic surfaces than in the presence of hydrophobic ones ($33 \pm 4 \text{ kcal.mol}^{-1}$ vs $10 \pm 2 \text{ kcal.mol}^{-1}$). This explains why HI remains stable for long times in the presence of hydrophilic surfaces at pH7. In contrast, the activation energy for the amyloid fiber growth rate was the same for hydrophobic and hydrophilic surfaces ($21 \pm 4 \text{ kcal.mol}^{-1}$). Similar conformational changes are thus likely to be associated with aggregate growth in solution or on the surface.

Second, we investigated the effect of pH on HI aggregation (Fig. 7C). In this experiment, an HI solution was agitated at various pHs at 37°C in the presence of hydrophilic surfaces and aggregate formation was recorded by both turbidity and ThT fluorescence. At low or high pH, no aggregation occurred after 16 hrs, as previously reported. At a pH close to the pI of HI, aggregation occurred within minutes, but the aggregates did not appreciably bind ThT (Fig. 7C). These aggregates are therefore essentially non-amyloidal, which is confirmed by their FTIR spectrum showing mainly α -helical structure (Fig. 4E, compare to Fig. 4C and D). In conclusion, HI aggregates can be amyloidal or not, and amyloidal HI aggregates form following two mechanisms: independently of the material surface at high temperature, and on hydrophobic surfaces at lower temperatures.

DISCUSSION

We first showed that hydrophobic surfaces stimulate the formation of large amounts of HI amyloid fibers. The characteristic structure of these aggregates was revealed by infrared spectroscopy and by Thioflavin T fluorescence. In contrast, aggregates obtained at a pH close to the pI of insulin keep an IR amide band similar to that of soluble insulin, and do not bind ThT. An irreversible conformational change is therefore required for the formation of insulin amyloid fibers. The seeding experiments of Fig. 1 and 2 clearly show that aggregation takes place on the surface, and not in the bulk solution. Large amounts of insulin indeed accumulate on hydrophobic surfaces before the onset of aggregation (Fig. 1A, Fig. 5). Amyloid fibers therefore form on pre-adsorbed insulin. This requires agitation, to prevent the formation of a diffusive layer that would strongly delay nucleation (Fig. 6A). Order of magnitude calculations explain why no aggregation is observed in multiwell plates below 600 rpm. Mixing requires that the kinetic energy of the fluid is sufficient to modify the shape of the free fluid surface, creating a rotating wave²². The kinetic energy is $E_c = \frac{1}{2} m_{\text{fluid}} v^2$, where m_{fluid} is the fluid mass (200 μg) and v the maximum linear speed ($v = 2\pi r\omega$, with r the well radius and ω the rotation rate). The surface energy of the free fluid surface is $E_s = \pi r^2 \gamma$, where γ is the fluid surface tension. The E_c/E_s ratio is equal to $2\pi m\omega^2/\gamma = 1.5$ for $\omega = 600 \text{ rpm}$ and $\gamma = 70 \text{ N.m}^{-2}$. At this rotation speed, the kinetic energy is high enough to deform the fluid.

Fig. 2B furthermore indicates that the aggregation promoting structures are fragile and can be partially washed away. The prefibrillar aggregates that form on the surface are thus likely to be released thanks to the mechanical forces provided by the agitation. Increasing the shaking rotation rate indeed accelerates the release of amyloid fibers in solution, in proportion to the average hydrodynamic shear stress (Fig. 6). This explains why small aggregates (< 100 nm) are not observed in suspension (Fig. 3). Micron-sized aggregates are thus released from the surfaces. The force exerted by the viscous shear stress on an object attached to a surface indeed increases as the square of its size ($F = \sigma \cdot S$, where σ is the wall hydrodynamical shear stress, S the projected surface area of the object). At the estimated shear stress experienced in multi-well plate experiments (1 Pa), the force exerted on a 100 nm particle attached to the side of the well is only 10^{-14} N, whereas it is 10^{-12} N for a 1 μm one. Assuming that the particles are associated to the surface by non-covalent interactions, ranging to a few Å and amounting to a few $k_B T$, only mechanical forces larger than 10^{-12} N can detach them. This is the order of magnitude to detach bacteria from surfaces^{23,24}. Concerning the lag time, agitation has two opposite effects: a promoting one, because it allows mixing and detachment of fully formed aggregates and an inhibiting one, because it breaks the fragile growing structures at the material surfaces.

Converting soluble insulin into amyloid fibers, involves the conversion of an overall α -helical conformation into extended β -sheets (Fig.4), which requires activation energy (Fig. 7). The activation energy for amyloid fiber growth is the same, whether aggregation takes place on the surface or in the bulk. It is comparable to the one obtained previously for bovine insulin²⁵. Interestingly, the activation energy for the nucleation step in the presence of hydrophobic surfaces is smaller than that for the growth of the fibers. This indicates that the surface acts as a catalyst. At a pH close to the pI, a fast aggregation mechanism takes place that does not lead to amyloid fibers. At extreme pHs (2 and 7), insulin does not readily form amyloid fibers in solution, unless the temperature is risen enough to denature the protein or a hydrophobic surface is provided. In solution, insulin molecules are indeed separated by electrostatic interactions. On the surface, this repulsion is compensated by the formation of hydrophobic interactions with the surface. This increases the local insulin concentration, which favours conformational changes. This explains why the surface is a catalyst of nucleation, both at pH 2 and 7. Since large amounts of insulin form on the surface, the initial conformational changes are reproduced in subsequent protein layers. Experimental evidences by several groups^{7, 26, 27} have pinpointed the LVEALYL peptide as a structural element able to connect insulin monomers within a fiber. We recently showed that this peptide indeed accelerates only hydrophobic surface-induced aggregation, both at pH 2 and pH 7, but it has no effect in the presence of hydrophilic surfaces²⁸. Hydrophobic surfaces are therefore necessary for the peptide to exert its catalytic role.

In support of our observations, it is noteworthy that hydrophobic surfaces influence the conformation of the beta amyloid peptide and the cellular prion protein^{29, 30}. Similarly to our findings, Giacomelli and Norde³¹ showed that the interaction between the A β (1-40) peptide and hydrophobic Teflon surfaces proceeds in two steps. At a low surface coverage, the A β peptide keeps the α -helical structure, but as the surface density increases, a cooperative conformational transition takes place, that results in β -sheet formation. Moreover, A β (10-35) monolayers adsorbed on such surfaces induce the aggregation of A β in solution³². This points out the importance of material surfaces in protein aggregation.

REFERENCES

1. B. Sharma, *Biotechnol Adv*, 2007, **25**, 318-324.
2. M. J. Treuheit, A. A. Kosky and D. N. Brems, *Pharmaceutical Research*, 2002, **19**, 511-516.
3. K. N. Ekdahl, J. D. Lambris, H. Elwing, D. Ricklin, P. H. Nilsson, Y. Teramura, I. A. Nicholls and B. Nilsson, *Adv Drug Deliv Rev*, **63**, 1042-1050.
4. E. A. Vogler, J. C. Graper, G. R. Harper, H. W. Sugg, L. M. Lander and W. J. Brittain, *Journal of Biomedical Materials Research*, 1995, **29**, 1005-1016.
5. V. Sluzky, J. A. Tamada, A. M. Klibanov and R. Langer, *Proc Natl Acad Sci U S A*, 1991, **88**, 9377-9381.
6. V. Sluzky, A. M. Klibanov and R. Langer, *Biotechnol Bioeng*, 1992, **40**, 895-903.
7. J. Brange, L. Andersen, E. D. Laursen, G. Meyn and E. Rasmussen, *J Pharm Sci*, 1997, **86**, 517-525.
8. B. J. Olson and J. Markwell, *Curr Protoc Protein Sci*, 2007, **Chapter 3**, Unit 3 4.
9. D. A. Smith and S. E. Radford, *Curr Biol*, 2000, **10**, R662-664.
10. K. J. Wiechelman, R. D. Braun and J. D. Fitzpatrick, *Analytical Biochemistry*, 1988, **175**, 231-237.
11. C. M. Stoscheck, *Methods Enzymol*, 1990, **182**, 50-68.
12. H. LeVine, 3rd, *Methods Enzymol*, 1999, **309**, 274-284.
13. W. D. Loughheed, A. M. Albisser, H. M. Martindale, J. C. Chow and J. R. Clement, *Diabetes*, 1983, **32**, 424-432.
14. Y. M. Kwon, M. Baudys, K. Knutson and S. W. Kim, *Pharm Res*, 2001, **18**, 1754-1759.
15. R. Khurana, C. Coleman, C. Ionescu-Zanetti, S. A. Carter, V. Krishna, R. K. Grover, R. Roy and S. Singh, *J Struct Biol*, 2005, **151**, 229-238.
16. M. Bouchard, J. Zurdo, E. J. Nettleton, C. M. Dobson and C. V. Robinson, *Protein Science*, 2000, **9**, 1960-1967.
17. T. Gervais and K. F. Jensen, *Chemical Engineering Science*, 2006, **61**, 1102-1121.
18. D. F. Waugh, *Journal of the American Chemical Society*, 1946, **68**, 247-250.
19. D. F. Waugh, R. E. Thompson and R. J. Weimer, *Journal of Biological Chemistry*, 1950, **185**, 85-95.
20. L. Nielsen, R. Khurana, A. Coats, S. Frokjaer, J. Brange, S. Vyas, V. N. Uversky and A. L. Fink, *Biochemistry*, 2001, **40**, 6036-6046.
21. R. Jansen, W. Dzwolak and R. Winter, *Biophys J*, 2005, **88**, 1344-1353.
22. G. Bai, J. S. Bee, J. G. Biddlecombe, Q. Chen and W. T. Leach, *Int J Pharm*, 2012, **423**, 264-280.
23. M. Demilly, Y. Brechet, F. Bruckert and L. Boulange, *Colloids Surf B Biointerfaces*, 2006, **51**, 71-79.
24. M. Mercier-Bonin, A. Dehouche, J. Morchain and P. Schmitz, *Int J Food Microbiol*, 2011, **146**, 182-191.
25. M. M. Varughese, 2011.
26. J. Brange, G. G. Dodson, D. J. Edwards, P. H. Holden and J. L. Whittingham, *Proteins*, 1997, **27**, 507-516.
27. M. I. Ivanova, S. A. Sievers, M. R. Sawaya, J. S. Wall and D. Eisenberg, *Proc Natl Acad Sci U S A*, 2009, **106**, 18990-18995.
28. T. Ballet, F. Bruckert, P. Mangiagalli, C. Bureau, L. Boulangé, L. Nault, T. Perret and M. Weidenhaupt, *Biochemistry*, 2012, **51**, 2172-2180.
29. C. Schladitz, E. P. Vieira, H. Hermel and H. Mohwald, *Biophys J*, 1999, **77**, 3305-3310.
30. T. Kowalewski and D. M. Holtzman, *Proc Natl Acad Sci U S A*, 1999, **96**, 3688-3693.
31. C. E. Giacomelli and W. Norde, *Biomacromolecules*, 2003, **4**, 1719-1726.
32. M. J. McMasters, R. P. Hammer and R. L. McCarley, *Langmuir*, 2005, **21**, 4464-4470.
33. R. E. Berson, M. R. Purcell, M. K. Sharp, K. A. Kang, D. K. Harrison and D. F. Bruley, Springer US, 2008, vol. 614, pp. 189-198.

ACKNOWLEDGEMENTS

We thank Benoît Duroux, Frédérique Crozet, Sébastien Janvier for excellent technical assistance in particle size analysis. We are grateful for the scientific input of Yves Bréchet (Grenoble-INP). We thank the CIME facility and BBSI laboratory (CEA Grenoble) for access to their equipment. This project was financed by a CNRS “Prise de risques” grant (CHAPROMAT). TB is a recipient of a CIFRE fellowship (371/2007). LN is a recipient of a Rhone-Alpes Region PhD fellowship (Macodev program).

TABLES

Table 1: **Cross-seeding experiments.**

Insulin seeds were prepared at pH 1.6, 60°C or at pH 7.4, 37°C on hydrophobic surfaces, as described in Materials and Methods. Aggregates were recovered by centrifugation and mixed with a fresh HI solution (5% w/w). A sample without seed was also prepared. The samples were then incubated at 60°C pH2 and the aggregation was monitored by OD_{600nm}. In addition, the mass of the aggregates in the solution was determined by the BCA assay after filtration (0.45 µm cutoff). The lag time and the maximum turbidity were determined using the OD_{600nm} measurements. The growth slope was determined using the BCA measurements of the aggregated protein.

Conditions	Lag time (hrs)	Growth slope (µg.hr⁻¹)	Maximum turbidity (OD_{600nm})
100 µg HI without seeds	7 ± 1	6.1 ± 0.3	0.08 ± 0.01
100 µg HI + 5 µg seeds obtained at pH 1.6 and 60°C	1.5 ± 0.5	34 ± 1	0.12 ± 0.01
100 µg HI + 5 µg seeds obtained at pH 7.4, 37°C, on hydrophobic surfaces	0	35 ± 1	0.13 ± 0.01

FIGURE LEGENDS

FIG 1. Precursors of insulin aggregates form on hydrophobic glass surfaces.

A: Kinetics of human insulin adsorption and aggregation on hydrophilic or hydrophobic beads. A HI solution was agitated at 37°C, pH 7, in a borosilicate tube, in the presence of plain (open symbols) or Surfasil[®]-treated (closed symbols) borosilicate beads. The amount of soluble (circles), aggregated (triangle) and adsorbed (squares) HI is plotted as a function of the incubation time.

B: Seeding experiments. A HI solution was pre-incubated for 2 hrs at 37°C, pH 7, in the presence of Surfasil[®]-treated borosilicate beads, then the fluid phase and the beads were separated. The fluid phase was transferred to a new borosilicate tube containing plain borosilicate beads (open symbols). The pre-incubated beads were washed and transferred to a new borosilicate tube containing a fresh HI solution (closed symbols). The amount of soluble (circles), aggregated (triangles) and adsorbed (squares) HI is plotted as a function of the incubation time after transfer.

FIG 2. Precursors of insulin aggregates form on hydrophobic plastic surfaces.

A: Kinetics of human insulin aggregation in hydrophilic or hydrophobic multi-well plates. A HI solution was agitated at 37°C, pH 7, in a hydrophilic (open symbols) or hydrophobic (closed symbols) polystyrene multi-well microplate. The optical density at 600 nm is represented as a function of the incubation time.

B: Aggregation centers can be partially removed from hydrophobic surfaces by washing. a HI solution was pre-incubated at 37°C, pH 7, for the indicated times in a hydrophobic multi-well microplate, then the solution was removed and the plate was filled with a fresh HI solution, either without (open squares) or after washings (closed squares). The incubation was continued at 37°C, pH 7, for 16 h. The lag time of HI aggregation was determined and is represented as a function of the pre-incubation time.

FIG 3. Particle quantification during insulin aggregation. A HI solution was agitated at 37°C, pH 7, in the presence of hydrophobic surfaces. At the indicated time, the number of large aggregates (> 1 μm) was determined by MFI (open diamonds). The size of HI oligomers and small aggregates was determined on filtrated (100 nm cut-off) and non-filtrated fluid phase samples with DLS (closed diamonds). The results shown are average \pm standard deviation.

A : Size of the HI oligomers and large aggregates present in the fluid phase. After the lag phase (2.5 h), the presence of HI aggregates larger than 0.1 μm could be deduced from the DLS signal of unfiltrated samples. However, their size could not be determined. The grey region represent aggregate sizes non accessible to DLS or MFI measurements.

B: Size distribution of insulin aggregates detected by MFI. The cumulated number of particles per μL is represented as a function of particle size in μm , for the HI solution harvested at the indicated times.

C: Number of large HI aggregates present in the fluid phase. The number of particle per μL counted by MFI (open diamonds) is plotted as a function of the incubation time, alongside with ThT fluorescence (crosses), normalized to its maximum value.

FIG 4. FTIR spectra of HI solutions and final aggregates. HI solutions were prepared at different pHs (2, 5.5 and 7). The solution at pH5.5 spontaneously aggregated in hydrophilic containers. HI solutions at pH 2 and 7 were aggregated in the presence of hydrophobic surfaces.

A and C represent FTIR spectra before and after aggregation at pH7. B and D represent FTIR spectra before and after aggregation at pH2. E represents the FTIR spectrum of the aggregated HI solution at pH5.5.

The FTIR spectra (bold lines) were decomposed into β -sheet (1626-1636 cm^{-1}), α helix (1650-1656 cm^{-1}) and β -sheet/ β -turn (1672-1677 cm^{-1}) contributions (thin lines).

F summarizes the relative contribution of each spectral component to the overall absorbance in the range 1600-1700 cm^{-1} .

FIG 5. Morphology and structure of HI aggregates on hydrophobic surfaces.

A: AFM images of dried HI aggregates. A HI solution was incubated for the indicated times at 37°C, pH 7, in the presence of Surfasil[®]-treated borosilicate beads, then the beads were separated from the fluid phase, washed, mildly dried and imaged by AFM. Images were taken before (1h30) and at the onset (3h) of the aggregation phase, and after full aggregation of the sample (18h). Scale bar = 0.5 μm. Arrowheads point to dendritic (1h30) and spherical (3h, 18h) HI aggregates.

FIG 6. Effect of agitation on HI aggregation kinetics.

A: Effect of agitation on HI aggregation lag time. A HI solution was agitated at 37°C, pH 7, in a hydrophobic polystyrene multi-well microplate, at the indicated rotation speed. HI aggregation was monitored using ThT fluorescence and the lag time was determined as explained in Materials and Methods. The grey region defines rotation speeds insufficient to ensure mixing of the initial HI solution. The solid line represent a fit of the data with the equation $k(\omega) = A \omega^{3/2}$, which indicates that the growth rate is proportional to the average wall shear stress in an orbital shaker³³. The dashed line represents the effect of shaking on the mixing efficiency and is hand-drawn.

B: Effect of agitation on HI aggregation growth rate. Filled squares : A HI solution was agitated at 37°C, pH 7, in a hydrophobic polystyrene multi-well microplate, at the indicated rotation speed. Open squares : A HI solution was agitated at 37°C, pH 7, in a hydrophobic polystyrene multi-well microplate, at 1200 rpm until the onset of aggregation, then the agitation was pursued at the indicated rotation speed. HI aggregation was monitored using ThT fluorescence and the growth rate is expressed as the percentage of insulin aggregated per hour. Error bars are smaller than the symbol size. Note that once aggregation has started, the fluid phase is well mixed in micro-wells even at rotation speeds as low as 100 rpm. The solid line is defined as in Fig. 6A.

FIG 7. Effect of pH, temperature and material surfaces on HI aggregation kinetics.

A: HI aggregation at pH 2 is also accelerated by hydrophobic surfaces. A HI solution was agitated at 37°C, pH 2, in a hydrophobic (closed symbols) or hydrophilic (open symbols) polystyrene multi-well microplate. HI aggregation was monitored by ThT fluorescence. Under these conditions, aggregation starts at 6 h and 26 h on hydrophobic and hydrophilic surfaces, respectively.

B: Determination of activation energies for the nucleation and growth rate of HI aggregates. A HI solution (pH 7) was agitated at different temperatures, in a hydrophobic or hydrophilic polystyrene multi-well microplate. HI aggregation was monitored by ThT fluorescence. The aggregation nucleation and growth rates were determined as explained in Materials and Methods and are plotted as a function of the inverse of the absolute temperature (K) to determine the activation energies. The solid line represents the best fit of the data with the equation $k(T) = k_0 \exp(-E_a/RT)$, where E_a is the activation energy. The growth rates obtained in the presence of hydrophilic or hydrophobic surfaces at different temperatures were fitted with the same equation.

C: HI aggregation on hydrophilic surfaces as a function of the pH. A HI solution was prepared at different pH, using glycine, MES or phosphate as buffers, and agitated at 37°C in a hydrophilic polystyrene multi-well microplate, for 16 hours. HI aggregation was monitored by turbidity (closed symbols) and amyloid fiber formation by ThT fluorescence (open symbols). ThT fluorescence is expressed as percentage of the fluorescence signal obtained after 12h incubation in hydrophobic multi-well microplates.

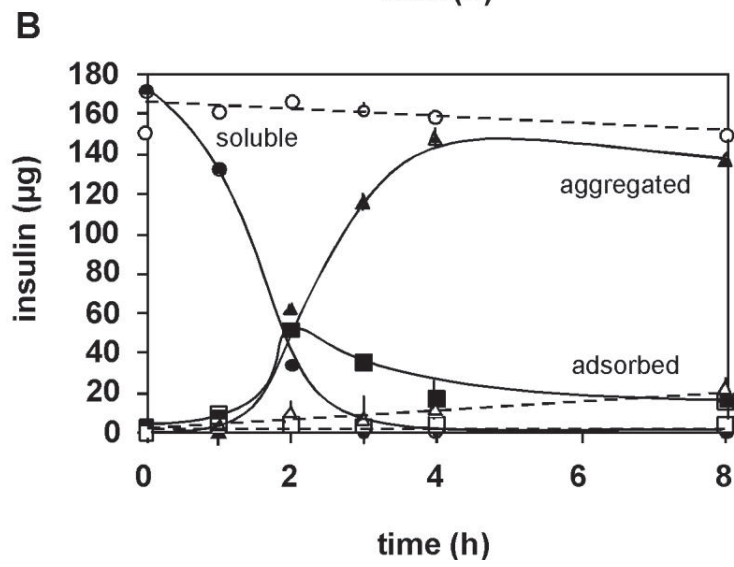
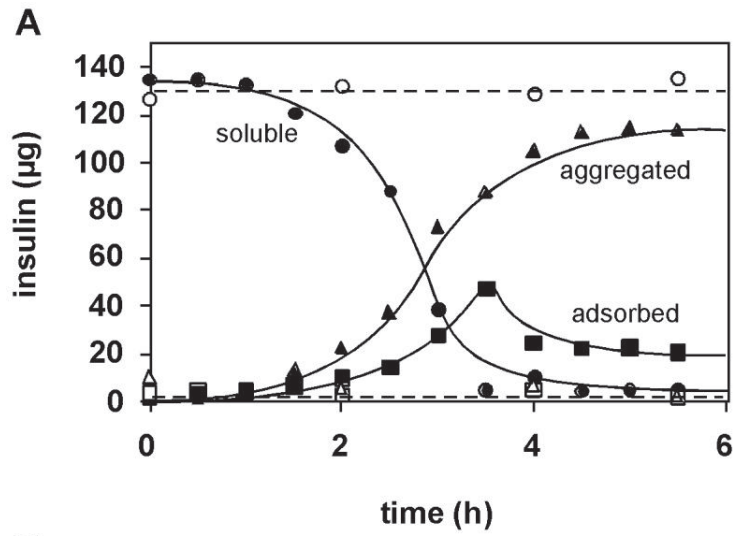


FIG. 1

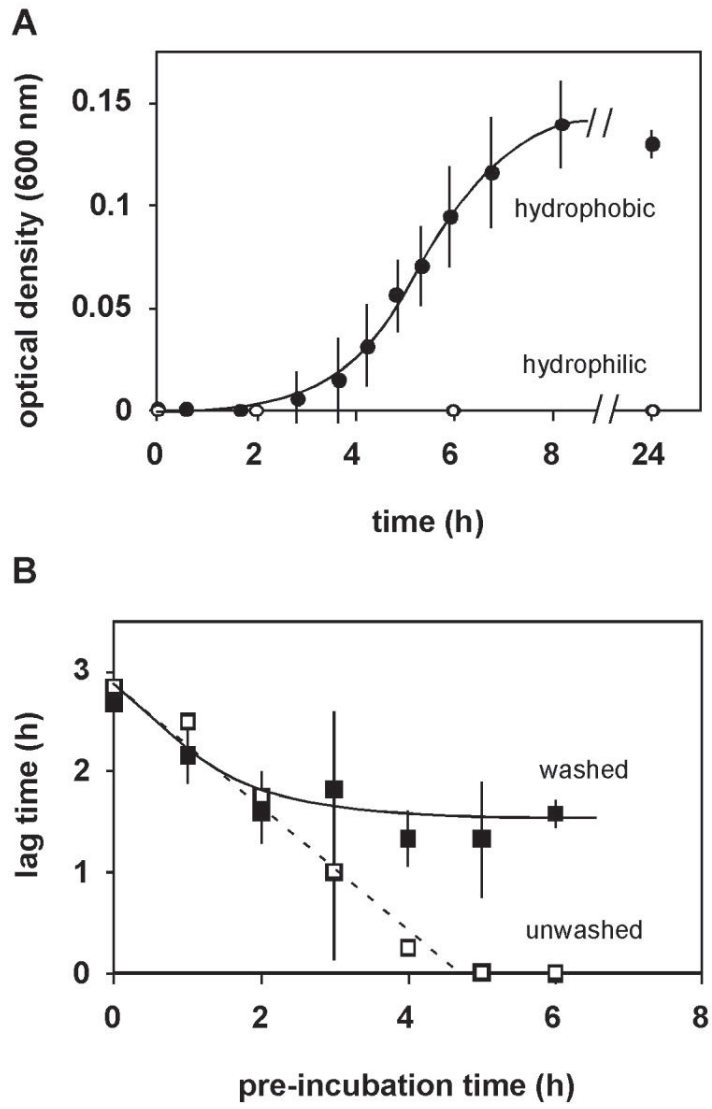


FIG. 2

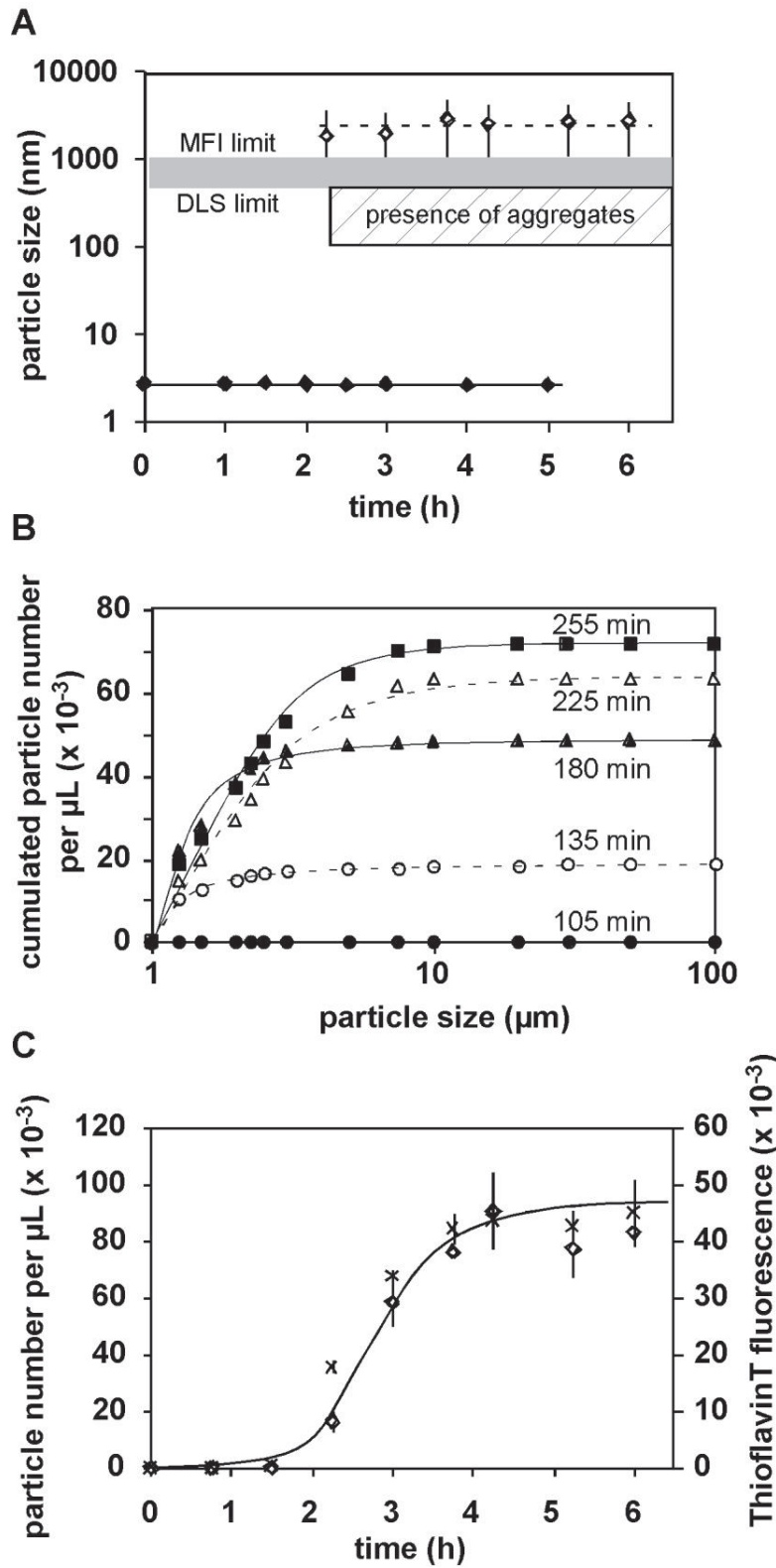


FIG. 3

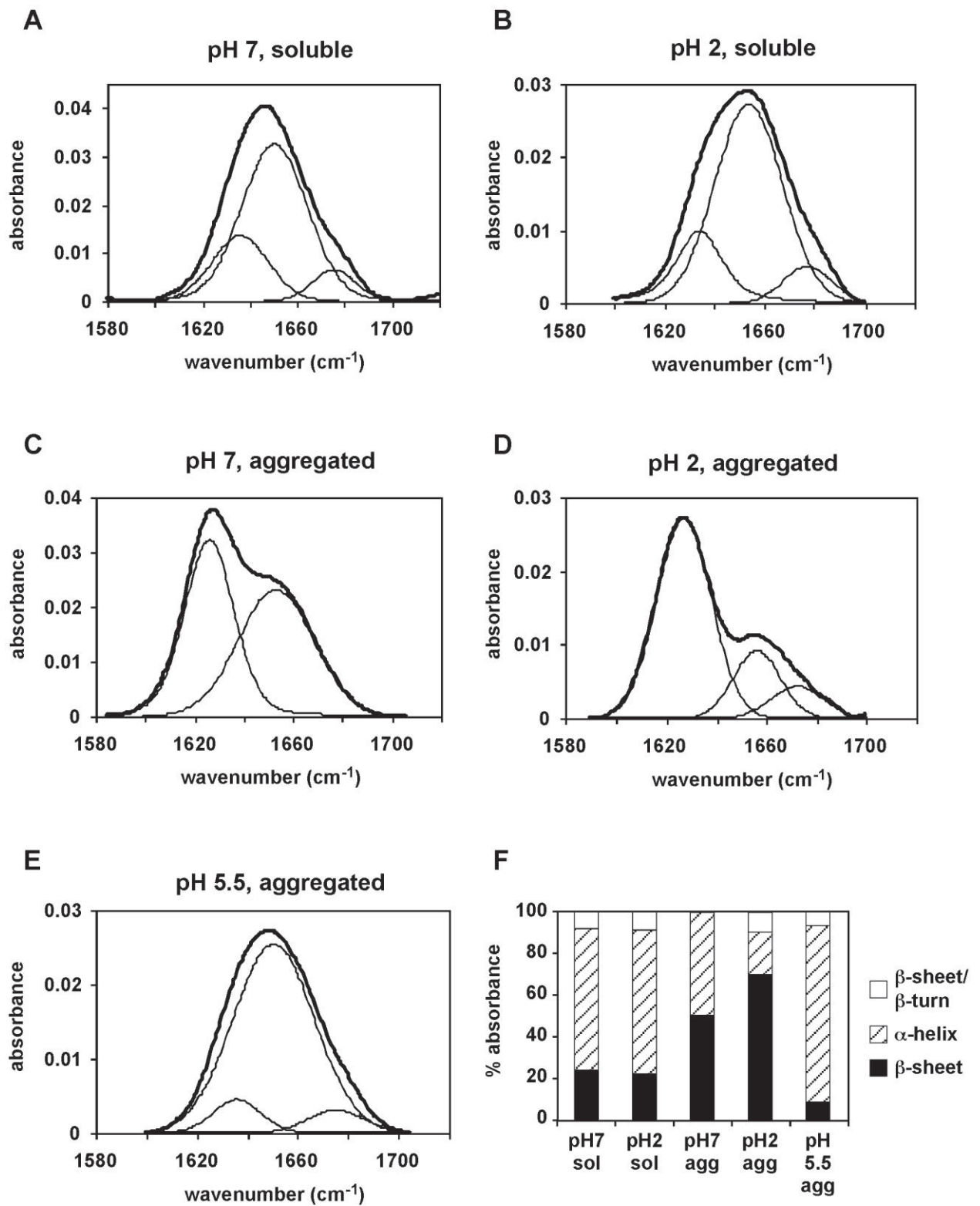


FIG. 4

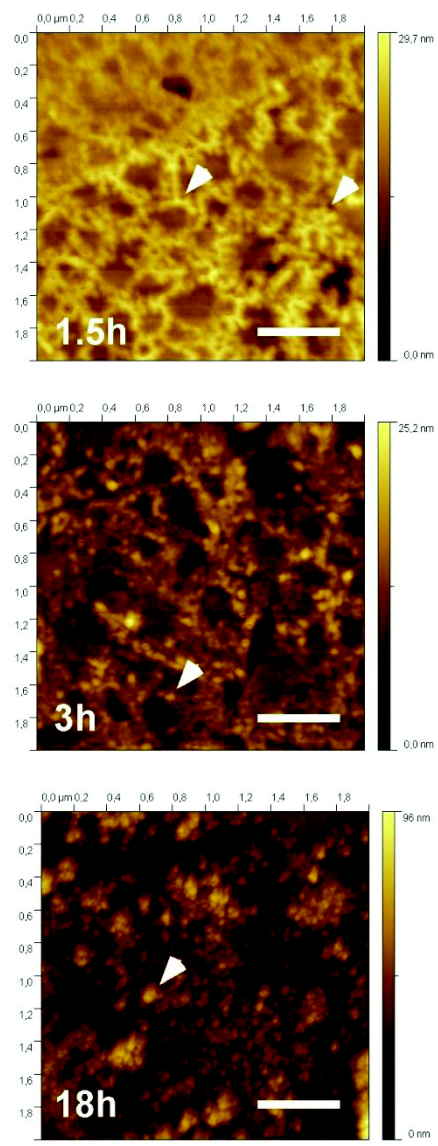


FIG. 5

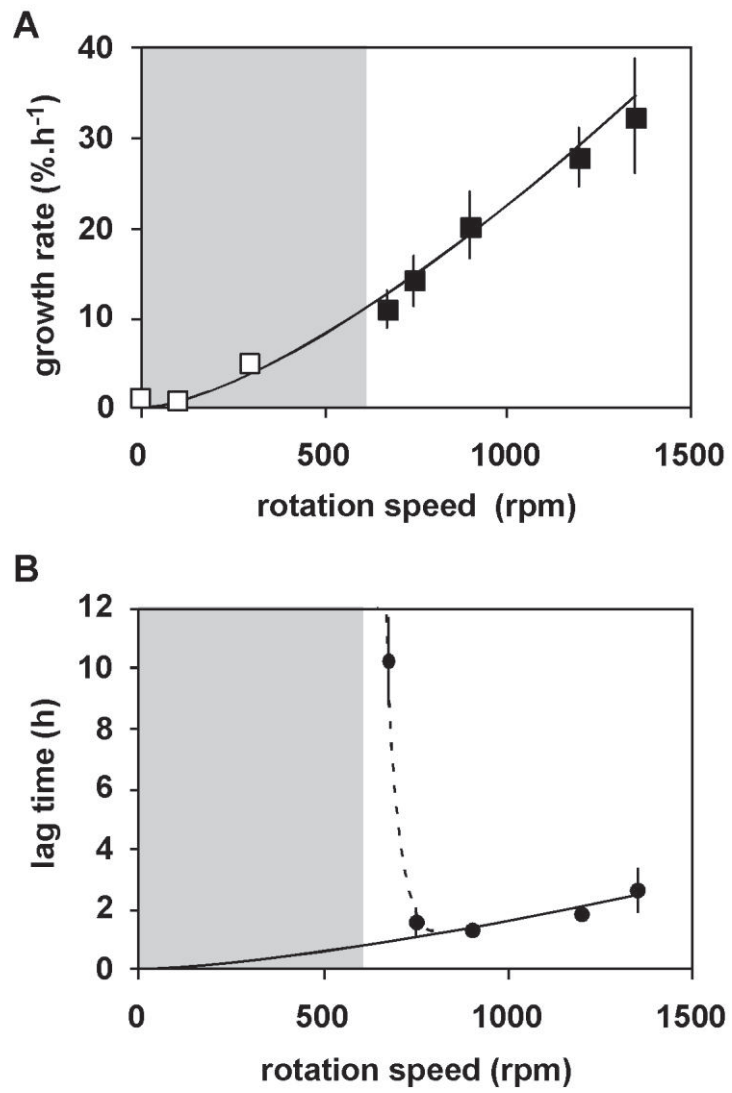


FIG. 6

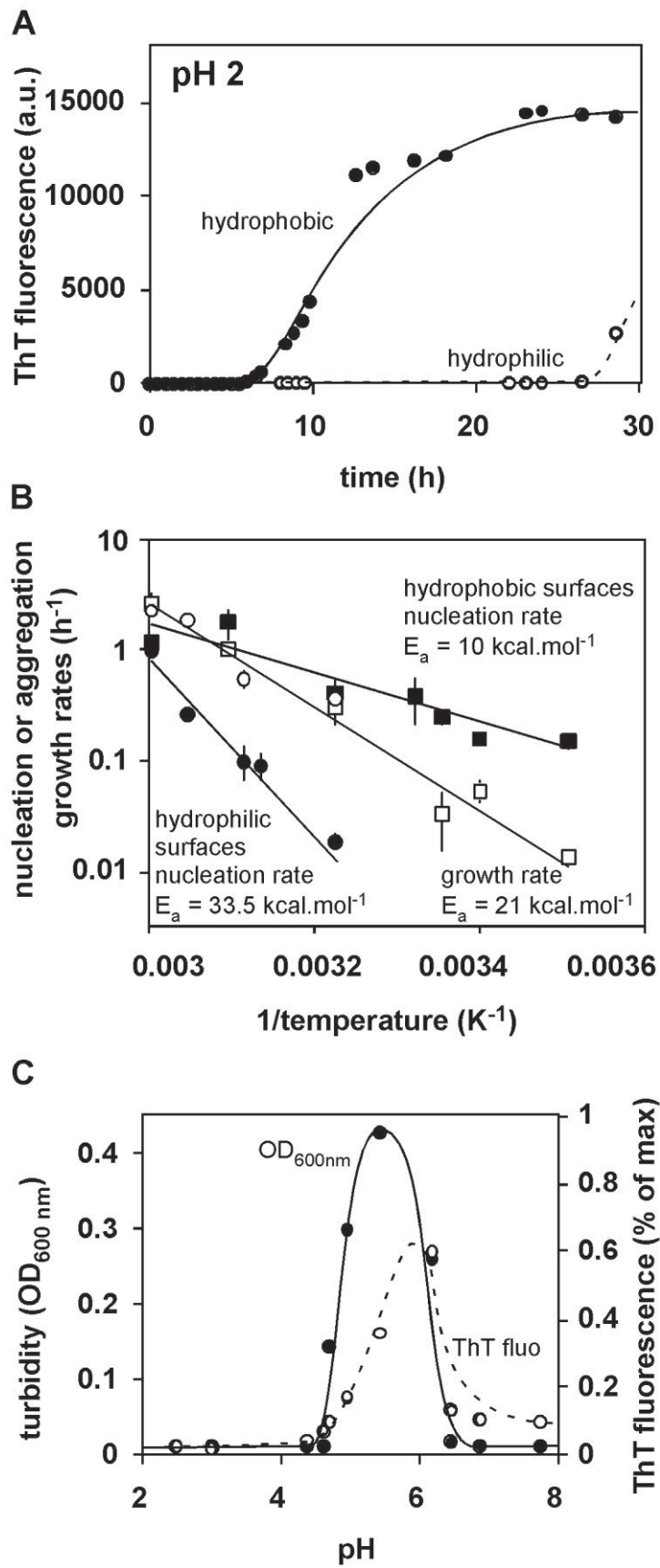


FIG. 7

Chapter 4: Human insulin adsorption kinetics, conformational changes and amyloidal aggregate formation on hydrophobic surfaces

4.1. Aim of the study

As seen in the introduction and in previous chapter, insulin nucleation on hydrophobic surfaces is an important parameter of insulin aggregation on surfaces. In order to analyze the nuclei formation at the surface, we needed both to obtain information of the mass of protein that adsorbs on the surfaces, and to have information of the structure of the adsorbed proteins. Precedent study⁸⁸ and first chapter shown that the protein amounts adsorbed during the lag phase are extremely low, of the order of the 100 nanogram in a 1.8 cm² microwell. Moreover, the time evolution of the adsorbed amount of protein and protein structure changes has to be studied. Little is known about the characteristic time of insulin adsorption on hydrophobic surfaces. Consequently, we needed to choose a technique able to detect protein adsorptions as low as a few hundreds of pictograms per cm² with real time resolution.

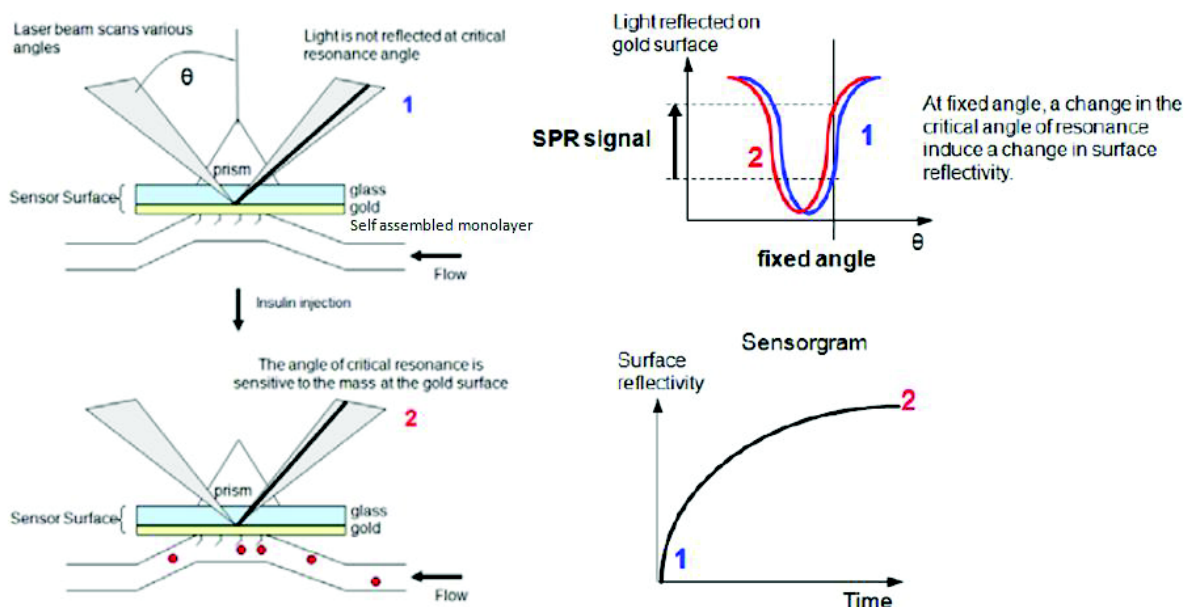
The bicinchoninic acid assay, which directly measures the protein mass, is not sensitive enough to obtain confident measurements of protein adsorption lower than the hundred of nanograms per cm². Another technique used in precedent studies is Thioflavin T (ThT) fluorescence measurements in fluorometer. ThT fluorescence is sensitive to protein conformation. Indeed, ThT binds to extended β -sheets, which induces a specific fluorescence of the dye. As amyloid fibers are very rich in intermolecular β -sheets but not native insulin, ThT can be used to detect amyloid fibers formation. But this technique is usually used for solution fluorescence and fluorometers do not have enough numeric aperture to perform sensitive measurements of the small signal produced at the surface. Furthermore, to study the protein on the surface, these two techniques require different washes, which increase the measurement time to about ten minutes, which is not sufficient to monitor real time protein adsorption and aggregation kinetic on the surfaces. Consequently, the techniques used in the precedent chapter and in Ballet's PhD thesis⁸⁸ are not appropriate to analyze the insulin adsorption kinetic and the amyloid aggregate formation on the surfaces.

Other techniques can be used to study protein adsorption and association on surfaces. The Quartz Cristal Microbalance in dispersive mode (QCM-D) uses the piezo-electric effect to monitor the mass adsorption on a surface. This technique has excellent time resolution with high sensitivity on the mass adsorbed. Nevertheless, it is also sensitive to the hydration of the structures adsorbed on the surface. It is likely that the protein conformation changes related to fibril formation is accompanied with a change in the hydration of the protein on the surface. Consequently, QCM-D should be sensitive both to protein adsorption kinetic and to protein

conformational changes in a single signal. We therefore didn't use this signal to start with, although it will be very useful later, to confirm the presence of conformational changes. Atomic Force Microscopy (AFM) after washing and drying has give information about aggregate structure on the surface with very high spatial resolution (nanometer scale, see AFM images in figure 5 in precedent chapter, page 77), but the lack of time resolution of that technique (~15 minutes) makes it unable to monitor the protein adsorption kinetic correctly. Here, we developed Surface Plasmon Resonance, Infrared Spectroscopy and fluorescence microscopy protocols in order to study insulin adsorption and structural changes on hydrophobic surfaces.

4.2. Insulin adsorption kinetic and conformational changes

Surface Plasmon Resonance imaging (SPRi) is a real time optical technique that is sensitive to optical index changes on the first 100 nanometers of a metal surface, usually a gold layer. At a certain angle, called critical angle of resonance, a metal layer does not reflect light as the electric and magnetic fields of the light are in resonance with an electron wave induced in the metal layer. This critical angle of resonance is decreased when the refractive index on the first nanometers of the surface is increased. As an accumulation of proteins on the surface will locally increase the refractive index, the reflectivity of the gold layer will be increased. This reflectivity change of the gold layer is monitored in real-time, revealing as small material accumulation as tens of picograms per millimeter square on the gold surface. Contrary to QCM-D, Surface Plasmon Resonance is not sensitive to the hydration of the structures at the surface. Consequently, it allows monitoring in real time of insulin mass adsorption kinetic during the few first minutes of insulin solution contact with hydrophobic surface up to one hour, which gives information on insulin nucleus formation on the surface. Here, a protocol was developed to obtain a gold layer treated both with PEG-thiol, a hydrophilic compound, and alkyl (C16)-thiol, a hydrophobic compound. So, we managed to analyze proteins adsorbed on systems with both hydrophilic and hydrophobic areas in a single SPRi experiment. Moreover, the use of both alkyls (C₁₆) treated (hydrophobic) and Poly Ethylene Glycol (PEG) (hydrophilic, often used as a protein-repellent surface¹⁰⁸⁻¹¹⁰) treated surfaces allowed to separate the contribution of the index changes due to the bulk solution from the index changes due to insulin accumulation on the surface (see Fig. 3 of following article).

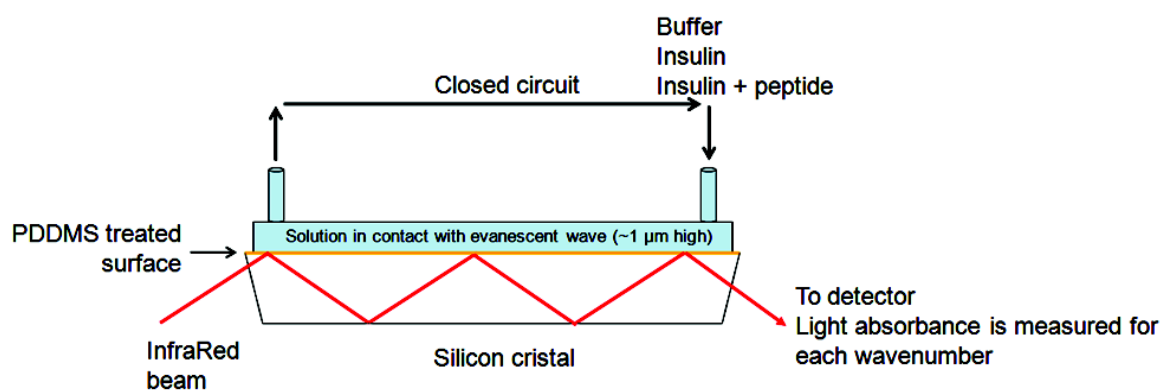


Scheme 4.1: Scheme of the experimental device used in SPR sensorgrams acquisition.

SPRi results shows that two pools of insulin exist on hydrophobic surfaces: a first pool of weakly adsorbed insulin molecules and a second pool of more strongly adsorbed insulin molecules. When the duration of the contact between the insulin solution and the hydrophobic surface is increased, the pool of strongly adsorbed insulin is increased compared to the pool of weakly adsorbed insulin. Moreover, both weakly and strongly adsorbed pools of insulin are more strongly adsorbed as the time of contact increases. These results also indicate that the apparition of the strongly adsorbed insulin pool, which is proposed to be the insulin population involved in nuclei formation and fibril growth, has a time scale evolution of several minutes. This indicates that insulin conformation changes have to be analyzed with techniques of time resolution of the few minutes.

Since protein structures change during aggregation the vibrations of atoms within the protein structure are also changing. These vibrations can be detected by infrared spectroscopy. The molecular infrared wavelength absorption is linked to the covalent bond vibrations in molecules. In proteins, the most important vibrations are the C=O and N–H amide bonds. As these bonds are involved in H–bonding, they are very sensitive to changes in secondary structure. The insulin structures formed on hydrophobic surfaces were monitored using a silicon prism by Total Attenuated Reflectance Fourier Transformed Infrared Spectroscopy (ATR-FTIR) (See Scheme 4.2.). The prism was treated with phenyldimethylmethoxysilane, to obtain a hydrophobic (water contact angle = 103.1 +/- 3.7 °) sensor surface. Infrared spectroscopy has a time resolution of about 2 minutes, which is sufficient to analyze the

insulin conformation changes during the growth of the strongly surface adsorbed insulin pool, according to the SPRi results. Since the penetration depth of ATR-FTIR is about $1\mu\text{m}$, the sensor integrates both the contribution of adsorbed protein and the soluble protein contained in the $1\mu\text{m}$ thick layer above the sensor. In our case, the baseline was done with the buffer solution, consequently, when proteins are added to the solution, the monitored absorbance is due to protein. The adsorption kinetics is obtained during 1 hour of solution flow on the surface, with regular absorbance measurements. Then, the surface is washed in buffer and strongly adsorbed insulin remains bound to the surface. Here, minimum protein remains in the solution, and the specific contribution of the adsorbed layer is obtained (see Experimental Procedures in the following article).



Scheme 4.2: Scheme of the experimental device used in ATR-FTIR experiments with silicon crystal treated with PDMMS.

Different signals can be obtained thanks to infrared spectroscopy. Absorbance frequencies depend on the nature of the bond (C–H, O–H, C–O, C=O...), on the vibration mode (stretch, twist, scissor...) and on the interactions with the environment. Consequently, infrared absorbance frequencies are specific for each chemical compound. Different signals are known for proteins in infrared spectroscopy. As the amide bond is the basic repeat unit of proteins, the prominent absorbance signals are due to amide bond vibrations. In addition, amino acid side chains may contribute to specific signals.

Amide bonds give 9 characteristic bands called amide A, B, I, II...VII. Only amide A, I and II contain information related to protein conformation. The amide A band (about 3500 cm^{-1}) corresponds to N–H vibration. It is highly sensitive to H bonding, its wavenumber increasing as the strength of H–bonds decreases. The amide I band (between 1600 and 1700 cm^{-1}) is mainly associated with stretching vibration of the C=O, a chemical group which is directly related to the backbone structure. Most protein conformation changes involve C=O

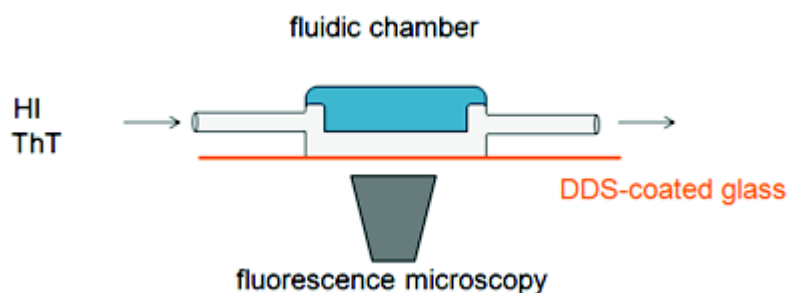
H-bonds within the polypeptide main chain. As a result, the amide I signal consists of different peaks characteristic of the secondary structures in the protein (see Table 4.1). Amide II (between 1510 and 1580 cm^{-1}) results from a combination between the N-H bending vibrations, the C-N stretching vibrations and the C-C stretching vibrations. This band is also conformational sensitive but, since several bonds and vibration modes are involved in the signal, extracting structural information from the amide II band is difficult.

D ₂ O	
Mean frequencies	Assignment
1624±4.0	β-sheet
1631±3.0	β-sheet
1637±3.0	β-sheet
1641±2.0	₃ ₁₀ Helix
1645±4.0	Random
1653±4.0	α-Helix
1663±4.0	β-Turn
1671±3.0	β-Turn
1675±5.0	β-sheet
1683±2.0	β-Turn
1689±2.0	β-Turn
1694±2.0	β-Turn

Table 4.1: Deconvoluted amide I band frequencies and assignments to secondary structure for protein in D₂O. Frequencies are given in cm^{-1} . From Kong *et al.*¹¹¹

Using ATR-FTIR, the nature of insulin conformational changes induced by adsorption on hydrophobic surface was studied. The magnitude of the signal confirmed that insulin adsorption increased with contact time and that most of insulin is strongly adsorbed. A slow change in insulin structure was characterized, that corresponds to the formation of structure with high β-sheet content. The spectrum of adsorbed insulin is different from that of fully aggregated insulin released in solution. The slow infrared rising signal at 1708 cm^{-1} could therefore possibly be related to aggregation nuclei on the surface.

The use of fluorescence microscopy monitoring thioflavin T (ThT) fluorescence has then been used to confirm the slow apparition of β-sheet structures on hydrophobic surface. ThT is a fluorescent dye with high changes in excitation and emission wavelengths in presence of extended β-sheets. Fluorescence microscopy of insulin flowing in a flow cell on Dimethyl dichlorosilane (hydrophobic compound) treated glass slide was developed, see Scheme 4.3. Using fluorescence filters adapted to ThT fluorescence (see Figure 2.1) this system monitors at a micrometer scale the apparition of ThT fluorescence on the surface, which monitors the apparition of protein structures with high β-sheet content on the surface.



Scheme 4.3: Scheme of the experimental device used in fluorescence microscopy experiments.

The major difficulty of that technique is that ThT binds by itself to hydrophobic surfaces, inducing a fluorescence shift, so the signal is not specific to extended β -sheet protein structures. Consequently, we first monitored the evolution of ThT fluorescence on the surface without protein. Free ThT adsorbs and desorbs in ~ 30 minutes. Then, it appears that the addition of protein decreases the ThT fluorescence, due to a competition on surface binding between ThT and proteins, analogous to the Vroman effect. The addition of a non-aggregative protein known to binds strongly to surfaces, Bovine Serum Albumin (BSA), shows that ThT fluorescence decrease with time and then stabilizes at a low level. Insulin addition, similarly to BSA shows a similar ThT fluorescence decrease during the first 20 minutes. But the surface fluorescence increases again after 40 minutes. Consequently, the ThT fluorescence signals obtained with this developed instrument shows the appearance of extended β -sheets on the surface after 30 to 40 minutes, which is consistent with ATR-FTIR results. ThT binds then strongly to this protein covered surface. Moreover, it was confirmed with this technique that adsorbed insulin β -sheet structures build on the surface are hardly affected by buffer washing.

The techniques we developed for that study gives much new information on insulin/hydrophobic surfaces interactions. It appears that insulin adsorbs rapidly on the surface. Then, insulin stabilizes its interaction with the surface, which is characterized by the apparition of a strongly adsorbs insulin population. This stronger adsorption is also characterized by an α to β transition of insulin structure and the apparition of ThT positive protein aggregates on the surface in less than 1 hour (see Figure 4.1). These structures may then be released in solution in high shear stress conditions. Consequently, our results are consistent with data seen in the precedent chapter showing that insulin nucleation takes place on the surface⁸⁸.

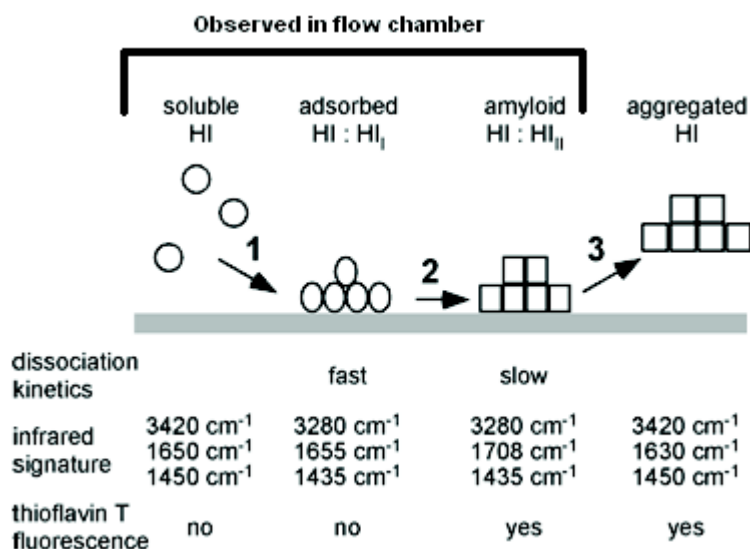


Figure 4.1: Model of insulin accumulation and aggregation on hydrophobic surfaces. **1:** fast protein adsorption without conformational changes. **2:** slow conformational changes of adsorbed protein, and slow additional protein accumulation. **3:** release in solution of formed amyloid fibrils.

In the precedent chapter, AFM images (see Figure 4.2) of hydrophobic beads incubated with insulin show that, during the lag-phase, different large filamentous structures of 20 nm large per 20 nm high and 100 nm long were detectable on the surface. These structures could be insulin aggregation nuclei. Their volume can be estimated to be 40000 nm³, with a contact area with the surface of 2000 nm². Assuming that insulin monomers are cubes of 3.2nm x 3.2nm x 3.2nm (Crowfoot *et al.*¹¹²), an order of magnitude of the size of stable nuclei composition would be of ~1250 insulin monomers per nuclei. This corresponds to a mass of 1.2*10⁻¹⁷g per nucleus (human insulin molecular mass is almost 5808 g.mol⁻¹). Estimating nucleus surface occupation at 2000 nm², a surface fully covered with insulin nuclei should present an insulin surface concentration of 6 mg.m⁻². As the surface coverage is estimated by ImageProPlus software at ~40 %, insulin concentration at the surface can be evaluated at 2.4 mg.m⁻². In microplates, we can observe that BCA measurements give ~3 mg.m⁻² of adsorbed insulin for similar insulin incubation time. Considering the differences between BCA and AFM conditions (low precision of protein concentration evaluation with AFM images, AFM samples were dried before observation which can highly change the protein structures size) it can be proposed that BCA measurements are in the same order of magnitude than AFM observations: stable insulin aggregation nucleus on the hydrophobic surface should be composed of ~1250 insulin monomers, which is consistent with previously published results that estimated the repeating unit of insulin fibril to about 1240 insulin monomers⁷⁸. This order of magnitude could be a basis for insulin aggregation mathematical modeling. Nevertheless, the AFM images used for these calculations were obtained from

hydrophobic beads with surfaces geometries that are not clearly defined. Moreover, they were shaken in a rotation shaker, where different beads collide together, so the mechanic forces are badly defined in such cases. A solution consists of using a flow chamber on flat surfaces. Surface geometry and hydrodynamic forces are well defined in such experiment. In that procedure, the diminution of hydrodynamic shear stress and mechanic collisions leads to the formation of larger nuclei on the surface (see Figure 4.3). Indeed, the protein accumulation spots rises to 50x50x30nm and 100x100x50nm for the biggest ones, which corresponds to 5000 to 6500 insulin molecules in respect to the calculation exposed above. This increase of nucleus size is in agreement with the studied effects of agitation on insulin nucleation and aggregation in the previous chapter. No protein concentration BCA measurements have been done in such conditions, but according to the above calculation, the protein concentration on the surface should reach 10 mg.m⁻². Further studies of protein accumulation on the surface with time in flow chamber experiments could give important information for theoretical modeling of the protein/surface interactions and the nuclei formation process.

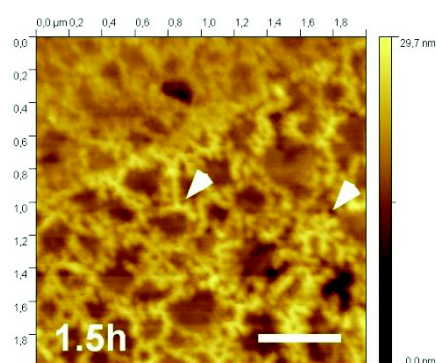


Figure 4.2: AFM image of dried surface incubated 1.5h at 37°C with HI solution pH 7.3 under agitation and buffer wash. Scale bar = 0.5 μ m. Arrowheads point to filamentous structures used for insulin surface coverage evaluations discussed in the text.

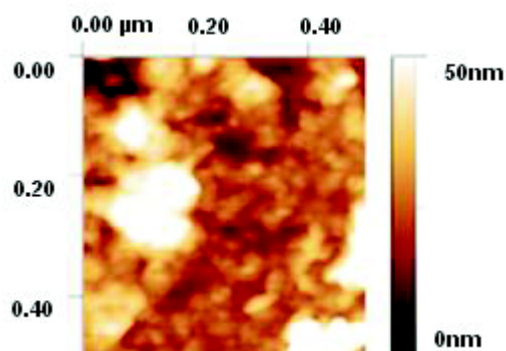
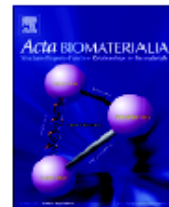


Figure 4.3: AFM image of dried surface incubated 30minutes at room temperature with HI solution pH 7.3 and buffer wash.



Human insulin adsorption kinetics, conformational changes and amyloid aggregate formation on hydrophobic surfaces

Laurent Nault^a, Perry Guo^a, Bhagyashree Jain^a, Yves Bréchet^b, Franz Bruckert^a, Marianne Weidenhaupt^{a,*}

^aLaboratoire des Matériaux et du Génie Physique, Phelma-Minatec, 3 parvis Louis Néel, BP257, F-38016 Grenoble Cedex, France

^bLaboratoire de Science et Ingénierie des Matériaux et des Procédés, Phelma-Campus, 1130 rue de la Piscine, BP 75, F-38402 Saint-Martin d'Hères Cedex, France

ARTICLE INFO

Article history:

Received 12 June 2012

Received in revised form 14 September 2012

Accepted 19 September 2012

Available online 25 September 2012

Keywords:

Protein adsorption on material surfaces

Protein aggregation

Insulin

Surface plasmon resonance imaging (SPRI)

Fourier transform infrared spectroscopy

(FTIR)

ABSTRACT

The formation of insulin amyloid aggregates on material surfaces is a well-known phenomenon with important pharmaceutical and medical implications. Using surface plasmon resonance imaging, we monitor insulin adsorption on model hydrophobic surfaces in real time. Insulin adsorbs in two phases: first, a very fast phase (less than 1 min), where a protein monolayer forms, followed by a slower one that can last for at least 1 h, where multilayered protein aggregates are present. The dissociation kinetics reveals the presence of two insulin populations that slowly interconvert: a rapidly dissociating pool and a pool of strongly bound insulin aggregates. After 1 h of contact between the protein solution and the surface, the adsorbed insulin has practically stopped dissociating from the surface. The conformation of adsorbed insulin is probed by attenuated total reflection–Fourier transform infrared spectroscopy. Characteristic shifts in the amide A and amide II' bands are associated with insulin adsorption. The amide I band is also distinct from that of soluble or aggregated insulin, and it slowly evolves in time. A 1708 cm^{-1} peak is observed, which characterizes insulin adsorbed for times longer than 30 min. Finally, Thioflavin T, a marker of extended β -sheet structures present in amyloid fibers, binds to adsorbed insulin after 30–40 min. Altogether, these results reveal that the conformational change induced in insulin upon binding to hydrophobic surfaces allows further insulin binding from the solution. Adsorbed insulin is thus an intermediate along the α -to- β structural transition that results in the formation of amyloid fibers on these material surfaces.

© 2012 Acta Materialia Inc. Published by Elsevier Ltd. All rights reserved.

1. Introduction

Amyloid fibers are protein aggregates stabilized by intermolecular β -sheets [1]. They are characterized by staining with Congo red and Thioflavin T (ThT), and by a specific cross β X-ray diffraction pattern [2]. Several proteins or polypeptides are able to form amyloids under both natural and artificial conditions [3,4], e.g. islet amyloid polypeptide, which is associated with diabetes II, or the A β (1–40) peptide, which fibrillates in Alzheimer's disease [5]. Insulin is a well-known hormone that regulates blood glucose concentration. Its structure in solution is essentially helical [6]. Daily insulin injections are used to treat type I and many type II diabetic patients. It has long been recognized that insulin solutions also form amyloid fibers in the presence of hydrophobic materials [7–9], especially in contact with peristaltic pump tubing [10]. Furthermore, the daily injection of insulin solutions at the same place

occasionally induces local amyloidogenesis, characterized by the presence of insulin amyloid aggregates [11,12]. Similarly, the formation of A β (1–40) peptide amyloid fibers is also strongly influenced by material surfaces [13,14], such as Teflon [15], alkane-thiol self-assembled monolayers [16] and the air–water interface [17,18]. Understanding the role of material surfaces in protein instability is therefore useful.

Pioneering work by Sluzky et al. [19,20] shows that human insulin (HI) indeed aggregates on hydrophobic material surfaces, at pH 7 and 37 °C under agitation, and that aggregation proceeds in two phases: a nucleation phase or lag time, where no insulin aggregation is observed, followed by an aggregation phase, where most of the insulin aggregates. The length of both phases is influenced by the material hydrophobicity, its surface area compared to the fluid volume, the extent of agitation and the temperature. Ballet et al. [21] further investigated the aggregation mechanism, and showed that the aggregates form on the surface and are later released in the fluid phase. Using DnaK, a bacterial chaperone, as a marker of protein denaturation, they showed that adsorbed HI has a conformation different from soluble and aggregated HI.

* Corresponding author.

E-mail address: marianne.weidenhaupt-blackledge@grenoble-inp.fr (M. Weidenhaupt).

A limitation of these previous studies is that the relatively small amount of adsorbed HI could not be detected with sufficient sensitivity during the nucleation time, with prefibrillar aggregates forming on the material surface. The evidence for the insulin conformational change upon adsorption was also indirect. Finally, in the 96-well plate configuration used in these experiments, ThT binding on adsorbed proteins was detected only after the onset of the aggregation phase. More sensitive methods are therefore required to monitor the adsorption and the interaction of HI molecules on hydrophobic model surfaces in real time.

In this study, we combine three biophysical approaches to study HI adsorption and conformational changes on hydrophobic surfaces (Fig. 1): surface plasmon resonance is sensitive to refractive index changes close to the surface and is used to monitor adsorption kinetics with good temporal resolution; attenuated total reflection–Fourier transform infrared spectroscopy (ATR-FTIR) monitors infrared vibrational bands and is therefore sensitive to conformational changes in surface-adsorbed protein, especially the conversion of α -helices into β -sheets; and ThT binds to amyloidal aggregates and is a sensitive marker of the final insulin state. The common trait of these experiments is that the surface of interest is put into contact with a continuous flow of an HI solution, in contrast with previous experiments, where an HI solution was incubated in a container with a specific surface chemistry. In the configuration presented here, the soluble HI concentration is almost constant throughout the duration of the experiment. A time-resolved sequence of events can thus be defined and studied, from the start of HI adsorption to the formation of amyloidal aggregates on the surface.

2. Materials and methods

2.1. Chemicals

Unless otherwise stated, all chemicals were purchased from Sigma–Aldrich. Experiments were conducted in TBS (25 mM Tris–HCl, pH 7.4, 125 mM NaCl). HI (recombinant, expressed in yeast) solutions were prepared at 0.5 mg ml^{-1} ($86 \text{ }\mu\text{M}$). All solutions were filtered ($0.22 \text{ }\mu\text{m}$, Millipore Stericup filter unit) before use. For the ATR-FTIR experiments, insulin solutions were prepared at $86 \text{ }\mu\text{M}$ in phosphate-buffered saline (10 mM H_3PO_4 , 2.7 mM KCl and 137 mM NaCl) in D_2O and filtered at $0.22 \text{ }\mu\text{m}$. The pD was adjusted to 6.89 using a pH-meter, which corresponds to pH 7.30 in H_2O . The refractive index of the solutions was measured with an Abbe refractometer.

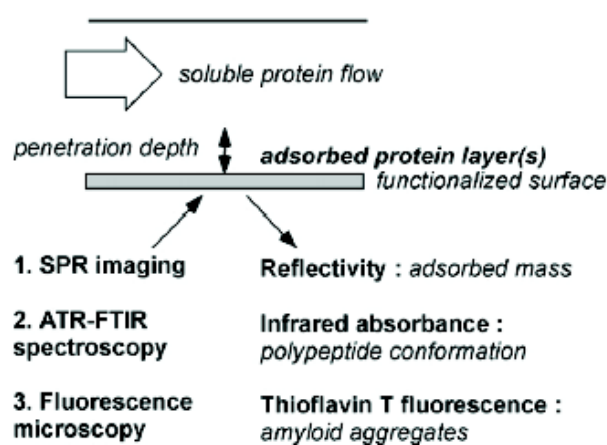


Fig. 1. Scheme of the experimental procedures used in this study. The sensor surface (gray bar) is coated with a hydrophobic self-assembled monolayer and a protein solution is passed over it. Contributions to the signal originate from the adsorbed protein layer and from the soluble protein contained in the penetration depth, which is technique dependent. The different physico-chemical parameters monitored during the studies are summarized below.

2.2. Surface functionalization

Gold-coated prisms (SPRi Biochips) were obtained from Horiba. Prisms were cleaned using oxygen plasma (12 W, 2 min), and half of the gold surface was functionalized with polyethylene glycol thiol (SH-PEG, 8 monomer units, $\text{MW} = 569.8 \text{ g mol}^{-1}$, from Iris Biotech GmbH) at 1 mg ml^{-1} in water at room temperature to obtain a hydrophilic surface. The other half was then treated with hexadecane thiol (SH- C_{16}) at 1 mg ml^{-1} , diluted in toluene at room temperature to obtain a hydrophobic surface. The water surface contact angle was measured (DSA100 Krüss) and found to be $38 \pm 3^\circ$ and $100 \pm 2.5^\circ$ for the hydrophilic and hydrophobic sides, respectively. After each experiment, the prisms were washed with 1% sodium dodecyl sulfate (SDS) and distilled water to remove insulin aggregates.

Round (35 mm diameter) glass coverslips were cleaned using oxygen plasma (12 W, 2 min), siliconized with dimethyldichlorosilane (DDS) (5% in toluene, 2 h, room temperature), washed in toluene and ethanol, and cured at 110°C for 2 h. The water surface contact angle was $102.1 \pm 1.3^\circ$.

For ATR-FTIR measurements, a silicon prism was purchased from Specac Ltd, cleaned using oxygen plasma (12 W, 2 min), functionalized with phenyldimethylmethoxysilane (PDMMS) (5% in toluene, 2 h, room temperature), washed in toluene and ethanol, and cured at 110°C for 2 h. The water surface contact angle was $103.1 \pm 3.7^\circ$.

2.3. Surface plasmon resonance sensorgram acquisition and analysis

Buffer and protein solutions were injected in the SPRi chamber using syringe pumps at $100 \text{ }\mu\text{l min}^{-1}$ at room temperature (22°C). Reflectivity images were taken every 3 s. The SPRi instrument (Horiba Scientific SPRi-Lab+™) records reflectivity changes of manually predefined spots on the treated gold surface. Calibration was performed using a 50 mM NaCl solution, to adjust the response of the spots to a known refractive index change (3×10^{-4}). A background image was acquired at the beginning of the experiment, which was then subtracted from the subsequent ones. Three zones of interest were defined on the SH-PEG and SH- C_{16} sides of the prism, and the sensorgrams obtained on each side were averaged. A difference sensorgram $\Delta R(t)$ was finally obtained by subtracting the SH-PEG sensorgram from the SH- C_{16} one.

The adsorption kinetics were analyzed with the following equation:

$$\Delta R(t) = A(1 - \exp(-kt)) + bt \quad (1)$$

where A and k are the amplitude and rate of the fast adsorption component, and b is the rate of the slow protein binding component.

The desorption kinetics were analyzed with the following equation:

$$\Delta R(t) = A_1 \exp(-k_1 t) + A_2 \exp(-k_2 t) \quad (2)$$

where A_1 and A_2 are the amplitude of the fast and slow desorption components, respectively, and k_1 and k_2 are the rate constants of the fast and slow desorption components, respectively. Data are obtained from several independent experiments, using different functionalized prisms and HI solutions.

The conversion between the ΔR and the adsorbed mass per area is given in pg mm^{-2} by the equation:

$$\text{mass} = 122.25 \Delta R - 0.6557 \quad (3)$$

assuming that the signal is in the linear range of the instrument and solution refractive index changes have been corrected (equation provided by Horiba SPRi+). The relationship between ΔR and the refractive index changes, Δn , was determined using NaCl solutions

at different concentrations and was found to be: $\Delta R = 28333\Delta n$. This relation was used to calculate the amplitude of the refractive index change in protein solutions compared to buffer.

Having recorded the dissociation kinetics, the hydrophobic surface was regenerated with SDS (5%, 5 min).

2.4. FTIR recordings

Aggregated HI solutions were prepared in 96-well plates (Greiner Bio-One, contact angle = $85 \pm 4.7^\circ$) as follows. The plates were covered by plastic sheets, incubated at 37°C and shaken at 1200 rpm (Heidolph Titramax, 1.5 mm vibration orbit) for 12 h. The aggregated solution was analyzed using a Bruker Vertex 70 FTIR instrument. The liquid cell was a CaF_2 cell from Perkin Elmer Instruments. Using the OPUS software, compensation was applied to filter the contributions of H_2O and CO_2 to the spectra. Smoothing was done using the Savitzky–Golay equation. Baselines were flattened using a linear correction.

2.5. ATR-FTIR recordings

Buffer and protein solutions were prepared in D_2O and injected in the chamber using a peristaltic pump at 10 ml min^{-1} in a closed circuit, at room temperature. A tubing diameter of 5 mm was used to reduce shear stress. No amyloid fibers were formed on the tubing during the time of the experiment. The total volume of the sample was 10 ml. During recording of the spectra (about 2 min), the flow was stopped. Spectra were acquired from 1400 to 4000 cm^{-1} . Baselines were flattened using a linear correction in the range 4000 – 2800 cm^{-1} and in the range 2000 – 1400 cm^{-1} . H_2O and CO_2 compensations were done as described for FTIR recordings. Further smoothing was performed using a Savitzky–Golay algorithm. Spectral decomposition of the amide I band (1600 – 1700 cm^{-1}) was done using the second derivative of the spectra to find peak positions. Then, using the Levenberg–Marquardt algorithm, 3–5 peaks were fitted to the experimental data (residual relative error less than 2.5×10^{-5}).

The spectra $A(t)$ recorded at time t contain two contributions: $A(t) = A_{\text{ads}}(t) + A_{\text{sol}}$, where $A_{\text{ads}}(t)$ is the spectrum of adsorbed HI at time t and A_{sol} is the constant soluble HI contribution. With this notation, the spectrum recorded after 80 min in the presence of HI and 1 min wash with buffer is $A_{\text{ads}}(80)$. The spectra of HI adsorbed at time t , $A_{\text{ads}}(t)$, can therefore be calculated by the following equation:

$$\begin{aligned} A_{\text{ads}}(t) &= A(t) - A(0) + A_{\text{ads}}(80) - [A(80) - A(0)] \\ &= A(t) + A_{\text{ads}}(80) - A(80) \end{aligned} \quad (4)$$

2.6. Surface fluorescence measurements

A flow chamber was built on a DDS-coated glass coverslip using a Glycotech flow chamber (channel width = 2.5 mm, channel thickness = 0.127 mm). A $20 \mu\text{l min}^{-1}$ flow rate was applied by a syringe pump. When indicated, ThT was added to the buffer and protein solutions at a $20 \mu\text{M}$ final concentration. The surface fluorescence was observed by a $\times 63$ objective (NA = 1.4) on an IX-71 Olympus microscope fitted with a DAPI fluorescence cube ($\lambda_{\text{ex}} = 435 \pm 10 \text{ nm}$, $\lambda_{\text{em}} = 485 \pm 25 \text{ nm}$) and connected to an Olympus DP30BW camera. The image of the field stop was used to ensure proper focusing on the glass surface. Fluorescence images of the surface were recorded at the indicated times. To avoid photobleaching, each image was recorded at a different position, using a motorized stage. Using the ImageProPlus software, the average fluorescence

monitored during the studies are summarized below.

intensity was calculated on the image of the field stop and the value of the dark background was subtracted.

3. Results

3.1. Insulin adsorption and dissociation kinetics on hydrophobic surfaces

Surface plasmon resonance imaging (SPRI) is a sensitive method to measure the amount of molecules adsorbed on functionalized gold surfaces (see Fig. 1). A gold prism was prepared with half of the surface coated with SH-PEG and the other half with C_{16} alkyl-thiol. SPR is sensitive to refractive index changes within the penetration distance of the evanescent wave. When a solution is bathing the prism, the SPR signal sums up two contributions, one due to the refractive index of the bulk solution, the other due to the mass adsorbed on the gold surface. The response time of the setup was determined by passing a 50 mM NaCl solution over the functionalized prism. In this case, no adsorption is expected. The sensorgrams indeed indicate a fully reversible, fast ($<1 \text{ min}$) signal, the amplitude of which minimally depends on the surface functionalization (Fig. 2A and B). This corresponds to the time needed to exchange solutions over the prism surface. The linearity of the technique with respect to the amount of adsorbed material was assessed by adsorbing a polyelectrolyte multilayer film on the prism layer by layer. In this experiment, the prism was not functionalized and a 10 mg ml^{-1} polyethyleneimine (PEI) solution in TBS was passed first to provide an anchoring layer. Solutions of 5 mg ml^{-1} polystyrene sulfonate (PSS, negatively charged) and 5 mg ml^{-1} polyallylaminehydrochloride (PAH, positively charged) in TBS were passed alternately over the surface, separated by washes with TBS (Fig. 2C). Previous work showed that the thickness of these films increased linearly with the number of layers deposited, each polystyrene sulfonate layer forming a 3–5 nm thick layer [22]. Using QCM-D and waveguide spectroscopy, up to 12 layers could be monitored. In contrast, with SPRI, the deposition of the same polyelectrolytes gave signals that rapidly decreased as the number of layers increased (Fig. 2C and D). The amplitude of the signal was plotted as a function of the thickness of the multilayered film, obtained by waveguide spectroscopy [23] and fitted as $S[1 - \exp(-z/d_p)]$, where S represents the maximum reflectivity change and d_p is the penetration distance. From Fig. 2C and D, a penetration distance of $18.7 \pm 1 \text{ nm}$ and a maximum signal of $26.5 \pm 1 \text{ RU}$ can be estimated. A single layer of PSS corresponds to 6 RU, which is 0.73 mg m^{-2} according to Eq. (3).

A typical HI adsorption kinetics experiment is shown in Fig. 3A. A $86 \mu\text{M}$ HI solution (0.5 mg ml^{-1}) was passed over the functionalized prism during 14 min, then the surface was washed with buffer for 45 min. Sensorgrams were recorded on both the hydrophilic SH-PEG-coated side and the hydrophobic C_{16} alkyl-thiol-coated side. On the hydrophilic side, a fast reversible signal was observed, which could be attributed to refractive index changes solely. On the hydrophobic side, a much larger signal was observed, which rose in two phases and decreased much more slowly after the buffer had replaced the protein solution. This signal is due to both the refractive index change and the binding of HI on the hydrophobic surface. After a 5 min wash, the reflectivity remained 0.5 RU higher than on the PEG-coated side.

Subtracting the sensorgram acquired on the PEG-coated surface from the one acquired on the C_{16} alkyl-coated surface allows the common component due to refractive index changes to be eliminated and the HI adsorption and desorption kinetics on the hydrophobic surface to be specifically obtained (Fig. 3B). The association curve consists of two components – a fast signal, rising to 1 RU in refractive index changes, Δn , was determined using NaCl solutions

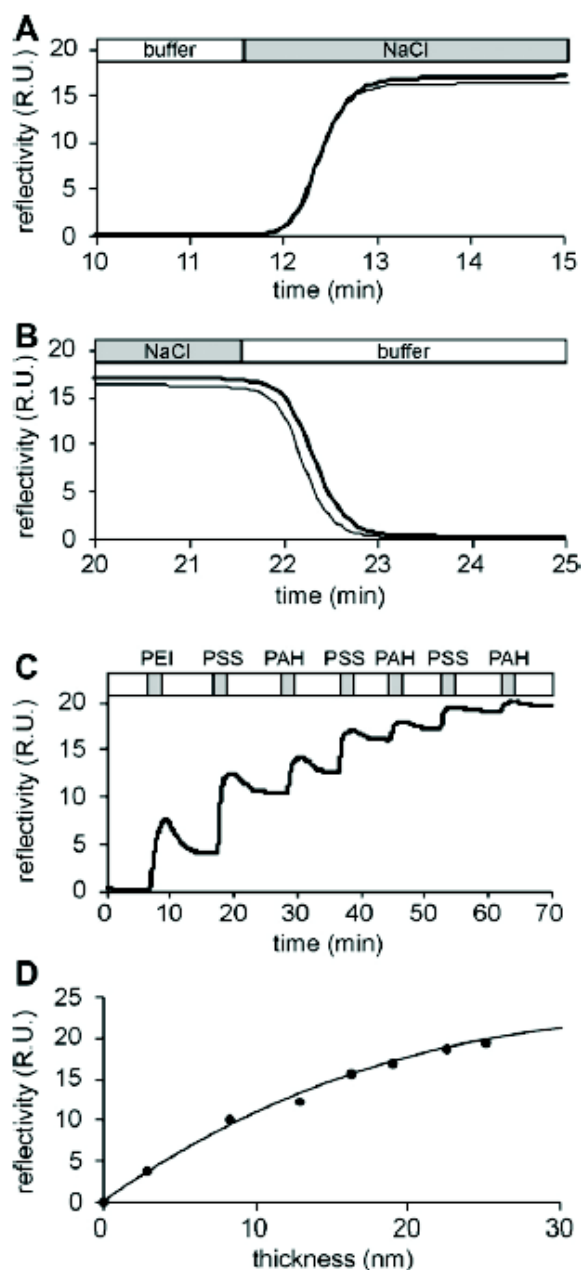


Fig. 2. Calibration of the SPRi apparatus. A and B. Changes in C_{16} -coated (heavy line) and PEG-coated (thin line) gold surface reflectivity were monitored by surface plasmon resonance during injection of 50 mM NaCl (A) and washing in buffer (B). (C) SPRi recording of a PSS and PAH polyelectrolyte layer-by-layer film built on a gold surface. PEI is first deposited as an anchoring layer. (D) The amplitude of the SPRi signal after depositing the successive layers and washing with buffer (data from (C)) is plotted as a function of the adsorbed layer thickness (z) determined by Picart et al. [23]. The solid line is a fit with the equation: $S(z) = S[1 - \exp(-z/d_p)]$, where S (26.5 ± 1 RU) is the maximum reflectivity change and d_p (18.7 ± 1 nm) is the penetration distance.

about 1 min, followed by a slow, almost linear increase. During the wash, the dissociation curve also consists of two components – a fast signal, going up to 1.3 RU in about 5 min, followed by a much slower decrease that lasted for more than 30 min. The association and dissociation kinetics were adequately fitted by the phenomenological equations 1 and 2 (see Materials and methods), giving seven parameters: A , k , b , A_1 , k_1 , A_2 and k_2 . A and k represent the amplitude and rate constant of the fast association component, and b represents the slope of the slow association component. A_1 and k_1 (and A_2 and k_2) represent the amplitudes and rate constants of the fast (and slow) dissociation components, respectively. These biphasic association and dissociation curves show that HI binding

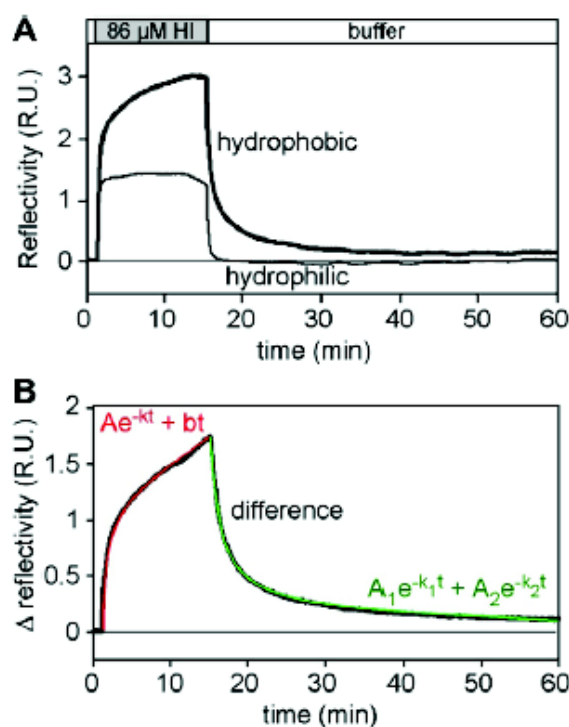


Fig. 3. HI association and dissociation kinetics on hydrophobic surfaces. (A) SPRi signal for 0.5 mg ml^{-1} HI injection and buffer washing on a prism functionalized with C_{16} -thiol (heavy line) or SH-PEG (thin line). (B) The difference signal obtained by subtracting the signals recorded on the SH-PEG and SH- C_{16} sides reveals the HI adsorption and desorption kinetics (black line). The red and green curves represent a mathematical fit of the data with Eqs. (1) and (2), respectively. $A = 1.076 \pm 0.005$; $k = 1.32 \pm 0.02$; $b = 0.0545 \pm 0.0005$. $A_1 = 1.153 \pm 0.005$; $k_1 = 0.707 \pm 0.007$; $A_2 = 0.570 \pm 0.004$; $k_2 = 0.0595 \pm 0.0007$.

on hydrophobic surfaces is not a reversible process. The slow dissociation component indicates that some HI is strongly bound to the surface, whereas the fast dissociation component suggests that another pool of HI is much more weakly bound to the surface.

In a parallel experiment, the surface concentrations of HI adsorbed on a hydrophilic PEG-coated microwell or on a hydrophobic polystyrene plastic surface (2 cm^2) were directly determined using the bicinchoninic assay [24]. No HI was detectable on the hydrophilic surface, whereas 0.4 mg m^{-2} was quantified on hydrophobic surfaces. Comparing this value to the corresponding SPRi experiments shows that $1 \text{ RU} = 0.2 \text{ mg m}^{-2}$. This is close to the value obtained with Eq. (3) (0.12 mg m^{-2} per RU). Assuming that the calibration determined for the fast phase of the SPRi association signal holds also for the slow phase, the rate of insulin adsorption would be about $0.013 \text{ mg m}^{-2} \text{ min}^{-1}$.

Since SPRi is a very sensitive technique, HI adsorption could easily be monitored on hydrophobic surfaces at different concentrations down to $0.1 \mu\text{M}$. Fig. 4A shows an SPRi difference sensorgram obtained on the same surface where successive HI concentrations ranging from 0.49 to $86 \mu\text{M}$ were applied. Each HI concentration was applied for 10 min, after which the surfaces were washed. It is apparent from the difference sensorgram that the slope of the slow dissociation kinetics and the amplitude of the slow dissociation kinetics both increase with HI concentration. In Fig. 4B and C, the effect of increasing HI concentrations on the parameters A , k (Fig. 4B) and b (Fig. 4C) describing the association kinetics are displayed. The amplitude A of the fast association component increases with HI concentration and saturates at 1 ± 0.05 RU (2.6 mg m^{-2}), with an apparent binding constant of $2.5 \pm 0.5 \mu\text{M}$, showing that the amount of HI was limited by the available surface. The rate constant of the fast association kinetics k remains constant at $1.3 \pm 0.1 \text{ min}^{-1}$. The fast rise of the

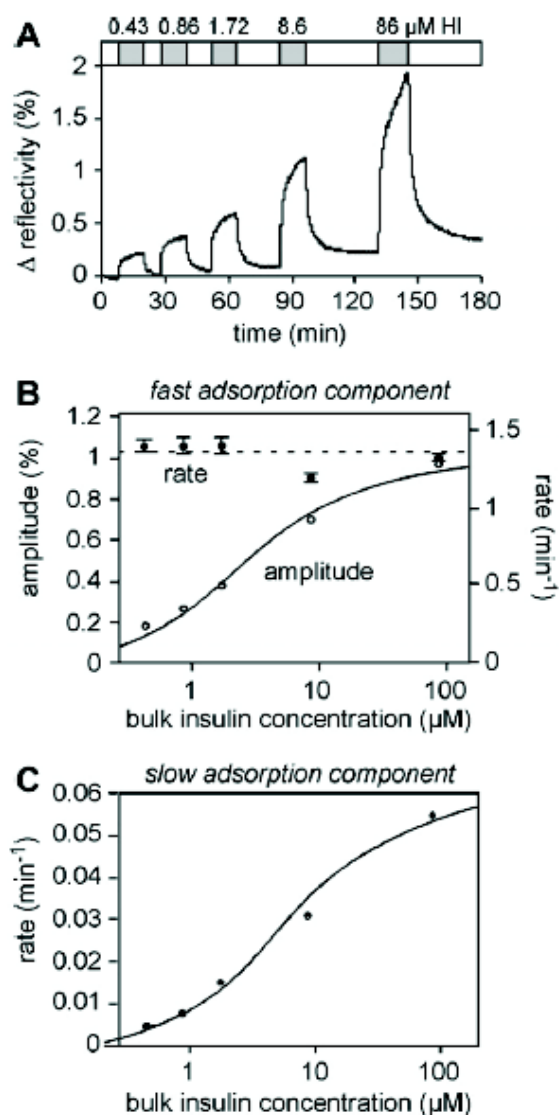


Fig. 4. Effect of HI concentration on HI adsorption and desorption kinetics. (A) Successive HI adsorption and desorption difference SPRi signals recorded at the indicated HI concentrations. (B, C) The adsorption kinetics were fitted with Eq. (1) to calculate the amplitude A and the rate constant k of the fast component and the slope b of the slow component. (B) Parameters A and k are plotted as a function of the HI concentration. The error in A is smaller than the symbol size. The solid curve is a fit with the following relationship: $A = A_{\max}[\text{HI}]/([\text{HI}] + K)$, where A_{\max} (1 ± 0.05 RU) is the HI binding site concentration and K (2.5 ± 0.5 μM) is the apparent binding constant. (C) Parameter b is plotted as a function of the HI concentration. The error on b is smaller than the symbol size. The solid curve is a fit with the following relationship: $b = b_{\max}[\text{HI}]/([\text{HI}] + K')$, where b_{\max} (0.058 ± 0.002 RU min⁻¹) is the maximum HI association rate and K' (6.1 ± 1 μM) is the apparent binding constant.

association kinetics is thus limited by the response time of the SPRi setup. The slope of the slow association component b also increases with HI concentration and saturates at 0.058 ± 0.002 RU min⁻¹ (0.023 ± 0.001 mg m⁻² min⁻¹), with an apparent binding constant of 6.1 ± 1 μM. The growth of HI aggregates on the hydrophobic surface thus occurs at a limited number of specific sites.

In a second set of experiments, we varied the time during which the HI solution was in contact with the prism surface (Fig 5A). As the contact time is increased, the slow association component lasts longer (not shown) and the slow dissociation component becomes more important (Fig 5B) and slower (Fig 5C). This indicates that, as time progresses, insulin binds more strongly to the alkyl surface and an increasing amount of insulin remains adsorbed in a strongly bound form on the hydrophobic surface. The parameters describing the association kinetics are similar to those described in the experiments where the HI concentration was varied. For the dissociation kinetics, both sets of experiments were analyzed together,

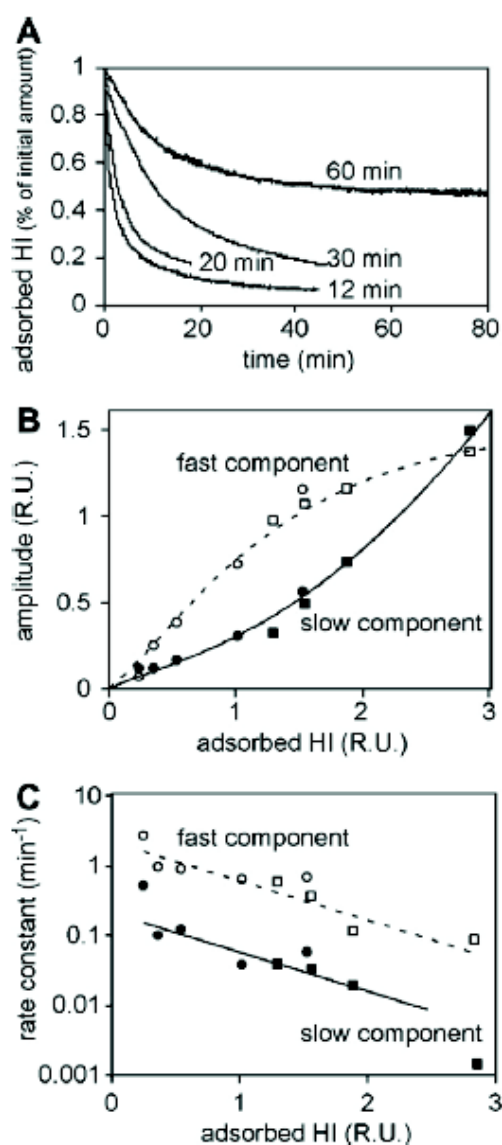


Fig. 5. Effect of incubation time on HI desorption kinetics. (A) SPRi desorption difference sensorgrams obtained after application of 86 μM HI for the indicated time. The SPRi difference signals have been normalized to the values reached at the beginning of the washing with buffer. (B) Amplitudes of the fast (open symbols) and slow (dosed symbols) components of the desorption sensorgrams, represented as a function of the SPRi value at the onset of the washing with buffer. They correspond to parameters A_1 and A_2 in Eq. (2). The lines are hand-drawn. (C) Rate constant of the fast (open symbols) and slow (closed symbols) components of the desorption sensorgrams, represented as a function of the SPRi value at the onset of the buffer wash. They correspond to parameters k_1 and k_2 in Eq. (2). The lines are exponential fits of the data. In the case of the slow component, the two extreme points were omitted. In (B) and (C), squares and circles correspond to desorption kinetics obtained after applying either different HI concentrations for the same time or 86 μM HI for different times, respectively. The errors in the determination of the kinetic desorption parameters are smaller than the symbol size.

and the kinetic parameters were plotted as a function of the amount of HI adsorbed on the surface at the beginning of the wash. The relative amplitude of the fast dissociation component A_1 decreased and the amplitude of the slow dissociation component A_2 increased as the amount of adsorbed HI increased. Furthermore, the fast and the slow dissociation rate constants k_1 and k_2 decreased exponentially, in a parallel manner, as the amount of adsorbed HI increased. This shows that the presence of adsorbed HI further stabilizes HI binding. HI adsorption is therefore a cooperative process.

It has been shown that agitation has two opposite effects on HI aggregation induced by hydrophobic surfaces: on the one hand, it prevents the formation of a depleted diffusion layer that slows

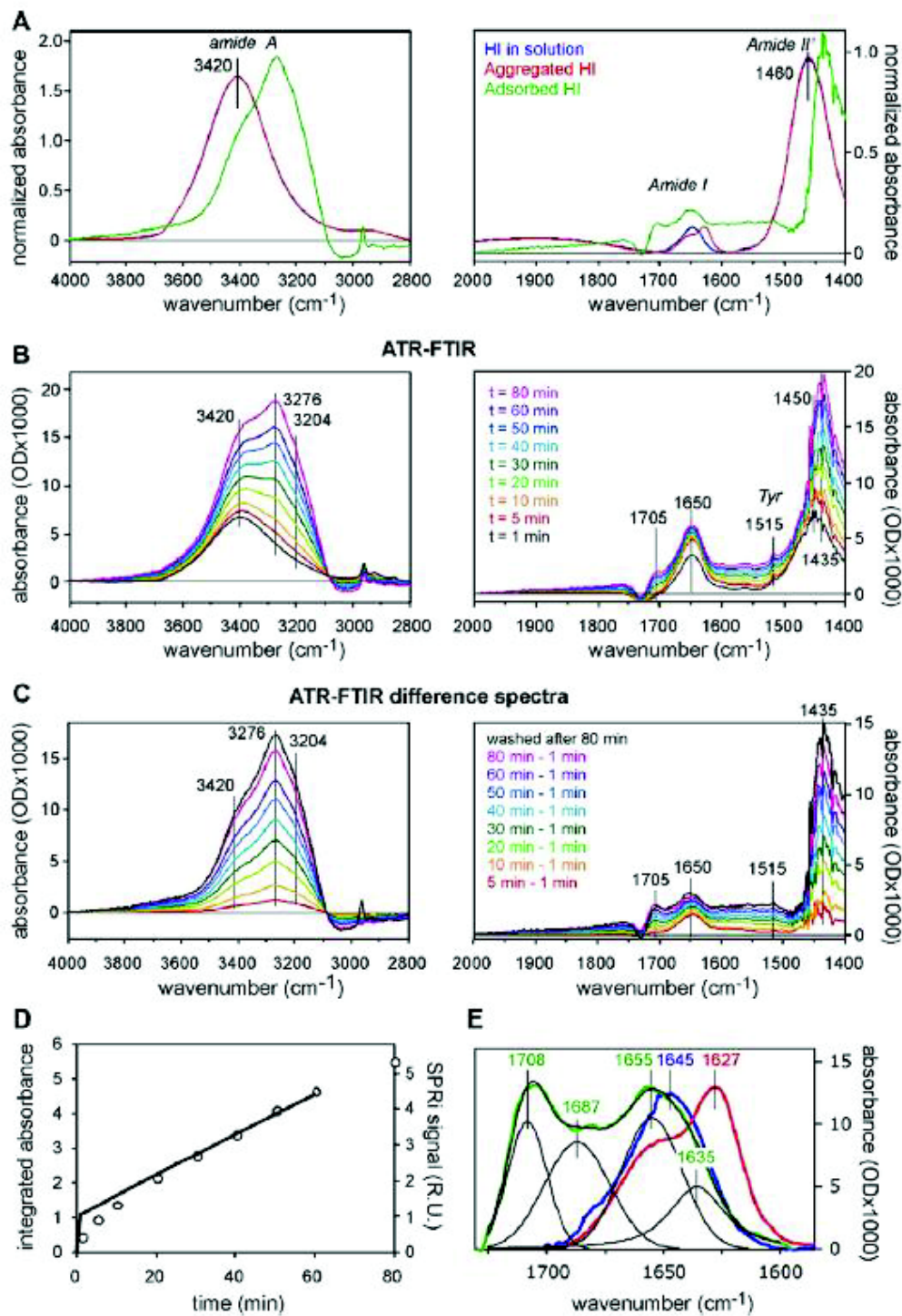


Fig. 6. ATR-FTIR spectra of HI adsorbed on hydrophobic surfaces. In (A), (B) and (C), the left and the right panels display the spectra in the 4000–2800 cm^{-1} or the 2000–1400 cm^{-1} ranges, respectively. In the left and right panels, the baseline was zeroed at 4000 or 2000 cm^{-1} , respectively, except in the right panel of (A), where the zero was set at the minimum. Data are representative of three experiments. (A) Transmission FTIR spectra of soluble (blue) and aggregated (red) HI. ATR-FTIR spectrum of HI adsorbed for 80 min on a hydrophobic surface and washed (green). The spectra have been normalized to the same total area. (B) Successive ATR-FTIR spectra recorded on the same hydrophobic surface while passing an 86 μM HI solution during 80 min. The time is indicated in the right panel. (C) Same data as in (B). The ATR-FTIR spectrum recorded after 1 min has been subtracted from those recorded later to show the increase in adsorbed HI. In addition, the spectrum obtained after 80 min of contact with the HI solution and a 1 min wash is also displayed. (D) Total absorbance of adsorbed HI calculated according to Eq. (3) integrated over the 4000–2800 cm^{-1} and the 2000–1400 cm^{-1} ranges, as a function of time. For comparison, the association SPRi difference signal is represented as a thick line. (E) Amide I band of soluble HI (blue), aggregated HI (red) and HI adsorbed for 80 min on hydrophobic surfaces (green). Data are from (A). The baseline is linearly adjusted between 1700 and 1570 cm^{-1} for soluble HI and aggregated HI spectra, and between 1730 and 1570 cm^{-1} for the adsorbed HI spectrum. In the case of the adsorbed HI spectrum, the decomposition of the band into four peaks is displayed as thin lines that represent the individual peaks and their sum.

down the accumulation of protein on the surface; on the other hand, it helps to detach already formed aggregates. The fluid flow rate was therefore changed to mimic the effect of agitation (data not shown). The rate of HI adsorption was monitored as the fluid flow was stopped. No change was observed, showing that HI diffusion is fast enough to allow HI aggregation at surfaces.

3.2. Insulin conformational changes on hydrophobic surfaces

Insulin conformational changes during its adsorption on hydrophobic surfaces were investigated by ATR-FTIR (Fig. 1). The infra-red spectrum of a protein is indeed sensitive to its secondary structure. For this purpose, the top contact surface of an ATR-FTIR

silicon prism was functionalized with phenyldimethylmethoxysilane, which forms a hydrophobic self-assembled monolayer. The baseline spectrum was recorded with the buffer solution. An 86 μM HI solution prepared in $^2\text{H}_2\text{O}$ was then passed over the prism and 4000–1400 cm^{-1} infrared spectra were recorded at the times indicated during 80 min at room temperature (20 °C). Since recording a single spectrum takes about 1 min, the infrared spectrum referring to time point 1 corresponds to insulin already adsorbed on the prism for 1–2 min. Infrared spectra were therefore recorded early after the fast initial HI adsorption (time 1) and during the slow phase of the HI adsorption kinetics (subsequent times).

In comparison, Fig. 6A shows the spectra of the initial HI solution and of a suspension of aggregated HI, obtained after agitation in a hydrophobic multi-well plate [21], both recorded by transmission FTIR. The spectra are displayed in two parts, the 4000–2800 cm^{-1} region in the left panel and the 2000–1400 cm^{-1} region in the right one, skipping the intermediate 2800–2000 cm^{-1} region, where the signal is almost flat or does not contain any protein contributions. In proteins, the peptide bond (amide group) is the main contributor to the infrared spectrum, but specific amino acid side chains may also contribute significantly in spectral regions where no other chemical group absorbs, e.g. tyrosines at 1515 cm^{-1} . In the 4000–1400 cm^{-1} range, amide groups contribute to three groups of peaks: the amide A peak, in the 3600–3100 cm^{-1} range, the amide I peaks, in the 1700–1600 cm^{-1} range, and the amide II' peaks, in the 1500–1400 cm^{-1} range [25]. The prime refers to the fact that in the presence of $^2\text{H}_2\text{O}$, hydrogen is exchanged for deuterium in the amide NH group. The soluble and aggregated HI spectra are similar in the amide A/B and amide II' bands (3420, 3100 and 1460 cm^{-1} , respectively), but are characteristically different in the amide I band, with one prominent 1650 cm^{-1} band for soluble HI and two bands around 1660 and 1630 cm^{-1} for aggregated HI, as reported previously [26].

The successive ATR-FTIR spectra clearly show the progressive accumulation of protein material on the PDMMS surface (Fig. 6B). The first spectrum (time 1) is very similar to the spectrum of soluble HI and displays the amide A peak at 3420 cm^{-1} , the amide I peak at 1650 cm^{-1} , the tiny tyrosine contribution at 1515 cm^{-1} and the amide II' peak at 1450 cm^{-1} . At later times, however, specific peaks appear and increase rapidly, especially at 3276 and 3204 cm^{-1} in the amide A band and at 1705 cm^{-1} in the amide I band. Since the penetration distance of the infrared evanescent waves in ATR-FTIR is about 2 μm , the recorded spectra are indeed the sum of the soluble HI contribution and the adsorbed HI contribution. Assuming that the adsorbed HI layer remains negligible compared to the 2 μm penetration depth, the contribution of soluble HI is constant during the association phase. Difference spectra thus reveal the adsorbed HI contribution. In Fig. 6C, the spectrum recorded at $t = 0$ has been subtracted from subsequent spectra. These difference spectra are quite similar in shape, except in the range 1730–1670 cm^{-1} (see below), but are clearly distinct from the spectrum of HI in solution or aggregated (Fig. 6A). Besides the aforementioned amide A and amide I differences, the amide II' is clearly shifted to 1435 cm^{-1} . Furthermore, these difference spectra are very similar to the ATR-FTIR spectrum recorded at the end of the experiment, once HI had been passed over the prism surface for 80 min and washed with buffer for 1 min (black curve in Fig. 6C). This proves that adsorbed HI has a specific spectrum and that spectra recorded subsequently in time (Fig. 6B) are the sum of a constant soluble HI contribution and increasing adsorbed HI contributions. Curve fitting confirmed this analysis, except in the 1730–1670 cm^{-1} region (see below). After washing with 1% SDS, the flat initial baseline was restored, showing that this detergent is able to remove all adsorbed proteins. The spectrum recorded after buffer wash is therefore due to adsorbed HI. In Fig. 6A, this

spectrum has been normalized and displayed along the soluble and aggregated HI ones to facilitate their comparison.

The difference between the spectrum obtained after washing the prism surface (Fig. 6C, black curve) and the last difference spectrum (80 min – 1 min, Fig. 6C, pink curve) corresponds to the HI adsorbed during the first minute. It is therefore possible to calculate the spectrum of adsorbed HI as a function of time from Eq. (3). In Fig. 6D, the absorbance is summed over the 4000–2800 cm^{-1} and 2000–1400 cm^{-1} ranges, and plotted as a function of time. The fact that the integrated absorbance continuously increases over 80 min confirms that HI is indeed able to adsorb not only on the hydrophobic surface, but also on HI molecules already adsorbed on the surface. To compare this plot with the SPRi results, the SPRi association signal was also plotted, and displayed using a scale that allows its comparison to the integrated absorbance signal. The integrated absorbance signal is quite comparable to the SPRi signal: it rises rapidly during the first 10 min (fast component), then increases linearly for about 1 h (slow component). It should nevertheless be noted that the FTIR signal rises less rapidly than the SPRi signal in the first 10 min.

The amide I band of adsorbed HI is strikingly different from that of soluble and aggregated HI. First, the entire band is shifted from the 1700–1600 cm^{-1} range to 1730–1630 cm^{-1} . Second, the substructure of the amide I band exhibits four main peaks, at 1635, 1655, 1687 and 1708 cm^{-1} (Fig. 6E). The relative contributions of these peaks to the amide I band are 18, 33, 29 and 20%, respectively. A detailed analysis of the evolution of the amide I band of adsorbed HI with time reveals that, initially, the 1708 cm^{-1} peak is minimal, but increases over about 30–40 min (Fig. 7A and B). In contrast, the 1655 cm^{-1} peak reaches its maximum level in less than 5 min and remains almost constant thereafter. The evolution of the 1708 cm^{-1} peak parallels that of the relative amplitude of the slow dissociation component of the SPRi signal (Fig. 7B). This documents the complexity of conformational changes and reveals the existence of slow conformational rearrangements within adsorbed HI.

3.3. Insulin aggregate formation on hydrophobic surfaces

Amyloid aggregates are characterized by the formation of large intermolecular β -sheets, which can be probed by the binding of ThT, resulting in a specific fluorescence signal, distinct from soluble ThT fluorescence. We used a Glycotech flow chamber to pass an HI solution over a surface of interest in the presence of ThT and monitor the fluorescence associated with the surface. The coverslip was functionalized with dimethyldichlorosilane, which forms a hydrophobic self-assembled monolayer on glass. Fig. 8A shows a typical experiment. When a buffer solution containing ThT was introduced in the chamber, a small but significant surface fluorescence signal was detected. Washing the surface with buffer alone resulted in a fast decrease in surface fluorescence down to the background level, showing that the fluorescence signal was due to ThT that was loosely bound to the hydrophobic surface (Fig. 8A). When an 86 μM HI solution containing ThT was passed over the coverslip, the fluorescence signal first decreased close to zero, then increased sharply after 40 min and was saturated by about 90 min. No ThT fluorescence signal appeared on a hydrophilic surface (plain glass coverslip, data not shown). Passing a BSA solution over the hydrophobic surface also decreased the surface fluorescence signal, but gave rise to little or no fluorescence recovery. We therefore interpret the surface fluorescence decrease as a strong competitive protein binding, replacing the weakly bound ThT. The fluorescence increase is due to the formation of insulin amyloid aggregates on the surface. BSA indeed does not readily form amyloid aggregates on hydrophobic surfaces (data not shown). Once HI had accumulated on the surface, washing with a

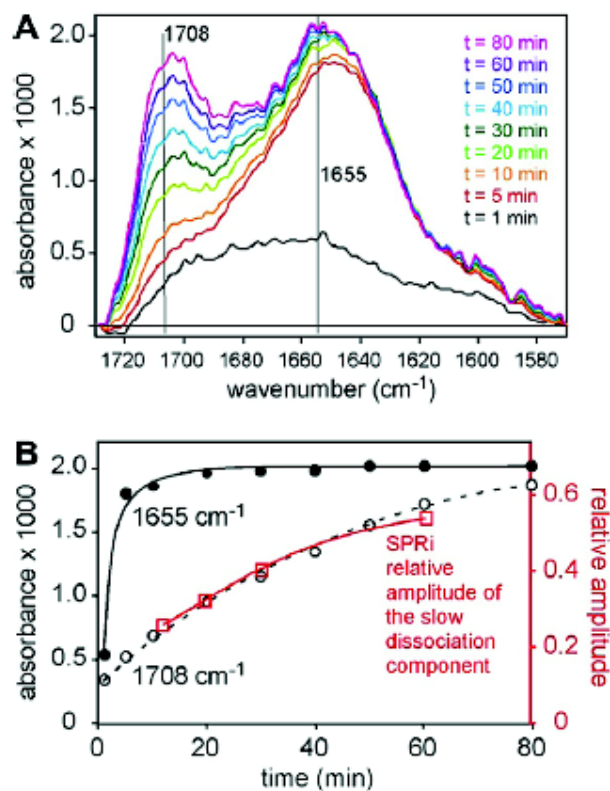


Fig. 7. (A) Evolution of the HI amide I band as a function of the time of contact between an 86 μM HI solution and the hydrophobic surface. Data are from Fig. 6. The adsorbed HI spectra are calculated using Eq. (3). The baselines of the amide I bands are linearly adjusted between 1730 and 1570 cm^{-1} . (B) The infrared absorbances of adsorbed HI at 1655 cm^{-1} (closed circles) and at 1708 cm^{-1} (open circles), and the relative amplitude of the slow component of the SPRi dissociation signal (squares), are plotted as a function of the time of contact between an 86 μM HI solution and the hydrophobic surface. The lines are hand-drawn.

buffer solution devoid of ThT resulted in a very slow fluorescence decrease, showing that ThT was now strongly bound to HI adsorbed on the surface (Fig. 8B). Quantitatively, the ThT dissociation kinetics was five times lower from adsorbed HI than from plain hydrophobic surfaces. The surface fluorescence decreased very slowly (typically for 15 h) during washing with a buffer solution containing ThT, confirming that amyloid HI does not easily dissociate from the surface (Fig. 8B). In contrast, washing with SDS allowed a fast and complete disappearance of the surface fluorescence (data not shown). Altogether, these results show that a lag phase of 40 min precedes the appearance of ThT positive aggregates on hydrophobic surfaces, that ThT binds more strongly to adsorbed HI than to hydrophobic surfaces and that ThT-positive aggregates are strongly bound to the surface.

4. Discussion

In this work, we reconstituted the formation of insulin amyloid aggregates on hydrophobic surfaces and delineated in time a series of sequential molecular events that occur on the material surface (Fig. 9). Amyloid aggregates, evidenced by ThT fluorescence, appear about 40 min after the hydrophobic surface is put into contact with an insulin solution. It should be noted that the experimental conditions are slightly different from those used in previous insulin aggregation assays such as in Slutzky et al. [19,20] or Ballet et al. [21]. First, the protein solution flows over the surface of interest, instead of being simply incubated. The bulk protein concentration therefore remains constant, except during ATR-FTIR experiments, where the solution is recirculated. Note that in this case, the total HI content of the setup (5 mg) is in large excess to the HI expected

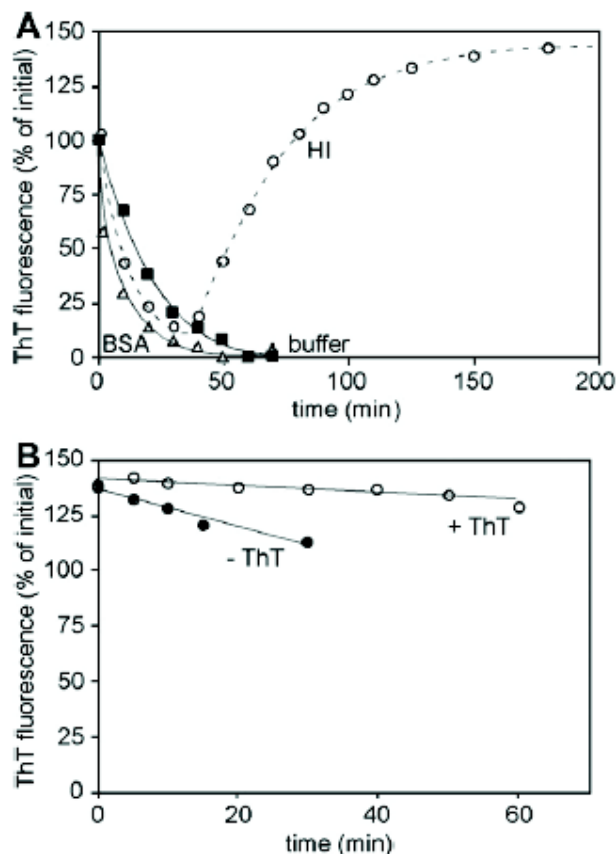


Fig. 8. Formation of HI amyloid fibers on hydrophobic surfaces. The surface fluorescence of a PDMMMS-coated coverslip is monitored to detect the presence of bound ThT. The fluorescence levels are normalized to the value obtained after passing a 20 μM ThT solution for 120 min on the surface. The curves displayed are representative of three independent experiments. (A) At $t = 0$, either TBS buffer without ThT (black squares) or TBS buffer containing 0.5 mg ml^{-1} (6.5 μM) BSA and 20 μM ThT (open triangle) or TBS buffer containing 0.5 mg ml^{-1} (86 μM) HI and 20 μM ThT (open circle) are passed over the surface. Surface fluorescence was measured every 10 min. The lines are hand-drawn. (B) After passing a 20 μM ThT solution for 120 min on the surface, the surface is washed at $t = 0$ with either ThT-free TBS buffer (closed circles) or ThT-containing buffer (open circles). The lines represent a linear fit to the data.

to bind to the tubing and the ATR-FTIR sensor area (4 cm^2 ; after 1 h, the bound HI is $4 \times 10^{-4} \text{ cm}^2 \times (0.2 \text{ mg cm}^{-2} + 0.013 \text{ mg cm}^{-2} \text{ min}^{-1} \times 60 \text{ min}) = 3.9 \mu\text{g}$, according to Eq. (1)). Second, the experimental temperature, a key parameter in protein unfolding, was 20 $^\circ\text{C}$ instead of 37 $^\circ\text{C}$. From the temperature dependence studied by Ballet et al. [24], the lag time before the onset of massive aggregation increases to 5 h at 20 $^\circ\text{C}$ compared to 2.5 h at 37 $^\circ\text{C}$. Note that the hydrophobic surface treatment used to treat the SPRi and the ATR-FTIR prisms or the coverslip are not exactly the same. A sixteen-carbon moiety was grafted onto gold, but only a six-carbon one was attached onto silicon or glass. Additional SPRi experiments were performed on a gold prism functionalized with an eight-carbon moiety (octyl-thiol) that gave similar results. We therefore believe that the length of the alkyl molecule used to make the material surface hydrophobic does not play a prominent role in HI adsorption and aggregation as long as the contact angle is close to 100 $^\circ$.

Bovine insulin aggregation at acidic pH and high temperature was studied by Bouchard et al. using FTIR [27]. These authors observe a heat-induced conformational transition characterized by the gradual disappearance of the characteristic α -helix peak (1651 cm^{-1}) concomitantly with the appearance of characteristic β -sheet peaks (1670 and 1627 cm^{-1}). In our study, the final HI aggregates obtained upon contact with hydrophobic surfaces present a very similar FTIR signature (Fig. 6E): a major peak at

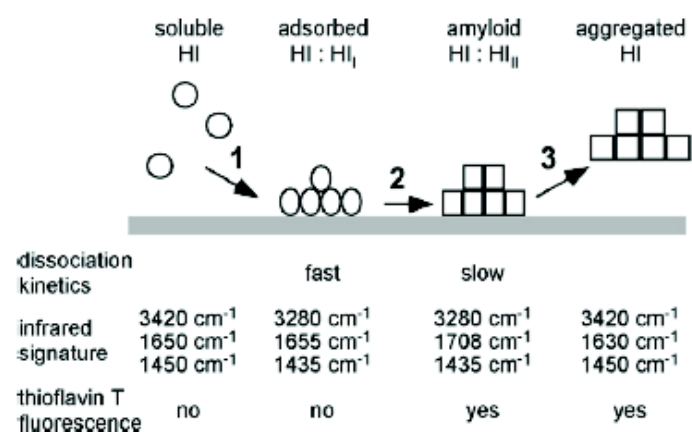


Fig. 9. Intermediates in the formation of HI amyloid fibers on hydrophobic surfaces. The scheme summarizes the different steps in the conversion of soluble HI into amyloid HI aggregates that takes place on hydrophobic surfaces. (1) Soluble insulin adsorption and accumulation on the surface; it is accompanied by changes in the infrared amide A and I' bands. (2) Formation of HI amyloid fibers adsorbed on the surface, characterized by the appearance of the 1708 cm⁻¹ peak, ThT fluorescence and reinforcement of HI binding to the surface. (3) Dissociation of the HI amyloid fibers.

1628 cm⁻¹ (72.1%) and three additional peaks at 1652 cm⁻¹ (16.6%), 1662 cm⁻¹ (2.4%) and 1669 cm⁻¹ (8.9%) (data not shown). The 1628 cm⁻¹ peak fits with the observation that characteristic FTIR β -sheet maxima of protein amyloid fibrils extend from 1611 to 1630 cm⁻¹ [28]. The final insulin aggregates formed at hydrophobic surfaces are therefore similar to the ones formed in solution at high temperature and acidic pH. Nevertheless, Bouchard and co-workers did not characterize any intermediate conformational state, in contrast to our study. We describe a conformation for adsorbed insulin, which has a different FTIR signature than the final HI aggregates (see below).

A clear accumulation of HI on the surface precedes the onset of ThT-positive fluorescence. This accumulation was reported by Ballet et al. [21], but the limited sensitivity and long processing time of the direct biochemical method prevented their documenting it precisely. SPRI experiments show that HI adsorption proceeds in two phases: first, the very fast binding of an HI monolayer, followed by the slow but steady accumulation of HI on top of the monolayer. Assuming that HI adsorbs uniformly, about two protein layers would be present on the surface at the onset of the ThT fluorescence. This signal pattern illustrates the mechanism of insulin aggregation on hydrophobic surfaces: soluble HI is indeed able to bind to adsorbed HI, increasing the local HI concentration tremendously, which is a prerequisite to the formation of aggregates. The precision of SPRI further allows differentiating two HI populations adsorbed on the material surface, characterized by their dissociation kinetics: one strongly bound to the surface, which dissociates slowly, and another one less strongly bound, which dissociates more easily.

Infrared spectroscopy reveals that adsorbed HI is in a conformational state that is distinct from soluble HI and from suspended HI amyloid aggregates. The amide A and amide I' bands are indeed both shifted to lower energy. It is known that the position of the amide A band, which corresponds to NH stretching, is sensitive to hydrogen bonding [29]. Its shift from 3420 cm⁻¹ to 3276 and 3204 cm⁻¹ thus indicates that adsorbed HI is involved in more hydrogen bonding than soluble HI. The existence of a specific conformation for adsorbed HI is in accordance with Ballet et al. [21], who showed that the bacterial chaperone DnaK recognizes a specific conformation on adsorbed HI. DnaK could bind, though with a diminished affinity, on aggregated HI fibers released in solution, indicating that adsorbed HI and aggregated HI have distinct confor-

mations. In ATR-FTIR, the amide I band in adsorbed HI is also unique. As shown in Fig. 7, it consists of four peaks, at 1635, 1655, 1687 and 1708 cm⁻¹. Assuming that the assignation of the different amide I peaks provided in the literature for soluble proteins [29,30] also holds for adsorbed proteins, we can interpret the 1635 and 1687 cm⁻¹ peaks as indicative of the presence of β -sheet, and the 1655 cm⁻¹ peak as the residual presence of α -helices. By analogy with the case of cytochrome c [31] and fibroin [32], the 1708 cm⁻¹ peak could be due to intermolecular β -sheets. Furthermore, its shape slowly evolves as HI accumulates over the surface, showing that some maturation takes place (Fig. 7A). Since the kinetics of the 1708 cm⁻¹ peak's appearance roughly matches that of the slow dissociation component evidenced by SPRI, we propose that two states of adsorbed HI are present, corresponding to the fast and slow dissociation components. The first one (HI_I), characterized by a prominent peak at 1655 cm⁻¹ (Fig. 7A, HI adsorbed after 1 or 5 min), very similar to that of soluble HI, would dissociate fastest. The second one (HI_{II}), with a characteristic peak at 1708 cm⁻¹ (Fig. 7A, HI adsorbed at 80 min), would dissociate ten times more slowly. Both would be intermediates in the transition from soluble HI to HI amyloid aggregates. Since the HI_I \rightarrow HI_{II} transition is completed in about 30–40 min (Fig. 7), it is tempting to assume that HI_{II} is ThT-positive whereas HI_I is not. HI_I would thus represent pre-amyloid adsorbed HI and HI_{II} amyloid aggregates (adsorbed HI and amyloid HI in Fig. 9). HI_{II} dissociation from the material surface would allow the formation of mature amyloid fibers in solution. In this state, the infrared signature is different from that of amyloid aggregates bound to the surface, but both are ThT-positive. The mechanical detachment of insulin amyloid fibers has been studied by Ballet et al. [24].

This study underlines the importance of considering the material surface when dealing with protein stability issues. It reveals the complexity of a multi-step adsorption mechanism and the existence of conformationally different protein species that cooperate to form amyloid fibers. Insulin–material interactions are governed by a complex interplay between the hydrophobicity, surface charge and topography of the material. Indeed, it was shown that insulin, although carrying a net negative charge at physiological pH, accumulates in significant amounts on negatively charged, hydrophilic polystyrene sulfonate (water contact angle: 50–60°) [33]. On uncharged poly(ethylene oxide)-coated surfaces (water contact angle: 3.5°), however, no insulin adsorption is measurable [21]. Moreover, Pandey and co-workers have studied the influence of increasing surface hydrophobicity and topography on the nucleation rate using mixed self-assembled monolayers of amine- and octyl-silanes [34]. They show that the lag time of insulin aggregation varies as a function of the amine fraction on the surface and that the morphology of the aggregates depends on the surface chemistry and topography. From these studies we conclude that the conditions that inhibit insulin adsorption on materials and material-induced aggregation, are maximal wettability (water contact angle <5°) and the absence of charges. Further work is clearly needed to examine whether the mechanisms outlined in the case of HI also hold true for other proteins in contact with hydrophobic surfaces, or for HI in contact with other surface chemistries.

Acknowledgements

This work was supported by the ANR grant "Stabilization of Therapeutic Proteins". L.N. was supported by a PhD grant from the Rhone-Alpes Region (Macodev program). B.J. was an exchange student from Delhi University. P.G. was a summer student from Toronto University, supported by a mobility grant from the Rhone-Alpes Region. We thank Catherine Picart and Flora Gilde for access and help with the ATR-FTIR apparatus. The authors acknowledge the "Pôle de Capteurs Thermométriques et

Calorimétrie" of the Institut Néel laboratory for the use of the oxygen plasma etcher.

Appendix A. Figures with essential colour discrimination

Certain figures in this article, particularly Figs. 3, 6 and 7, are difficult to interpret in black and white. The full colour images can be found in the on-line version, at <http://dx.doi.org/10.1016/j.actbio.2012.09.025>.

References

- [1] Westermark P, Benson MD, Buxbaum JN, Cohen AS, Frangione B, Ikeda S, Masters CL, Merlini G, Saraiva MJ, Sipe JD. Amyloid fibril protein nomenclature. *J. Amyloid* 2002;9:197–200.
- [2] Astbury WT, Dickinson S, Bailey K. The X-ray interpretation of denaturation and the structure of the seed globulins. *Biochem J* 1935;29:2351–2360.1.
- [3] Dobson CM. Protein misfolding, evolution and disease. *Trends Biochem Sci* 1999;24:329–32.
- [4] Rudall KM. The proteins of the mammalian epidermis. *Adv Protein Chem* 1952;7:253–90.
- [5] Koo EH, Lansbury PT, Kelly JW. Amyloid diseases: abnormal protein aggregation in neurodegeneration. *Proc Natl Acad Sci USA* 1999;96:9989–90.
- [6] Adams MJ, Blundell TL, Dodson EJ, Dodson GG, Vijayan M, Baker EN, et al. Structure of rhombohedral 2 zinc insulin crystals. *Nature* 1969;224:491–5.
- [7] Feingold V, Jenkins AB, Kraegen EW. Effect of contact material on vibration-induced insulin aggregation. *Diabetologia* 1984;27:373–8.
- [8] Loughheed WD, Albisser AM, Martindale HM, Chow JC, Clement JR. Physical stability of insulin formulations. *Diabetes* 1983;32:424–32.
- [9] Sefton MV, Antonacci GM. Adsorption isotherms of insulin onto various materials. *Diabetes* 1984;33:674–80.
- [10] Loughheed WD, Woulfe-Flanagan H, Clement JR, Albisser AM. Insulin aggregation in artificial delivery systems. *Diabetologia* 1980;19:1–9.
- [11] Dische FE, Wernstedt C, Westermark GT, Westermark P, Pepys MB, Rennie JA, et al. Insulin as an amyloid-fibril protein at sites of repeated insulin injections in a diabetic patient. *Diabetologia* 1988;31:158–61.
- [12] Störkel S, Schneider HM, Müntefering H, Kashiwagi S. Iatrogenic, insulin-dependent, local amyloidosis. *Lab Invest* 1983;48:108–11.
- [13] Moores B, Drolle E, Attwood SJ, Simons J, Leonenko Z. Effect of surfaces on amyloid fibril formation. *PLoS One* 2011;6:e25954.
- [14] Kowalewski T, Holtzman DM. In situ atomic force microscopy study of Alzheimer's beta-amyloid peptide on different substrates: new insights into mechanism of beta-sheet formation. *Proc Natl Acad Sci USA* 1999;96:3688–93.
- [15] Giacomelli CE, Norde W. Influence of hydrophobic Teflon particles on the structure of amyloid beta-peptide. *Biomacromolecules* 2003;4:1719–26.
- [16] McMasters MJ, Hammer RP, McCarley RL. Surface-induced aggregation of beta amyloid peptide by ω -substituted alkanethiol monolayers supported on gold. *Langmuir* 2005;21:4464–70.
- [17] Chi EY, Frey SL, Winans A, Lam KLH, Kjaer K, Majewski J, et al. Amyloid-beta fibrillogenesis seeded by interface-induced peptide misfolding and self-assembly. *Biophys J* 2010;98:2299–308.
- [18] Schladitz C, Vieira EP, Hermel H, Möhwald H. Amyloid-beta-sheet formation at the air-water interface. *Biophys J* 1999;77:3305–10.
- [19] Sluzky V, Tamada J, Klibanov A, Langer R. Kinetics of insulin aggregation in aqueous solutions upon agitation in the presence of hydrophobic surfaces. *Proc Natl Acad Sci USA* 1991;88:9377–81.
- [20] Sluzky V, Klibanov AM, Langer R. Mechanism of insulin aggregation and stabilization in agitated aqueous solutions. *Biotechnol Bioeng* 1992;40:895–903.
- [21] Ballet T, Bruckert F, Mangiagalli P, Bureau C, Boulangé L, Nault L, et al. DnaK prevents human insulin amyloid fiber formation on hydrophobic surfaces. *Biochemistry* 2012;51:2172–80.
- [22] Lavalle P, Gergely C, Cuisinier FJG, Decher G, Schaaf P, Voegel JC, et al. Comparison of the structure of polyelectrolyte multilayer films exhibiting a linear and an exponential growth regime: an in situ atomic force microscopy study. *Macromolecules* 2002;35:4458–65.
- [23] Picart C, Ladam G, Senger B, Voegel J-C, Schaaf P, Cuisinier FJG, et al. Determination of structural parameters characterizing thin films by optical methods: a comparison between scanning angle reflectometry and optical waveguide lightmode spectroscopy. *J Chem Phys* 2001;115:1086.
- [24] Ballet T, Nault L, Pandey L, Bruckert F, Bureau C, Boulangé L, et al. Insulin adsorbed on hydrophobic surfaces stimulates the formation and release of insulin amyloid fibers. Submitted for publication.
- [25] Barth A, Zscherp C. What vibrations tell us about proteins. *Q Rev Biophys* 2002;35:369–430.
- [26] Dzwolak W, Smirnovas V, Jansen R, Winter R. Insulin forms amyloid in a strain-dependent manner: an FT-IR spectroscopic study. *Protein Sci* 2004;13:1927–32.
- [27] Bouchard M, Zurdo J, Nettleton E, Dobson CM, Robinson CV. Formation of insulin amyloid fibrils followed by FTIR simultaneously with CD and electron microscopy. *Protein* 2000;9:1960–7.
- [28] Zandomenighi G, Krebs MRH, McCammon MG, Fändrich M. FTIR reveals structural differences between native beta-sheet proteins and amyloid fibrils. *Protein Sci* 2004;13:3314–21.
- [29] Kong J, Yu S. Fourier transform infrared spectroscopic analysis of protein secondary structures. *Acta Biochim Biophys Sin* 2007;39:549–59.
- [30] Mizushima S-I, Tsuboi M, Shimanouchi T, Tsuda Y. Spectroscopic investigation of the strength of hydrogen bonds formed by amides. *Spectrochim Acta* 1955;7:100–7.
- [31] Marboutin L, Boussac A, Berthomieu C. Redox infrared markers of the heme and axial ligands in microperoxidase: bases for the analysis of c-type cytochromes. *J Biol Inorg Chem* 2006;11:811–23.
- [32] Hu X, Kaplan D, Cebe P. Determining beta-sheet crystallinity in fibrous proteins by thermal analysis and infrared spectroscopy. *Macromolecules* 2006;39:6161–70.
- [33] Jeworrek C, Hollmann O, Steitz R, Winter R, Czeslik C. Interaction of IAPP and insulin with model interfaces studied using neutron reflectometry. *Biophys J* 2009;96:1115–23.
- [34] Pandey LM, Le Denmat S, Delabouglise D, Bruckert F, Pattanayek SK, Weidenhaupt M. Surface chemistry at the nanometer scale influences insulin aggregation. *Colloids Surf B* 2012;100C:69–76.

Chapter 5: Kinetic modification of surface-induced insulin aggregation by short peptide sequences

5.1. Aim of the study

In the previous chapter, we studied insulin adsorption and changes in structure by Surface Plasmon Resonance, Infrared spectroscopy and fluorescence microscopy. In the following, we used those techniques to study the aggregative activity of peptide LVEALYL.

Our interest to this peptide was driven by the paper by Ivanova *et al.* (2009) who showed that this peptide was able to reduce insulin lag-time, at sub-stoichiometric amounts and at pH 2.5⁴⁸. In their work, two insulin peptides were studied: LVEALYL (Residues B11-B17 in insulin sequence) and SLYQLENY (Residues A12-A19 in insulin sequence). Both are able to form amyloid fibers at pH 2.5. Only the first one influences insulin aggregation, in a complex manner. At substoichiometric concentrations, the peptide accelerates insulin nucleation, shorting the nucleation times without changing the aggregation growth rate (Fig.5.1). At stoichiometric concentrations and above, the peptide decreases the insulin aggregation growth rate. (see Figure 5.1)

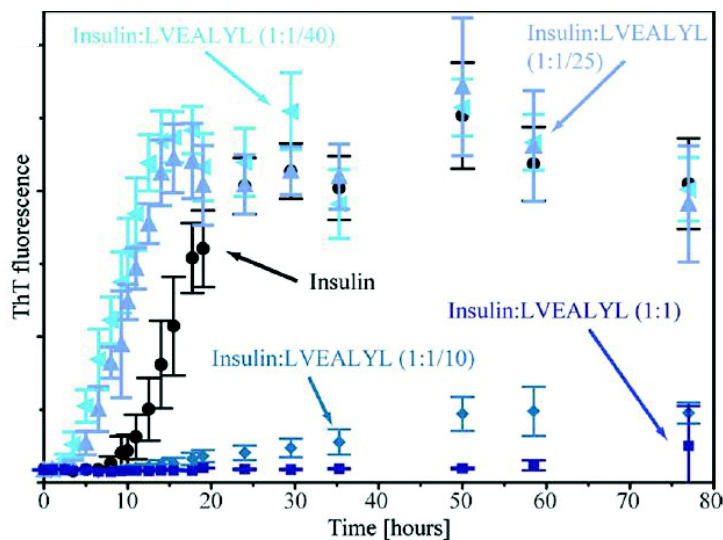


Figure 5.1: Fibrillation assay showing that B-chain LVEALYL accelerates insulin fibril formation when added to the reaction mixture at low concentrations, but inhibits insulin fibril formation at higher concentrations.

(Figure from Ivanova *et al.*⁴⁸)

5.2. Surface-dependant effect of LVEALYL peptide on insulin aggregation

The effect at sub-stoichiometric concentration was puzzling. We hypothesized that the acceleration of nucleation could be due to a surface effect. In Ivanova *et al.*, experiments were performed at pH 2.5, as they usually are. I first reproduced their work at pH 2.5, 37°C, and observed that hydrophobic surfaces were required. No aggregation took place on PEG-coated microwell plates. Then, I showed that at pH 7.3⁸⁸, substoichiometric amounts of the LVEALYL peptide also accelerated insulin nucleation, but not aggregation growth rate. I also proved that hydrophobic surfaces were required to obtain this effect of the peptide at pH 7.3. As a conclusion, I proved that the LVEALYL peptide accelerates insulin nucleation in a surface-dependant manner, independently to the pH¹⁰⁵. Moreover, it was previously⁸⁸ proven

that the chaperone DnaK was able to bind aggregated insulin and surface adsorbed insulin, but was not able to bind soluble insulin. This shows that adsorbed insulin involves some conformational changes and exposes a segment recognized by DnaK. Rüdiger *et al.*¹¹³ showed that DnaK binds to an insulin B chain peptide encompassing the LVEALYL segment. This exposed segment is therefore likely to be involved in insulin aggregation mechanism. I further proved that (i) DnaK is also able to counterbalance the LVEALYL peptide effect on insulin aggregation, and (ii) DnaK binds aggregated LVEALYL peptide. These results suggest that the LVEALYL segment may be a part of the sequence exposed by insulin when adsorbed to the surface.

This work and the structural model proposed by Ivanova *et al.* convinced us that the LVEALYL sequence played a central role in insulin aggregation. Furthermore, the fact that the peptide act only in presence of hydrophobic surfaces leads us to hypothesize that the peptide first interacted with the surface, providing a surface that helped the insulin conformational change. We therefore demonstrated this hypothesis (see following article). To this purpose, we first pre-incubated a hydrophobic surface with the peptide and observed that the lag-time for insulin aggregation increased thanks to the adsorbed peptide. Furthermore, the presence of the peptide potentializes insulin binding on hydrophobic surfaces. In addition, we showed that the adsorbed peptide adopts a β -sheet rich conformation. Finally, ATR-FTIR experiments confirm that the supplementary HI bound in the presence of the peptide adsorbed in a β -sheet structure. This is shown in the paper exposed below.

5.3. Minimum structure of an amyloidogenic peptide consists of alternating hydrophilic and hydrophobic amino-acids

We then took advantage of the peptide effect on insulin aggregation to gain insights in the molecular motives needed to induce insulin conformational change. This is going to be the second part of the article. To this purpose, we decided to use mutants of the peptide, mixed with insulin solution and to observe the insulin aggregation kinetic changes induced by the different peptide sequences. See amino acid structures and energy of transfert in water pH 7 in table 5.1.

Looking at the model of insulin amyloid fibers⁴⁸, we noticed that two glutamate (E) residues are close in the structure (Figure 5.2). We assumed that, at pH 7.3, the presence of these two negative charges was unfavorable for the protein/peptide interaction. Consequently, we imagined that changing the charged E residue for a polar residue, like Threonine (T), would increase the interaction with insulin and hence increase its effect on insulin aggregation. In the same line of thought, a positively charged residue, like Lysine (K) or Ornithine (O) should even present a stronger interaction with insulin and a higher acceleration of insulin aggregation. Assuming that the peptide could have the same conformation on the surface that the amyloid structure, a repulsive electrostatic interaction could therefore take place between the E (residue 3) in the peptide sequence and the E (residue B13) in insulin.

amino acid ($\Delta G_{\text{transfer}}$)	one letter code	structure	amino acid ($\Delta G_{\text{transfer}}$)	one letter code	structure
glutamic acid (-8.2)	E		tyrosine (-0.7)	Y	
aspartic acid (-9.2)	D		phenylalanine (3.7)	P	
threonine (1.2)	T		tryptophane (1.9)	W	
serine (0.6)	S		alanine (1.6)	A	
lysine (-8.8)	K		leucine (2.8)	L	
ornithine (-9.8)	O		proline (-0.2)	P	

Table 5.1: Structure, one letter code and energy of transfer in water of amino acids used in this thesis. Energy of transfer of the amino acid in water at pH 7 ($\Delta G_{\text{transfer}}$) is in kcal.mol⁻¹.

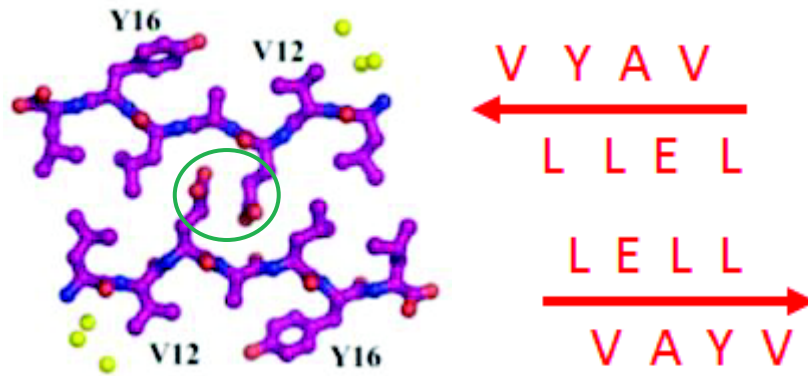


Figure 5.2: LVEALYL segments interactions in fibril aggregates at pH 2. Inside the green circle: two Glutamate (E) residues (negatively charged at pH 7 but neutral at pH 2).

(Image from Ivanova et al.⁴⁸)

As expected, the LVTALYL peptide further decreased the insulin lag-time compared to the wild type peptide LVEALYL, specifically in the presence of hydrophobic surfaces. However, it appeared that the LVKALYL and LVOALYL peptides (O is Ornithine amino-acid) had no effect on insulin aggregation albeit they bear positive charge. Consequently, it seems that the charge interaction between the two glutamate (E) residues between the peptide and the insulin molecule is not a key parameter of the peptide efficiency to enhance insulin aggregation.

Then, we studied another mutant peptide, LVÆALYL, which conserved the same amino-acid composition, but contains a single inversion in the middle of the sequence. This inversion was chosen because we supposed it should be highly disturbing the peptide/insulin interactions due to the change in the position of the glutamate (E) charge, leading to an ineffective peptide. To our surprise, it appeared that this peptide was even more efficient than the wild-type in decreasing the lag-phase. It was as effective as the LVTALYL peptide. Again, LVTALYL and LVÆALYL peptides have significant effects only in presence of hydrophobic surface. It must be noted that none of the peptide tested aggregated by itself in the conditions studied (37°C pH 7.3 for 24 hours). The strong effect of the inverted LVÆALYL was puzzling until I did a seeding experiment showing that peptide binding to the surface was required. Preincubating a hydrophobic surface with the LVÆALYL peptide induces an important decrease of insulin nucleation time (see Table 1 and Figure 3 in following paper). The adsorbed peptide acts as a seed for further insulin aggregation.

The seeding experiments prompted us to examine how a peptide could bind on a hydrophobic surface. Since insulin is α -helical in solution, and converted into β -sheets in amyloid aggregates, it is likely that the peptide would bind in β -sheet conformation to the surface through hydrophobic amino-acids, and would be stabilized by inter-peptidic H-bonds (see Figure 5.3). In a β -sheet structure, the lateral chains of the amino-acids are organized in a planar structure, perpendicularly to the β -sheet plan. Furthermore, these lateral chains are alternatively distributed on both sides on the main chain. In the case of hydrophobic surface, it is thus likely that half of the amino-acids are orientated to the hydrophobic surface, and the

other half are orientated to the solution, or to the incoming insulin molecules. Taking in account the hydrophobicity of each lateral chain, it is possible to evaluate which of the two conformations of the peptide β -strand should be energetically favored compare to the other. The negative charge on the glutamate (E) residue makes it very polar and hydrophilic. It follows that the wild type and swapped peptides will bind to hydrophobic surfaces with a different configuration (see Figure 5.4). As a consequence, the LVEALYL peptide presents only 3 hydrophobic lateral chains to the hydrophobic surface, whereas LVAELYL peptide has 4 hydrophobic amino-acids facing the surface. This justifies to a higher adsorption of this mutant peptide on the surface, observed by BCA, which could explain the effect of the EA \rightarrow AE swap. Similarly, LVTALYL (peptide 3) peptide conformation analysis on hydrophobic surface shows that this peptide could have a similar organization than the LVAELYL peptide, with 4 hydrophobic amino-acids facing the surface (see Figure 5.4), because T is weakly hydrophobic, which leads to similar adsorbed stability than the LVAELYL peptide. Since the effect of the peptides is related to their presence on the hydrophobic surface, a better peptide adsorption could explain a stronger effect of the peptides on insulin aggregation. Consequently, according to these results, it seems that the peptide action on insulin aggregation kinetic is dependent on its stability to form stable β -sheets on the surface.

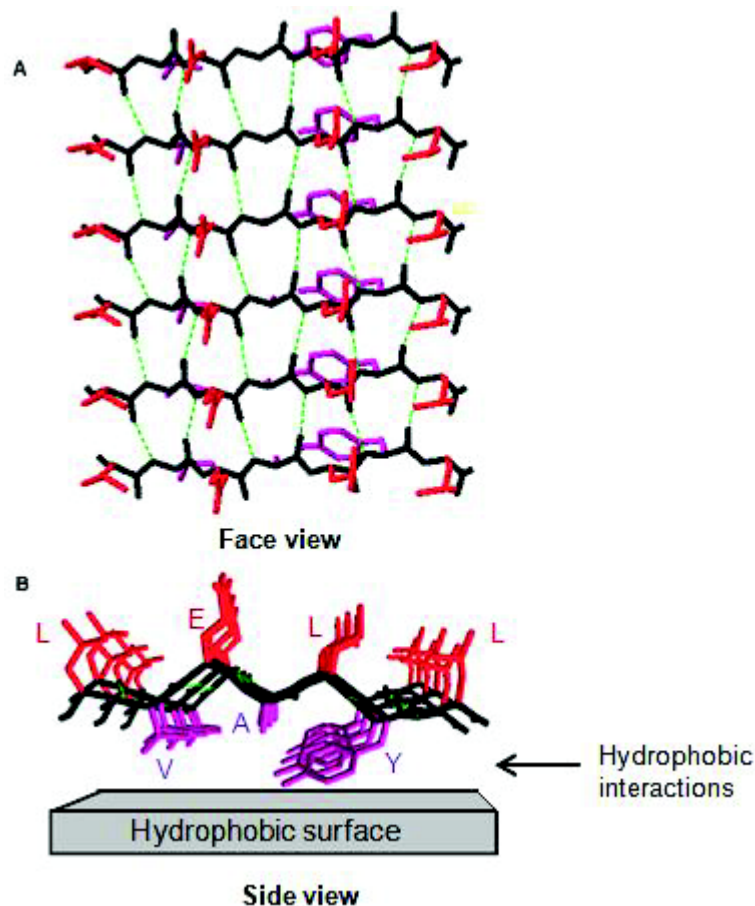


Figure 5.3: **A.** Face view of LVEALYL peptide organized in β -sheet, stabilized by intermolecular H-bonds (green dot points). **B.** Side view of LVEALYL peptide, organized in β -sheet on a hydrophobic surface. Main chain in dark, lateral chains in red or violet, depending on their position (top or bottom) to the main chains plan. Figure made with *Protein Data Base Swiss PDB Viewer* using the atomic coordinates of the LVEALYL segment in the putative HI amyloid structure.

To test for the importance of the peptide secondary structure organization on the surface, we introduced a proline (P) amino-acid in the sequence, which is known to be a structure-disruptor residue. It appears that all the proline-containing peptides (*LPEALYL*, *LVEPLYL*, *LVPTLYL* and *LVTPLYL*) have no effect on insulin aggregation, confirming the importance of peptide secondary structure for its interaction with insulin.

In order to confirm that the peptides effect on insulin is dependent on the β -conformation of the adsorbed peptide, but not (or weakly) dependant on the sequence, we used peptides with alternating hydrophilic and hydrophobic residues. First, half of the amino-acid sequence was modified from the *LVEALYL*, keeping all amino-acids that presumably face the hydrophobic surface and changing all the others into Serine (S) (see Scheme 4.2). We obtained the *SVSASYS* peptide (peptide 4). We similarly, modified the *LVAELYL* peptide to get the *LSASLSL* peptide (peptide 5). These 2 peptides reduced insulin aggregation lag-time. Nevertheless, the *LSASLSL* adsorbed more on surfaces and reduced more the insulin aggregation lag-time than the *SVSASYS*. This again can be related to the fact that *LSASLSL* could present 4 hydrophobic residues to the hydrophobic surface (L-A-L-L) compared to the *SVSASYS* which would present only 3 hydrophobic residues (-V-A-Y-) (see Scheme 5.2).

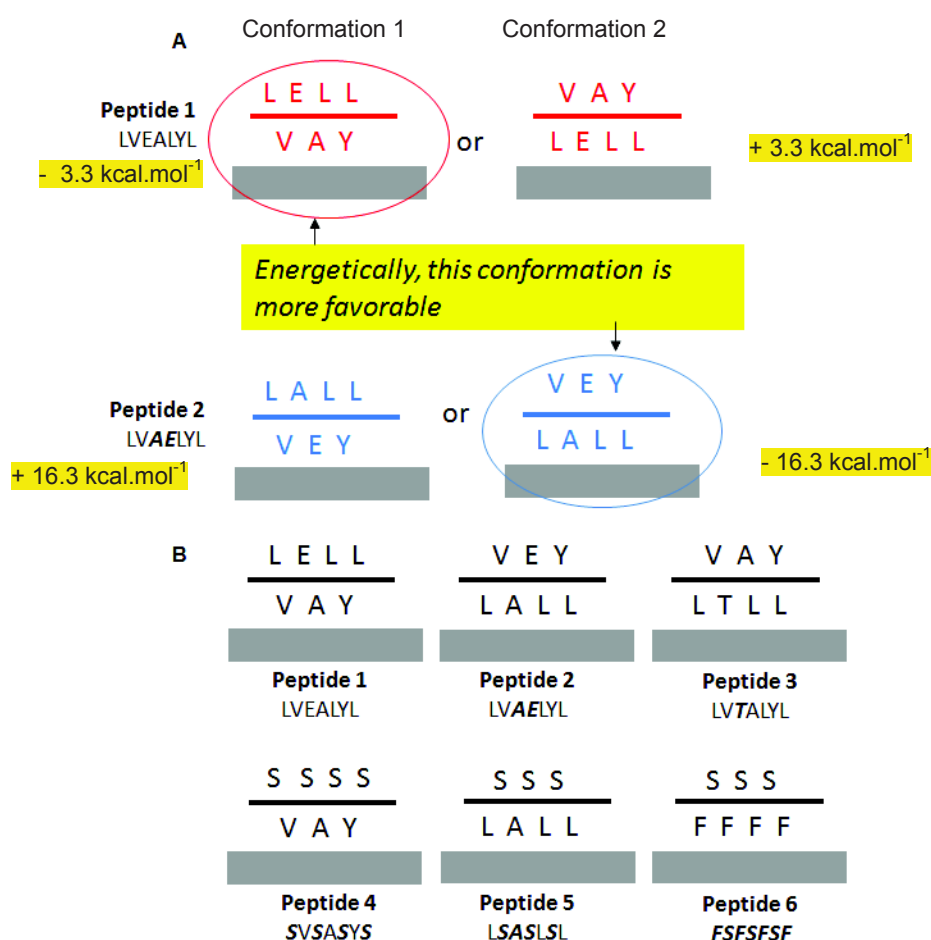


Figure 5.4: **A.** LVEALYL (peptide 1, red) and LVAELYL (peptide 2, blue) peptides possible β -strand conformations on hydrophobic surface. Activation energies are shown in yellow and calculated as explain in Material and Methods in the following article. **B.** Most energetically favorable β -strand conformation of LVEALYL, LVAELYL, LVTALYL, *SVSASYS*, *LSASLSL* and *FSFSFSF* peptides on hydrophobic surface.

Moreover, the *FSFSFSF* peptide presents a significant ability to reduce insulin aggregation lag-time (lag time = 3.1 h ± 0.3), although it has no common amino-acid with the wild-type peptide. Nevertheless, the presence of phenylalanine residue (F) seems to reduce the activity of the peptide compare to the Tyrosine (Y). In line with this observation, the *LVEVLF* (lag time = 3.6 h ± 0.2) was also less efficient than the *LVEVLYL* peptide (lag time = 2.4 h ± 0.2) to induce insulin nucleation time reduction. Similarly, the same effect is observed for tryptophan residue (W), as the *LVEALW* induced less insulin nucleation time reduction (lag time = 3.8 h ± 0.3) than the *LVEALYL* peptide (lag time = 1.5 h ± 0.2). It could be due to a steric effect, as these residues are among the largest amino acids.

In addition to these aggregation kinetic studies, insulin adsorption on hydrophobic surfaces in presence of the *LVAELYL* peptide was analyzed with Surface Plasmon Resonance. The peptide adsorption by itself gives a small signal, but in the presence of the peptide, more insulin binds to the surface (see Figure 1 in following paper). Moreover, Infrared spectroscopy confirmed that the wild type, the *LVAELYL* and the *LSASLSL* peptides adsorb on hydrophobic surface in a β -sheet conformation (see Figure 2 in following paper). It remains to be shown that *FSFSFSF* and *LSASLSL* peptides are adsorbed in a β -strand conformation.

5.4. Model of action of amyloidogenic peptides on surface-induced insulin aggregation

Our results show that the local increase of insulin concentration on the surface due to the peptide would lead to fast nuclei formation on the surface and consequently to shorter lag-times in insulin aggregation kinetics. One remaining question is the nature of these nuclei that are formed rapidly. A nucleus is a site or a structure where insulin fibril elongation kinetics constants prevail on fibril dissociation constants. It is unclear if, in presence of the peptide, (i) the insulin nuclei are build on the surface similarly to insulin nuclei without the peptide, or if (ii) the peptide-covered surface became itself a large nucleus. The fact that the presence of the peptide does not change significantly the growth phase of insulin aggregation suggests that the number of nuclei is not modified by the peptide, which is not consistent with the second hypothesis. Nevertheless, further investigations are needed to answer this question.

This is the first model of action of pro-aggregating peptides taking in account the presence of surfaces (see Figure 5.3). This molecular mimicry is mostly sequence independent and could have an effect on other proteins that aggregates in highly β -sheet structures in presence of surfaces (some monoclonal antibodies, IAPP, A β peptide...). Conversely, we propose that the peptides that bind to surfaces in alpha-helical conformation could be able to prevent protein aggregation by covering the surface in a conformation which would not be able to stabilize proteins in high β -sheet content.

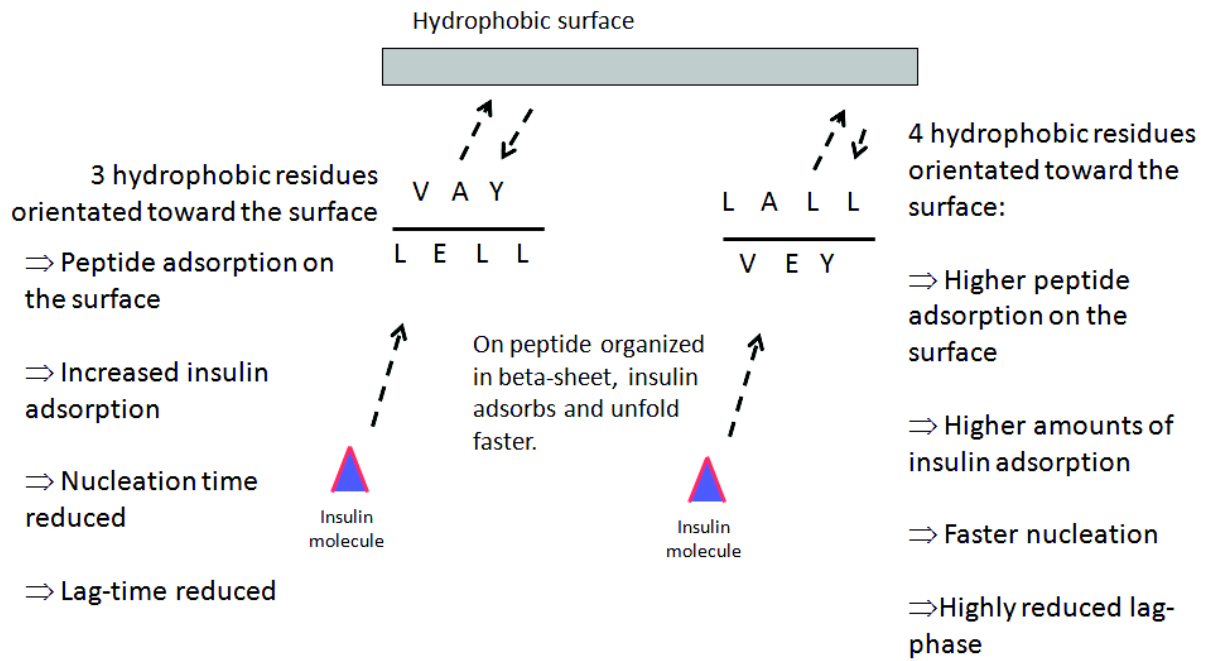


Figure 5.3: Model of peptide action on insulin aggregation lag-time: examples of the LVEALYL and LVAELYL peptides.

A question that remains after this study is the peptide/insulin interaction. For the wild type peptide, the peptide interaction with insulin can be similar to what Sawaya *et al.*⁷⁹ and Ivanova *et al.*⁴⁸, with antiparallel β -sheet interaction of the LVEALYL sequence (see Figure 5.4, case 1). Nevertheless, for mutant peptides, the sequence exposed to insulin is different. It can be proposed that insulin interact in antiparallel (Fig. 5.4 case 2) or parallel β -sheets (not shown), involving the LVEALYL sequence. It can also be proposed that the interaction involves the SLYQLENY sequence, in antiparallel (Fig. 5.4 case 3) or parallel (Fig. 5.4 case 4) interaction with the peptide. In the both 2 cases, the LVEALYL insulin sequence, which is proposed to be the main contributor to fibril formation, is exposed to solvent. As a result, further insulin/insulin interactions could be facilitated.

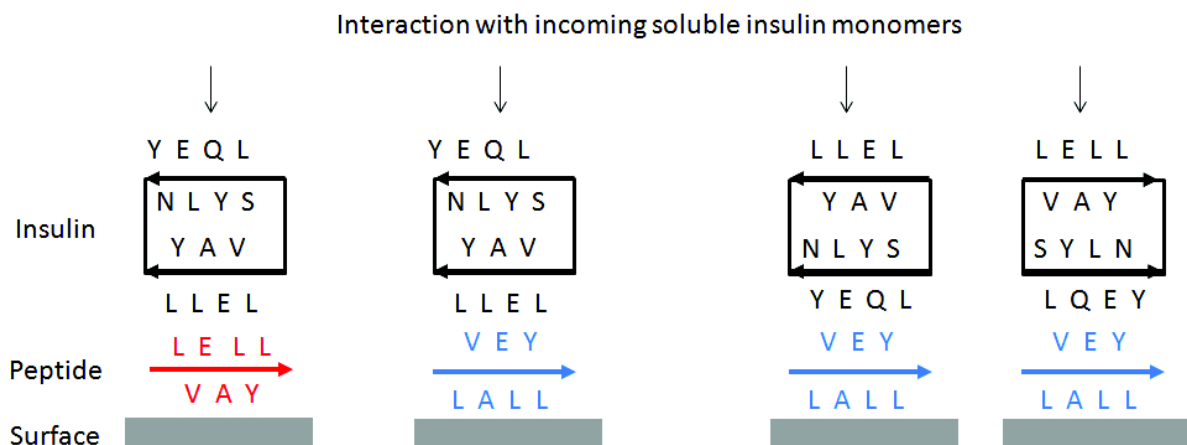


Figure 5.4: Model of peptide/insulin interaction, examples of the LVEALYL and LVAELYL peptides. Surfaces are in grey, LVEALYL peptide in red, LVAELYL peptide in blue and insulin molecules in black. Insulin is schemed here with LVEALYL and SLYQLENY sequences in β -sheets similar to those described in Ivanova *et al.*⁴⁸

Peptides that form β -sheets on hydrophobic surfaces accelerate surface-induced insulin amyloidal aggregation

Laurent Nault¹, Charlotte Vendrely¹, Yves Bréchet², Franz Bruckert¹, and Marianne Weidenhaupt^{1*}

(1) Laboratoire des Matériaux et du Génie Physique, Phelma-Minatec, 3 parvis Louis Néel BP257, F-38016 Grenoble Cedex

(2) Laboratoire de Science et Ingénierie des Matériaux et des Procédés, Phelma-Campus, 1130 rue de la Piscine, BP 75, F-38402 Saint-Martin d'Hères Cedex

* corresponding author

Accepted to FEBS Letters the 16th November 2012.

Abstract

Interactions between proteins and material or cellular surfaces are able to trigger protein aggregation *in vitro* and *in vivo*. The human insulin peptide segment LVEALYL is able to accelerate insulin aggregation in the presence of hydrophobic surfaces. We show that this peptide needs to be previously adsorbed on a hydrophobic surface to induce insulin aggregation. Moreover, the study of different mutant peptides proves that its sequence is less important than the secondary structure of the adsorbed peptide on the surface. Indeed, these pro-aggregative peptides act by providing stable β -sheets to incoming insulin molecules, thereby accelerating insulin adsorption locally and facilitating the conformational changes required for insulin aggregation. Conversely, a peptide known to form α -helices on hydrophobic surfaces delays insulin aggregation.

Introduction

Many protein solutions are prone to aggregation *in vitro*. This is particularly critical for therapeutic proteins because aggregate formation decreases drug activity and can induce immunogenic reactions when injected in patients. For instance, the most used protein hormone, insulin, can be found in fibrillar form at the site of frequent insulin injections, which causes injection amyloidosis [1]. Moreover, the increasing prevalence of human diseases, characterized by the presence of large amounts of aggregated proteins, like amyloidosis, Alzheimer's, Parkinson's and prion diseases, requires mechanistic studies to understand protein aggregate formation.

The mechanism of protein fibrillation is generally modeled in three steps. 1- Conformational changes, due to defects in the cellular folding processes or due to an abnormal protein environment. 2- Nucleation, during which the misfolded individual proteins

are stabilized, mostly by intermolecular interactions, which drives the formation of oligomers. Such oligomers can then evolve into stable nuclei. 3- Growth, during which the nuclei will grow upon binding of other misfolded proteins, leading to the formation of large fibrils. *In vivo*, the growing step has a major impact on cell survival [2].

Human insulin (HI) has often been used as a model protein in fibrillation studies as it is a non-expensive protein which fibrillates rapidly *in vitro*, particularly at low pH, high temperature, high ionic strength and on hydrophobic surfaces [3–5]. In a preceding study [6], we have shown that the presence of hydrophobic surfaces is essential for HI fibrillation at pH 7.3 and 37°C. Such surfaces were assumed to induce the unfolding of HI monomers adsorbed on them, but it appears that all three steps, including nucleation and fibril elongation also take place on the surface, leading eventually to the release of mature fibrils into solution.

Different studies show that the onset of aggregate nucleation can be accelerated by the addition of peptides, which present a pro-aggregative activity [7–10]. Such amyloidogenic peptides are mostly hydrophobic, have beta-sheet conformation and are capable to fibrillate by themselves. They are commonly derived from protein sequences suspected to be involved in fibrillation. In 2009, Ivanova *et al.* [11] showed that a 7 amino-acid peptide sequence, present in the B chain of native HI (LVEALYL, residues B11–B17), was able, at sub-stoichiometric concentrations, to accelerate the nucleation step of human HI at pH 2.5. On the other hand, it is known that surface hydrophobicity has an important effect on the HI nucleation rate [12] and, given the hydrophobic nature of this peptide, its amyloidogenic properties are likely to rely on its interaction with hydrophobic surfaces. We recently demonstrated that the LVEALYL peptide-driven acceleration of HI aggregation is strictly dependent on the presence of hydrophobic surfaces [6].

In this study, we use mutants of the LVEALYL peptide together with HI to investigate the effects of amino acid changes in this sequence on HI aggregation kinetics, protein adsorption on hydrophobic surfaces and changes in peptide secondary structure. When compared to previous studies measuring the effects of amyloidogenic peptides on HI aggregation kinetics, we have introduced two novel and important parameters: first, the experiments are done at physiological pH and, second, the effect of material surface hydrophobicity is analyzed. Our work suggests that the LVEALYL peptide and mutants thereof induce HI aggregation only if they are previously adsorbed on the material surface. Moreover, it appears that their primary sequence is less important than their ability to stably adsorb in beta-structure on the surface.

Materials and Methods

Chemicals

If not otherwise stated, all chemicals were purchased from Sigma-Aldrich. Experiments were conducted in TBS (25 mM TRIS-HCl, pH 7.3, 125 mM NaCl and 2 mM MgCl₂). HI (recombinant human HI, expressed in yeast) solutions were prepared at 0.5 mg.mL⁻¹ (86 μM). All solutions were filtered (0.22 μm) before use. Peptides were purchased from Genecust (Luxembourg) and a concentrated stock solution was made at 860 μM in 20 mM NaOH.

Monitoring of aggregation kinetics

HI aggregation assays were conducted as 8 replicates in plastic 96-well microplates. Polystyrene (Greiner Bio-One, water contact angle = 85° ± 4.7), or PEO-coated, (Corning 3651 microplate, water contact angle = 3.5° ± 5.8) microplates were used. In fluorescence assays, black polystyrene microplates were used (Nunc Nunclon® Δ Surface). The plates were covered by plastic sheets, incubated at 37°C and shaken at 1,200 rpm (Heidolph Titramax, 1.5

mm vibration orbit). Thioflavin T (ThT, 20 μ M) fluorescence was directly measured ($\lambda_{ex} = 450$ nm, $\lambda_{em} = 482$ nm) in the wells [6].

Kinetic analysis

The aggregation kinetics proceeds in three phases: a lag phase, where the signal is not statistically different from the baseline (mean \pm standard deviation), a linear growth phase and a plateau phase. Experimentally, the lag time was defined by the intercept between the linear growth phase and the baseline. The growth rate was defined as the slope of the linear phase and the plateau as the maximum value attained. The parameters were calculated on individual kinetics corresponding to different replicates, and the given statistics represent the average and the standard deviation for each parameter.

Surface seeding using peptides

96-well microplates were filled with peptides diluted at 8.6 μ M in TBS and incubated at 37°C, 1200 rpm for 10 minutes. Wells were then washed once with TBS and filled with HI (86 μ M) and incubated at 37°C, 1200 rpm. HI aggregation kinetics was monitored using ThT as described.

Quantification of adsorbed protein

HI (86 μ M) and/or peptide solutions (8.6 μ M) were incubated in 96-well hydrophobic microplates in TBS for 30 minutes at 37°C, 1200 rpm. Wells were then washed with TBS and adsorbed peptides and protein were desorbed using Sodium Dodecyl Sulfate (5 %) for 30 minutes at 37°C and 1200 rpm. The peptide and/or protein concentrations were determined using the Bicinchoninic Assay.

Adsorption kinetics and infrared spectroscopy

Peptide and HI association and dissociation kinetics were studied on PEG- and C₁₆-coated surfaces by SPRi as described in Nault *et al.* [13]. The peptide conformation in solution and adsorbed on hydrophobic surfaces was determined by FTIR transmission or ATR-FTIR experiments, respectively [13].

Estimation of the hydrophobic contribution to the peptide binding energy to hydrophobic surfaces

The hydrophobic contribution to the binding energy of 7 amino acid long peptides with a hydrophobic surface was calculated for two β -sheet configurations by the following formula:

$$\Delta G_{conf1} = \sum_{1,3,5,7} \Delta G_i - \sum_{2,4,6} \Delta G_i \quad (\text{Eq. 1})$$

$$\Delta G_{conf2} = \sum_{2,4,6} \Delta G_i - \sum_{1,3,5,7} \Delta G_i \quad (\text{Eq. 2})$$

$$\Delta G_{sol} = \sum_1^7 \Delta G_i \quad (\text{Eq. 3})$$

where ΔG_i is the free transfer energy of the i^{th} amino acid side chain [14]. Conformation 1 and 2 correspond to the exposure of even or odd amino acids to solvent, respectively. The third calculation corresponds to the hydrophobic contribution of the peptide transfer energy into solution, with all amino acids exposed to the solvent. This calculation does not consider the

contribution of N- and C-termini, which is identical for all peptides and conformations. In the interpretation of the data, peptides are assumed to adopt the conformation having the lowest interaction energy.

Results

The LVEALYL peptide accelerates HI aggregation kinetics when bound to hydrophobic surfaces

As shown before [6], the LVEALYL peptide accelerates HI aggregation kinetics at pH 7.3 and 37°C, only in the presence of hydrophobic surfaces (polystyrene) but not in the presence of PEG-coated surfaces preventing HI binding. The maximum effect is observed at a peptide concentration of 8.6 μM , and the lag time is reduced by 66% on average (Table 1). We quantified the peptide adsorption on microwells. Table 1 shows that 0.06 μg LVEALYL peptide remains adsorbed on the hydrophobic surface after 30 min, corresponding to 4.5 % of the initial peptide amount. These minute amounts have a dramatic effect on HI aggregation, as shown by the following seeding experiment. Hydrophobic surfaces were pre-incubated for 10 minutes with peptide, washed and exposed to HI. Peptide pre-adsorption decreases the lag-time of HI aggregation by 63 % (Table 1). It is noteworthy that preincubating the surface with HI does not decrease the lag time (Table 1, line1). Moreover, supplying the solution with 0.06 μg LVEALYL peptide, does not affect HI aggregation kinetics. The pro-aggregative effect of the peptide is therefore due to the adsorbed fraction on the surface. Upon adsorption, but not in solution, the LVEALYL peptide presents molecular features that strongly accelerate HI binding and aggregation.

The pro-aggregative peptides LVEALYL and LVAELYL have a strong effect on HI aggregation and adsorption kinetics

The strong effect of the LVEALYL peptide on HI aggregation kinetics prompted us to study different peptide variants (Table 1). All experiments were done at the same peptide (8.6 μM) and HI (86 μM) concentrations. None of the peptides studied here aggregates on its own, nor triggers HI aggregation in the presence of PEG-coated surfaces, confirming that the kinetic enhancement is dependent on the presence of hydrophobic surfaces. Among the peptides studied, the swapped peptide LVAELYL, where the third and fourth amino acid are exchanged, exhibits a remarkably short lag time (0.4 h). This peptide binds also strongly to hydrophobic surfaces (0.1 μg) and pre-adsorption reduces the lag time of HI aggregation down to 2.3 h (Table 1).

The binding kinetics of both peptides, alone and in combination with HI, were studied by SPRi (Fig. 1A and B). As shown before [13], HI alone binds specifically to hydrophobic surfaces, in a biphasic manner. Fast, reversible binding is followed by a slower increase of HI adsorption, resulting in the formation of a strongly bound HI pool ([13] and Fig. 1). The LVEALYL and LVAELYL peptides alone bind weakly to the hydrophobic surface (Fig. 1A and B). Mixing one of the peptides with HI enhances protein adsorption on the hydrophobic surface but has no effect on HI adsorption on the hydrophilic surface (Fig. 1A and B). More specifically, upon injection of HI with either peptide, there is an increase of the fast association component (first minutes of Fig. 1A and B) and of the slow dissociation component of the SPRi signal (last 10 min of Fig. 1A and last 20 min of Fig.1B), compared to HI alone. The addition of sub-stoichiometric amounts of both peptides to HI therefore induces the formation of strongly adsorbed HI on the hydrophobic surface. A direct measurement of protein binding to microwell plastic surfaces confirms this result (Table 1). In the presence of the swapped peptide, the total protein bound is larger than in the presence of HI or peptide

alone. The wild-type peptide also enhances, but to a lesser extent, protein binding on the surface (Table 1).

The wild type and the swapped peptides adopt a β -sheet conformation on hydrophobic surfaces

Infrared spectroscopy is sensitive to protein secondary structure in the amide I band and was used to analyze the conformational state of different peptides in solution (FTIR) or adsorbed on hydrophobic surfaces (ATR-FTIR). Decomposing the band into peaks shows that in solution, the wild type and swapped peptides adopt mostly unstructured conformations (Fig. 2A and B, left panels). Indeed, they present a major peak around 1645 cm^{-1} , indicative of random coil conformation, which accounts for 37 and 32 % in the wt and swapped peptides' solution spectra, respectively (Table 1S). After 30 min adsorption on hydrophobic surfaces, the amide I band of both peptides changes and reveals prominent peaks around 1694, 1680, 1664, 1648, 1633 and 1622 cm^{-1} (Fig. 2A and B, right panels). This indicates that the conformation of the adsorbed wild type and swapped peptides consists predominantly of internal and intermolecular β -sheets and β -turns, the residual unstructured coil contribution consisting of 17 and 22 %, respectively (Table 1S).

Characterization of other amyloidogenic peptides: influence of primary and secondary structure

In order to explain the peptide effect on the HI aggregation rate, a simple model was built, assuming that amyloidogenic peptides adopt a β -sheet conformation parallel to the material surface, stabilized by intermolecular hydrogen bonds and side chain interactions with the hydrophobic surface on one side, and the solvent on the other side. Amino acid side chains indeed alternatively point to one side or the other of a β -strand. For a 7 amino acid long peptide, two such conformations exist, with odd or even amino acids exposed to solvent. For each conformation, the hydrophobic contribution of amino acid side chains to the binding energy was summed up using the transfer energies from benzene to water, amino acids exposed to solvent contributing positively, while those in contact with the surface contributing negatively (Eq. 1 and 2). In this way, one can determine the energetically most favorable conformation of a given peptide adsorbed on a hydrophobic surface. For a stable adsorption, this energy should be lower than the one for the peptide in solution (Eq. 3). For the LVEALYL peptide, the most stable β -sheet conformation exposes the L-E-L-L amino acids towards the solution, and the -V-A-Y- amino acids towards the surface (interaction energy = $-3.3\text{ kcal.mol}^{-1}$). For the LVAELYL peptide, the most stable conformation exposes the -V-E-Y- amino acids towards the solution, and the L-A-L-L amino acids towards the surface (interaction energy = $-16.3\text{ kcal.mol}^{-1}$). This justifies the better stability of the swapped peptide.

Two other peptides were studied, SVSASYS and LSASLSL, based on the wild-type and the swapped peptides respectively, where the amino acids supposed to face the surface were conserved and the ones turned to the solvent replaced by serines (S). For both peptides, the most stable conformation exposes hydrophilic S to the solution and hydrophobic amino acids to the surface (interaction energy = $-8.2\text{ kcal.mol}^{-1}$ for LSASLSL and $-1.1\text{ kcal.mol}^{-1}$, for SVSAVYS). In the HI aggregation assay, the SVSASYS and the LSASLSL peptides behaved similarly to their parent peptides (Table 1), showing that the primary sequence exposed to the solvent was not critical. The stronger effect of the LSASLSL peptide compared to the SVSASYS one is again justified by its higher stability on hydrophobic surfaces. The LSASLSL peptide also presents a β -sheet rich conformation when adsorbed on hydrophobic surfaces (Fig. 2C and Table 1S), and enhances HI binding on the surface (Fig. 1).

To confirm the importance of peptide conformation on the surface, the (LKKLLKL)₂ peptide, known to form α -helices on hydrophobic surfaces [15] was tested. This peptide

indeed proved to have a completely different FTIR spectrum in solution or, when adsorbed on a hydrophobic surface when compared to the wildtype or swapped peptides (Fig. 2D, left and right panels). Its solution spectrum indicates that the (LKKLLKL)₂ peptide adopts β -sheet, random coil and α -helix conformations (60, 7 and 33 %, respectively; Table 1S). Strikingly, when adsorbed on a hydrophobic surface, its ATR-FTIR signature reveals a typical peak around 1655 cm⁻¹, which indicates that this peptide retains α -helical conformation (27%, Table 1S). When used in seeding experiments, no HI aggregation was observed for up to 30 h (Table 1). We therefore conclude that the conformation of the adsorbed (LKKLLKL)₂ peptide is not pro-aggregative but rather stabilizes HI.

Furthermore a proline residue (P), was introduced to disrupt the wildtype peptide secondary structure: LPEALYL, LVEPLYL and SVSPSYS. None of these three peptides affect HI aggregation kinetics (Table 1), which consolidates the importance of peptide β -sheet conformation on the surface.

Replacing the negatively charged glutamate residue (E) by a threonine (T) in the wild type or swapped peptide had no effect on the pro-aggregative property of the peptides, showing that electrostatic interactions were not determinant (LVTALYL and LVATLYL in Table 1). Again, the additional A to P mutation abolished the pro-aggregative effect of these peptides (LVTPLYL and LVPTLYL in Table 1).

Finally, we analyzed a peptide, ISISISI, exposing a series of three Ser (S) to the solution and being adsorbed via four Ile (I) to the hydrophobic surface. This peptide has a sequence that is similar to the LKLKLLKL peptide, known to form β -sheets on hydrophobic surfaces [15–17], and has no common residues with LVEALYL. The HI aggregation lagtime, obtained using this peptide in seeding experiments is 0.4 h. This peptide therefore also shows a pro-aggregative effect on HI-surface aggregation and confirms that the primary sequence is not paramount.

Discussion

In this study, we show that the LVEALYL peptide, adsorbed on hydrophobic surfaces at sub-stoichiometric concentrations, favors HI binding and the formation of HI amyloid fibers. We previously showed that HI adsorbed on hydrophobic surfaces exposes a motive containing the LVEALYL peptide, which is recognized by the DnaK/DnaJ bacterial chaperones [6]. Combining these two observations indicates how HI amyloid aggregates form on hydrophobic surfaces. HI molecules adsorb and change their conformation, exposing the LVEALYL peptide that allows further HI binding in a β -sheet conformation. The conformational change induced on HI directly adsorbed on the surface thus propagates to incoming HI that binds to adsorbed HI. This mechanism is in accordance with the insulin amyloid fiber model proposed by Ivanova *et al.* [11]. There is some similarity with the prion self-replication mechanism, with soluble and adsorbed HI playing the role of PrP^C and PrP^{Sc}, respectively. An important difference is that HI amyloid aggregates released into solution do not seed efficiently fiber growth.

This work confirms the central role played by the LVEALYL peptide, pointed out by Ivanova *et al.* [11]. We confirm that the SLYQLENY peptide, another HI segment putatively involved in the HI amyloid structure, does not stimulate HI aggregation in contact with hydrophobic material surfaces. This is reasonable since this peptide is globally hydrophilic ($\Delta G_{\text{sol}} = -12.3 \text{ kcal.mol}^{-1}$) and therefore not likely to adopt a β -sheet conformation on hydrophobic surfaces. Interestingly, introducing two mutations so that hydrophobic amino acids are placed at even locations (LYQLEAY peptide, $\Delta G_{\text{conf 1}} = -13.9 \text{ kcal.mol}^{-1}$) has a mild but significant effect on HI aggregation kinetics (lag time = 3.4 h \pm 0.1). Our study, although

limited to a subset of all possible peptides, strongly suggests that the interaction of HI with the adsorbed peptide is not highly sensitive to the primary structure, as long as the adsorbed peptide provides a stable β -structure on the surface. Furthermore, the effect of the short peptides on insulin aggregation is related to their surface binding energy (minimum -5 kcal.mol^{-1}) and requires a β -sheet conformation (Fig. 3). The interaction with the peptide-borne β -structure drives stable HI adsorption by triggering an α to β transition in HI and consequent β -sheet formation between neighboring peptides and incoming HI molecules. This effect is reminiscent of the effect of silver iodide crystals on super-cooled H_2O that induces the formation of ice crystals because of a match between the crystal structures of β -AgI and ice. It is already known that short peptides are able to influence full-length protein amyloid aggregation [7–9]. Nevertheless, the impact of container surface chemistry is not systematically taken into account, despite the fact that hydrophobic interfaces are known to be able to induce the aggregation of different proteins [5,18].

Acknowledgements

This work was supported by the ANR grant “Stabilization of Therapeutic Proteins”. Laurent Nault held doctoral fellowship from la Région Rhône-Alpes. We thank Catherine Picart and Flora Gilde for access to and assistance with the ATR-FTIR. The authors acknowledge the "Pôle de Capteurs Thermométriques et Calorimétrie" of the Institut Néel laboratory for the use of the oxygen plasma etching.

References

- [1] Dische, F.E., Wernstedt, C., Westermark, G.T., Westermark, P., Pepys, M.B., Rennie, J.A., Gilbey, S.G. and Watkins, P.J. (1988) Insulin as an amyloid-fibril protein at sites of repeated insulin injections in a diabetic patient. *Diabetologia* 31, 158-61.
- [2] Wogulis, M., Wright, S., Cunningham, D., Chilcote, T., Powell, K. and Rydel, R.E. (2005) Nucleation-dependent polymerization is an essential component of amyloid-mediated neuronal cell death. *J. Neurosci.* 25, 1071-80.
- [3] Brange, J., Andersen, L., Laursen, E.D., Meyn, G. and Rasmussen, E. (1997) Toward understanding insulin fibrillation. *J. Pharma. Sci.* 86, 517-25.
- [4] Ahmad, A., Uversky, V.N., Hong, D. and Fink, A.L. (2005) Early events in the fibrillation of monomeric insulin. *J. Biol. Chem.* 280, 42669-75.
- [5] Sluzky, V., Tamada, J., Klibanov, A. and Langer, R. (1991) Kinetics of insulin aggregation in aqueous solutions upon agitation in the presence of hydrophobic surfaces. *Proc. Natl. Acad. Sci. USA* 88, 9377-81.
- [6] Ballet, T., Brukert, F., Mangiagalli, P., Bureau, C., Boulangé, L., Nault, L., Perret, T. and Weidenhaupt, M. (2012) DnaK prevents human insulin amyloid fiber formation on hydrophobic surfaces. *Biochemistry* 51, 2172-80.

- [7] Scrocchi, L.A., Ha, K., Chen, Y., Wu, L., Wang, F. and Fraser, P.E. (2003) Identification of minimal peptide sequences in the (8–20) domain of human islet amyloid polypeptide involved in fibrillogenesis. *J. Struct. Biol.* 141, 218-227.
- [8] Du, H-N., Li, H-T., Zhang, F., Lin, X-J., Shi, J-H., Shi, Y-H., Ji, L-N., Hu, J., Lin, D-H. and Hu, H-Y. (2006) Acceleration of alpha-synuclein aggregation by homologous peptides. *FEBS lett.* 580, 3657-64.
- [9] Kim, J.R. and Murphy, R.M. (2004) Mechanism of accelerated assembly of beta-amyloid filaments into fibrils by KLVFFK(6). *Biophys. J.* 86, 3194-203.
- [10] Hong, D-P. and Fink, A.L. (2005) Independent heterologous fibrillation of insulin and its B-chain peptide. *Biochemistry* 44, 16701-9.
- [11] Ivanova, M.I., Sievers, S.A., Sawaya, M.R., Wall, J.S. and Eisenberg, D. (2009) Molecular basis for insulin fibril assembly. *Proc. Natl. Acad. Sci. USA* 106, 18990-5.
- [12] Sluzky, V., Klibanov, A.M. and Langer, R. (1992) Mechanism of insulin aggregation and stabilization in agitated aqueous solutions. *Biotech. and Bioeng.* 40, 895-903.
- [13] Nault, L., Guo, P., Jain, B., Bréchet, Y., Bruckert, F. and Weidenhaupt, M. (2012) Human insulin adsorption kinetics, conformational changes and amyloid aggregate formation on hydrophobic surfaces. *Acta Biomaterialia*, in press.
doi:10.1016/j.actbio.2012.09.025
- [14] Engelman, D.M., Steitz, T.A. and Goldman, A. (1986) Identifying nonpolar transbilayer helices in amino acid sequences of membrane proteins. *Annu. Rev. Biophys. Chem.* 15, 321-53.
- [15] DeGrado W.F. and Lear J.D. (1985) Induction of peptide conformation at apolar water interfaces. 1. A study with model peptides of defined hydrophobic periodicity. *J. American Chemical Society.* 107:7684-7689.
- [16] Collier G., Vellore N.A., Yancey J.A., Stuart S.J. and Latour R.A. (2012) Comparison Between Empirical Protein Force Fields for the Simulation of the Adsorption Behavior of Structured LK Peptides on Functionalized Surfaces. *Biointerphases.* 7:24.
- [17] Weidner T., Apte J.S., Gamble L.J. and Castner D.G. (2010) Probing the orientation and conformation of alpha-helix and beta-strand model peptides on self-assembled monolayers using sum frequency generation and NEXAFS spectroscopy. *Langmuir.* 26:3433-40.
- [18] McMasters, M.J., Hammer, R.P. and McCarley, R.L. (2005) Surface-Induced Aggregation of Beta Amyloid Peptide by ω -Substituted Alkanethiol Monolayers Supported on Gold. *Langmuir* 21, 4464-4470.

Tables

Legend to Table 1

Physico-chemical and pro-aggregative properties of different peptides. The binding energy corresponds to the hydrophobic contribution to the minimum interaction energy of the peptide bound to the surface, calculated by Eq. 1 or 2 (column 2). For the (LKKLLKL)₂ peptide no interaction energy was calculated since this peptide is in α -helical configuration. Lag times were determined from the aggregation kinetics of a 1:10 peptide:protein mixture (column 3) and for a surface first exposed to the indicated peptide (8.6 μ M) for 10 min, washed and then incubated with a fresh HI solution (86 μ M) (column 4). Adsorption of peptides and peptide plus HI mixtures on hydrophobic surfaces (2 cm²) was determined as described in Materials and Methods (column 5 and 6).

Table 1

Peptide sequence	Interaction energy (kcal. mol ⁻¹)	Lag time of HI aggregation kinetics (h)		Protein adsorbed on the surface after 30 min (μ g)	
		8.6 μ M peptide mixed with 86 μ M HI	After 10 min seeding	8.6 μ M peptide alone	8.6 μ M peptide mixed with 86 μ M HI
No peptide		4.4 \pm 0.4	4.3 \pm 0.4*		0.19 \pm 0.01
LVEALYL	- 3.3	1.5 \pm 0.2	1.7 \pm 0.3	0.06 \pm 0.01	0.21 \pm 0.01
LVAELYL	-16.3	0.4 \pm 0.1	2.3 \pm 0.3	0.10 \pm 0.01	4.28 \pm 0.10
LSASLSL	-8.2	0.5 \pm 0.1	2.5 \pm 0.3	0.13 \pm 0.01	0.25 \pm 0.01
SVSASYS	-1.1	2.0 \pm 0.1	ND	ND	ND
LPEALYL	-0.5	4.1 \pm 0.3	ND	ND	ND
LVEPLYL	-1.5	4.2 \pm 0.2	ND	ND	ND
SVSPSYS	-0.7	4.3 \pm 0.4	ND	ND	ND
LVTALYL	-6.1	0.5 \pm 0.1	2.7 \pm 0.3	0.16 \pm 0.04	1.6 \pm 0.2
LVATLYL	-6.9	0.6 \pm 0.1	1.8 \pm 0.3	0.15 \pm 0.02	0.5 \pm 0.2
LVTPLYL	-7.9	4.3 \pm 0.1	ND	ND	ND
LVPTLYL	-5.1	4.6 \pm 0.1	ND	ND	ND
ISISISI	-10.6	0.4 \pm 0.1	ND	ND	ND
(LKKLLKL) ₂	ND	> 30	ND	ND	ND

* seeding with 86 μ M HI

Legend to Figures

Figure 1: SPRi sensorgrams of protein adsorption on hydrophobic surfaces. The protein solutions (8.6 μM peptide, 86 μM HI or a mixture of 8.6 μM peptide and 86 μM HI) were injected at $t=0$ min and the association kinetics were monitored for 10 min (A) or 15 min (B). The surface was then washed with buffer and the protein dissociation kinetics were monitored for 15 min (A) or 20 min (B). The signal represented is the difference between the signal recorded on the C_{16} -coated side and the PEG-coated side of the prism. **(A)** SPRi curves obtained with peptides LVEALYL and LSASLSL, **(B)** SPRi curves obtained with peptide LVAELYL.

Figure 2: Amide I band of the LVEALYL (A), LVAELYL (B) and LSASLSL (C) and (LKKLLKL)₂ peptides in solution (left) and adsorbed on hydrophobic surfaces (right). Transmission FTIR spectra were recorded with 8.6 μM peptides in deuterated buffer. For ATR-FTIR, peptides were introduced at 8.6 μM in the flow chamber of a hexylmethyl-coated silicon prism. After 30 min, the prism surface was washed with buffer and the infrared spectra were recorded. Thick line: amide I band after linear baseline correction. Thin lines: decomposition of the amide I band into individual peaks.

Figure 3: Effect of different peptides on insulin kinetics. Aggregation kinetics of HI (86 μM) alone or mixed with 8.6 μM peptide were determined. The nucleation rates k (in the presence of peptides) and k_0 (in the absence of peptide) were calculated as the inverse of the lag time. For each peptide, the k/k_0 ratio is plotted as a function of the binding energy of the peptide on hydrophobic surfaces in β -strand conformation (Eq. 1 or 2). Circles: peptides without proline residue. Squares: peptides containing one proline residue. Data are from table 1. Lines are hand drawn.

Figures

Figure 1

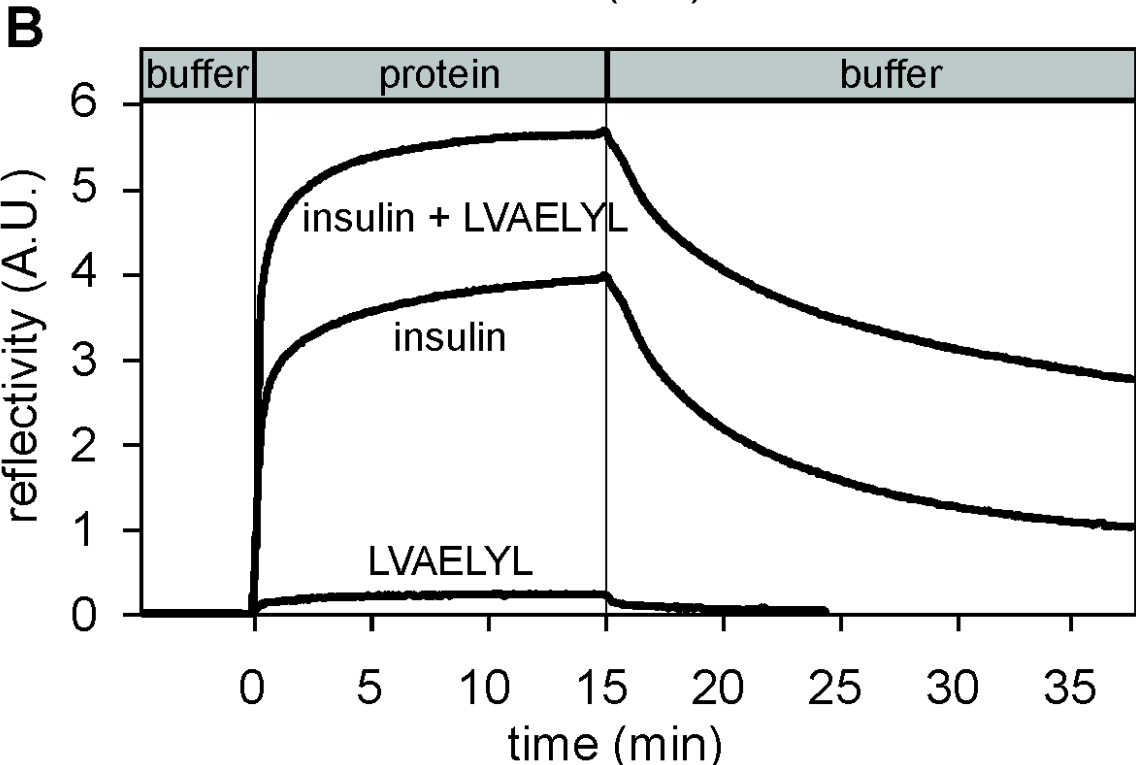
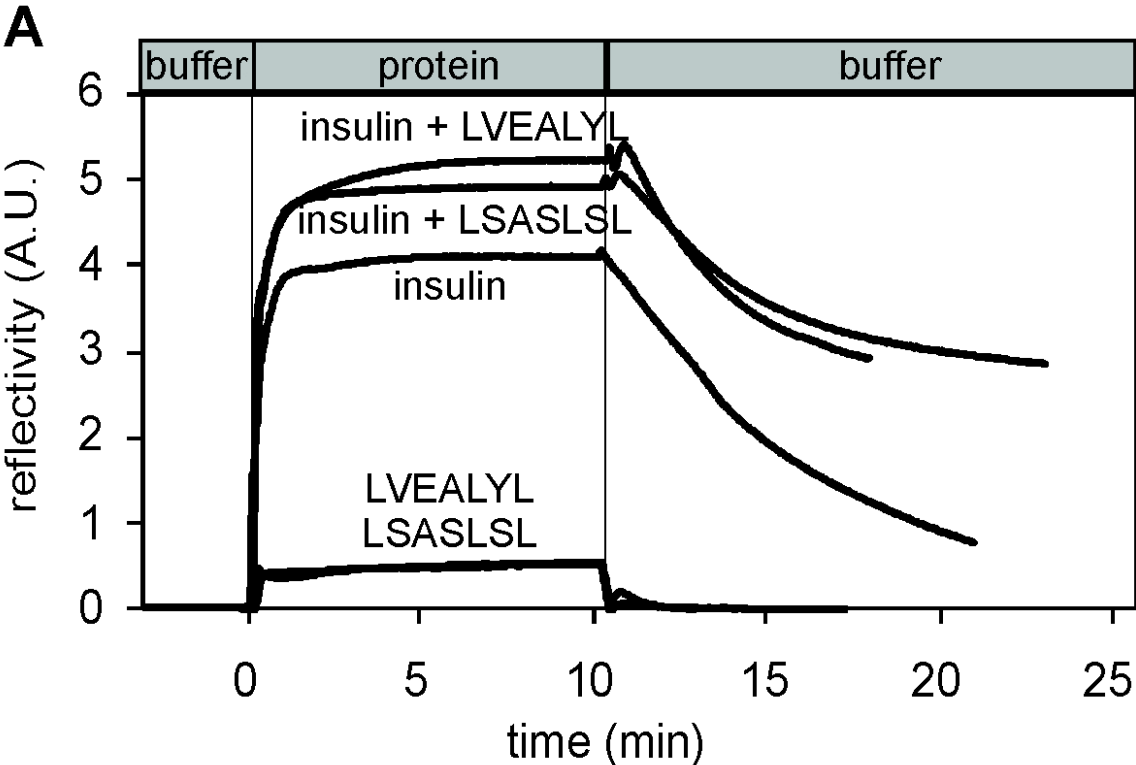


Figure 2

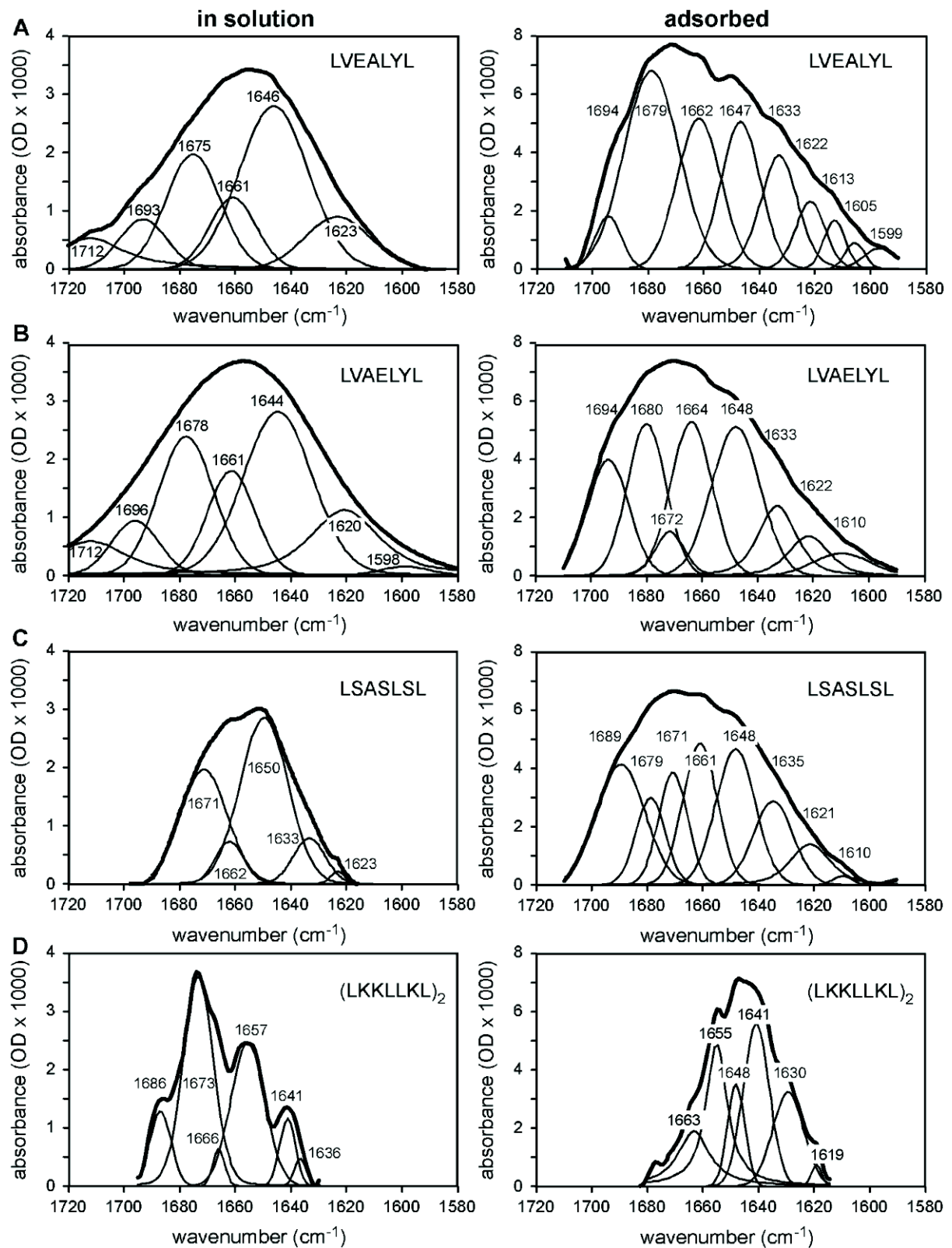
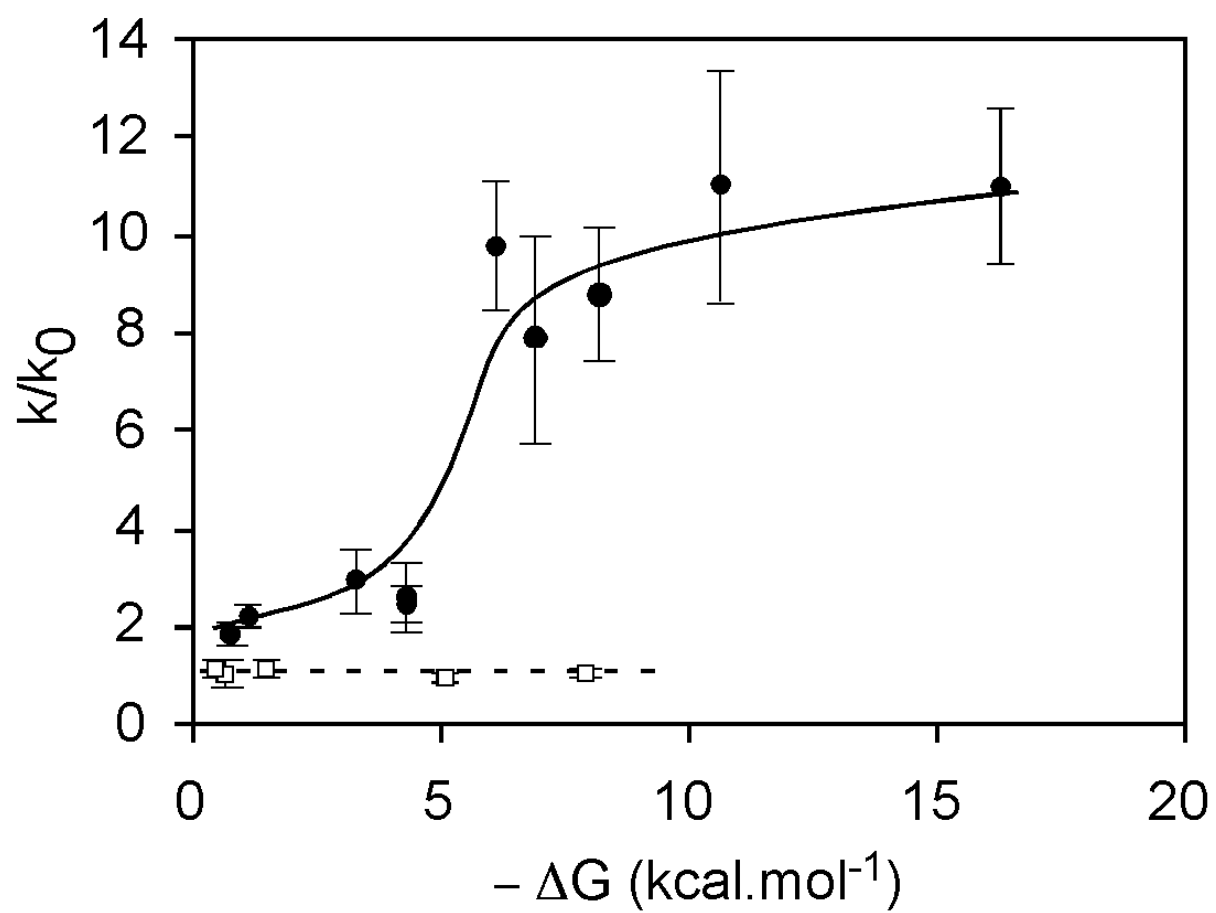


Figure 3



Supplementary data

Table 1S

	FTIR		ATR-FTIR		
	wavenumber (cm-1)	ratio %	wavenumber (cm-1)	ratio %	
LVEALYL			1596,9	2,0	
			1605,7	1,5	
			1613,0	3,2	
		1623,3	11,6	1621,7	6,2
			1632,9	13,5	
		1646,2	37,7	1646,8	17,4
		1661,0	11,2	1661,8	19,6
		1675,3	21,0	1678,8	32,5
		1693,3	8,0	1694,3	4,1
LVAEYL		1712,4	10,7		
		1598,2	1,1	1609,8	4,1
		1620,3	16,0	1621,6	6,2
			1633,0	10,1	
		1644,4	32,0	1647,8	22,4
		1661,3	13,7	1663,8	19,6
			1671,6	4,6	
		1677,7	21,1	1679,9	18,2
LSASLSL		1696,2	7,1	1693,7	14,8
		1712,5	9,0		
			1609,5	0,6	
		1622,9	1,1	1621,2	7,3
		1633,2	9,0	1634,6	12,2
		1649,5	49,2	1648,1	19,5
		1662,0	7,5	1660,8	17,9
(LKKLLKL) ₂		1671,3	33,2	1670,6	11,9
			1678,7	9,4	
			1689,4	21,2	
			1619,0	1,4	
		1636,5	2,2	1629,2	18,2
		1641,1	7,1	1640,7	26,1
			1648,0	10,8	
		1655,5	32,7	1655,0	27,0
	1666,0	3,0	1663,2	16,1	
	1673,4	44,5	1676,9	0,3	
	1687,1	10,5			

Table 1S summarizes the decomposition of the FTIR spectra presented in Fig. 2 into individual peaks and presents their relative contribution in %. Cells coloured in orange represent peaks assigned to β -sheets and β -turns. Cells coloured in yellow represent peaks assigned to random coil. Cells coloured in green represent peaks assigned to α -helices (Kong and Yu, 2007, Hu *et al.*, 2006).

Kong J and Yu S. Fourier Transform Infrared Spectroscopic Analysis of Protein Secondary Structures. 2007, *Acta Biochimica et Biophysica Sinica* 39:549-559.

Hu X, Kaplan D and Cebe P. Determining β -sheet crystallinity in fibrous proteins by thermal analysis and infrared spectroscopy. 2006, *Macromolecules* 39, 6161-6170.

Chapter 6: Discussion and conclusion

6.1. Thesis summary

This thesis aimed at improving our understanding of the aggregation mechanism of protein in contact with hydrophobic surfaces. We experimentally focused on the lag-time, which corresponds to the formation of aggregation nuclei. To this purpose, we investigated a protein of high therapeutic importance, human insulin, which is not expensive, and known to aggregate in contact with hydrophobic surfaces in time scales (less than 10 hours) that are compatible with daily experimental procedures. We managed to define the different molecular events that happen at the interface between hydrophobic materials and fluid phase leading to nucleus formation, fibril growth and the release of amyloid fibrils in solution.

Microwells plates aggregation kinetics monitored by Thioflavin T fluorescence have been used for studying nucleation time and fibril growth phase at different temperature and under different rotation speeds. Previous works ^{40,85} showed that insulin aggregation was promoted by hydrophobic surfaces and by agitation rates. We proposed a model ⁸⁸, explaining surface-induced insulin aggregation by insulin adsorption on surfaces, inducing an unfolding and an organization in amyloid fibers. These fibers were supposed to be released in solution after reaching a certain size but no mechanism was proposed to explain the release. Furthermore, even if it was observed that insulin adsorption on hydrophobic surfaces induced nuclei formation, alternative experimental protocols exist where no agitation is required. Delineating the exact proportion of aggregates formed in solution (homogeneous nucleation) and on surfaces (heterogeneous nucleation) is thus important. Evidences are brought here that nucleation takes place on the hydrophobic surfaces due to a decreased activation energy compare to nucleation in solution. Moreover, agitation has two antagonist effects on insulin nucleation: (i) it increases protein interactions and solution homogeneity, leading to shorter nucleation times, but (ii) it also destabilizes nuclei on the surfaces, leading to longer nucleation times. Finally, we showed that the release of completely formed fibrils in solution is due to hydrodynamic shear-stress that detaches the fibril grown on the surface adsorbed nuclei.

Nevertheless these initial studies did not give enough information on the nucleation molecular mechanism. The development of a protocol for studying the adsorbed protein ThT fluorescence microscopy and of surface treatment for Surface Plasmon Resonance imaging, coupled to the use of Infrared spectroscopy allowed obtaining adsorption and desorption kinetics of insulin on hydrophobic surfaces (SPRi) and extended inter-molecular β -sheets

formation detection (Infrared and Fluorescence Microscopy). We observed that insulin first accumulates on hydrophobic surfaces, and then forms in 30 to 40 minutes large amounts of inter-molecular β -sheets that are positive to ThT fluorescence and can be supposed to be pre-fibrillar aggregates. These β -sheet structures are strongly adsorbed to the surface and cannot be detached easily with buffer flowing, which is consistent with the mechanism of large surface fibrils detachment due to hydrodynamic shear-stress observed earlier, and with the fact that dynamic light scattering and micro-flow imaging experiments do not detect in solution insulin oligomers intermediates between monomeric insulin and 100 nm long fibrils⁴⁰.

Moreover, using these developed techniques, the study of mutants of an insulin segment peptide that is known to impact insulin aggregation⁴⁸ shown that, contrary to what was supposed previously, these peptides only act in presence of hydrophobic surfaces where they adsorb and enhance the insulin adsorption amounts. Furthermore, it appears that the peptide effect on insulin aggregation kinetic is not sequence dependant but requires a peptide spontaneous adsorption in β -strand conformation on the surface. That conformation seems to increase insulin affinity for the surface and to accelerate insulin unfolding and aggregation nuclei formation. These results indicate that any peptide long enough (7 amino-acids or more) composed of alternative hydrophobic and neutral hydrophilic residues should be able at sub-stoichiometric concentrations to highly reduce insulin nucleation time in presence of hydrophobic surfaces. Nevertheless, steric effects of biggest amino-acids residues could disturb that insulin nucleation time reduction.

Consequently, in this thesis, different ancient observations on insulin aggregation (agitation effect, pro-aggregative peptides actions) have been explained. Moreover, insulin adsorption, unfolding kinetics and fibrils growth have been described and a model of insulin aggregation in contact of hydrophobic surfaces can be proposed, explaining precedent insulin studies and the observations done in this thesis.

6.2. Surface-induced aggregation mechanism

Initial model for the mechanism of insulin aggregation in aqueous solutions in contact with hydrophobic surfaces was proposed by Sluzky *et al*⁸⁵. This model is exposed in Figure 6.1. According to this model, monomers as well as dimers and hexamers can reversibly adsorb on the surface. However, monomers are the least stable species and therefore may undergo conformational changes at hydrophobic interfaces. The partially unfolded monomers are then released in bulk solution, and can either refold to the native conformation (most

likely event) or combine with other unfolded monomers, initiating nucleation. Once a critical size is reached, the nuclei have sufficient surface area for stability and can start reacting with native molecules. The slow formation of stable nuclei would explain the lag phase observed in insulin fibrillation experiments, and the fast insulin depletion following the formation of stable nuclei would imply that native molecules participate in the final aggregation steps. Nevertheless, in this model, the nuclei assemble and grow in solution. But, seeding experiments showed (see Chapter 3) that nuclei are not present in solution but are adsorbed on the surface.

A new model was more recently proposed by Ballet *et al*^{88,105}. This model (see Figure 6.2) expose that in order to act as catalysts of amyloid fiber formation, hydrophobic surfaces have first to be covered with insulin monomers, which allows local increase of unfolded insulin concentration. That catalyzes the formation of aggregation nucleus formation. These aggregation nuclei catalyze insulin fibril growth on the surface, before their release in solution. Consequently, contrary to Sluzky's model, all the nucleation and fibril growth steps takes place on the surface in this model. In my work, different results exposed in precedent chapters show that insulin molecules adsorbs rapidly in few minutes on hydrophobic surfaces (part 1 in figure 6.2). Then, these monomers partially unfold and slowly acquire β -sheet conformation, as seen by Infrared spectroscopy (part 2 in Figure 6.2). The presence on the surface of these β structures increases insulin accumulation on the surface and accelerate insulin unfolding and α to β transition (part 3 in Figure 6.2). These locally accumulated unfolded insulin molecules can interact with each other, leading to large intermolecular β -sheets formations, positive to ThT fluorescence in 40 to 60 minutes. These structures are proposed to be growing fibrils. The mechanism of fibril growth on the surface (part 4 in Figure 6.2) is still non-understood. Nevertheless, in chapter 3, I was able to calculate activation energy of this fibril growth step. I also demonstrated that fibrils are mechanically detached from the surface when they reach a sufficient size (part 5 in Figure 6.2). New fibrils can then grow on the liberated surface, until the system reaches steady-state between insulin monomers and fibrils.

In addition, I propose a model of insulin aggregation in contact with hydrophobic surfaces in presence of pro-aggregative peptide, see Figure 6.3. Pro-aggregative peptide action is explained by that model. Due to their small size and their amino-acid sequence properties, peptides can diffuse faster than insulin and adsorbs rapidly in β -strand conformation on the surface. Then, similarly to what was observed previously, the presence

on the surface of β structures increases insulin affinity for the surface and accelerate insulin α to β transition. This faster local accumulation of unfolded insulin leads to faster aggregation nuclei formation, which is the major pro-aggregative peptide effect observed in that study.

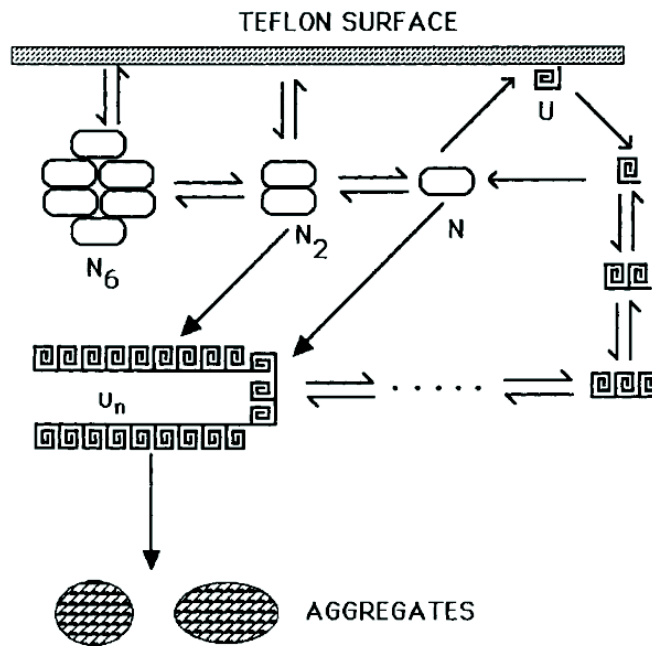


Figure 6.1: Schematic representation of the proposed mechanism of insulin aggregation on the teflon-water interface proposed by Sluzky *et al.*

(Figure modified from Sluzky *et al.* 85)

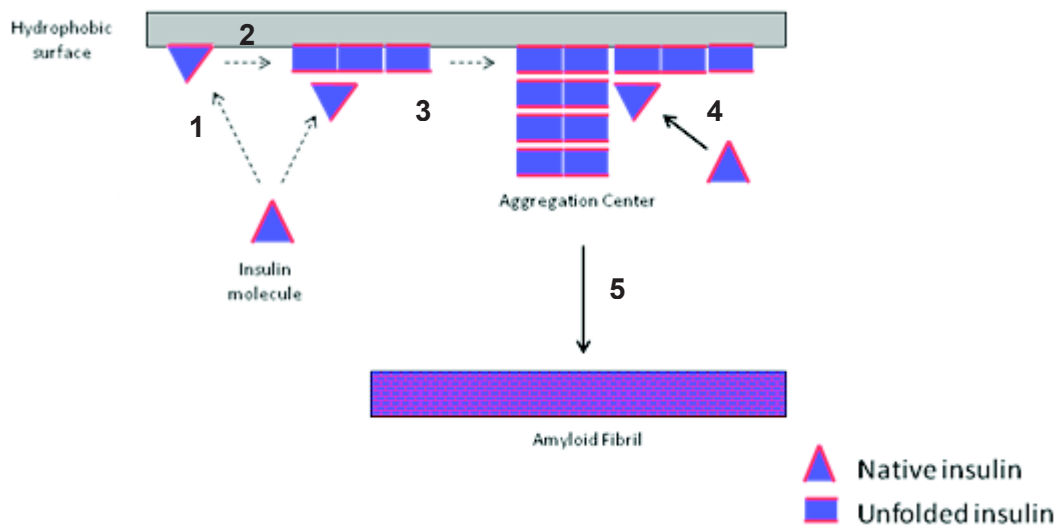


Figure 6.2: Schematic representation of the proposed mechanism of insulin aggregation on hydrophobic surfaces as proposed by Ballet *et al.*¹⁰⁵

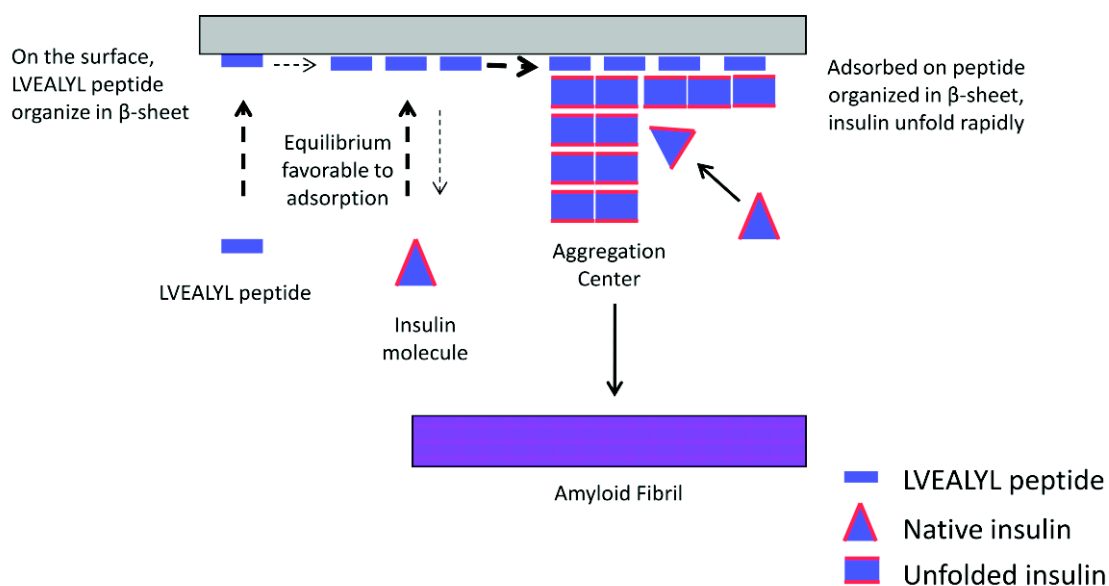


Figure 6.3: Schematic representation of the proposed mechanism of pro-aggregative peptides on insulin aggregation on hydrophobic surfaces proposed in this thesis.

6.3. Thesis discussion

A weakness of our strategy could be the difference in surface chemistry used in the different kinds of experiments. Aggregation kinetics were indeed measured on microwell plastic surfaces. SPRi, fluorescence in microscopy and ATR-FTIR were measured on C₁₆ alkyl-thiol, Dimethyl dichlorosilane and Phenyl dimethyl methoxysilane self-assembled monolayers. Nevertheless, despite the differences between the surfaces, protein accumulation and the presence of a strongly bound insulin fraction are always observed. Moreover, we observed that replacing dimethyl-dichloro silane by phenyldimethylmethoxysilane in microscopy experiments gives similar results. The same observation is done for C₁₆ alkyl-thiol or C₈ alkyl-thiol treated surface in SPRi. In microwell plates, the use of plates from different producers and of different composition does not change significantly the insulin aggregation kinetic. Moreover, Sluzky *et al.*^{40,85} performed experiments in presence of chemically different hydrophobic surfaces (water-air, teflon, polypropylene, surfacil siliconized glass). Changes in nucleation time and fibril growth characteristic time were observed, but the global shape of aggregation kinetics remained similar. Consequently, we can be confident that, as long as surface is hydrophobic enough (contact angle > 100°), the insulin aggregation mechanisms are not significantly changed.

An unexplained observation is the absence at pH 7 of pro-aggregative activity of mutant peptides LVKALYL and LVQALYL, where the negatively charged glutamate (E)

residue is replaced by a positively charged residue of similar size. According to our sequence independent model, the LVKALYL and LV~~O~~ALYL peptides should have similar effect than the LVEALYL peptide. Further work is needed to understand why the charge of that residue is important in this case. One possibility could be that the charged glutamate residue present on the insulin segment could electrostatically interact with the peptide. Nevertheless, at pH 2.5, the glutamate residue is not charged whereas the LVEALYL peptide stimulates insulin aggregation, as at pH 7. The effects of these two mutated peptides on insulin aggregation at pH 2.5 should be studied for a better understanding. Moreover, the LVTALYL peptide, where E residue is replaced by a neutral residue is extremely efficient, at both pH 7 and pH 2.5. But as explained in the precedent chapters, this is not comparable as the T residue is less hydrophilic than the charged E residue, which changes the most energetically conformation of the peptide on hydrophobic surface. The replacement of the E residue for a neutral polar residue, like serine (S) or asparagine (N) (forming peptides LVSALYL and LVNALYL respectively) should give more information on the importance of that charge. Other tested peptides could already give information on the importance of that residue. The SVSASYS peptide presents pro-aggregative activity similar to that of the LVEALYL peptide. It can consequently be anticipated that the LVSALYL peptide would also present a similar pro-aggregative activity. In conclusion, the effect of the charge on the third position of peptide sequence is yet not fully understood, but neutral or negatively charged residue seems to conserve the peptide pro-aggregative activity, whereas positively charged residue seems to prevent it. Molecular dynamics of surface/peptide and protein/peptide interactions could give information on that issue.

6.4. Future directions

The main goal of this research project was to understand the molecular mechanisms of surface-induced protein aggregation, in order to propose ways to better protein stability. We observed that peptides adsorbing in β -strand on hydrophobic surfaces are able to enhance insulin aggregation. We propose that peptides able to adsorb in α -helix conformation on the surface may inhibit insulin aggregation induced by surfaces. For instance, the α -helical peptide LKLLKLLKLLKLL is shown to adsorb on hydrophobic surfaces^{114,115}. Its adsorption on hydrophobic surfaces may delay insulin aggregation and inhibit the different phenomena. This could be observed by SPRi, FTIR and fluorescence microscopy. This peptide is positively charged, but a negatively charged peptide like LEELLEELLEELLE, or neutral peptide like LSSLLSLLSLLSLL may also be α -helical and adsorb on hydrophobic

surfaces. These could be used as a general protein stabilizing agent acting at sub-stoichiometric concentrations. Such result could be of high interest for the stabilization of therapeutic protein.

This study was done using hydrophobic surfaces. Nevertheless, it is known that insulin aggregation can be enhanced by other surfaces, particularly by amine-coated surfaces¹¹⁶. Other proteins, like antibodies and amyloid β , can also present similar aggregation enhancement in presence of amine surfaces and other charged surfaces¹¹⁷. On all these surfaces, aggregation mechanism could be similar to what is observed in this study: (i) protein accumulation on the surface due to interactions between charges on the protein and charges on the surface, (ii) protein partial unfolding involved by charges interactions between surface and proteins, (iii) unfolded proteins interactions leading to aggregation nucleus formation and (iv) fibril growth on the surface, followed by large fibril detachment due to agitation. Nevertheless, on charged surfaces, the peptides studied so far should have hardly any effect on insulin aggregation kinetic, as their adsorption and their conformation on the surface should be highly different from what is observed on hydrophobic surfaces. We plan to study, using amine-coated microwells plates provided by Becton-Dickinson. Results obtained with these surfaces should give important information on the generalization possibilities of our model for various surfaces chemistries. This should require the design of peptides that may adsorb on charged surfaces in β -strands. ESESESE or DSDSDSD peptides could be proposed as peptides that could accelerate insulin aggregation for negatively charged surfaces, and KSKSKSK peptide could be proposed for positively charged surfaces.

Furthermore, it appears that insulin adsorption was increased in presence of pro-aggregative peptide. This adsorption effect seems to be increased when using peptide with higher pro-aggregative effects. It can be supposed that an anti-aggregative peptide should have the opposite effect, reducing the insulin adsorption on the surface. This could be of great interest in protein stability studies. For instance, one could prepare surfaces exposing a large number of different peptides. These “peptide microarrays” could be incubated with a protein solution of interest to test whether some peptides induce protein aggregation. In addition, SPRi measurements and ThT fluorescence microscopy could be used to determine the effect of immobilized peptide on protein affinity for the surface and on extended β -sheets formation. That could facilitate and accelerate the determination of stabilizing peptides and of protein sequences involved in protein aggregation. Moreover, pre-filled syringes and insulin pump delivery systems could be improved by the grafting of anti-aggregative peptide in the chamber

and the tubing. Insulin and other therapeutic solutions stabilities could be improved thanks to the development of such techniques.

Some data are still missing for a complete understanding of protein induced insulin aggregation. We proposed that some peptides induce fast insulin aggregation nuclei, due to their β -sheet conformation on the surface. But no information was obtained about the presence of the peptide in the nuclei structure at the surface or inside the final protein fibril. Peptides with the tyrosine (Y) to tryptophan (W) ($Y \rightarrow W$) mutation have been tried, as tryptophan presents an easily detectable fluorescence which is sensitive to its environment. Since insulin does not contain any tryptophan residue, insulin/peptide ratio in precipitated insulin fibrils or on the surface could be quantified with a tryptophan mutated peptide. But it appears that aromatic residues decreased the pro-aggregative peptide effect, probably due to steric effects, reducing the interest of tryptophan mutated peptides. Another way to determine the proportion of peptide/insulin on the surface could be to use mass spectrometry. Furthermore, after a buffer wash of the surface to detach all weakly bound compounds, a coupling agent could covalently link proteins and peptides that are spatially close. Analyzing the complexes formed would shed light on the composition and arrangement of aggregation nuclei.

Another limitation of our observations is that in SPRi, ATR-FTIR and fluorescence microscopy, due to the low experimental flow rate, hydrodynamic shear-stress on fibrils growing on the surface is considerably reduced, compare to microwells plate aggregation experiments. Moreover, in these experiments, temperature was decreased to room temperature compare to microwells plate aggregation experiments (37°C). Consequently, aggregation kinetics are slow down due to the decreased temperature, and fibrils growing on the surface cannot be detached from the surface due to low shear-stress. This results in mass accumulation and ThT fluorescence on the surface which rapidly reaches a plateau (Fig. 8A of article in chapter 4). No aggregates were detected in the collected solution at the outlet. The leak of released insulin aggregates limits the observations to surface events. Nevertheless, temperature control could be easily added in these three techniques, and predicted effects of temperature on the insulin nucleation (faster α to β transition) and fibril growth (faster ThT fluorescence apparition on the surface) could be measured. But due to limited flow rate acceptable in flow chambers, no easy adaptation can be done to increase the shear-stress in these experiments to values comparable to that reached in microwells plate aggregation experiments.

Insulin is not the sole therapeutic protein that forms amyloid fibrils. Some monoclonal antibodies, IAPP (islet amyloid peptide or amylin), calcitonine and some other proteins of therapeutic interest form amyloid fibers in presence of hydrophobic surfaces. According to our sequence non-specific model, the action of pro-aggregative peptides, like the LVEALYL peptide and mutants should be conserved for these proteins. This has to be tested. Moreover, if an α -helix peptide is found to delay insulin aggregation, its effect should be conserved for other proteins, which could be of great interest in pharmaceutical research.

It must be noted that some peptides aggregates in α -helix conformation, contrary to the proteins forming amyloid fibrils which are composed mostly of β -sheets. For instance, in the presence of the helix-inducing agent TFE (Trifluoroethanol) the tau protein is known to be able to aggregate *in vitro* in an α -helix rich conformation and to form Paired Helical Filaments (PHFs)^{118,119}. It should be interesting to study whereas material surfaces and specific peptides are also able to induce that α -helix rich aggregation.

Our results can be of great interest in pharmaceutics of protein drug solutions in general and type 1 diabetes mellitus insulin therapy in particular. Indeed, new techniques of protein stabilization and protein/surface interaction study may be developed based on this work. Moreover, in medicine, the importance of surfaces in protein aggregation is often neglected. Considering that the extracellular matrix can be considered as a material surface which is generally composed of hydrophobic compounds, it can be hypothesized that taking in account the protein/extracellular matrix interactions could leads to new therapeutics development against some diseases like Alzheimer, prion diseases and amyloidosis.

7. References

1. Anfinsen, C. B. Principles that govern the folding of protein chains. *Science (New York, N.Y.)* **181**, 223–30 (1973).
2. Fink, A. L. Compact intermediate states in protein folding. *Annu. Rev. Biophys. Biomol. Struct.* **24**, 495–722 (1995).
3. Wang, W., Nema, S. & Teagarden, D. Protein aggregation--pathways and influencing factors. *International journal of pharmaceutics* **390**, 89–99 (2010).
4. Gsponer, J. & Vendruscolo, M. Theoretical approaches to protein aggregation. *Protein and peptide letters* **13**, 287–93 (2006).
5. Wood, E. Protein Purification Methods: A Practical Approach. *Biochemical Education* **19**, 39–40 (1991).
6. FDA Guidance, Compliance & Regulatory information. *Guidances (Drugs)* at <<http://www.fda.gov>>
7. Cleland, J. L., Powell, M. F. & Shire, S. J. The development of stable protein formulations: a close look at protein aggregation, deamidation, and oxidation. *Critical reviews in therapeutic drug carrier systems* **10**, 307–77 (1993).
8. Shirwaikar, A. *et al.* Stability of proteins in aqueous solution and solid state. *Indian Journal of Pharmaceutical Sciences* **68**, 154 (2006).
9. Dobson, C. M. Protein folding and misfolding. *Nature* **426**, 884–90 (2003).
10. Kelly, J. W. Mechanisms of amyloidogenesis. *Nature structural biology* **7**, 824–6 (2000).
11. Yang, W. Y., Larios, E. & Gruebele, M. On the extended beta-conformation propensity of polypeptides at high temperature. *Journal of the American Chemical Society* **125**, 16220–7 (2003).
12. Perutz, M. F., Pope, B. J., Owen, D., Wanker, E. E. & Scherzinger, E. Aggregation of proteins with expanded glutamine and alanine repeats of the glutamine-rich and asparagine-rich domains of Sup35 and of the amyloid beta-peptide of amyloid plaques. *Proceedings of the National Academy of Sciences of the United States of America* **99**, 5596–600 (2002).
13. Tycko, R. Molecular structure of amyloid fibrils: insights from solid-state NMR. *Quarterly reviews of biophysics* **39**, 1–55 (2006).
14. Halling, P. J. Proteins: Structures and molecular properties (2nd edition). by Thomas E. Creighton, W. H. Freeman, New York, 1992, xiii + 512 pp, price £22.95. ISBN 0-7167-7030-X. *Journal of Chemical Technology AND Biotechnology* **62**, 105–105 (1995).

15. Hammarström, P., Wiseman, R. L., Powers, E. T. & Kelly, J. W. Prevention of transthyretin amyloid disease by changing protein misfolding energetics. *Science (New York, N.Y.)* **299**, 713–6 (2003).
16. Baskakov, I. V, Legname, G., Baldwin, M. A., Prusiner, S. B. & Cohen, F. E. Pathway complexity of prion protein assembly into amyloid. *The Journal of biological chemistry* **277**, 21140–8 (2002).
17. Kiefhaber, T., Rudolph, R., Kohler, H.-H. & Buchner, J. Protein Aggregation in vitro and in vivo: A Quantitative Model of the Kinetic Competition between Folding and Aggregation. *Bio/Technology* **9**, 825–829 (1991).
18. Jarrett, J. T. & Lansbury, P. T. Seeding “one-dimensional crystallization” of amyloid: a pathogenic mechanism in Alzheimer’s disease and scrapie? *Cell* **73**, 1055–8 (1993).
19. Andreu, J. M. & Timasheff, S. N. The measurement of cooperative protein self-assembly by turbidity and other techniques. *Methods in enzymology* **130**, 47–59 (1986).
20. Norde, W. My voyage of discovery to proteins in flatland ...and beyond. *Colloids and surfaces. B, Biointerfaces* **61**, 1–9 (2008).
21. Chi, E. Y., Krishnan, S., Randolph, T. W. & Carpenter, J. F. Physical stability of proteins in aqueous solution: mechanism and driving forces in nonnative protein aggregation. *Pharmaceutical research* **20**, 1325–36 (2003).
22. Hellman, B., Gylfe, E., Grapengiesser, E., Dansk, H. & Salehi, A. [Insulin oscillations-clinically important rhythm. Antidiabetics should increase the pulsative component of the insulin release]. *Läkartidningen* **104**, 2236–9
23. Banting, F. G., Best, C. H., Collip, J. B., Campbell, W. R. & Fletcher, A. A. Pancreatic extracts in the treatment of diabetes mellitus: preliminary report. 1922. *CMAJ*: *Canadian Medical Association journal = journal de l’Association medicale canadienne* **145**, 1281–6 (1991).
24. World Health Organization Media Centre Diabetes. at <http://www.who.int/mediacentre/factsheets/fs312/en/index.html>
25. Abel, J. J. Crystalline Insulin. *Proceedings of the National Academy of Sciences of the United States of America* **12**, 132–6 (1926).
26. Scott, D. A. Crystalline insulin. *The Biochemical Journal* **28**, 1592–1602.1 (1934).
27. Irsigler, K. & Kritz, H. Long-term continuous intravenous insulin therapy with a portable insulin dosage-regulating apparatus. *Diabetes* **28**, 196–203 (1979).
28. Loughheed, W. D., Woulfe-Flanagan, H., Clement, J. R. & Albisser, A. M. Insulin aggregation in artificial delivery systems. *Diabetologia* **19**, 1–9 (1980).
29. Feingold, V., Jenkins, A. B. & Kraegen, E. W. Effect of contact material on vibration-induced insulin aggregation. *Diabetologia* **27**, 373–378 (1984).

30. Sefton, M. V & Antonacci, G. M. Adsorption isotherms of insulin onto various materials. *Diabetes* **33**, 674–80 (1984).
31. Ryle, a P., Sanger, F., Smith, L. F. & Kitai, R. The disulphide bonds of insulin. *The Biochemical journal* **60**, 541–56 (1955).
32. Adams, M. J. *et al.* Structure of Rhombohedral 2 Zinc Insulin Crystals. *Nature* **224**, 491–495 (1969).
33. Reddy, G. B., Narayanan, S., Reddy, P. Y. & Surolia, I. Suppression of DTT-induced aggregation of abrin by alphaA- and alphaB-crystallins: a model aggregation assay for alpha-crystallin chaperone activity in vitro. *FEBS letters* **522**, 59–64 (2002).
34. Blundell, T. L., Cutfield, J. F., Dodson, G. G., Dodson, E. & Hodgkn, D. C. The Structure and Biology of Insulin. *The Biochemical journal* **112**, 21P–36P (1969).
35. Jeffrey, P. D., Milthorpe, B. K. & Nichol, L. W. Polymerization pattern of insulin at pH 7.0. *Biochemistry* **15**, 4660–4665 (1976).
36. Milthorpe, B. K., Nichol, L. W. & Jeffrey, P. D. The polymerization pattern of zinc(II)-insulin at pH 7.0. *Biochimica et biophysica acta* **495**, 195–202 (1977).
37. Pekar, A. H. & Frank, B. H. Conformation of proinsulin. Comparison of insulin and proinsulin self-association at neutral pH. *Biochemistry* **11**, 4013–4016 (1972).
38. Mitra, R., Pezron, I., Chu, W. a & Mitra, a K. Lipid emulsions as vehicles for enhanced nasal delivery of insulin. *International journal of pharmaceutics* **205**, 127–34 (2000).
39. Lougheed, W. D., Albisser, A. M., Martindale, H. M., Chow, J. C. & Clement, J. R. Physical stability of insulin formulations. *Diabetes* **32**, 424–32 (1983).
40. Sluzky, V., Tamada, J. ., Klibanov, A. . & Langer, R. Kinetics of insulin aggregation in aqueous solutions upon agitation in the presence of hydrophobic surfaces. *Proceedings of the National Academy of Sciences of the United States of America* **88**, 9377–81 (1991).
41. Dische, F. E. *et al.* Insulin as an amyloid-fibril protein at sites of repeated insulin injections in a diabetic patient. *Diabetologia* **31**, 158–61 (1988).
42. Störkel, S., Schneider, H. M., Müntefering, H. & Kashiwagi, S. Iatrogenic, insulin-dependent, local amyloidosis. *Laboratory investigation; a journal of technical methods and pathology* **48**, 108–11 (1983).
43. Brange, J., Andersen, L., Laursen, E. D., Meyn, G. & Rasmussen, E. Toward understanding insulin fibrillation. *Journal of pharmaceutical sciences* **86**, 517–25 (1997).
44. Westermark, P. Aspects on human amyloid forms and their fibril polypeptides. *The FEBS journal* **272**, 5942–9 (2005).

45. Astbury, W. T., Dickinson, S. & Bailey, K. The X-ray interpretation of denaturation and the structure of the seed globulins. *The Biochemical journal* **29**, 2351–2360.1 (1935).
46. Geddes, A. J., Parker, K. D., Atkins, E. D. & Beighton, E. “Cross-beta” conformation in proteins. *Journal of molecular biology* **32**, 343–58 (1968).
47. Sunde, M. & Blake, C. The structure of amyloid fibrils by electron microscopy and X-ray diffraction. *Advances in protein chemistry* **50**, 123–59 (1997).
48. Ivanova, M. I., Sievers, S. a, Sawaya, M. R., Wall, J. S. & Eisenberg, D. Molecular basis for insulin fibril assembly. *Proceedings of the National Academy of Sciences of the United States of America* **106**, 18990–5 (2009).
49. Jansen, R., Dzwolak, W. & Winter, R. Amyloidogenic self-assembly of insulin aggregates probed by high resolution atomic force microscopy. *Biophysical journal* **88**, 1344–53 (2005).
50. Millican, R. L. & Brems, D. N. Equilibrium Intermediates in the Denaturation of Human Insulin and Two Monomeric Insulin Analogs. *Biochemistry* **33**, 1116–1124 (1994).
51. Waugh, D. A fibrous modification of insulin. I. The heat precipitate of insulin. *Journal of the American Chemical Society* **68**, 247–250 (1946).
52. Langmuir, I. Pressure-soluble and pressure-displaceable components of monolayers of native and denatured proteins. *Journal of the American Chemical* **1089**, 2771–2793 (1940).
53. Waugh, D. The linkage of corpuscular protein molecules. I. A fibrous modification of insulin. *Journal of the American Chemical Society* **497**, 1944 (1944).
54. Waugh, D. F., Thompson, R. E. & Weimer, R. J. Assay of insulin in vitro by fibril elongation and precipitation. *The Journal of biological chemistry* **185**, 85–95 (1950).
55. Waugh, D. & Wilhelmson, D. Studies of the nucleation and growth reactions of selected types of insulin fibrils. *Journal of the American Chemical Society* **1048**, 2592–2600 (1953).
56. Waugh, D. F. A mechanism for the formation of fibrils from protein molecules. *Journal of Cellular and Comparative Physiology* **49**, 145–164 (1957).
57. Bischoff, F. & Sahyun, M. Denaturation of insulin protein by concentrated sulfuric acid. *Journal of Biological Chemistry* **81**, 167–173 (1929).
58. Krogh, A. & Hemmingsen, A. M. The destructive action of heat on insulin solutions. *The Biochemical journal* **22**, 1231–8 (1928).
59. Balbirnie, M., Grothe, R. & Eisenberg, D. S. An amyloid-forming peptide from the yeast prion Sup35 reveals a dehydrated beta-sheet structure for amyloid. *Proceedings*

- of the National Academy of Sciences of the United States of America* **98**, 2375–80 (2001).
60. López de la Paz, M. & Serrano, L. Sequence determinants of amyloid fibril formation. *Proceedings of the National Academy of Sciences of the United States of America* **101**, 87–92 (2004).
 61. Tenidis, K. *et al.* Identification of a penta- and hexapeptide of islet amyloid polypeptide (IAPP) with amyloidogenic and cytotoxic properties. *Journal of molecular biology* **295**, 1055–71 (2000).
 62. Reches, M., Porat, Y. & Gazit, E. Amyloid fibril formation by pentapeptide and tetrapeptide fragments of human calcitonin. *The Journal of biological chemistry* **277**, 35475–80 (2002).
 63. Tjernberg, L., Hosia, W., Bark, N., Thyberg, J. & Johansson, J. Charge attraction and beta propensity are necessary for amyloid fibril formation from tetrapeptides. *The Journal of biological chemistry* **277**, 43243–6 (2002).
 64. Tjernberg, L. O. *et al.* Arrest of beta-amyloid fibril formation by a pentapeptide ligand. *The Journal of biological chemistry* **271**, 8545–8 (1996).
 65. Findeis, M. A. *et al.* Modified-peptide inhibitors of amyloid beta-peptide polymerization. *Biochemistry* **38**, 6791–800 (1999).
 66. Kapurniotu, A., Schmauder, A. & Tenidis, K. Structure-based design and study of non-amyloidogenic, double N-methylated IAPP amyloid core sequences as inhibitors of IAPP amyloid formation and cytotoxicity. *Journal of molecular biology* **315**, 339–50 (2002).
 67. Chabry, J., Caughey, B. & Chesebro, B. Specific inhibition of in vitro formation of protease-resistant prion protein by synthetic peptides. *The Journal of biological chemistry* **273**, 13203–7 (1998).
 68. Hashimoto, M., Rockenstein, E., Mante, M., Mallory, M. & Masliah, E. beta-Synuclein inhibits alpha-synuclein aggregation: a possible role as an anti-parkinsonian factor. *Neuron* **32**, 213–23 (2001).
 69. Ghanta, J., Shen, C. L., Kiessling, L. L. & Murphy, R. M. A strategy for designing inhibitors of beta-amyloid toxicity. *The Journal of biological chemistry* **271**, 29525–8 (1996).
 70. Pallitto, M. M., Ghanta, J., Heinzelman, P., Kiessling, L. L. & Murphy, R. M. Recognition sequence design for peptidyl modulators of beta-amyloid aggregation and toxicity. *Biochemistry* **38**, 3570–8 (1999).
 71. Du, H.-N. *et al.* Acceleration of alpha-synuclein aggregation by homologous peptides. *FEBS letters* **580**, 3657–64 (2006).

72. Kim, J. R. & Murphy, R. M. Mechanism of accelerated assembly of beta-amyloid filaments into fibrils by KLVFFK(6). *Biophysical journal* **86**, 3194–203 (2004).
73. Ma, J., Yee, A., Brewer, H. B., Das, S. & Potter, H. Amyloid-associated proteins alpha 1-antichymotrypsin and apolipoprotein E promote assembly of Alzheimer beta-protein into filaments. *Nature* **372**, 92–4 (1994).
74. Eriksson, S., Janciauskiene, S. & Lannfelt, L. Alpha 1-antichymotrypsin regulates Alzheimer beta-amyloid peptide fibril formation. *Proceedings of the National Academy of Sciences of the United States of America* **92**, 2313–7 (1995).
75. Evans, K., Berger, E. & Cho, C. Apolipoprotein E is a kinetic but not a thermodynamic inhibitor of amyloid formation: implications for the pathogenesis and treatment of Alzheimer disease. *Proceedings of the* **92**, 763–7 (1995).
76. Wisniewski, T., Castaño, E. M., Golabek, A., Vogel, T. & Frangione, B. Acceleration of Alzheimer's fibril formation by apolipoprotein E in vitro. *The American journal of pathology* **145**, 1030–5 (1994).
77. Jiménez, J. L. *et al.* The protofilament structure of insulin amyloid fibrils. *Proceedings of the National Academy of Sciences of the United States of America* **99**, 9196–201 (2002).
78. Vestergaard, B. *et al.* A helical structural nucleus is the primary elongating unit of insulin amyloid fibrils. *PLoS biology* **5**, e134 (2007).
79. Sawaya, M. R. *et al.* Atomic structures of amyloid cross-beta spines reveal varied steric zippers. *Nature* **447**, 453–7 (2007).
80. Gibson, T. J. & Murphy, R. M. Inhibition of insulin fibrillogenesis with targeted peptides. *Protein Science* **15**, 1133–41 (2006).
81. Bouchard, M., Zurdo, J., Nettleton, E., Dobson, C. M. & Robinson, C. V Formation of insulin amyloid fibrils followed by FTIR simultaneously with CD and electron microscopy. *Protein* **9**, 1960–7 (2000).
82. Nettleton, E. J. *et al.* Characterization of the oligomeric states of insulin in self-assembly and amyloid fibril formation by mass spectrometry. *Biophysical journal* **79**, 1053–65 (2000).
83. Yu, N. T., Jo, B. H., Chang, R. C. & Huber, J. D. Single-crystal Raman spectra of native insulin. Structures of insulin fibrils, glucagon fibrils, and intact calf lens. *Archives of biochemistry and biophysics* **160**, 614–22 (1974).
84. Turnell, W. G. & Finch, J. T. Binding of the dye congo red to the amyloid protein pig insulin reveals a novel homology amongst amyloid-forming peptide sequences. *Journal of molecular biology* **227**, 1205–23 (1992).

85. Sluzky, V., Klibanov, A. M. & Langer, R. Mechanism of insulin aggregation and stabilization in agitated aqueous solutions. *Biotechnology and bioengineering* **40**, 895–903 (1992).
86. Thurow, H. & Geisen, K. Stabilisation of dissolved proteins against denaturation at hydrophobic interfaces. *Diabetologia* **27**, 212–8 (1984).
87. Chawla, A. S., Hinberg, I., Blais, P. & Johnson, D. Aggregation of insulin, containing surfactants, in contact with different materials. *Diabetes* **34**, 420–4 (1985).
88. Ballet, T. *et al.* DnaK prevents human insulin amyloid fiber formation on hydrophobic surfaces. *Biochemistry* **51**, 2172–80 (2012).
89. Nilsson, P., Nylander, T. & Havelund, S. Adsorption of insulin on solid surfaces in relation to the surface properties of the monomeric and oligomeric forms. *Journal of Colloid and Interface Science* **144**, 145–152 (1991).
90. Blundell, T., Dodson, G. & Hodgkin, D. Insulin: the structure in the crystal and its reflection in chemistry and biology. *Adv. Protein Chem* **26**, 279 – 402 (1972).
91. Rudiuk, S., Cohen-Tannoudji, L., Huille, S. & Tribet, C. Importance of the dynamics of adsorption and of a transient interfacial stress on the formation of aggregates of IgG antibodies. *Soft Matter* **8**, 2651 (2012).
92. McMasters, M. J., Hammer, R. P. & McCarley, R. L. Surface-Induced Aggregation of Beta Amyloid Peptide by ω -Substituted Alkanethiol Monolayers Supported on Gold. *Langmuir* **21**, 4464–4470 (2005).
93. Arora, A., Ha, C. & Park, C. B. Inhibition of insulin amyloid formation by small stress molecules. *FEBS letters* **564**, 121–5 (2004).
94. Grau, U. & Saudek, C. D. Stable insulin preparation for implanted insulin pumps. Laboratory and animal trials. *Diabetes* **36**, 1453–9 (1987).
95. Brewster, M. E., Hora, M. S., Simpkins, J. W. & Bodor, N. Use of 2-hydroxypropyl-beta-cyclodextrin as a solubilizing and stabilizing excipient for protein drugs. *Pharmaceutical research* **8**, 792–5 (1991).
96. Kuroda, Y. & Kawahara, M. Aggregation of amyloid beta-protein and its neurotoxicity: enhancement by aluminum and other metals. *The Tohoku journal of experimental medicine* **174**, 263–8 (1994).
97. Wang, M. S., Boddapati, S. & Sierks, M. R. Cyclodextrins promote protein aggregation posing risks for therapeutic applications. *Biochemical and biophysical research communications* **386**, 526–31 (2009).
98. Stefani, M. & Dobson, C. M. Protein aggregation and aggregate toxicity: new insights into protein folding, misfolding diseases and biological evolution. *Journal of molecular medicine (Berlin, Germany)* **81**, 678–99 (2003).

99. Schröder, H. DnaK, DnaJ and GrpE from a cellular chaperone machinery capable of repairing heat-induced protein damage. *EMBO J* **12**, 4137–44 (1993).
100. Mogk, A. *et al.* Identification of thermolabile Escherichia coli proteins: Prevention and reversion of aggregation by DnaK and ClpB. *EMBO J* **18**, 6934–49 (1999).
101. Rasmussen, T., Kasimova, M. ., Jiskoot, W. & Van de Weert, M. The caperone-like Protein alpha-crystallin dissociates insulin dimers and hexamers. *Biochemistry* **48**, (2009).
102. Rasmussen, T., Tantipolphan, R., Van de Weert, M. & Jiskoot, W. The molecular chaperone alpha-crystallin as an excipient in an insulin formulation. *Pharmaceutical research* **27**, (2010).
103. Ritossa, F. A new puffing pattern induced by temperature shock and DNP in drosophila. *Cellular and molecular life sciences* **18**, 571–573 (1962).
104. Ritossa, F. Discovery of the heat shock response. *Cell stress chaperones* **1**, 97–98 (1996).
105. Ballet, T. *et al.* Insulin adsorbed on hydrophobic surfaces stimulates the formation and release of insulin amyloid fibers. (submitted)
106. Nault, L. *et al.* Human insulin adsorption kinetics, conformational changes and amyloid aggregate formation on hydrophobic surfaces. *Acta biomaterialia* **9**, 5070–9 (2013).
107. Nault, L., Bréchet, Y., Bruckert, F. & Weidenhaupt, M. Peptides that form beta-sheets on hydrophobic surfaces accelerate surface-induced insulin amyloid aggregation. *FEBS letters* (2013) (in publication).
108. Bergström, K. *et al.* Reduction of fibrinogen adsorption on PEG-coated polystyrene surfaces. *Journal of biomedical materials research* **26**, 779–90 (1992).
109. Kingshott, P., McArthur, S., Thissen, H., Castner, D. G. & Griesser, H. J. Ultrasensitive probing of the protein resistance of PEG surfaces by secondary ion mass spectrometry. *Biomaterials* **23**, 4775–85 (2002).
110. Michel, R., Pasche, S., Textor, M. & Castner, D. G. Influence of PEG architecture on protein adsorption and conformation. *Langmuir*: the ACS journal of surfaces and colloids **21**, 12327–32 (2005).
111. Kong, J. & Yu, S. Fourier Transform Infrared Spectroscopic Analysis of Protein Secondary Structures. *Acta Biochimica et Biophysica Sinica* **39**, 549–559 (2007).
112. Crowfoot, D. X-Ray Single Crystal Photographs of Insulin. *Nature* **135**, 591–592 (1935).

113. Rüdiger, S., Germeroth, L., Schneider-Mergener, J. & Bukau, B. Substrate specificity of the DnaK chaperone determined by screening cellulose-bound peptide libraries. *The EMBO journal* **16**, 1501–7 (1997).
114. Collier, G., Vellore, N. a., Yancey, J. a., Stuart, S. J. & Latour, R. a. Comparison Between Empirical Protein Force Fields for the Simulation of the Adsorption Behavior of Structured LK Peptides on Functionalized Surfaces. *Biointerphases* **7**, 24 (2012).
115. Weidner, T., Apte, J. S., Gamble, L. J. & Castner, D. G. Probing the orientation and conformation of alpha-helix and beta-strand model peptides on self-assembled monolayers using sum frequency generation and NEXAFS spectroscopy. *Langmuir*: the ACS journal of surfaces and colloids **26**, 3433–40 (2010).
116. Pandey, L. M. *et al.* Surface chemistry at the nanometer scale influences insulin aggregation. *Colloids and surfaces. B, Biointerfaces* **100C**, 69–76 (2012).
117. Cabaleiro-Lago, C., Quinlan-Pluck, F., Lynch, I., Dawson, K. a. & Linse, S. Dual Effect of Amino Modified Polystyrene Nanoparticles on Amyloid β Protein Fibrillation. *ACS Chemical Neuroscience* **1**, 279–287 (2010).
118. Sadqi, M. *et al.* Alpha-helix structure in Alzheimer's disease aggregates of tau-protein. *Biochemistry* **41**, 7150–5 (2002).
119. Kunjithapatham, R. *et al.* Role for the alpha-helix in aberrant protein aggregation. *Biochemistry* **44**, 149–56 (2005).

Appendix: Ballet *et al.* (2012)

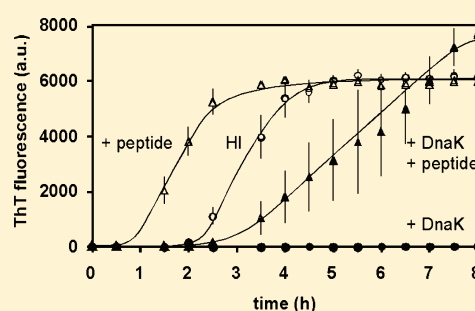
DnaK Prevents Human Insulin Amyloid Fiber Formation on Hydrophobic Surfaces

Thomas Ballet,^{†,‡} Franz Brukert,[†] Paolo Mangiagalli,[‡] Christophe Bureau,[‡] Laurence Boulangé,^{‡,§} Laurent Nault,[†] Thomas Perret,[†] and Marianne Weidenhaupt^{*,†}

[†]Laboratoire des Matériaux et du Génie Physique, Grenoble Institute of Technology, 3 parvis Louis Néel, 38016 Grenoble Cedex 1, France

[‡]Becton-Dickinson Pharmaceutical Systems, 11, Rue Aristide Bergès, 38801 Le Pont de Claix, France

ABSTRACT: We have developed a multiwell-based protein aggregation assay to study the kinetics of insulin adsorption and aggregation on hydrophobic surfaces and to investigate the molecular mechanisms involved. Protein–surface interaction progresses in two phases: (1) a lag phase during which proteins adsorb and prefibrillar aggregates form on the material surface and (2) a growth phase during which amyloid fibers form and then are progressively released into solution. We studied the effect of three bacterial chaperones, DnaK, DnaJ, and ClpB, on insulin aggregation kinetics. In the presence of ATP, the simultaneous presence of DnaK, DnaJ, and ClpB allows good protection of insulin against aggregation. In the absence of ATP, DnaK alone is able to prevent insulin aggregation. Furthermore, DnaK binds to insulin adsorbed on hydrophobic surfaces. This process is slowed in the presence of ATP and can be enhanced by the cochaperone DnaJ. The peptide LVEALYL, derived from the insulin B chain, is known to promote fast aggregation in a concentration- and pH-dependent manner in solution. We show that it also shortens the lag phase for insulin aggregation on hydrophobic surfaces. As this peptide is also a known DnaK substrate, our data indicate that the peptide and the chaperone might compete for a common site during the process of insulin aggregation on hydrophobic surfaces.



Adsorption of protein on material surfaces is of widespread importance in fields like cellular biology, pharmacology, and medicine. It can be quantitatively measured either biochemically after desorption or in situ by sensitive biophysical methods, like QCM-D or surface plasmon resonance (SPR). Protein adsorption is accompanied by conformational changes upon contact with the material surface, leading sometimes to protein aggregation. It is not easy to monitor these conformational changes on the material in a fast, convenient, and preferentially multiplexed assay. Albeit greatly sensitive, techniques like attenuated total reflectance Fourier transform infrared spectroscopy (ATR-FTIR) are not readily available and do not provide unambiguous information about the nature of the changes in protein folding.

Within cells, chaperones constitute a set of proteins whose function is to check the folding state of other proteins, and to refold them,^{1–3} using ATP hydrolysis energy to drive protein disaggregation and renaturation. In *Escherichia coli*, Bukau and co-workers identified DnaK, DnaJ, and ClpB as the minimum set of bacterial chaperones needed to help the cell recover from a heat shock.⁴ DnaK is an ATPase specific for unfolded hydrophobic amino acid stretches. DnaJ forms a complex with DnaK and stimulates DnaK ATPase activity.⁵ ClpB is a hexameric ATPase that interacts with aggregated proteins and disaggregates them, in cooperation with DnaK and DnaJ.^{4,6,7} Furthermore, in *E. coli*, ~250 proteins are disaggregated and

refolded when DnaK, DnaJ, and ClpB are present, which supports the broadness of their protein substrates.⁴ Chaperones detect general conformational unfolding characteristics, rather than specific targets. In addition, many chaperones work in complexes; hence, chaperone combination is likely to enhance the recognition process. We therefore hypothesized that this protein family could provide new sensors for protein conformational changes at material surfaces.

We chose human insulin (HI) as a model because its aggregation has been studied under different physicochemical conditions.^{8–10} It was shown that HI aggregation is formulation-dependent and that insulin undoubtedly changes its conformation upon binding to hydrophobic surfaces, leading to the formation and release of amyloid fiber aggregates.¹¹ From a concentration dependence study, Sluzky et al. deduced that the HI monomer was the molecular species leading to aggregation.⁹ Using recombinant chaperones, we observe that different sets of them are able to prevent HI aggregation by binding preferentially to surface-bound insulin. Rüdiger et al.¹² have shown that DnaK binds to the insulin B chain peptide SHLVEALYLVCGER, and Ivanova et al.¹³ demonstrated that the shorter LVEALYL peptide is the minimal sequence that can

Received: September 19, 2011

Revised: January 23, 2012

Published: February 21, 2012

accelerate the lag time of insulin fiber formation at acidic pH in a concentration-dependent manner. We show that this same peptide also accelerates the lag time of insulin aggregation on hydrophobic surfaces and that bacterial chaperones are able to counterbalance this effect.

■ EXPERIMENTAL PROCEDURES

If not otherwise stated, all chemicals were purchased from Sigma-Aldrich. Experiments were conducted in TBS [25 mM Tris-HCl (pH 7.4) and 125 mM NaCl]. HI (recombinant, expressed in yeast) solutions were prepared at 0.5 mg/mL (86 μ M). All solutions were filtered (0.22 μ m) before being used. The LVEALYL peptide was purchased from Genecust (Luxembourg) and dissolved in 20 mM NaOH at a concentration of 4.3 mM.

Bacterial Chaperone Preparation and Activity Assay.

The bacterial strains used to produce DnaK (Hsp70), ClpB (Hsp100), and DnaJ (Hsp40) were kindly provided by B. Bukau and A. Mogk (Zentrum für Molekulare Biologie Heidelberg, Universität Heidelberg, Heidelberg, Germany). His-tagged ClpB and DnaJ were purified using nickel-nitrilotriacetic acid (Ni-NTA) metal affinity chromatography columns (Qiagen) according to the manufacturer's instructions. DnaK was purified as described by Cegielska and Georgopoulos¹⁴ and McCarty and Walker,¹⁵ with minor modifications by Buchberger et al.¹⁶ The refolding activity of the purified proteins was controlled using the malate dehydrogenase (MDH) renaturation assay.^{6,17} The three proteins and ATP were essential for the refolding activity (2 ± 0.3 nM min⁻¹ at 1 μ M DnaK, 0.2 μ M DnaJ, and 1 μ M ClpB).

Insulin Aggregation Assays. HI aggregation assays were conducted as eight replicates in plastic 96-well microplates. Polystyrene (Greiner Bio-One, contact angle of $85 \pm 4.7^\circ$) or PEO-coated (Corning, contact angle of $3.5 \pm 5.8^\circ$) microplates were used. In fluorescence assays, black polystyrene microplates were used (Nunc Nunclon Δ Surface). The plates were covered by plastic sheets, incubated at 37 °C, and shaken at 1200 rpm (Heidolph Titramax, 1.5 mm vibration orbit). At each time point, the solution was pipetted out of the microwells. Part of the solution was filtered to remove aggregated HI (100 nm cutoff). The wells were washed twice with 300 μ L of TBS. The adsorbed HI fraction was desorbed with 100 μ L of 5% SDS for a 1 h agitation at 37 °C. Negligible protein material remained on the surface thereafter. The total amounts of HI in solution (nonfiltered), soluble HI, and HI adsorbed in the wells were determined using the bicinchoninic acid (BCA) assay.^{18–21} In addition, turbidity ($\lambda = 600$ nm) or thioflavin T (ThT, 20 or 50 μ M) fluorescence was directly measured in the wells. Free and bound forms of ThT were measured at a λ_{ex} of 342 nm and a λ_{em} of 430 nm and at a λ_{ex} of 450 nm and a λ_{em} of 482 nm, respectively,²² with a 5 nm excitation and emission slit (Tecan Infinite M1000).

Kinetic Analysis. The aggregation kinetics proceed in three phases: a lag phase, where the signal was not statistically different from the baseline (mean \pm standard deviation), a linear growth phase, and a plateau phase. Experimentally, the lag time was defined by the intercept between the linear growth phase and the baseline. The growth rate was defined as the slope of the linear phase and the plateau as the maximal value attained. The parameters were calculated on individual kinetics corresponding to different samples, and the given statistics represent the average and standard deviation for each parameter.

Protection of Insulin Aggregation by Bacterial

Chaperones. HI aggregation was monitored by turbidity or ThT fluorescence and confirmed by protein quantification after filtration at the end of the experiment. The TBS buffer solution was supplemented with 2 mM MgCl₂ (TBS-M), because Mg²⁺ ions are needed for the chaperone ATPase activity. Magnesium itself does not affect HI aggregation. All chaperones were stable in this buffer. The efficiency of chaperone protection was expressed as the lag time before the onset of HI aggregation. As Zn²⁺ influences the equilibrium of HI hexamer formation,²³ we tested the effect of Zn²⁺ addition (up to 10 μ M) on HI aggregation: neither HI aggregation kinetics nor DnaK protection was modified.

Chaperone Binding Assays. Polystyrene microplates [96 wells, Greiner enzyme-linked immunosorbent assay (ELISA)] were incubated at 37 °C and 1200 rpm with insulin for various amounts of time and blocked with 10 mg/mL bovine serum albumin (BSA) in TBS-M (blocking buffer) for 30 min at room temperature (RT) with shaking (1000 rpm). DnaK, DnaJ, or both (diluted in blocking buffer) were then added for 30 min (RT) with shaking (1000 rpm). The plate was blocked again with BSA for 30 min (RT) with shaking (1000 rpm).

For DnaK detection, a mouse anti-DnaK (*E. coli*) monoclonal antibody (8E2/2; diluted 1:2500 in blocking buffer) was used, and for DnaJ detection, a mouse anti-penta-His antibody (diluted 1:1000 in blocking buffer) was added to each well and the mixture incubated for 15 min (RT) with shaking (1000 rpm). Finally, a goat horseradish peroxidase-conjugated anti-mouse antibody (diluted 1:2500 in blocking buffer) was added to each well and the mixture incubated for 15 min (RT) with shaking (1000 rpm). Wells were then washed three times with 200 μ L of TBS, and 200 μ L of ECL substrate solution was added per well. Chemiluminescence signals were immediately recorded using a TriStar LB 941 microplate multimode reader.

To relate luminescence values to the amount of DnaK adsorbed, a calibration experiment was conducted in parallel. Increasing amounts of DnaK were incubated in 96-well polystyrene microplates (Greiner ELISA). The amounts of adsorbed DnaK were determined using the NanoOrange assay, according to the manufacturer's instructions. An ELISA was performed on the adsorbed DnaK as described previously. A calibration curve was then obtained that related luminescence values to the amount of adsorbed DnaK.

■ RESULTS

HI Aggregation in the Presence of Hydrophobic

Surfaces. To study the mechanisms of insulin aggregation on hydrophobic surfaces, we developed a HI aggregation assay using commercial hydrophilic or hydrophobic 96-well plates, to allow rapid screening of different experimental conditions. A HI solution was placed in the presence of hydrophilic or hydrophobic plastic surfaces and agitated at 37 °C. At the indicated times, the solution was recovered and filtered to separate the soluble and aggregated HI pools. The microwell surface was then washed, and adsorbed HI was desorbed with SDS. These three protein pools were then quantified using the BCA assay. In the presence of hydrophilic surfaces, HI remained soluble for several days and less than 1 μ g of protein was adsorbed on the hydrophilic microwell surfaces (data not shown). In contrast, in the presence of hydrophobic surfaces, the concentration of soluble HI remained constant for \sim 4 h (lag phase), after which the amount decreased

sharply to trace amounts (Figure 1A). The amount of aggregated HI in solution increased in parallel at a similar rate.

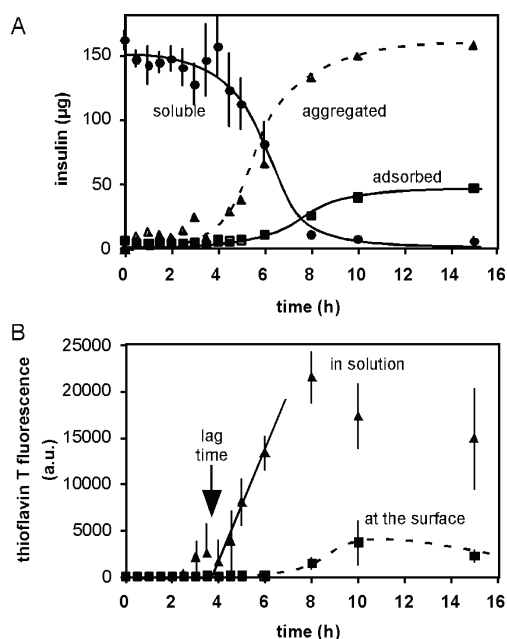


Figure 1. Kinetics of human insulin adsorption and aggregation in hydrophobic microplates. (A) Amount of soluble (●), aggregated (▲), and adsorbed (■) HI after the indicated incubation time. (B) Amyloid fiber-bound ThT fluorescence in solution (▲) and on the surface (■) plotted as a function of incubation time. The lag time as the intercept between the growth rate (—) and the baseline is denoted with an arrow. Other curves are hand-drawn and provided as a guide for the eye.

The amount of HI adsorbed on hydrophobic surfaces increased during the aggregation process, reaching a maximum amount of ~40 µg.

Amyloid aggregates are characterized by the formation of intermolecular β-sheets, which can be probed by the binding of thioflavin T (ThT), resulting in a characteristic fluorescence signal. Both the aggregated and the adsorbed HI pools were stained with ThT, and the fluorescence intensity per microgram of protein was the same in both pools (Figure 1B). The ThT fluorescence is therefore a convenient method for monitoring the appearance of HI aggregates. In the following experiments, we defined the lag time as the intercept between the linear growth phase and the baseline of the ThT fluorescence kinetics. Depending on HI preparations, the lag time varied from 2 to 4 h. Within an experiment, using the same HI preparation in the same multiwell plate, the lag time was also variable from well to well, which explains the variation observed in the aggregation kinetics. HI aggregates exhibited elongated fiberlike rods with a diameter of 5–10 nm and a length of 50–100 nm when imaged using electron microscopy (data not shown). Their morphology and dimensions are similar to those of the fibers obtained after incubation of insulin at pH 2 and an elevated temperature.^{24,25}

Effect of Bacterial Chaperones on Insulin Aggregation. We then studied whether bacterial chaperones could have an effect on the kinetics of HI aggregation. In the presence of 1 mM ATP, the simultaneous presence of the three chaperones delayed HI aggregation as shown by the 9-fold increase in the

aggregation lag time (Figure 2A). DnaK alone slightly increased the lag time, whereas DnaJ was without effect. The combined

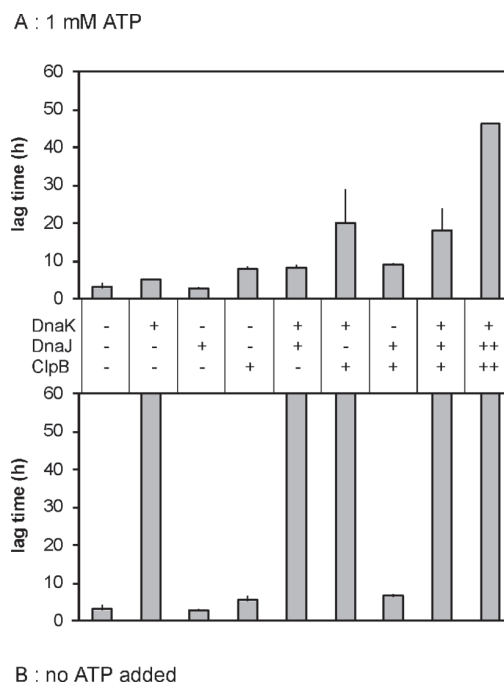


Figure 2. Effect of bacterial chaperones on human insulin aggregation. A HI solution was agitated in a hydrophobic microplate, in the presence of DnaK (0.3 µM), DnaJ [0.06 µM (+) and 0.3 µM (++)], and ClpB [0.3 µM (+) and 0.6 µM (++)] as indicated (A) in the presence of 1 mM ATP or (B) in the absence of ATP. The aggregation kinetics were monitored by turbidity, and the lag times were determined as explained in Experimental Procedures.

presence of DnaK and DnaJ significantly increased the lag time, to a level similar to that obtained in the presence of ClpB alone. Moreover, the combined presence of ClpB with DnaK, but not DnaJ, further delayed HI aggregation in the presence of 1 mM ATP. When the concentrations of DnaJ and ClpB were increased (++ vs +), the lag time further increased. These results show that HI undergoes conformational changes during the aggregation process that are recognized and could possibly be repaired by a minimal set of bacterial chaperones. Nevertheless, incubation of 150 µg of final amyloid insulin aggregates with DnaK, DnaJ, and ClpB for 24 h does not allow recovery of more than 1 µg of soluble insulin (data not shown). This suggests that the three chaperones do not dissociate final aggregates but more likely block intermediate aggregation states.

Surprisingly, in the absence of ATP, no protein aggregation was observed whenever DnaK was present (Figure 2B). The effect was specific for DnaK because, in the absence of ATP, the presence of the other chaperones alone or in combination did not significantly change the HI aggregation kinetics. Addition of comparable and larger amounts of BSA, which is routinely used as a blocking agent to cover material surfaces and works by competitive adsorption, had no effect (data not shown). The peculiar role of DnaK is further investigated in the next section.

Prevention of Insulin Aggregation by DnaK in the Absence of ATP. In the presence of 1 mM ATPγS, a

nonhydrolyzable form of ATP, DnaK did not prevent HI aggregation (Figure 3A), which showed that no ATP hydrolysis

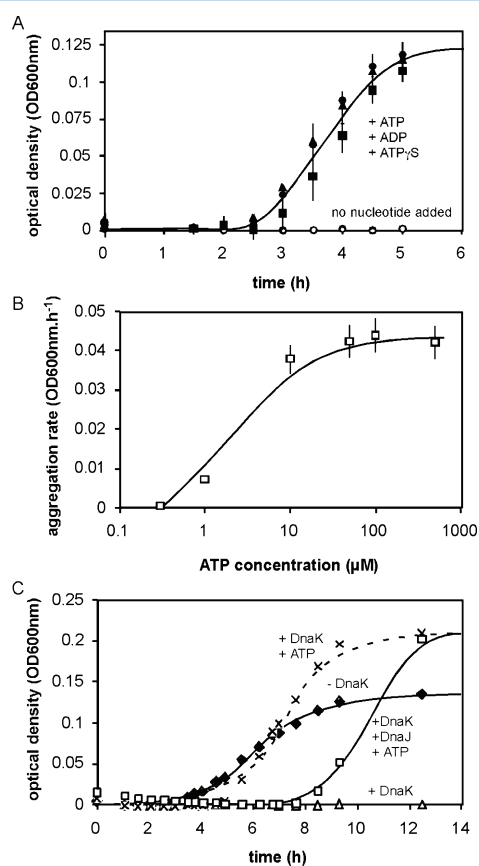


Figure 3. Nucleotide requirements for DnaK protection of human insulin aggregation on hydrophobic surfaces. A HI solution was agitated in a hydrophobic microplate in the presence of the indicated chaperones and nucleotides. HI aggregation was monitored by optical density measurements at 600 nm. (A) The HI solution was supplemented with 1 μ M DnaK and either no nucleotide (○) or 1 mM ATP, ADP, or ATP γ S (●, ▲, and ■, respectively). (B) The HI solution was supplemented with 0.3 μ M DnaK, and the aggregation rate is plotted as a function of ATP concentration. (C) The HI solution was not supplemented with chaperones (◆), supplemented with 0.3 μ M DnaK in the absence of ATP (△) or with 1 mM ATP (×), or supplemented with 0.3 μ M DnaK and 0.06 μ M DnaJ with 1 mM ATP (□).

took place on the HI substrate. Furthermore, addition of 1 mM ADP also abolished the protective effect of DnaK on HI aggregation. The similar effect obtained by the presence of ADP, ATP, or a nonhydrolyzable nucleotide suggested that the molecular species, active at preventing the formation of HI amyloid fibers, was the nucleotide-free DnaK_{empty}-HI complex. This fits well with the biochemical properties of this protein because in the presence of ATP, DnaK indeed has a decreased affinity for its protein substrate^{26,27} and hence could be less protective against aggregation. A series of HI aggregation experiments were performed in the presence of DnaK at different ATP concentrations ranging from 1 μ M to 5 mM. The HI aggregation rate was used to measure the effect of added ATP on DnaK (Figure 3B). An apparent affinity of 2 μ M was determined, which fits with the reported values of the affinity of DnaK for ATP.²⁸ Furthermore, in the presence of ATP, DnaJ

increased the protective effect of DnaK on HI aggregation (Figure 3C). It is indeed known that the DnaK-DnaJ complex has a higher affinity for the protein substrate than DnaK alone.^{29,30}

Several lines of evidence indicate that DnaK prevented early phases of HI aggregation. First, in the continuous presence of DnaK, the amount of HI that adsorbed on hydrophobic surfaces remained small (Figure 4A) and ThT did not stain the adsorbed HI (Figure 4B, vs Figure 1B). Second, in two-stage experiments, when the protective effect of DnaK was released after 5 h by addition of ATP, HI aggregation took place after the same lag time observed in the absence of DnaK (Figure 4C). Similarly, when DnaK was added after incubation for 1 h, the lag time was reduced by 1 h after the addition of ATP. This showed that, as long as it was present in a nucleotide-free form, DnaK prevented the formation of amyloid aggregates on hydrophobic surfaces. To confirm the early effect of DnaK, a constant amount of DnaK was added at different times after the beginning of the incubation. After a 1 h preincubation, DnaK considerably slowed HI aggregation kinetics, but after 2 h, it had no significant effect, although aggregation had not yet started (Figure 4D).

DnaK Binds to HI Adsorbed on Hydrophobic Surfaces.

We then determined the minimal amount of DnaK that should be added as a function of preincubation time to prevent HI aggregation for at least 18 h (Figure 5). This amount increased very rapidly without exceeding the amount of HI adsorbed on the surface, on a molar ratio basis.

Because insulin aggregates are present both on the plastic surface and in solution, we studied the binding of DnaK to the HI pool adsorbed on the surface and to HI aggregates in suspensions. BCA and sodium dodecyl sulfate-polyacrylamide gel electrophoresis (SDS-PAGE) analysis were combined to quantify the amount of DnaK and HI adsorbed on the surface or to aggregates in suspension (Table 1). For these experiments, we used an experimental setup similar to that of Sluzky et al.⁸ SurfSil-treated borosilicate beads were incubated with HI under agitation overnight. After the beads had been washed, 20 ± 2 μ g of HI remained adsorbed to the beads. The HI solution fully aggregated, and 150 μ g of HI aggregates was recovered by centrifugation and washed.

In a first set of experiments, the adsorbed HI pool was incubated with 8 μ g of DnaK, or buffer alone, in the presence or absence of ATP, for 8 min, and the amount of insulin and DnaK adsorbed on the beads after the incubation was determined. The material released in solution after the incubation was also analyzed by centrifugation, to separate soluble and aggregated proteins, and the amount of DnaK associated with the aggregates was also quantified. In the absence of DnaK, 35% of the initially adsorbed HI detached from the bead surfaces (7 μ g/20 μ g), corresponding to the spontaneous detachment of HI aggregates from the surface. In the presence of DnaK, larger amounts of protein, which contained both DnaK and HI, were released from the surface (15.4 μ g + 2.4 μ g = 17.8 μ g). Under these conditions, 77% of the initially adsorbed HI detached from the beads (15.4 μ g/20 μ g). This material could be recovered by centrifugation, showing that it contained only HI aggregates. Moreover, an ELISA confirmed that <0.1 μ g of HI could be recovered in soluble form. No protein renaturation had thus taken place. A large fraction of DnaK (2.4 μ g of 8 μ g) cosedimented with the released HI material, and small but significant amounts of DnaK (0.2 μ g) remained at the bead surface. This strongly suggested that

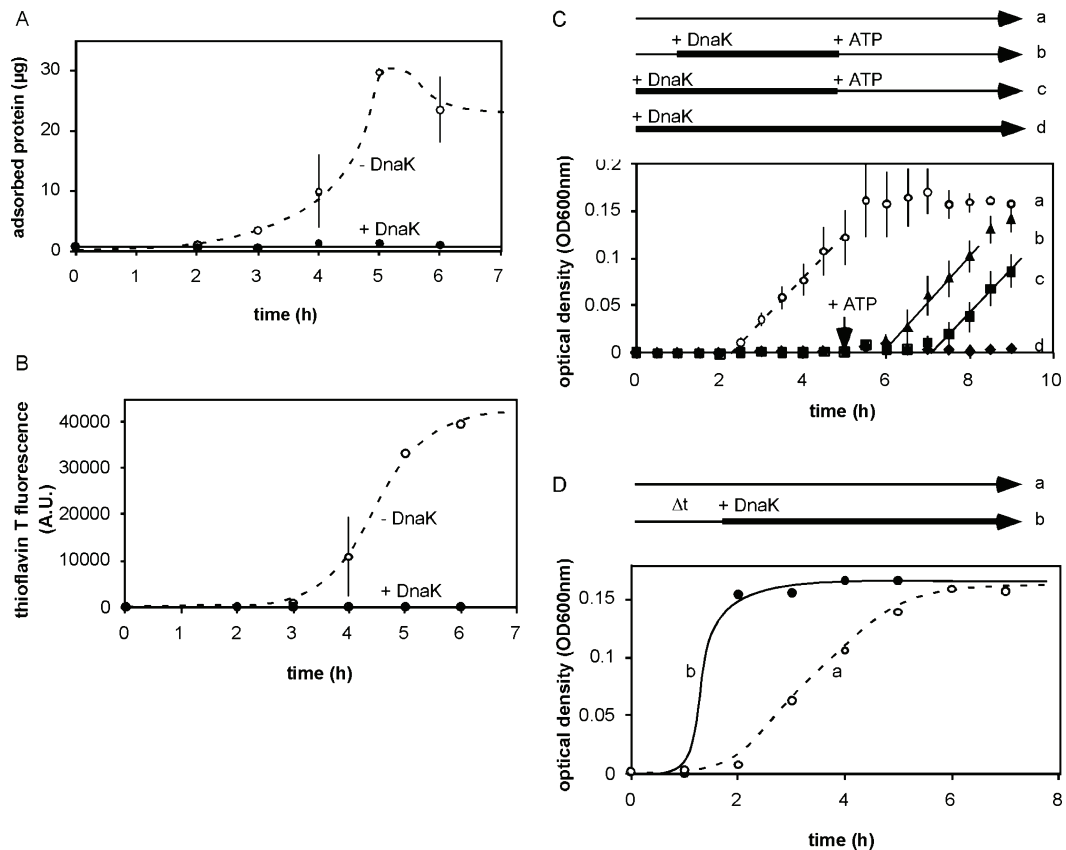


Figure 4. DnaK prevents the formation of prefibrillar insulin aggregates on hydrophobic surfaces. (A) Time course of adsorption of HI on hydrophobic surfaces in the presence of $0.3 \mu\text{M}$ DnaK without ATP (●) compared to the adsorption in the absence of DnaK (○). (B) Time course of amyloid fiber formation on hydrophobic surfaces in the presence of $0.3 \mu\text{M}$ DnaK without ATP (●) compared to the aggregation in the absence of DnaK (○). (C and D) Two-stage experiments. (C) A HI solution was incubated in the presence (filled symbols, b–d) or absence (○, a) of $0.3 \mu\text{M}$ DnaK. At the indicated time, 1 mM ATP was added to the DnaK-containing sample (b and c) and the HI solution was further incubated. Bold lines represent the time during which DnaK protects HI from aggregation. HI aggregation was monitored by turbidity. (D) DnaK ($0.3 \mu\text{M}$) was added at the indicated time (Δt) after the beginning of HI agitation in a hydrophobic microplate, and the incubation was further continued for $8 - \Delta t$ hours (●). In comparison, the kinetics of HI aggregation as measured in panel C (a) is shown (○). HI aggregation was monitored by turbidity after 8 h.

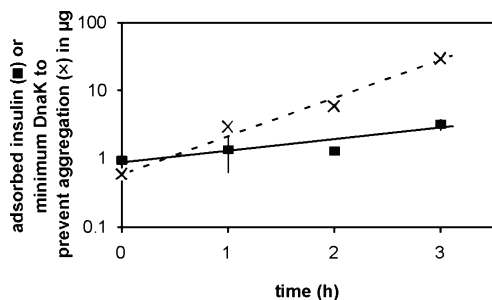


Figure 5. Stoichiometry of the interaction of DnaK with insulin adsorbed on hydrophobic surfaces. A HI solution was agitated in hydrophobic microplates for the indicated preincubation time. DnaK was then added at different concentrations, and the HI solution was further incubated for 18 h. The extent of HI aggregation was determined by ThT staining. A 2-fold increase in the level of ThT staining over background was used as a criterion for the onset of HI aggregation. The minimal amount of DnaK needed to prevent the onset of HI aggregation is represented as a function of preincubation time. The amount of adsorbed HI is also represented.

DnaK detached insulin aggregates from the bead surface, remaining associated to them. The time course of this process

was ~20 min (data not shown). In contrast, no DnaK could be detected on hydrophilic surfaces where similar amounts of HI had been preadsorbed (data not shown). Qualitatively similar results were obtained in the presence and absence of ATP. However, less insulin was detached, and ~50% of the DnaK remained bound to insulin aggregates in the presence of 1 mM ATP.

In a second set of experiments, DnaK ($8 \mu\text{g}$) was incubated with HI aggregates that had already been released in solution. Under these conditions, ~ $0.5 \mu\text{g}$ of DnaK was bound to $150 \mu\text{g}$ of a HI aggregate suspension. This shows that DnaK does not bind efficiently to HI aggregates already present in solution. DnaK therefore binds specifically to HI adsorbed on hydrophobic surfaces.

Making use of the affinity of DnaK for insulin adsorbed on hydrophobic surfaces, we subsequently designed an assay for the sensitive detection of aggregated insulin on material surfaces. Insulin (or BSA as a control) was incubated in the presence of hydrophobic or hydrophilic surfaces for 1 h. The adsorbed protein ($1-2 \mu\text{g}$) was incubated with increasing amounts of DnaK, in the presence or absence of DnaJ and/or ATP. After the sample had been gently washed, DnaK was detected using anti-DnaK antibodies in a chemoluminescence

Table 1. DnaK Binding to HI-Covered Surfaces and HI Aggregates and LVEALYL Aggregates in Solution^a

	fraction		
	adsorbed	released from beads	
		aggregates	soluble
Hydrophobic Surfaces, No DnaK Added			
human insulin (μg)	11 \pm 2	7 \pm 3	<0.1
Hydrophobic Surfaces, with DnaK (8 μg)			
human insulin (μg)	4.6 \pm 1	15.4 \pm 2.5	<0.1
DnaK (μg)	0.2 \pm 0.1	2.4 \pm 0.6	5.4 \pm 0.7
DnaK:HI molar ratio	277	77	
Hydrophobic Surfaces, with DnaK (8 μg) and Aggregated Insulin in Solution			
human insulin (μg)		150 \pm 10	
DnaK (μg)		0.5 \pm 0.2	
Molar ratio (HI:DnaK)		4200	
Hydrophobic surfaces, with DnaK (1.5 μg)			
LVEALYL (μg)		25	
DnaK (μg)		0.5	
Molar ratio (peptide:DnaK)		4000	

^aAcid-washed borosilicate glass beads (diameter of 1 mm) were silicized by immersion in SurfaSil (Pierce, 10%, w/w) in acetone and stabilized by being cured at 100 °C for 1 h. The water contact angle was measured (DSA100 Krüss) ($93.5 \pm 3.5^\circ$). SurfaSil-treated beads were incubated with HI in TBS-M buffer overnight. The fully aggregated HI solution was removed, and the beads were washed three times with 500 μL of TBS-M. The initial amount of HI adsorbed on the beads was determined. DnaK was then added, in the presence or absence of ATP, and the beads were further incubated for 1 h at 37 °C under agitation. The total protein content and the amount of HI or DnaK were determined in three fractions: the one adsorbed on the beads, the aggregated one, and the soluble ones released from the beads and separated by centrifugation (5000g for 10 min). The total amount of protein was quantified by the BCA assay; the amount of soluble HI was quantified by an ELISA (12018 mouse monoclonal anti-insulin antibody), and the amount of DnaK was determined using SDS-PAGE and Coomassie staining. Quantification was performed with ImageJ. For the interaction of DnaK with the aggregated LVEALYL peptide, the peptide solution was prepared at 1 mM glycine buffer (pH 2.5). This solution was incubated in hydrophobic 96-well plates overnight at 37 °C with agitation (1200 rpm). The resulting aggregates were centrifuged and washed three times in TBS-M buffer (pH 7.4) before being resuspended and incubated in TBS-M buffer containing 1.5 μg of DnaK over 30 min. The DnaK/peptide solution was then centrifuged and washed three times in TBS-M buffer before SDS-PAGE analysis.

assay (see Experimental Procedures). In Figure 6A, the amount of adsorbed DnaK is plotted as a function of the total amount of DnaK. In the absence of DnaJ, small but significant amounts of DnaK (26 ng) were bound to insulin adsorbed on hydrophobic surfaces compared to the amount of DnaK bound on adsorbed BSA (14 ng). In contrast, almost no DnaK was recovered when insulin was incubated with hydrophilic surfaces (data not shown). The amount of DnaK bound to adsorbed insulin was only slightly reduced in the presence of 1 mM ATP (23 ng). In the presence of DnaJ, much larger amounts of DnaK were bound to adsorbed HI (372 ng), but not on adsorbed BSA (27 ng). Addition of ATP reduced the amount of DnaK binding in the presence of DnaJ to 147 ng. To study the DnaJ requirement for DnaK binding, the amount of DnaK was kept constant at 2.5 μg (0.18 μM) and the DnaJ concentration was increased (Figure 6B). DnaK binding reached a maximum for amounts of DnaJ larger than 1.28 μg (0.16 μM), which corresponds to a 1:1 DnaJ:DnaK ratio. These

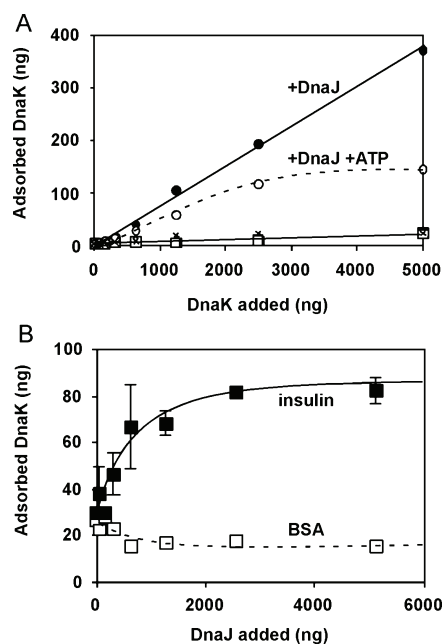


Figure 6. Amount of DnaK adsorbed on surface-bound HI. A 0.5 mg/mL insulin or 0.5 mg/mL BSA control solution (\times) was agitated for 1 h in a hydrophobic microplate. After removal of the solution, a DnaK solution was added. (A) The DnaK solution was not supplemented with ATP (\blacksquare), supplemented with 1 mM ATP (\square), and supplemented with DnaJ (0.16 μM) in the presence of 1 mM ATP (\circ) or in the absence of ATP (\bullet). The amount of adsorbed DnaK was measured using an ELISA as described in Experimental Procedures and is represented as a function of the total amount of DnaK added. (B) A 0.18 μM DnaK solution supplemented with different amounts of DnaJ was added to the adsorbed insulin (\blacksquare) and the adsorbed BSA (\square). The amount of adsorbed DnaK was measured using an ELISA as described in Experimental Procedures and is represented as a function of the total amount of DnaJ added. Lines are hand-drawn and provided as a guide for the eye.

data show that DnaK specifically interacts with HI adsorbed on hydrophobic surfaces and that the molecular chaperone DnaJ reinforces this binding. The weak binding of DnaK in the presence of ATP is consistent with its lack of a protective effect against aggregation.

Competition between the LVEALYL Amyloidogenic Peptide and Bacterial Chaperones during HI Aggregation on Hydrophobic Surfaces.

Recent studies by Ivanova et al.¹³ pinpointed the role of two HI amino acid stretches that are likely to change extensively their conformation when HI spontaneously goes from a soluble form to amyloid aggregates at pH 2 and 60 °C. These sequences are SLYQLENY (A12–19) and LVEALYL (B11–17). Both contain hydrophobic residues and are mainly involved in α -helices in the HI monomer. In amyloid fibers, two LVEALYL stretches from two monomers are assumed to associate into antiparallel extended β sheets that tightly interact via their hydrophobic side chains. The SLYQLENY sequence shows similar properties and also contributes to the formation of fibrillar structures. In this model, the core of HI amyloid fibers is therefore provided by hydrophobic interactions between these polypeptides and stabilized by the stacking of extended β -sheets. To investigate whether hydrophobic surfaces drive similar conformational changes, we studied the effect of the LVEALYL and the SLYQLENY peptides on HI aggregation kinetics. The SLYQLENY peptide

had no effect on HI aggregation kinetics, whereas the LVEALYL peptide strongly reduced the lag time in HI aggregation kinetics at substoichiometric concentrations relative to HI (Figure 7A). At higher concentrations, the

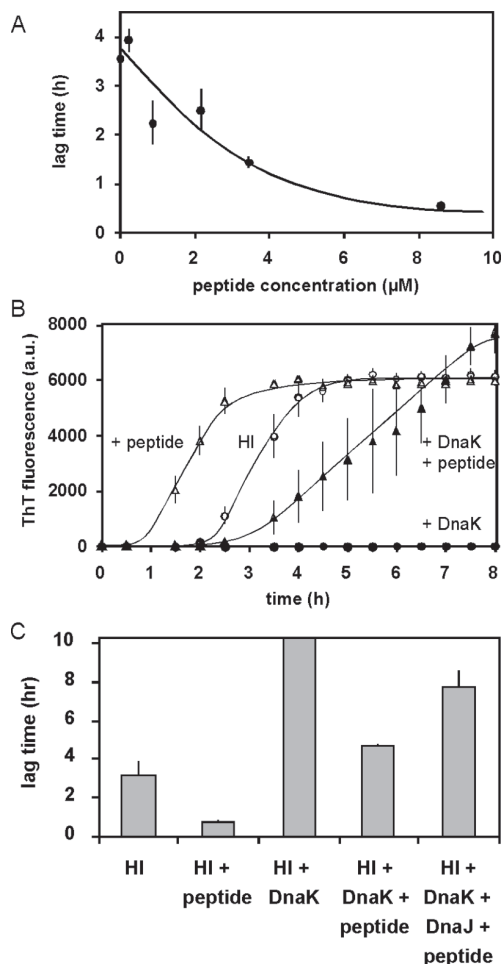


Figure 7. Effect of the LVEALYL peptide on HI aggregation kinetics. (A) A HI solution was agitated in a hydrophobic microplate in the presence of different amounts of the LVEALYL peptide, and aggregation was monitored using ThT fluorescence. The lag time (as defined in Experimental Procedures) is represented as a function of peptide concentration. (B) Aggregation kinetics of HI alone (○) or HI supplemented with 26 μM LVEALYL peptide (Δ), with 0.3 μM DnaK (●), or with both peptide and DnaK (\blacktriangle). Aggregation was assessed using ThT fluorescence. Lines are hand-drawn and provided as a guide for the eye. (C) A HI solution was agitated in a hydrophobic microplate in the presence of the LVEALYL peptide (8 μM), DnaK (0.3 μM), and DnaJ (0.16 μM), as indicated. Aggregation was monitored using ThT fluorescence, and the lag time was determined. In the presence of DnaK, the lag time extended beyond 10 h.

LVEALYL peptide inhibited the growth of HI amyloid aggregates, as reported previously at pH 2.¹³ The effect of the LVEALYL peptide was observed only in the presence of hydrophobic surfaces, the HI solution remaining perfectly stable in hydrophilic multiwell plates, whatever the peptide concentration. It should be noted that none of the peptides alone aggregate in hydrophobic or hydrophilic plates under the same pH, temperature, and concentration conditions.

Rüdiger et al. showed that the SHLVEALYLVCGER and CTSICSLYQLENYCN sequences in insulin bind DnaK.¹² Both encompass the aforementioned peptides involved in amyloid fiber formation (underlined). The same portions of insulin sequence are likely to be recognized by DnaJ, because it shares its substrates with DnaK.⁵ It follows that DnaK should antagonize the aggregation promoting effects of the LVEALYL peptide. As shown in Figure 7B, adding 26 μM LVEALYL peptide reduced the HI aggregation lag time from 2.5 ± 0.2 to 1.1 ± 0.2 h. The addition of 0.3 μM DnaK antagonized the effect of the LVEALYL peptide, extending the HI aggregation lag time up to 4.2 ± 0.7 h and slowing aggregation (Figure 7B). The presence of DnaJ enhanced the effect of DnaK [lag time of 7.8 ± 0.9 h (Figure 7C)]. More DnaK was needed to block HI aggregation for longer times. Conversely, ~ 60 μM LVEALYL peptide was needed to reduce the lag time to the value obtained in the absence of DnaK. Moreover, DnaK binds to amyloid aggregates formed by the LVEALYL peptide alone. Table 1 shows that 0.5 μg of DnaK binds to 25 μg of LVEALYL peptide aggregates.

DISCUSSION

DnaK Recognizes a Conformational Change Occurring on HI Adsorbed on Hydrophobic Surfaces. During aggregation, three pools of insulin were evidenced in this study: the soluble insulin pool, the final amyloid aggregates, and insulin adsorbed on hydrophobic surfaces. In another article, we show that the latter pool contains prefibrillar insulin aggregates that are essential intermediates in the pathway(s) leading to insulin aggregation. The amount of DnaK needed to block insulin aggregation supports the view that DnaK binds to a minor portion of insulin present in the adsorbed insulin pool. The DnaK concentration (0.3–3 μM) is indeed much lower than the HI concentration in solution. Thus, DnaK cannot significantly displace the monomer–dimer–hexamer equilibria and therefore cannot significantly reduce the HI monomer concentration, which is the form of HI in solution that aggregates in the presence of hydrophobic surfaces.⁹ Because DnaK weakly interacts with preformed amyloid aggregates released in solution, the binding of DnaK to the end product of the aggregation reaction cannot explain its inhibitory effect (Table 1). The target of DnaK is therefore to be found at the material surface. Because the amount of DnaK needed to block HI aggregation increases during the lag time (Figure 5), we rule out competitive adsorption at the material surface as the reason for DnaK inhibition. Moreover, we show that DnaK directly binds to HI adsorbed on hydrophobic surfaces and to HI aggregates released from the surface (Figure 6 and Table 1). We therefore propose that DnaK blocks the formation of HI amyloid fibers on hydrophobic surfaces, by selective binding to target sequences in adsorbed HI. One of these targets is likely to be the hydrophobic LVEALYL peptide, aggregates of which also bind DnaK (see Table 1 and below).

There is kinetic competition between amyloid fiber growth and protection by DnaK, which is illustrated well by the effect of ATP and DnaJ. ATP-loaded DnaK is known to have a lower affinity for its protein substrate than ADP-loaded DnaK⁵ and DnaJ, which stimulates ATP hydrolysis on DnaK and reinforces its interaction with its substrate. Our results suggest that in the absence of nucleotides, DnaK binds strongly to adsorbed HI and DnaJ further stabilizes DnaK binding. When the mean residence time of DnaK on exposed hydrophobic HI stretches is sufficiently long, the formation of amyloid fibers is inhibited

(Figure 4). On the other hand, when the residence time of DnaK is reduced by addition of ATP, aggregates can form rapidly because of the liberation of previously occupied hydrophobic growing fiber ends (Figures 3 and 4). Thus, the absence of ATP, through a substrate affinity increase, allows DnaK to win the competition between adding a blocking DnaK to a growing fiber end and an additional HI molecule, which would promote fiber growth. The competition can also be promoted by a sufficiently high concentration of the LVEALYL peptide, which accelerates HI aggregation so that it overcomes DnaK protection (Figure 7). Although significant amounts of DnaK are released from the surface (Table 1), together with the HI amyloid aggregates, it is the surface-bound DnaK fraction that sets the pace for fiber growth. In the ATP-free state, this latter DnaK fraction exhibits an affinity for growing fiber ends that is sufficiently high to block fiber formation. The inhibitory effect of DnaK on HI aggregation is therefore linked to its presence on the material surfaces.

The Amyloidogenic LVEALYL Peptide Is Exposed on HI during Its Aggregation on Hydrophobic Surfaces.

The results of this work and others show that insulin aggregates are able to form and grow on hydrophobic surfaces. What is the likely mechanism of this self-assembly process? Up to 40 μg of HI accumulates on the 2 cm^2 surface area of a single microwell during aggregation (Figure 1A). This high surface concentration (0.2 g/m^2) corresponds to 50 protein layers, assuming a uniform coverage of the surface. A consequence of this observation is that insulin does not merely adsorb on the plain hydrophobic surface, but on insulin already bound to the surface. The effect of the hydrophobic surface should therefore be transmitted from the bottom to the top HI layers, where incoming HI binds. This implies the existence of global conformational changes that relay the effect of the hydrophobic surface. Adsorption of HI molecules on a hydrophobic surface will itself trigger the exposure of a hydrophobic stretch at the surface of adsorbed HI. Although we did not evidence these conformational changes directly, several results support this hypothesis. (i) DnaK binds to HI adsorbed on hydrophobic surfaces, which shows that the structure of the HI protein has changed, exposing one of the two hydrophobic peptides known to bind DnaK: SLYQLENY and LVEALYL. (ii) The LVEALYL peptide itself interacts with HI in the presence of hydrophobic surfaces at a substoichiometric concentration in such a way to accelerate aggregation. This peptide has been shown to form antiparallel β -sheets with itself¹³ and could therefore help stabilize a conformational change in insulin by binding to intermediate states. (iii) The antagonist effects of the LVEALYL peptide and DnaK binding on HI aggregation reveal the presence of the same aggregation intermediates in the adsorbed HI pool. (iv) DnaK binds to preformed LVEALYL peptide aggregates. We therefore conclude that the buildup of amyloid fibers on the hydrophobic surface is due to HI adsorption and consequent conformational changes, exposing hydrophobic aggregation-prone sites in the protein. This situation occurs for some proteins, but not all of them. BSA, for instance, strongly binds to hydrophobic surfaces but does not accumulate on them and does not aggregate within an entire week in the presence of hydrophobic surfaces.

Perspectives. Our results have interesting potential biochemical and pharmaceutical applications. First, substoichiometric DnaK and DnaJ, in the absence of ATP, could represent a novel and convenient stabilizing additive. Indeed, the low DnaK concentration (0.3 μM), needed to stabilize HI solutions,

and its selectivity for exposed hydrophobic peptide domains are characteristics that most traditional stabilizing agents lack. Two recent papers by Rasmussen et al.^{31,32} showed that the protein α -crystallin, a member of the small heat shock protein family (sHSP), prevents HI aggregation on hydrophobic surfaces. Molecular chaperones, therefore, represent alternative approaches to guaranteeing the long-term storage of proteins, either in solution or in contact with the container surface. One should nevertheless be aware that DnaK triggers inflammatory responses and thus cannot be injected into patients.³³ DnaK, or better the DnaK–DnaJ combination, could also provide a sensitive *in vitro* assay to test for protein conformational changes at material surfaces, as shown for HI in this study. By revealing the presence of hydrophobic stretches exposed at the surface of proteins adsorbed on hydrophobic materials, this assay could provide a screening tool for the optimization of protein stability conditions.

AUTHOR INFORMATION

Corresponding Author

*Telephone: ++ 33 4 56 52 93 35. Fax: ++ 33 4 56 52 93 01. E-mail: marianne.weidenhaupt@grenoble-inp.fr.

Present Address

[§]EIFFAGE Travaux Publics, Centre d'Etudes et de Recherches, 8 rue du Dauphiné, 69960 Corbas, France.

Funding

This project was financed by a CNRS "Prise de risques" grant (CHAPROMAT). T.B. is a recipient of a CIFRE fellowship (371/2007). L.N. holds a doctoral fellowship from La Région Rhône-Alpes.

Notes

The authors declare no competing financial interest.

ACKNOWLEDGMENTS

We thank Benoît Duroux, Frédérique Crozet, and Sébastien Janvier for excellent technical assistance in particle size analysis, Laetitia Rapenne and Isabelle Paintrand in EM analysis and Bernd Bukau, Alexander Mogk, and Matthias Mayer for providing chaperone plasmids and protocols. We are grateful for the scientific input of Yves Bréchet (Grenoble-INP). We thank the CIME facility and BBSI laboratory (CEA Grenoble) for access to their equipment.

REFERENCES

- (1) Ellis, R. J., and van der Vies, S. M. (1991) Molecular chaperones. *Annu. Rev. Biochem.* 60, 321–347.
- (2) Ellis, R. J., van der Vies, S. M., and Hemmingsen, S. M. (1989) The molecular chaperone concept. *Biochem. Soc. Symp.* 55, 145–153.
- (3) Ellis, R. J., and Hemmingsen, S. M. (1989) Molecular chaperones: Proteins essential for the biogenesis of some macromolecular structures. *Trends Biochem. Sci.* 14, 339–342.
- (4) Mogk, A., Tomoyasu, T., Goloubinoff, P., Rudiger, S., Roder, D., Langen, H., and Bukau, B. (1999) Identification of thermolabile *Escherichia coli* proteins: Prevention and reversion of aggregation by DnaK and ClpB. *EMBO J.* 18, 6934–6949.
- (5) Bukau, B., and Horwich, A. L. (1998) The Hsp70 and Hsp60 chaperone machines. *Cell* 92, 351–366.
- (6) Goloubinoff, P., Mogk, A., Zvi, A. P., Tomoyasu, T., and Bukau, B. (1999) Sequential mechanism of solubilization and refolding of stable protein aggregates by a bichaperone network. *Proc. Natl. Acad. Sci. U.S.A.* 96, 13732–13737.
- (7) Diamant, S., Ben-Zvi, A. P., Bukau, B., and Goloubinoff, P. (2000) Size-dependent disaggregation of stable protein aggregates by the DnaK chaperone machinery. *J. Biol. Chem.* 275, 21107–21113.

- (8) Sluzky, V., Tamada, J. A., Klibanov, A. M., and Langer, R. (1991) Kinetics of insulin aggregation in aqueous solutions upon agitation in the presence of hydrophobic surfaces. *Proc. Natl. Acad. Sci. U.S.A.* 88, 9377–9381.
- (9) Sluzky, V., Klibanov, A. M., and Langer, R. (1992) Mechanism of insulin aggregation and stabilization in agitated aqueous solutions. *Biotechnol. Bioeng.* 40, 895–903.
- (10) Brange, J., Andersen, L., Laursen, E. D., Meyn, G., and Rasmussen, E. (1997) Toward understanding insulin fibrillation. *J. Pharm. Sci.* 86, 517–525.
- (11) Sharp, J. S., Forrest, J. A., and Jones, R. A. (2002) Surface denaturation and amyloid fibril formation of insulin at model lipid-water interfaces. *Biochemistry* 41, 15810–15819.
- (12) Rüdiger, S., Germeroth, L., Schneider-Mergener, J., and Bukau, B. (1997) Substrate specificity of the DnaK chaperone determined by screening cellulose-bound peptide libraries, *EMBO J* 16, 1507–582.
- (13) Ivanova, M. I., Sievers, S. A., Sawaya, M. R., Wall, J. S., and Eisenberg, D. (2009) Molecular basis for insulin fibril assembly. *Proc. Natl. Acad. Sci. U.S.A.* 106, 18990–18995.
- (14) Cegielska, A., and Georgopoulos, C. (1989) Functional domains of the *Escherichia coli* dnaK heat shock protein as revealed by mutational analysis. *J. Biol. Chem.* 264, 21122–21130.
- (15) McCarty, J. S., and Walker, G. C. (1991) DnaK as a thermometer: Threonine-199 is site of autophosphorylation and is critical for ATPase activity. *Proc. Natl. Acad. Sci. U.S.A.* 88, 9513–9517.
- (16) Buchberger, A., Schroder, H., Buttner, M., Valencia, A., and Bukau, B. (1994) A conserved loop in the ATPase domain of the DnaK chaperone is essential for stable binding of GrpE. *Nat. Struct. Biol.* 1, 95–101.
- (17) Veinger, L., Diamant, S., Buchner, J., and Goloubinoff, P. (1998) The small heat-shock protein IbpB from *Escherichia coli* stabilizes stress-denatured proteins for subsequent refolding by a multi-chaperone network. *J. Biol. Chem.* 273, 11032–11037.
- (18) Olson, B. J., and Markwell, J. (2007) Assays for determination of protein concentration. *Current Protocols in Protein Science*, Chapter 3, Unit 3, 4, Wiley, New York.
- (19) Smith, D. A., and Radford, S. E. (2000) Protein folding: Pulling back the frontiers. *Curr. Biol.* 10, R662–R664.
- (20) Wiechelman, K. J., Braun, R. D., and Fitzpatrick, J. D. (1988) Investigation of the bicinchoninic acid protein assay: Identification of the groups responsible for color formation. *Anal. Biochem.* 175, 231–237.
- (21) Stoscheck, C. M. (1990) Quantitation of protein. *Methods Enzymol.* 182, 50–68.
- (22) LeVine, H. III (1999) Quantification of β -sheet amyloid fibril structures with thioflavin T. *Methods Enzymol.* 309, 274–284.
- (23) Blundell, T. L., Cutfield, J. F., Dodson, G. G., Dodson, E., Hodgkin, D. C., and Mercola, D. (1971) The structure and biology of insulin. *Biochem. J.* 125, 50P–51P.
- (24) Burke, M. J., and Rougvie, M. A. (1972) Cross- β protein structures. I. Insulin fibrils. *Biochemistry* 11, 2435–2439.
- (25) Garriques, L. N., Frokjaer, S., Carpenter, J. F., and Brange, J. (2002) The effect of mutations on the structure of insulin fibrils studied by Fourier transform infrared (FTIR) spectroscopy and electron microscopy. *J. Pharm. Sci.* 91, 2473–2480.
- (26) Theyssen, H., Schuster, H. P., Packschies, L., Bukau, B., and Reinstein, J. (1996) The second step of ATP binding to DnaK induces peptide release. *J. Mol. Biol.* 263, 657–670.
- (27) McCarty, J. S., Buchberger, A., Reinstein, J., and Bukau, B. (1995) The role of ATP in the functional cycle of the DnaK chaperone system. *J. Mol. Biol.* 249, 126–137.
- (28) Skowrya, D., and Wickner, S. (1995) GrpE Alters the Affinity of DnaK for ATP and Mg. *J. Biol. Chem.* 270, 26282–26285.
- (29) Suh, W.-C., Burkholder, W. F., Lu, C. Z., Zhao, X., Gottesman, M. E., and Gross, C. A. (1998) Interaction of the Hsp70 molecular chaperone, DnaK, with its cochaperone DnaJ. *Proc. Natl. Acad. Sci. U.S.A.* 95, 15223–15228.
- (30) Liberek, K., Wall, D., and Georgopoulos, C. (1995) The DnaJ chaperone catalytically activates the DnaK chaperone to preferentially bind the sigma 32 heat shock transcriptional regulator. *Proc. Natl. Acad. Sci. U.S.A.* 92, 6224–6228.
- (31) Rasmussen, T., Kasimova, M. R., Jiskoot, W., and van de Weert, M. (2009) The Chaperone-like Protein¹-Crystallin Dissociates Insulin Dimers and Hexamers, *Biochemistry* 4893139320.
- (32) Rasmussen, T., Tantipolphan, R., van de Weert, M. and Jiskoot, W. (2010) The molecular chaperone alpha-crystallin as an excipient in an insulin formulation. *Pharm Res* 2713371347.
- (33) Nolan, A., Weiden, M. D., Hoshino, Y., and Gold, J. A. (2004) Cd40 but not CD154 knockout mice have reduced inflammatory response in polymicrobial sepsis: A potential role for *Escherichia coli* heat shock protein 70 in CD40-mediated inflammation in vivo. *Shock* 22, 538–542.